The matrix of cold-water coral mounds: origin and early-diagenetic interactions

---

De matrix van koudwaterkoraal-mounds: oorsprong en vroeg-diagenetische interacties

Hans Pirlet

2010

Proefschrift tot het behalen van de graad van Doctor in de Wetenschappen: Geologie

Dit werk werd gefinancierd door een beurs van het Fonds voor Wetenschappelijk Onderzoek - Vlaanderen (FWO-Vlaanderen)

Promotor: Prof. Dr. Jean-Pierre Henriet
Co-promotor: Prof. Dr. Frank Vanhaecke

Universiteit Gent
Faculteit Wetenschappen
Vakgroep Geologie en Bodemkunde

Table of contents

Part 2 The terrigenous fraction in Challenger mound

List of figures

List of tables

Summary

Corals have long been associated with warm and shallow water in tropical settings. Nevertheless an important part thrives in deep and cold waters where they feed on plankton and suspended organic material in the water column. Cold-water corals have been observed along the entire NE Atlantic margin. In certain places these cold-water corals build important geological features on the seabed such as the kilometers-long *Lophelia* reef complexes which have been mapped off Norway. However, the most spectacular coral buildups are, without any doubt, mound structures which reach heights up to 300 meter and have diameters up to several kilometers. Hence, they represent some of the most impressive bioherms in the world. Clusters of cold-water coral mounds were found in the Porcupine Seabight and Rockall Trough, west of Ireland but also more to the south in the Gulf of Cadiz, in the Alboran Sea and Off Mauritania. In 2005, IODP (Integrated Ocean Drilling Program) expedition 307 drilled for the first time a complete sequence through a cold-water coral mound (i.e. Challenger Mound, Porcupine Seabight) revealing cold-water corals until the base of the mound. Hence, the corals are really the engineers for the build-up of these mound structures. Several generations of PhD theses and numerous international peer reviewed papers, conducted over the last two decades, have already provided a broad overview of cold-water coral mound distribution, morphology, habitat mapping and contemporary constraints on mound build-up. The present thesis will zoom in on two distinct niches which remained largely unexplored until now: (1) The terrigenous fraction in a cold-water coral mound as recorder of paleo-environmental conditions and (2) cold-water coral mounds as natural laboratory to study early-diagenetic processes in cool-water carbonate bodies.

(1) The terrigenous fraction in Challenger Mound

More than 50 percent of the sediment matrix in Challenger Mound consists of terrigenous material. However, until now, no in-depth study of this fraction has been conducted. A thorough characterization of the terrigenous fraction is crucial given that it potentially plays an important role in diagenetic processes and the magnetic properties of the sediment. Moreover, the terrigenous sediment also provides crucial information on the hydrodynamics in the study site, weathering intensity on the nearby continents and sedimentary processes such as ice-rafting, turbidity flows and current reworking which transport and/or erode sediments to and from the mound. Therefore, a research strategy was developed to study the terrigenous fraction in a Late Quaternary sequence of Challenger Mound (gravity core MD01-2451G) combining clay mineralogy, sedimentology, petrography and strontium and neodymium isotope analysis. This multidisciplinary approach was used to acquire information about the provenance of the terrigenous material, the routes and modes of transport and the sedimentary environment but also about the continental weathering processes. Ireland was identified as the main contributor of terrigenous material in Challenger Mound in the Late Quaternary. Besides this, a variable input of volcanic material from the northern volcanic provinces (Iceland and/or the NW British Isles) is recognized in most of the samples. This volcanic material was most likely transported to

Challenger Mound during cold climatic stages. Minor amounts of sediment deriving from the old cratons on Greenland, Scandinavia or Canada were noticed in a few samples. A clear shift in the sedimentary environment and modes of transport was observed in glacial compared to interglacial periods. During glacial periods, most of the terrigenous sediment was transported towards Challenger Mound as ice rafted debris and was subsequently deposited in an environment, characterized by a slow bottom current regime. In contrast, the terrigenous material present in interglacial intervals seems largely of glacial origin which was reworked by intense bottom currents. Furthermore, the importance of the nearby British-Irish Ice Sheet (BIIS) on mound growth is highlighted. It is put forward that the deglaciation of the BIIS seriously altered the hydrography and terrigenous input in the Porcupine Seabight and therefore inhibited coral growth.

In a second step, the latter research strategy was used as a stepping stone to go further back into the sequence of Challenger and the same multidisciplinary approach was applied on the terrigenous sediment fraction in the IODP expedition 307 drilling. Throughout the entire mound sequence, the British-Irish Isles appeared to be the dominant sediment contributor in Challenger Mound with a variable amount of volcanic material. The Early Pleistocene ice-rafted horizons, which occur in the lower mound sequence can be linked with the British-Irish Isles as well. Therefore, it is concluded that a recurring, marine-based ice sheet was present on the British-Irish Isles during the Early Pleistocene since 2.7 Ma. Hence, for the first time, the existence of early and significant ice accumulation in mid-latitudinal regions, such as the British-Irish Isles is evidenced. Finally, the potential of the clay mineralogy in Challenger Mound as proxy for the continental climate on the British Irish Isles is highlighted. Interglacial periods are characterized by enhanced smectite values indicating the presence of a temperate climate with sufficient water to allow hydrolysis. In contrast, glacial periods reveal increased illite concentrations which are attributed to the growing importance of direct rock erosion. During deglaciations, smectite peaks are recorded, caused by the initial chemical weathering after glacial retreat. A shift is observed in the chlorite and kaolinite content before and after the Mid-Pleistocene Transition (MPT). Higher chlorite and decreasing kaolinite concentrations point towards an increase of the physical weathering processes after the MPT which may be attributed to the prolonged and more extensive glaciations.

(2) Early diagenetic processes in cold-water coral mounds

After deposition, the sediment is affected by a series of early diagenetic processes which are mainly fueled by the microbial degradation of organic matter. These early diagenetic processes will overprint the original sediment sequence and may result in the dissolution of the aragonitic corals and precipitation of other carbonate and sulfur-bearing minerals. The precipitation of carbonate minerals is of particular interest as this process might stabilize the mound sediments which is crucial for mound build-up. In addition, the study of these early diagenetic processes helps to better recognize and disentangle the diagenetic features in fossil carbonate mounds. Also, early diagenetic features might form a template for later diagenetic processes.

Authigenic gypsum was found in a gravity core, retrieved from the top of Perseverance Mound, a giant cold-water coral mound in the Porcupine Basin, off Ireland. The occurrence of gypsum in such an environment is intriguing, since gypsum, a classic evaporitic mineral, is undersaturated with respect to sea water. Sedimentological, petrographic and isotopic evidence point to diagenetic formation of the gypsum, tied to oxidation of sedimentary sulfide minerals (i.e. pyrite). This oxidation is attributed to a phase of increased bottom currents which caused erosion and enhanced inflow of oxidizing fluids into the mound sediments. The oxidation of pyrite produced acidity, causing carbonate dissolution and subsequently leading to pore-water oversaturation with respect to gypsum and dolomite. Calculations based on the isotopic compositions of gypsum and pyrite reveal that between 21.6% and 28.6% of the sulfate incorporated into the gypsum derived from pyrite oxidation. Thus, authigenic gypsum can serve as a signature for diagenetic oxidation events in carbonate-rich sediments. The dissolution of carbonate increased the porosity in the affected sediment layer but promoted lithification of the sediments at the sediment-water interface. This lithified carbonate layer was subsequently buried by Holocene sediments which resulted in a new phase of bacterial sulfate reduction. The produced hydrogen sulfide, which acts as a weak acid, was not buffered in the lithified carbonate layer due to the limited pool of reactive iron. This led to the dissolution of aragonitic biogenic fragments, creating a moldic porosity in the lithified horizon. These observations demonstrate

that fluid flow, steered by environmental factors, has an important effect on the diagenesis of coral mounds.

Alpha, Beta and Gamma Mound are three cold-water coral mounds, located on the Pen Duick Escarpment in the Gulf of Cadiz amidst the El Arraiche mud volcano field where focused fluid seepage occurs. The diagenetic alteration of the sedimentary record of Alpha and Beta Mound is strongly influenced by the biochemical processes occurring at shallow sulfate methane transition zones (SMTZs). This resulted in various intervals containing authigenic carbonates, depleted in ^{13}C and sedimentary pyrite with heavy $\delta^{34}S$ values. However, despite the proximity of Alpha and Beta Mound, the mounds each contain a completely different assemblage of authigenic minerals. Alpha mound features diagenetic dolomite, framboidal pyrite and gypsum, whereas Beta Mound contains a barite layer, and euhedral pyrite. Our combined sedimentological, petrographic and isotopic analyses indicate that the contrast in mineral assemblages between Alpha and Beta Mound may be caused by differences in fluid and methane fluxes. Alpha Mound appears to be affected by strong fluctuations in the fluid flow, causing shifts in redox boundaries whereas Beta Mound seems a less dynamic system. Whereas it becomes evident that authigenic mineral assemblages are very sensitive recorders of the diagenetic history of specific cold water coral mounds, the reasons for the differences in the diagenetic environment remain speculative. It is postulated that diagenetic regimes within cold-water coral mounds are not only influenced by external forcings. Diagenetic processes such as dissolution of aragonite, lithification by precipitation of authigenic minerals and subsequent brecciation of these lithified layers may also exert a control on the advective and diffusive fluid flow within these mounds.
In contrast to Alpha and Beta Mound, the diagenetic processes in the upper 5 m of Gamma Mound are not influenced by a SMTZ. The large pool of iron-(oxyhydr)oxides, due to the Saharan dust input, resulted in the dominance of dissimilatory iron reduction over bacterial sulfate reduction. Therefore, corals are well preserved in the upper layer. Below 5 m, bacterial sulfate reduction becomes the dominant electron accepting pathway during organic matter degradation and relatively high $\delta^{34}S$ values of the sedimentary pyrite suggest the upward diffusion of hydrogen sulfide from a STMZ below. In this layer, corals are badly preserved and precipitation of calcite and dolomite occurs.

Samenvatting

Koralen werden tot voor kort voornamelijk geassocieerd met ondiep, warm water in tropische oorden. Desalniettemin leeft een belangrijk deel van de koraalgemeenschap in koud en diep water buiten het bereik van zonlicht, waar ze zich voeden met plankton en organisch materiaal dat in suspensie voorbij drijft. Dergelijke koudwaterkoralen zijn inmiddels teruggevonden langsheen de volledige noordoostelijke Altantische continentale rand. Op bepaalde plaatsen kunnen deze koralen belangrijke geologische structuren op de zeebodem vormen. Zo werden langs de kust van Noorwegen riffen gevonden van *Lophelia* koralen die ettelijke kilometers lang kunnen worden. De meest spectaculaire bouwwerken, gevormd door deze koudwaterkoralen, zijn zonder twijfel de mound-structuren die hoogtes kunnen bereiken tot 300 m en een diameter hebben van verscheidene kilometers. Dergelijke clustsers van koraal-mounds werden tot nu toe gevonden in het Porcupine Bekken en de Rockall Trough, ten westen van Ierland. Meer naar het zuiden zijn koraal-mounds echter ook bekend in de Alboran Zee (westelijke Middellandse Zee), in de Golf van Cadiz (ten westen van Marokko) en voor de kust van Mauritanië. In 2005 werd voor het eerst een volledige mound aangeboord (Challenger Mound in het Porcupine Bekken) in het kader van het IODP project. Deze boring toonde aan dat koralen voorkomen tot aan de basis van de mound en dat zij wel degelijk de 'ingenieurs' zijn van deze mound structuren. De voorbije twintig jaar zijn reeds verschillende studies uitgevoerd die een overzichtsbeeld schetsen van koudwaterkoraal-mounds. Deze studie zal echter focussen op twee niches die tot nu toe onderbelicht bleven in het mound onderzoek. (1) Het potentieel van de terrigene sedimentfractie (sediment dat van het continent afkomstig is) in een koraal-mound als recorder van veranderingen in de klimaats- en omgevings-condities. (2) Koudwaterkoraal-mounds als testobject om vroeg-diagenetische veranderingen (veranderingen die plaatsgrijpen na het afzetten van het sediment) in koudwater carbonaten te onderzoeken.

(1) De terrigene sedimentfractie in Challenger Mound

Uit onderzoek bleek dat meer dan de helft van de sediment matrix in Challenger Mound bestaat uit terrigeen materiaal. Toch werd er tot op heden nog nooit een gedetailleerde studie van deze terrrigene fractie uitgevoerd. Een dergelijke studie is nochtans van cruciaal belang aangezien de terrigene sedimentfractie een rol speelt in diagenetische processen en de magnetische eigenschappen van het sediment. Bovendien bevat het terrigeen materiaal belangrijke informatie over de hydrodynamische processen in het studiegebied, de intensiteit van verwering op de aanpalende continenten en sedimentaire processen zoals het transport van sediment door middel van ijsbergen, turbiditeitsstromingen of bodemstromingen. Bijgevolg is er nood aan een onderzoeksstrategie die deze informatie uit het terrigeen sediment kan extraheren. In een eerste stap werd daarom een pilootstudie opgestart op een Laat-Quartaire sediment sectie van de top van Challenger Mound (Kern MD01-2451G). Een multi-disciplinaire aanpak werd gehanteerd die zowel kleimineralogie, mineralogische en sedimentologische analysen en analyse van de strontium en neodymium isotopen gebruikt om informatie te verzamelen over de herkomst, de route en wijze van transport van het terrigeen materiaal. Verder werd er ook gefocust op het sedimentair milieu en de wijze en intensiteit van de continentale verweringsprocessen. Ierland

werd geïdentificeerd als belangrijkste leverancier van terrigeen sediment in het Laat-Quartaire sediment van Challenger Mound. In de meeste samples was ook een variabele hoeveelheid vulkanisch materiaal aanwezig dat afkomstig is van de grote vulkanische provincies ten noorden van het Porcupine Bekken (bijv. IJsland en de vulkanische provincies in de noordwestelijke Brits-Ierse Eilanden). Dit vulkanisch materiaal is waarschijnlijk door middel van ijsbergen aangevoerd naar Challenger Mound tijdens koude periodes. Soms werden kleine hoeveelheden sediment gedetecteerd die afkomstig zijn van oude cratons die terug te vinden zijn op Groenland, Scandinavië of Canada. Tijdens de overgang van glaciale naar interglaciale periodes wordt een belangrijke verandering vastgesteld in de sedimentaire omgeving en de wijze van transport van het terrigeen materiaal. Tijdens glacialen werd het sediment voornamelijk aangevoerd door ijsbergen en vervolgens afgezet in een sedimentaire omgeving met trage bodemwaterstromingen. In interglaciale periodes wordt er echter vastgesteld dat de terrigene sedimentfractie voornamelijk bestaat uit materiaal van glaciale origine dat herwerkt is door intense bodemwaterstromingen. Het wordt daarom voorgesteld dat deglaciaties van de Brits-Ierse ijskap (BIIS) een invloed uitoefenen op de mound groei. Tijdens dergelijke deglaciaties kunnen de hydrodynamische condities en terrigene input in het Porcupine Bekken dusdanig veranderen dat koraalgroei wordt verhinderd.
De voorgaande onderzoekstrategie werd in een tweede fase gebruikt om verder terug te keren in de sedimentaire sequentie van Challenger Mound die aangeboord werd tijdens IODP expeditie 307. Net als de top van Challenger Mound bleek ook doorheen de volledige boring de Brits-Ierse Eilanden de dominante leverancier van terrigeen sediment, meestal met een kleine bijmenging van vulkanisch materiaal. Bovendien konden de Vroeg-Pleistocene sedimentlagen met materiaal dat aangebracht werd door middel van ijsbergen ook gerelateerd worden met de Brits-Ierse Eilanden. Uit deze bevinding kon geconcludeerd worden dat er herhaaldelijk een Brits-Ierse ijskap aanwezig was in het Vroeg Pleistoceen sinds 2.7 miljoen jaar. Deze ijskap nam bovendien aanzienlijke proporties aan aangezien hij de zee bereikte zodat ijsbergen gevormd konden worden. Het is voor de eerste maal dat de aanwezigheid van een Vroeg-Pleistocene ijskap kon worden bewezen in een dergelijk mid-latitudinaal gebied. Tot slot werd het potentieel van de klei-mineralen als proxy voor het continentale klimaat op de Brits-Ierse Eilanden onder de loep genomen. Interglaciale periodes worden gekarakteriseerd door verhoogde smectiet-concentraties die wijzen op de aanwezigheid van een gematigd continentaal klimaat met voldoende neerslag zodat hydrolyse kon plaatsgrijpen. Tijdens glaciale periodes werd echter voornamelijk illiet geproduceerd door de toenemende invloed van fysische erosie door ijswerking. Deglaciaties van de BIIS gaan meestal gepaard met smectietpieken. Dit wordt toegeschreven aan het toenemende belang van chemische verwering tijdens het terugtrekken van de ijskap. Een belangrijke verandering in de concentraties van kaoliniet en chloriet wordt geobserveerd voor en na de Mid-Pleistocene Transitie (MPT). De toename van de chloriet-concentraties en afname van kaoliniet na de MPT wordt gelinkt aan langere en koudere glaciaties.

(2) Vroeg-diagenetische processen in koudwaterkoraal-mounds

Het sediment wordt na de afzetting onderworpen aan een reeks vroeg-diagenetische processen die aangedreven worden door de microbiële afbraak van organisch materiaal. Deze diagenetische processen zorgen voor veranderingen in de originele sedimentsequentie en kunnen resulteren in de oplossing van het aanwezige aragoniet, zoals de koralen, en de precipitatie van andere carbonaten, sulfiden en sulfaten. Vooral de precipitatie van authigene mineralen is interessant voor deze studie aangezien deze precipitatie kan zorgen voor een stabilisatie van het sediment, een cruciaal proces in het opbouwen van een mound structuur. Verder is de studie van vroeg-diagenetische processen van belang om vroeg-diagenetische structuren in fossiele carbonaat mound beter te herkennen en te kunnen onderscheiden van latere diagenetische kenmerken. Bovendien kunnen de vroeg-diagenetische structuren een blauwdruk vormen voor de latere diagenetische processen.

In een kern die genomen werd op de top van Perseverance Mound, een koudwaterkoraal-mound in het Porcupine Bekken, werd authigeen gips teruggevonden. Het voorkomen van gips kristallen in een dergelijke omgeving is onverwacht aangezien gips, een evaporitisch mineraal, onderverzadigd is ten opzichte van zeewater en er bijgevolg geen directe precipitatie kan plaatsgrijpen uit zeewater. Aan de hand van sedimentologisch, petrografisch en isotopisch onderzoek werd een innovatief model opgesteld die de gipsvorming linkt aan de oxidatie van de sulfidemineralen in het sediment zoals pyriet. Deze oxidatie wordt toegedicht aan een fase met snelle

bodemwaterstromingen die erosie veroorzaakte alsook de penetratie van oxiderend zeewater in de mound sedimenten. De daaropvolgende oxidatie van het pyriet leidde tot een verzuring van het poriënwater die gebufferd werd door de oplossing van aragoniet (bijv. de koralen). Bijgevolg resulteerde dit oxidatieproces in een verhoging van zowel de sulfaat- als de calcium-concentratie in het poriënwater, zodat gips kon neerslaan. Naast de vorming van gipskristallen leidde de sulfide oxidatie ook tot de precipitatie van dolomiet. Berekeningen, op basis van de isotopische verhoudingen van gips en pyriet, toonden aan dat tussen 21.6% en 28.6% van het sulfaat dat geïncorporeerd werd in het gips afkomstig is van de oxidatie van pyriet. Bijgevolg kan het voorkomen van authigeen gips dienen als indicator van diagenetische oxidatie events in carbonaatrijke sedimenten. De oplossing van het aragoniet resulteerde in een verhoging van de porositeit in de sedimentlaag die beïnvloed werd door de sulfide oxidatie. Dit opgeloste carbonaat sloeg uiteindelijk terug neer als calciet dichtbij de zeebodem wat leidde tot de vorming van een verharde laag. Tijdens het Holoceen werd deze verharde laag begraven onder een nieuw sedimentpakket en vond opnieuw bacteriële sulfaat reductie plaats geassocieerd met de afbraak van het organisch materiaal. Tijdens dit proces werd waterstofsulfide geproduceerd, dat zich gedraagt als een zwak zuur. Door de lage concentratie van reactief ijzer in de verharde laag werd waterstofsulfide niet gebufferd door de vorming van pyriet en vond aragonietoplossing plaats. Dit leidde tot de vorming van een secundaire porositeit in de verharde laag. Deze observaties tonen aan hoe vloeistofstromingen, gestuurd door omgevingscondities, een belangrijke rol uitoefenen of de vroegtijdige diagenese in koraal-mounds.

Alpha, Beta en Gamma Mound zijn drie koudwaterkoraal-mounds gesitueerd in de Golf van Cadiz op een steile richel (Pen Duick Escarpment). Deze drie mounds bevinden zich in een gebied met moddervulkanen (El Arraiche mud volcano field) waar fluïda zich vanuit de diepte een weg naar de zeebodem banen. De diagenetische veranderingen die plaatsgrijpen in het sediment van Alpha en Beta Mound worden in sterke mate bepaald door de bio-geochemische processen die zich afspelen in de buurt van een ondiepe sulfaat methaan transitie zone (SMTZ). De ondiepe SMTZ resulteerde in beide mounds in de precipitatie van carbonaten (voornamelijk calciet) met een lage $\delta^{13}C$ waarde en sedimentair pyriet met hoge $\delta^{34}S$ waarden. Ondanks de beperkte afstand tussen beide mounds, worden Alpha en Beta Mound gekarakteriseerd door een verschillende assemblage van authigene mineralen. In Alpha Mound komt onder meer dolomiet, framboïdaal pyriet en gips voor terwijl Beta Mound voornamelijk gekarakteriseerd wordt door bariet en euhedraal pyriet. Sedimentologische, petrografische en isotopische analyses wezen uit dat de verschillen tussen deze twee diagenetische systemen in de eerste plaats te wijten zijn aan verschillende fluxen van methaan en andere fluïda. Deze variërende fluxen veroorzaken verplaatsingen van de grenzen van de diverse redoxzones. Zo wordt Alpha Mound gekarakteriseerd door sterke schommelingen van de vloeistofstromingen terwijl Beta Mound eerder een minder dynamische diagenetisch systeem vertegenwoordigt. Onze waarnemingen tonen aan dat authigene mineralen goede indicatoren zijn om de diagenetische geschiedenis van specifieke mounds te reconstrueren. Desalniettemin blijft het onzeker welke processen exact de vloeistofstromingen in mounds bepalen. Wij geloven dat de diagenetische regimes niet enkel beïnvloed worden door externe factoren. Diagenetische processen zoals aragonietoplossing, de verharding van het sediment door precipitatie van authigene mineralen en de brecciatie van de verharde lagen spelen een belangrijke rol in de vloeistofstromingen in deze mounds.

In tegenstelling tot Alpha en Beta Mound, worden de diagenetische processen in Gamma Mound niet beïnvloed door een SMTZ in de bovenste 5 m van het sediment. De grote hoeveelheid ijzer-oxiden en -hydroxiden die aangevoerd worden door het eolisch stof van de Sahara zorgt ervoor dat de reductie van ijzer, de bacteriële reductie van sulfaat grotendeels wegconcurreert. Dit resulteert in een uitstekende bewaring van de koralen in de bovenste sedimentlagen. Beneden 5 m wordt bacteriële sulfaat reductie het belangrijkste proces in de afbraak van organisch materiaal. De relatief hoge $\delta^{34}S$ waarden van het sedimentair pyriet suggereren de invloed van waterstofsulfide dat opwaarts migreert van een diepergelegen SMTZ. Lager dan 5 m werden zowel calciet- en dolomiet-precipitatie als aragonietoplossing geobserveerd.

Part 1

Introduction and methodology

Chapter 1 - Introduction

1.1 Cold-water corals

Coral reefs usually evoke images of warm trade winds, swaying palm trees, tropical coral seas with coral sand islands and the crash of the surf on a rocky edifice (Stanley, 2001). However, the exploration of deep-water environments, using new technologies, revealed that corals can thrive in dark, cold and nutrient-rich waters as well (Fig. 1.1, 1.2). Reef-building cold-water corals are derived from several systematic groups. The most important of these are the colonial stony corals (Scleractinia), true soft corals (Octocorallia), black corals (Antipatharia) and calcifying lace corals (Hydrozoa). Several species of the cold-water coral groups create forest-like reefs on the sea floor comparable in size and complexity to their warm-water cousins (Fig. 1.2) (Freiwald *et al.,* 2004). These coral groups are azooxanthellate (i.e. no symbiosis with zooxanthellate algae) and often form colonies supported by a common skeleton, providing a structural habitat for many other species (Roberts *et al.,* 2006). During the European Atlantic Coral Ecosystem Study (ACES) over 1300 species were listed from cold-water reefs along the NW European margins, emphasizing the biodiversity of these unique ecosystems. However, the diversity of coral species in cold water is much lower compared to their shallow-water counterparts. Approximately, 800 species of reef-building Scleractinians are described in shallow water whereas fewer than 10 are known to make a substantial deep-water reef framework (Freiwald *et al.,* 2004; Roberts *et al.,* 2006). The dominant framework-building cold-water coral species along the NE Atlantic margin is *Lophelia pertusa* while *Madrepora oculata* is

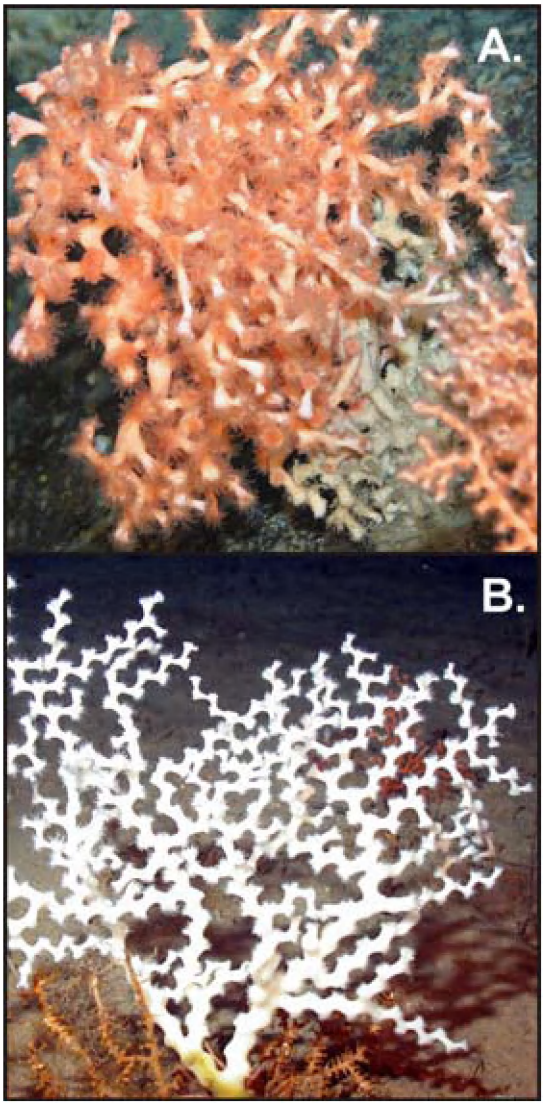

Fig. 1.1 *A detail of the two most common framework building cold-water corals in the NE Atlantic: A. Lophelia pertusa. and B. Madrepora oculata (Source: Photo library of the National Oceanic and Atmospheric Administration Department of Commerce).*

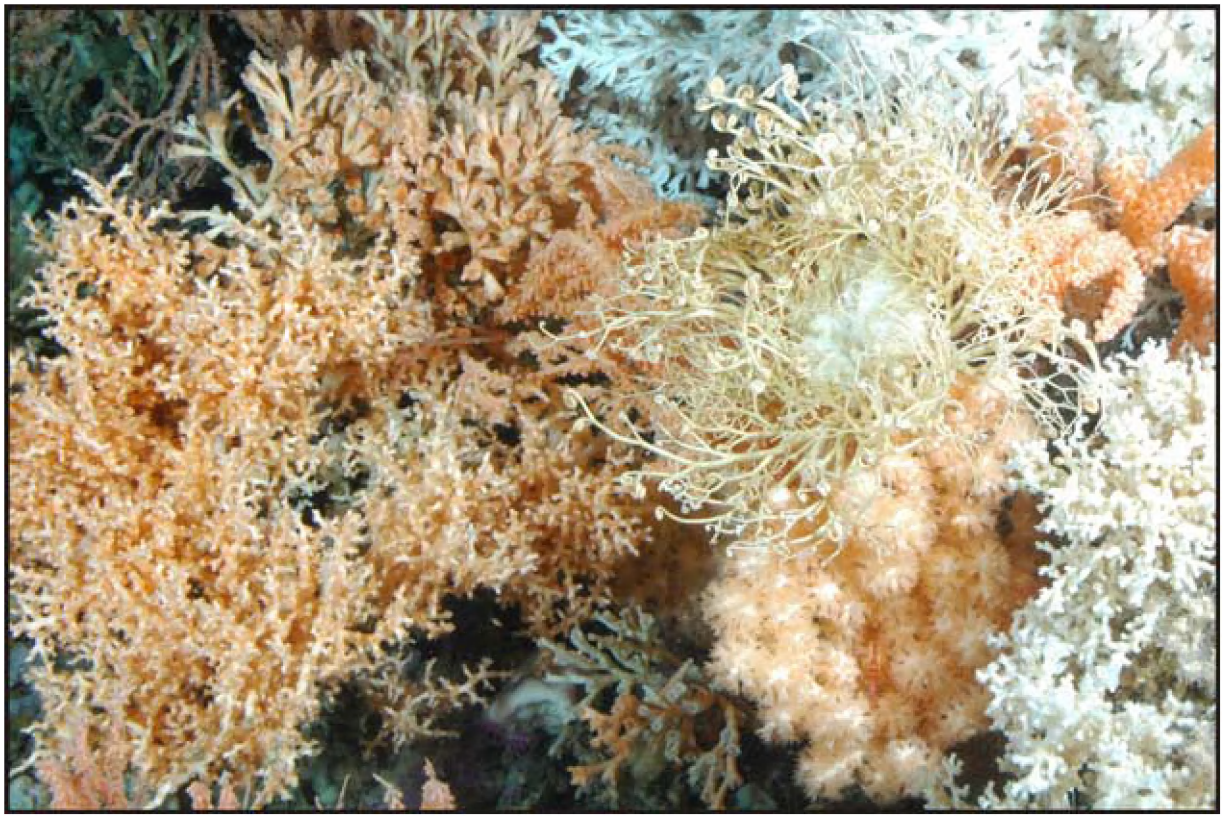

Fig. 1.2 *A detail of the biodiversity in Røst reef, a pristine cold-water coral reef off Norway (Picture taken by the JAGO-team, IFM-GEOMAR, Kiel).*

the second most reported species (Fig. 1.1) (e.g. Freiwald *et al.,* 2004; Le Danois, 1948; Rogers, 1999; Zibrowius, 1980). *Lophelia* forms strong, bush-like colonies measuring several meters across whereas the branched colonies of *Madrepora* are generally much more fragile, limiting its framework-building capacity (Freiwald *et al.,* 2004). Other important cold-water corals in the NE Atlantic deep waters are *Desmophyllum* spp. and *Dendrophyllia* spp. (Foubert and Henriet, 2009; Le Danois, 1948; Zibrowius, 1980).

1.1.1 Cold-water coral distribution

Nowadays, our view on the global distribution of cold-water corals (Fig. 1.3) still remains incomplete and is skewed by the geographically varying levels of research activity, exploration of human resources (oil and gas), fishing activities,... The highest occurrence of framework-building corals dominated by *Lophelia* and *Madrepora* is observed along the NE Atlantic margin (Fig. 1.3): off Norway (Fossa *et al.,* 2005; Fossa *et al.,* 2002; Freiwald *et al.,* 1997; Freiwald *et al.,* 1999; Hovland *et al.,* 2005; Lindberg *et al.,* 2007; Mortensen *et al.,* 2001), in the Rockall Trough and on the Rockall Bank (Akhmetzhanov *et al.,* 2003; de Haas *et al.,* 2009; Kenyon *et al.,* 2003; Masson *et al.,* 2003; van Weering *et al.,* 2003b; Wienberg *et al.,* 2008), on Hatton Bank (Roberts *et al.,* 2008) in the Sea of Hebrides (Davies *et al.,* 2009; Roberts *et al.,* 2005), in the Porcupine Seabight and on the Porcupine Bank (De Mol *et al.,* 2007; De Mol *et al.,* 2002; Dorschel *et al.,* 2009; Eisele *et al.,* 2008; Foubert *et al.,* 2005; Huvenne *et al.,* 2005; Huvenne *et al.,* 2007; Rüggeberg *et al.,* 2005), in the Bay of Biscay (De Mol *et al.,* 2010; Reveillaud *et al.,* 2008), on Galicia Bank (Duineveld *et al.,* 2004), in the Gulf of Cadiz (Foubert *et al.,* 2008; Wienberg *et al.,* 2009) and off Mauritania (Colman *et al.,* 2005). *Lophelia* reefs have also been discovered in the Mediterranean Sea (Freiwald *et al.,* 2009; Taviani *et al.,* 2009; Taviani *et al.,* 2005; Zibrowius, 1980), off Angola (Le Guilloux *et al.,* 2009), in the Gulf of Mexico (Becker *et al.,* 2009; Cordes *et al.,* 2008; Schroeder, 2002; Schroeder, 2007), off the Southeastern USA (Grasmueck *et al.,* 2006; Paull *et al.,* 2000), off Canada (Butler, 2005), off Brazil (Sumida *et al.,* 2004) and in the Indian and Pacific Ocean (Etnoyer and Morgan, 2005; Matsumoto, 2005).

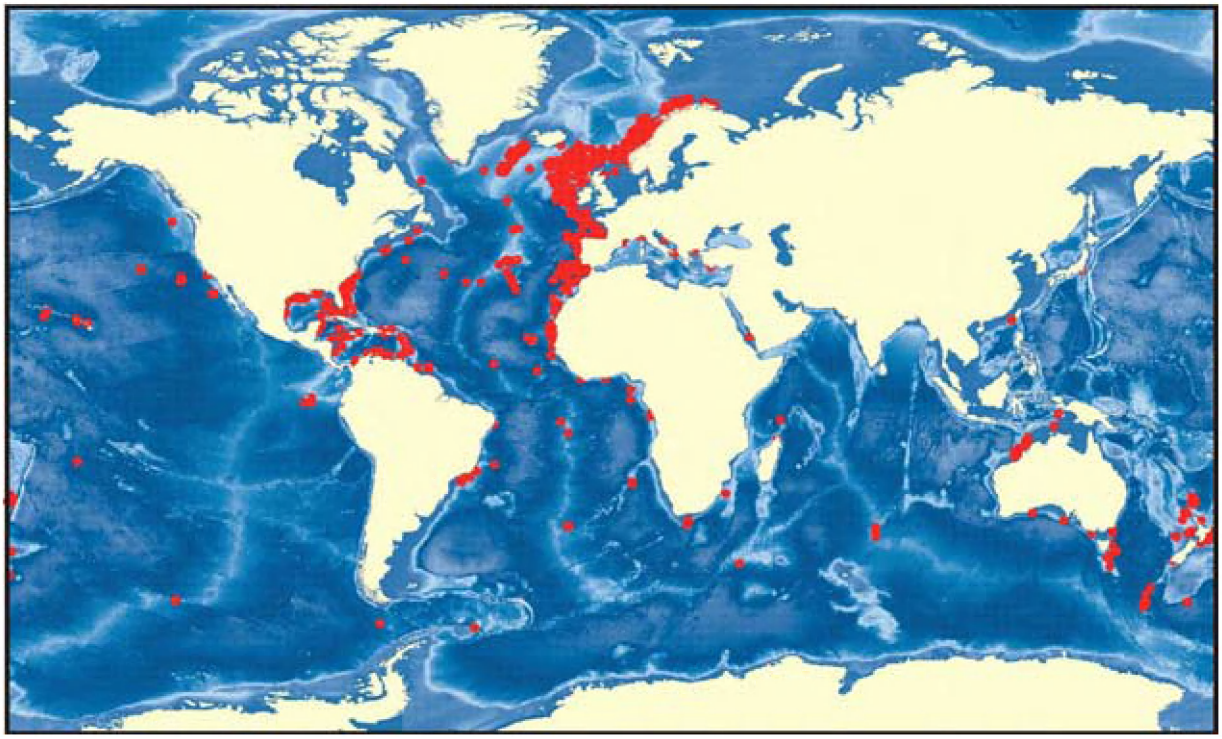

Fig. 1.3 *Map showing the current distribution of reef–forming cold-water corals (Freiwald et al., 2004; Roberts et al., 2006). High concentrations are observed on the shelves and continental slopes.*

The earliest Scleractinian corals appeared during the Middle Triassic and were of little importance for reef framework construction (Flügel, 2002). During the Cretaceous, the first deep-water thickets and mounds of azooxanthellate corals show up (primarily *Dendrophylliidae* and *Oculinidae*). The majority of the modern cold-water coral reef framework builders appeared during the Cretaceous (e.g. *Oculina*, *Petrophyllia*, *Madrepora*) and by the Early Cenozoic (e.g. *Lophelia*, *Dendrophyllia*, *Enallopsammia*, *Goniocorella*) at the latest (Roberts *et al.,* 2009). The first occurrence of the genus *Lophelia*, which is currently the dominant framework building cold-water coral, is not well constrained in the rock record. To date, the most reliable early occurrence of *Lophelia* derives from the Late Miocene, however, early Palaeocene *Lophelia* fossils have been reported which are badly preserved and therefore have to be treated with some caution (Roberts *et al.,* 2009). *Lophelia* records remain rare until the Plio-Pleistocene when *Lophelia pertusa* became common in the Mediterranean and Atlantic.

1.1.2 The biology of cold-water corals

The distribution and growth of cold-water corals is steered by the hydrographic conditions, geomorphology of the seabed, combined with environmental parameters such as temperature, salinity and nutrient supply (Freiwald *et al.,* 2004). Cold-water coral larvae preferably settle on hard substrates (such as: rock, shell, hardground, dead coral rubble, ridges…) (Freiwald *et al.,* 2004; Rogers, 1999). Most of the cold-water corals are found on the shelf break and the upper bathyal zones on the continental margins (Rogers, 1999), although they have also been discovered in Norwegian fjords as shallow as 39 m (Freiwald *et al.,* 2004) and on oil and gas platforms in the North Sea (Gass and Roberts, 2006). The deepest occurrence of *Lophelia pertusa* is reported on the New England seamount chain in the North Atlantic, at 3383 m, and off Morocco at 2775 m (Zibrowius, 1980).

The knowledge of the temperature and salinity range in which cold-water corals thrive, is incomplete. *Lophelia pertusa* tolerates temperatures between 4 and 13°C and salinity values from as low as 32‰ (Strømgren, 1971) to at least 38.78‰ (Freiwald *et al.,* 2004; Taviani *et al.,* 2005). In a recent study, Dullo *et al.* (2008) state that living *Lophelia* reefs occur within a density envelope of sigma-theta σ_θ = 27.35 to 27.65 kg m^{-3}, which is determined by the salinity

and temperature at a pressure of 1 atmosphere. Hence, these environmental parameters are of great importance for cold-water coral growth.
Cold-water corals are suspension feeders and capture live plankton and suspended particulate organic material using the polyp tentacles (Freiwald *et al.,* 2004). Therefore, cold-water corals generally occur in areas with a turbulent hydrodynamic regime (Frederiksen *et al.,* 1992; White, 2007). Corals benefit from high current speeds which increase the food supply (Mienis *et al.,* 2009). Moreover, enhanced currents prevent the corals from getting buried by sediments. Cold-water corals most likely feed on a mixed diet of animals and algae whereas a food source consisting of bacteria supported by methane seepage can be excluded (Duineveld *et al.,* 2004). The quality and availability of nutrients and food particles determine the fitness of coral habitats (Freiwald *et al.,* 2004). White *et al.* (2005), Kiriakoulakis *et al.* (2007) and Duineveld *et al.* (2007) highlight the importance of fresh suspended particulate organic matter, which is produced higher on the continental slope.
Little is known about the reproductive biology of the numerous species of deep-water scleractinians (Roberts *et al.,* 2009; Waller, 2005; Waller and Tyler, 2005). Most species have separate sexes (gonochoric) and spawn their gametes in the water column for external fertilization (Waller, 2005). Seasonal phytoplankton blooms may be the cue for *Lophelia* and *Madrepora* to initiate gametogenesis. During blooms, there is a substantial increase in the availability of particulate organic matter, which might support the energetically expensive production of gametes (Waller and Tyler, 2005). The larvae of the cold-water corals appear to have a pelagic stage before settlement (De Mol *et al.,* 2002). Although larvae can be dispersed along the European margin, the gene flow occurring among the subpopulations is likely to be sporadic and *Lophelia* does not form one panmitic population (Le Goff-Vitry and Rogers, 2005). *Lophelia* also reproduces asexually. Through intratenticular budding daughter polyps are formed from parental polyps (Freiwald, 1998).

1.2 Cold-water coral mounds

Cold-water corals are able to build up important geological structures on the seabed. Off Norway, pristine *Lophelia* reef complexes have been mapped with lengths of several kilometers and 2 to 30 m in height (Freiwald, 2002; Mortensen *et al.,* 2001). However, the most spectacular coral build-ups are mounds which reach heights up to 300 meter and represent some of the most impressive bioherms in the world. The mounds occur usually on continental slopes in intermediate water depths. Almost all of these giant mound build-ups are topped with coral reef patches of *Lophelia pertusa* and *Madrepora oculata,* which form low-relief frameworks, approximately 1 m thick (Freiwald *et al.,* 2004). In 2005, Integrated Ocean Drilling Program (IODP) expedition 307 drilled through an entire mound (Challenger Mound, Porcupine Seabight) revealing the occurrence of cold-water corals (mainly *Lophelia pertusa*) throughout the entire mound sequence (IODP 307 Expedition Scientists, 2005; Kano *et al.,* 2007). Hence, the corals are really the engineers for the build-up of these mound structures. The kick-off for the intensive study of cold-water coral mounds along the European margin was given by Hovland *et al.* (1994) who described a set of 'carbonate knolls' on industrial seismic lines in the Porcupine Seabight. During the subsequent two decades, coral mounds, clustered in provinces, were discovered on various sites along the European and northwest African margin.
In the Porcupine Seabight, SW of Ireland, the mounds occur in three well-delineated provinces (Fig. 1.4), featuring distinct morphologies. The Belgica Mounds, situated on the eastern slope of the Porcupine Seabight (550-1030 m mbsl), are outcropping or (partially) buried conical mounds (Fig. 1.4) (De Mol *et al.,* 2002; Van Rooij *et al.,* 2003). Their upslope side is typically partially buried while their seaward side is well-exposed and forms a steep step in the bathymetry (De Mol *et al.,* 2002). In total around 66 mounds are present with heights up to 200 m and diameters over 3.5 km (De Mol *et al.,* 2002; Foubert and Henriet, 2009). The Hovland Mounds, located on the northern slope of the basin (400-1100 m mbsl), have a conical shape and occur as single build-ups or in elongated clusters (Fig. 1.4) (De Mol *et al.,* 2002). Hovland *et al.* (1994) described the occurrence of 31 mounds in this province. The elongated mound clusters have a length up to 5 km and stand 150 m above the surrounding seafloor. The Magellan Mound Province (600-700 m mbsl) flanks the Hovland Mounds to the north (Fig. 1.4). The Magellan Mounds differ considerably from the two other provinces in the Porcupine Seabight (De Mol *et al.,* 2002;

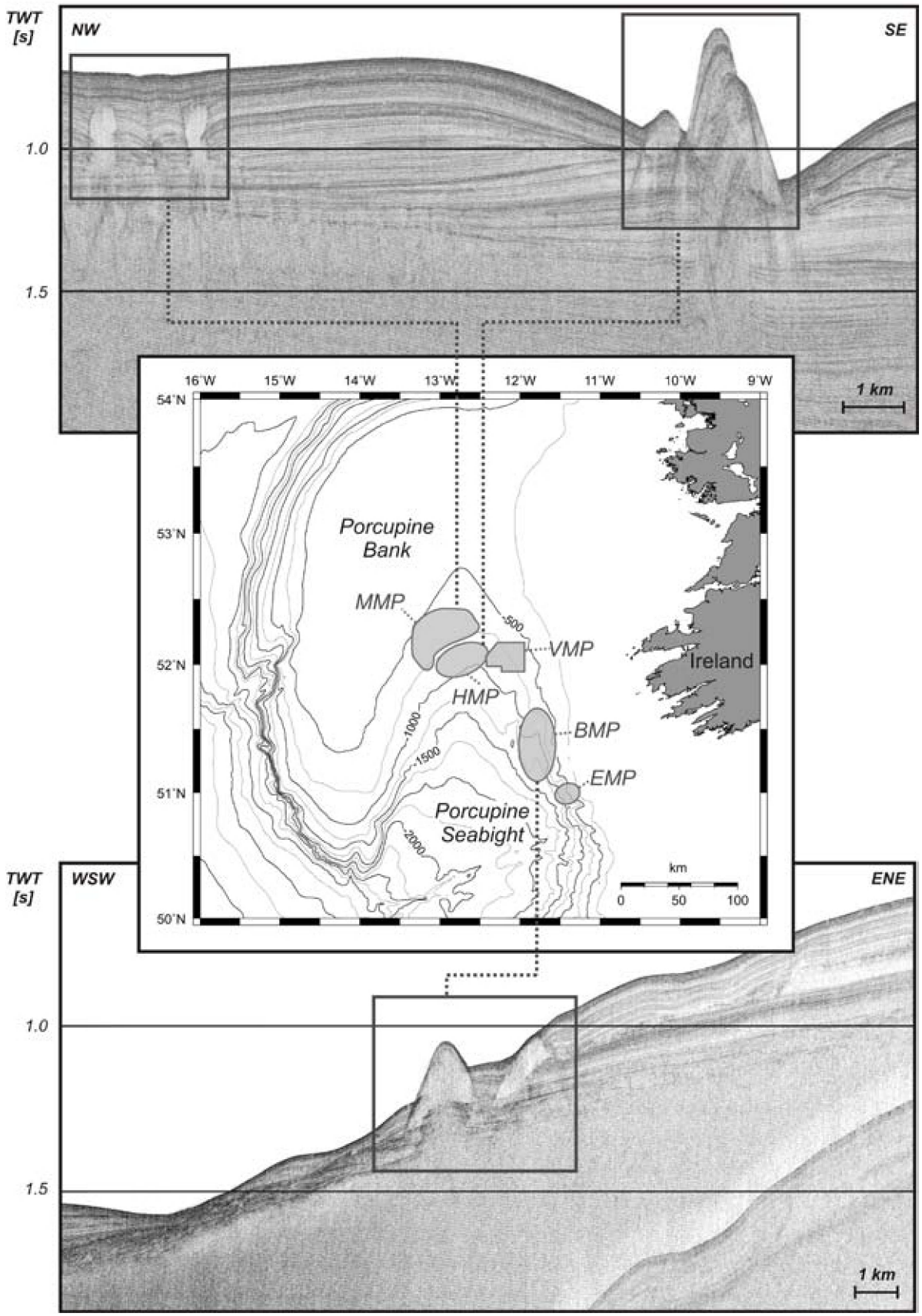

Fig. 1.4 *Location of the different mound provinces in the Porcupine Seabight. MMP: Magellan Mound Province, HMP: Hovland Mound Province, VMP: Viking Mound Province, Province BMP: Belgica Mound Province, EMP: Enya Mound Province. High-resolution seismic profiles of the various mound-types are shown (modified after De Mol (2002) and Van Rooij et al. (2007)).*

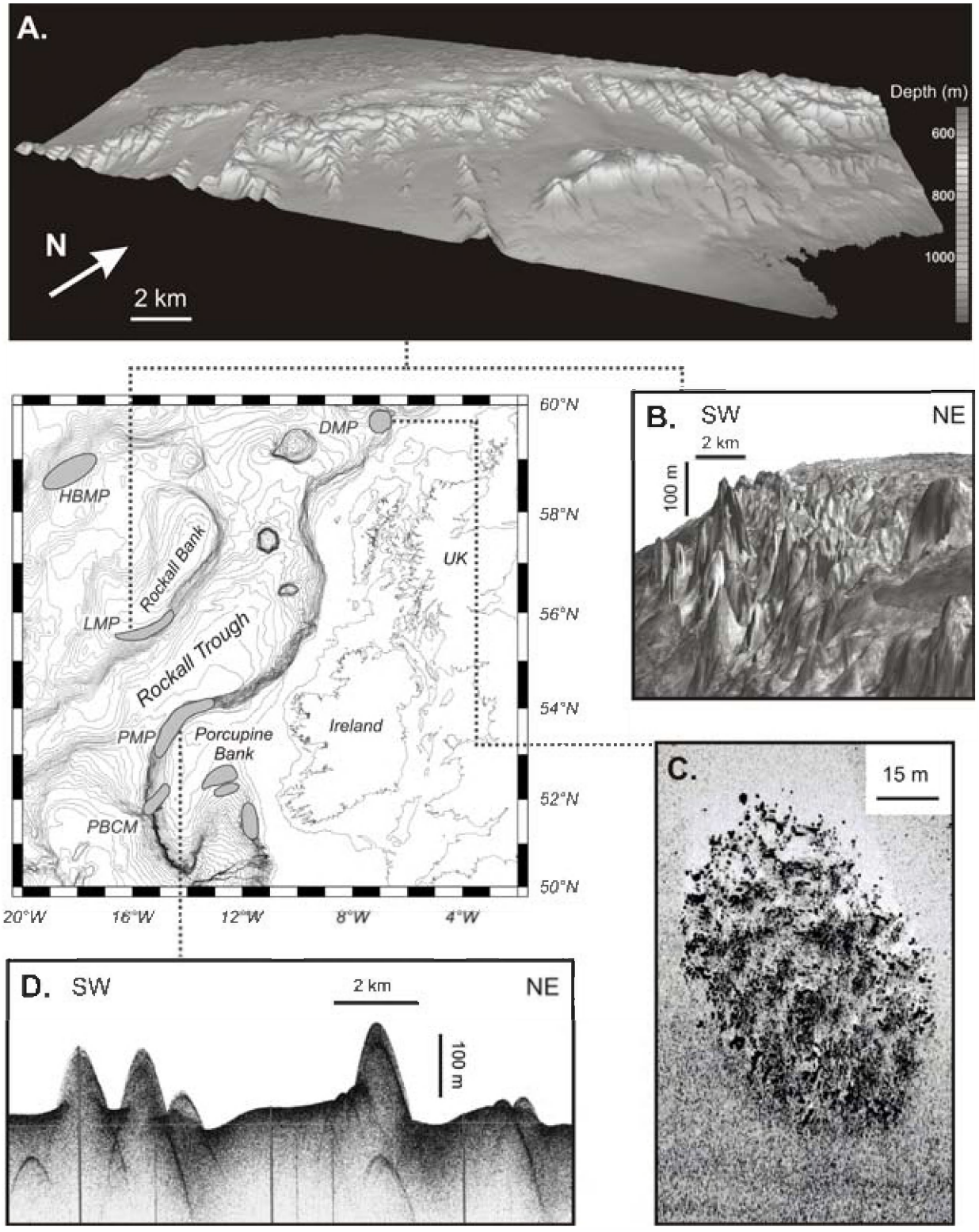

Fig. 1.5 *Location of the different mound provinces in the Rockall Trough. PMP: Pelagia Mound Province, PBCM: Porcupine Bank canyon mounds, LMP: Logachev Mound Province, HBMP: Hatton Bank Mound Province, DMP: Darwin Mound Province. A. Multibeam map (Courtesy of G. Duineveld) of carbonate mounds located at the SW Rockall Trough margin (Mienis et al., 2009). B. 3D image of the TOBI mosaic, projected on top of the bathymetry (SW Rockall Trough) (Mienis et al., 2006). C. Side-scan sonar image of a mound in the Darwin Mound Province (Masson et al., 2003). D. Echosounder profile of cold-water coral mounds in the SE Rockall Trough (O'Reilly et al., 2003).*

Huvenne *et al.,* 2007; Huvenne *et al.,* 2003). They are typically buried, although some do reach the seabed. In total, more than 1000 mounds are expected in this province, with a spatial density of ca. 1 mound/km². The mounds are on average 72 m tall and have widths varying between 25 and 1450 m (Huvenne *et al.,* 2007). Besides the three main mound provinces, two smaller provinces occur: the Enya Mounds (Van Rooij *et al.,* 2008) and the Viking Mounds (De Cock, 2005) (Fig. 1.4).

North of the Porcupine Seabight, in the Rockall Trough, several mound clusters can be identified as well (Fig. 1.5). The Logachev Mounds are located on the southeastern slope of the Rockall Bank (Fig. 1.5) (Akhmetzhanov *et al.,* 2003; Kenyon *et al.,* 2003; van Weering *et al.,* 2003a). They contain a large number of mainly elongated mound clusters up to 380 m high and several kilometers long in a water depth between 600 and 1000 m (Mienis *et al.,* 2006). At the opposing slope of the Rockall Trough, the Pelagia Mounds occur along the northwest flank of the Porcupine Bank in water depths between 600 and 800 m (Fig. 1.5) (Akhmetzhanov *et al.,* 2003; Kenyon *et al.,* 2003; O'Reilly *et al.,* 2003; van Weering *et al.,* 2003a). In contrast to the Logachev Mounds, the Pelagia Mounds are relatively isolated (Kenyon *et al.,* 2003). In the northern Rockall Trough, the Darwin Mounds were discovered (Fig. 1.5) (Huvenne *et al.,* 2009; Masson *et al.,* 2003; Wheeler *et al.,* 2008). It concerns small mounds up to 75 m diameter and 5 m high at a water depth of 1000 m (Masson *et al.,* 2003). West of the Rockall Trough, cold-water coral mounds occur on the southwestern slope of Rockall Bank (Wienberg *et al.,* 2008) and on the flanks of Hatton Bank (Roberts *et al.,* 2008) (Fig. 1.5).
In the Mediterranean Sea, the Melilla Mound Field was discovered in the southeastern margin of the Alboran Sea in a water depth of 250-400 m. Mounds occur as ridge-like build-ups 100-250 m wide, 2-6 km long and up to 100 m high (Comas and Pinheiro, 2007). In the Gulf of Cadiz, coral mounds are situated on escarpments in the close vicinity of mud volcanoes (Foubert *et al.,* 2008; Van Rensbergen *et al.,* 2005; Wienberg *et al.,* 2009). Here, they form build-ups with a height between 30 m and 60 m and a diameter of 250-500 m (Foubert *et al.,* 2008). Further south, coral mounds were mapped off Mauritania (Colman *et al.,* 2005) and along the Angola margin (Le Guilloux *et al.,* 2009). The occurrence of cold-water coral mounds was reported on the West Atlantic margin as well (Grasmueck *et al.,* 2006; Paull *et al.,* 2000).
Numerous hypotheses have been formulated to explain the presence of clusters of coral mounds in certain places and their absence in other ones. A first school hypothesizes that mound development and coral growth is related to hydrocarbon seepage (Henriet *et al.,* 1998; Hovland *et al.,* 1994; Hovland and Risk, 2003). In this view, mounds will form in association with deep-seated faults which act as a conduit for the hydrocarbons (Naeth *et al.,* 2007; Naeth *et al.,* 2005). The expulsion of hydrocarbons will attract microbial communities and nutrients which are beneficial for coral growth or form a lithified carbonate layer which will act as a suitable substrate for coral settlement. Henriet *et al.* (1998) suggested that the destabilization of gas hydrates could be responsible for hydrocarbon seepage and subsequent mound initiation in the Magellan Mound Province. However, the IODP drilling of the entire sequence of Challenger Mound revealed no indications that hydrocarbons play a significant role in mound formation, nor was a lithified hardground discovered at the base of the mound (Ferdelman *et al.,* 2006; Williams *et al.,* 2006). A second school hypothesizes that mound formation and growth is controlled by external factors rather than internal. In this view, mounds will form by a subtle interplay between sedimentation, hydrographic regime, water mass properties, nutrient supply... (De Mol *et al.,* 2005; Dorschel *et al.,* 2005; Foubert *et al.,* 2007; Freiwald, 2002; Rüggeberg *et al.,* 2007; White *et al.,* 2005). At this point, an exogenic steering of mound formation seems most plausible, however, a (partial) endogenic control cannot be excluded.

1.3 Ancient versus recent mound systems

Foubert and Henriet (2009) concluded that the term "cold-water coral carbonate mud mound" is most appropriate for Challenger Mound. However, it remains uncertain to what extent the (sub)-recent cold-water coral mounds along the NE Atlantic margin may be regarded as analogues of the ancient carbonate mud mound systems which occur throughout the geological history. According to Bosence and Bridges (1995)

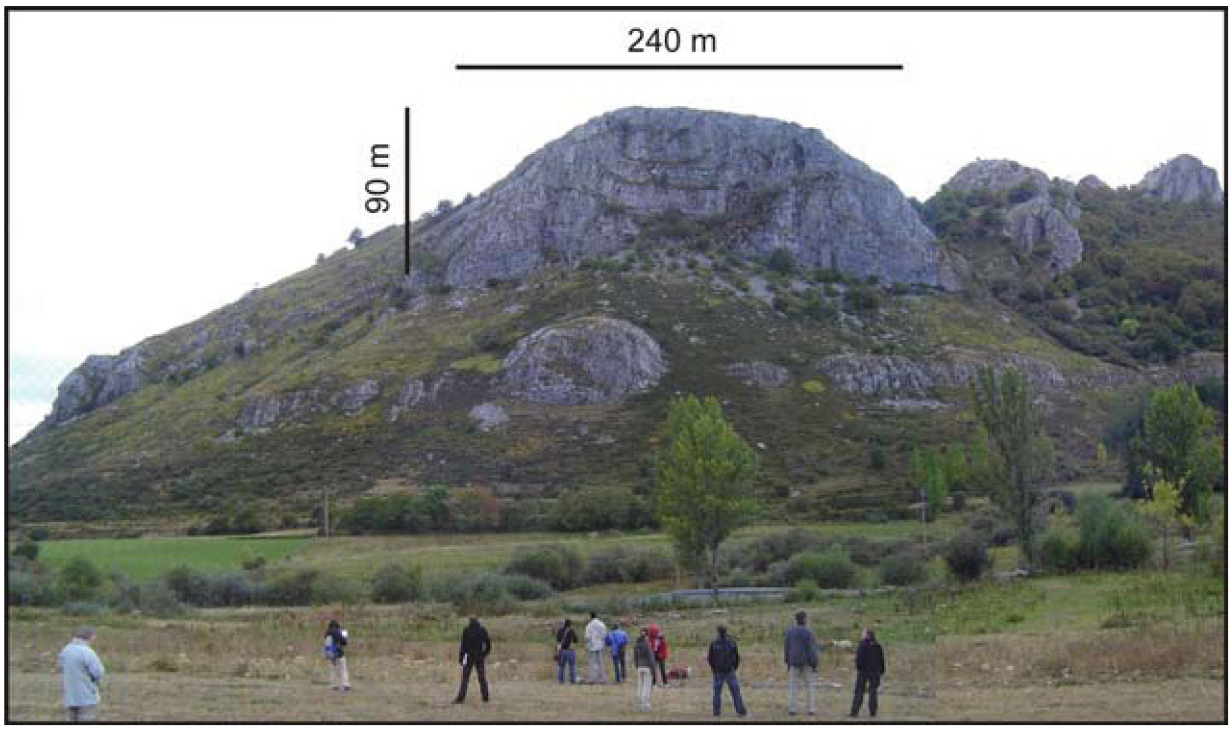

Fig. 1.6 *Late Carboniferous microbial mounds at Puebla de Lillo (Cantabria, Spain). Comparable to the recent cold-water coral mounds, they formed during glacial-interglacial cycles and reveal a cyclic layering of siliciclastic sediments interfering with carbonate deposits (von Allmen, 2006). (Picture by A. Rüggeberg).*

the definition of a carbonate mud mound is a carbonate build-up having depositional relief and being composed dominantly of carbonate mud, peloidal mud or micrite. Hence, not all recent cold-water coral mounds comply with this definition as some mounds are characterized by an important terrigenous component (e.g. Titschack *et al.,* 2009). Within the range of carbonate mud mounds, two major types can be recognized: microbial and biodetrital mud mounds (Bosence and Bridges, 1995).

The dominant texture, microfabric and composition in microbial mud mounds are considered to have a more or less in situ microbial origin (e.g. the Late Carboniferous mounds at Puebla de Lillo (Fig. 1.6)). The construction of mud mounds in the Late Precambrian and Paleozoic was mainly controlled by microbial activity (Bosence and Bridges, 1995). An important event in this regard is the rise of calcified cyanobacteria in the Late Precambrian (Monty, 1995). In the Paleozoic, benthic organisms such as sponges, corals, stromatoporoids and bryozoans play a subordinate role in mound build-up (Bosence and Bridges, 1995). The drilling of a recent cold-water coral mound (Challenger Mound, IODP exp. 307) revealed very low concentrations of methane in the mound sediments and the prokaryote cell counts are below global average (Ferdelman *et al.,* 2006; Webster *et al.,* 2008). Therefore, it is concluded that the microbial precipitation and/or microbial trapping and stabilization of particulate sediment did not play a significant role in the build-up of recent cold-water coral mounds. In this respect, the recent cold-water coral mounds are fundamentally different from the microbial mud mounds.

The (sub)-recent cold-water coral mounds reveal more similarities with the bio-detrital mud mounds in which the dominant composition is broken and transported skeletal debris (Bosence and Bridges, 1995). However, an important nuancing is that the dense skeletal framework on the cold-water coral mounds not only results in an accumulation of biogenic fragments but also actively traps particulate sediment which is transported onto the mound by currents or which is settling (Mienis *et al.,* 2009). Since the Mesozoic, a decline in the abundance and diversity of microbial mounds is recorded whereas biodetrital mounds become increasingly important and are dominant mound-type in the Cenozoic (Bosence and Bridges, 1995).

The closest analogue for the recent coral mounds

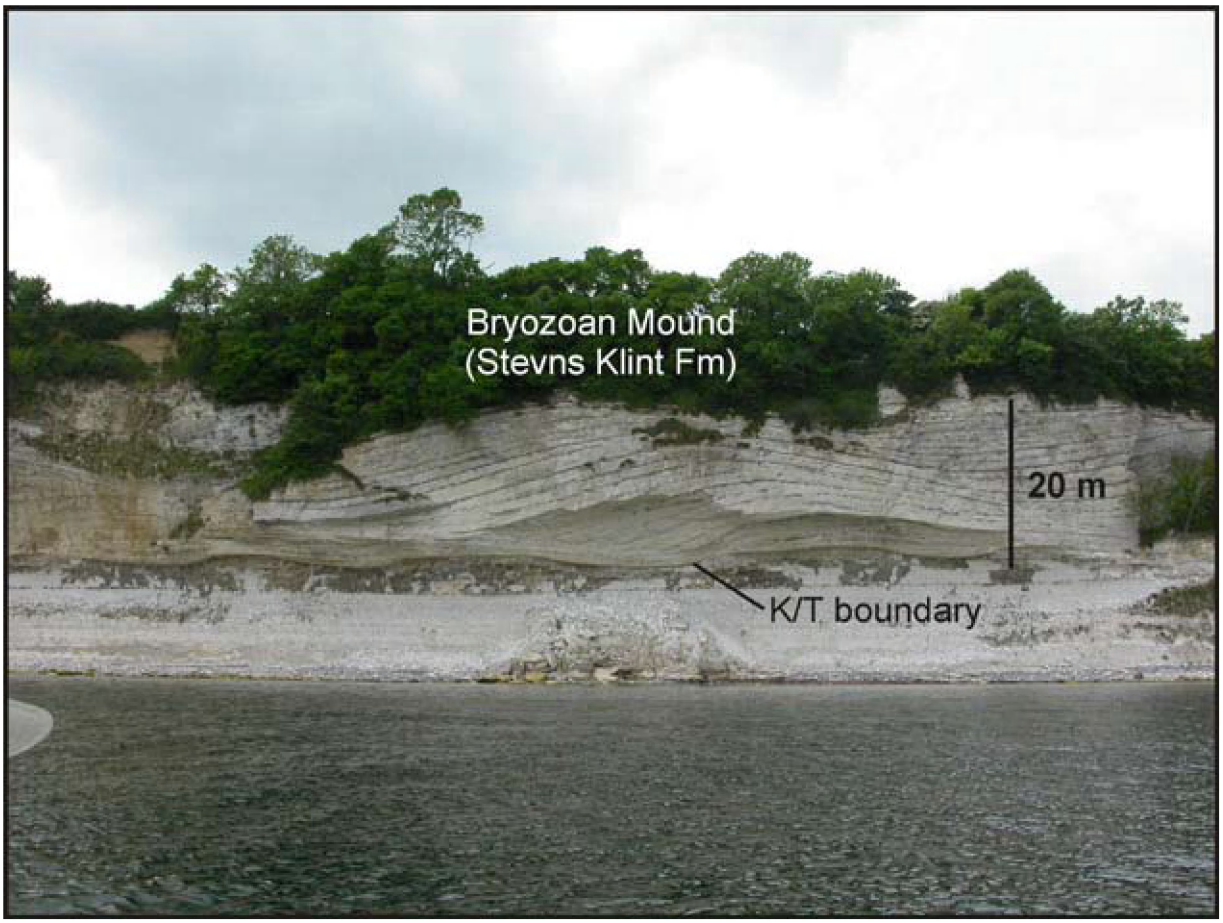

Fig. 1.7 *An example of a Danian Bryozoan mound at Stevns Klint (Denmark). Modified after Surlyk et al. (2006).*

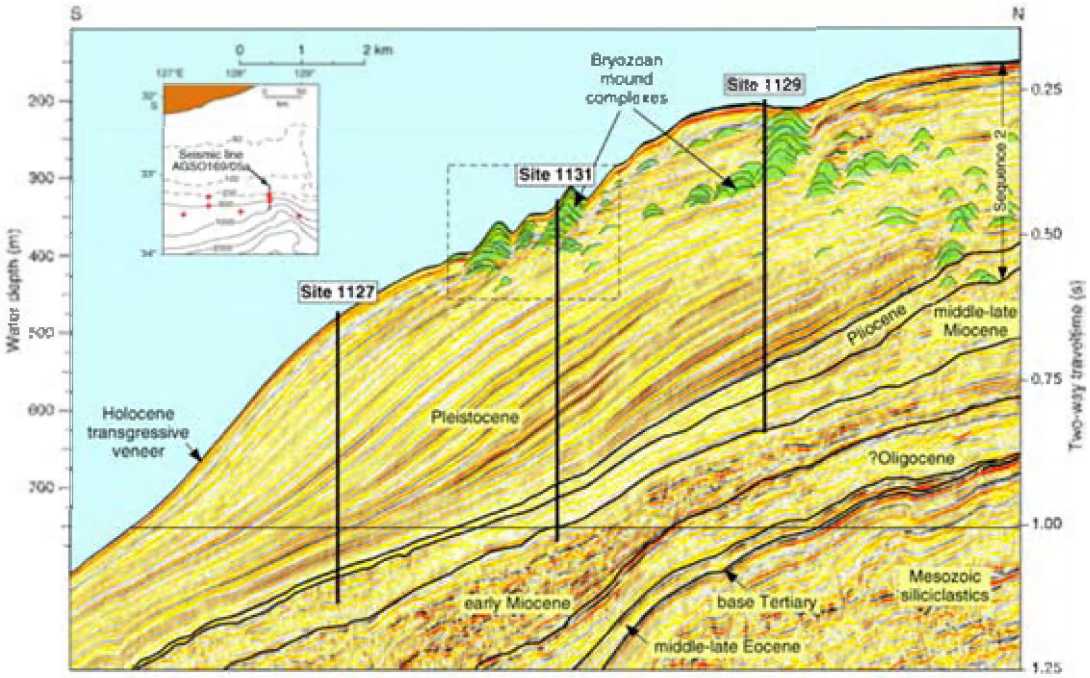

Fig. 1.8 *Seismic reflection image of the eastern drilling transect of ODP leg 182, showing the thick Pleistocene clinoform wedge underlying the modern outermost shelf and upper slope. Bryozoan mounds are visible as individual mounds and as stacked mound complexes immediately below the seafloor seaward of the shelf edge and also buried within the sediment wedge (James et al., 2000).*

may be the bryozoan mounds which occur in the Cenozoic. Danian cool-water bryozoan mounds which formed shortly after the Cretaceous-Tertiary mass extinction have been described in Sweden and Denmark (Fig. 1.7) (Bjerager and Surlyk, 2007a; Bjerager and Surlyk, 2007b; Nielsen *et al.,* 2009; Surlyk, 1997; Surlyk *et al.,* 2006). The mounds formed below the photic zone and comprise a typical cool and relatively deep-water fauna. The benthic fauna was dominated by suspension feeders of mainly delicate branching bryozoans. Comparable to the recent cold-water coral mounds, their formation was strongly influenced by bottom currents and influx of nutrients to the seafloor due to a high production in the surface waters, and an effective transport to the seafloor (Bjerager and Surlyk, 2007a).

During the Ocean Drilling Program Leg 182, bryozoan reef mounds of Pliocene-Pleistocene age were drilled in the Great Australian Bight (Fig. 1.8) (James *et al.,* 2000). The Bryozoan mounds in the Great Australian mounds have a paleorelief up to 65 m and along-slope extents of 2 km. The latter mounds grew periodically during glacial lowstands in upper slope environments as a result of increased nutrient supply and enhanced primary production in combination with beneficial current conditions. In analogy to the recent cold-water coral mounds, mound build-up was primarily attributed to the presence of in-place Bryozoans (James *et al.,* 2004).

1.4 Scope and rationale of this study

The present study builds upon several generations of PhD theses and international peer reviewed papers, conducted on cold-water coral mounds over the last two decades. The latter theses provided a broad overview of cold-water coral mound distribution, morphology, habitat mapping and contemporary constraints on mound build-up. The present thesis will zoom in on the matrix of cold-water coral mounds and more specifically on two distinct niches which remained largely unexplored until now: (1) the terrigenous fraction in a cold-water coral mound as recorder of paleo-environmental conditions and (2) cold-water coral mounds as natural laboratory to study early-diagenetic processes in cool-water carbonate bodies. These two niches do not stand alone and the interactions between the terrigenous fraction and early-diagenetic processes will be discussed in more detail in this work. A multidisciplinary approach was applied to tackle these subjects. The various methods used in this study are described in chapter 2.

(1) IODP expedition 307 revealed that Challenger Mound could possibly provide a unique record of the paleo-environmental conditions at intermediate water depths. Due to the presence of a stabilizing coral framework, a sedimentary sequence was preserved which has been eroded on most parts of the Atlantic continental slope (Foubert and Henriet, 2009). Numerous climatic cycles are expressed in the stable isotopes of foraminifera (Sakai *et al.,* 2009) and the carbonate content of the sediment (Titschack *et al.,* 2009). The present study will focus on the environmental signal which is recorded in the terrigenous fraction of the mound sediments. The terrigenous sediments provide information about the hydrographic and sedimentary processes which control mound growth but also about the continental weathering conditions and thus continental climate. In chapter 3 a research strategy is developed and applied on the terrigenous fraction of the upper section of Challenger Mound in order to elucidate the Late-Quaternary environmental conditions. The results of this study will be used as a stepping stone in chapter 4 to go further back into the sequence of Challenger Mound. The outcome of chapter 4 represents a major progress in the knowledge and understanding of the Early Quaternary climatic conditions on the British-Irish Isles and highlights the potential of the terrigenous material in cold-water mounds as environmental recorder.

(2) When sediments get buried they are affected by a series of biogeochemical processes, fueled by the mineralization of organic matter. These early diagenetic processes will overprint the original sediment sequence and may result in the dissolution of the aragonitic corals and precipitation of other carbonate and sulfur-bearing minerals (Ferdelman *et al.,* 2006; Foubert and Henriet, 2009; Foubert *et al.,* 2007). The precipitation of carbonate minerals is of particular interest as this process might stabilize the mound sediments which is crucial for mound build-up. In addition, the study of these early diagenetic processes helps to better recognize and disentangle the diagenetic features in fossil carbonate mounds. Also, early diagenetic features

might form a template for later diagenetic processes. In Chapter 5 a short introduction on early diagenesis is given and some general concepts are presented. Chapter 6 treats the diagenetic formation of calcite, dolomite and gypsum crystals and the dissolution of aragonitic corals in Perseverance Mound (Magellan Mound Province, Porcupine Seabight). Here, an innovative model is presented to explain the early-diagenetic formation of gypsum and dolomite. In contrast to Perseverance mound, the cold-water coral mounds on Pen Duick Escarpment in the Gulf of Cadiz (Off Morocco) are characterized by the presence of a shallow sulfate-methane transition zone (SMTZ). In chapter 7 the assemblages of authigenic minerals in three mounds, situated on Pen Duick Escarpment are studied. Different diagenetic processes are proposed to explain the specific assemblage of authigenic minerals, observed in each mound.

References

Akhmetzhanov, A.M., Kenyon, N.H., Ivanov, M.K., Wheeler, A.J., Shashkin, P.V. and van Weering, T.C.E., 2003. Giant Carbonate Mounds and Current-Swept Seafloors on the Slope of the Southern Rockall Trough. In: J. Mienert and P.P.E. Weaver (Editors), European margin sediment dynamics: side-scan sonar and seismic images. Springer-Verlag, Heidelberg, pp. 203-209.

Becker, E.L., Cordes, E.E., Macko, S.A. and Fisher, C.R., 2009. Importance of seep primary production to *Lophelia pertusa* and associated fauna in the Gulf of Mexico. Deep-Sea Research Part I-Oceanographic Research Papers, 56(5), 786-800.

Bjerager, M. and Surlyk, F., 2007a. Benthic palaeoecology of Danian deep-shelf bryozoan mounds in the Danish Basin. Palaeogeography Palaeoclimatology Palaeoecology, 250(1-4), 184-215.

Bjerager, M. and Surlyk, F., 2007b. Danian cool-water bryozoan mounds at Stevns Klint, Denmark - A new class of non-cemented skeletal mounds. Journal of Sedimentary Research, 77(7-8), 634-660.

Bosence, D.W.J. and Bridges, P.H., 1995. A review of the origin and evolution of carbonate mud-mounds. In: C.L.V. Monty, D.W.J. Bosence, P.H. Bridges and B.R. Pratt (Editors), Carbonate mud-mounds: Their origin and evolution. Blackwell, Oxford, pp. 3-9.

Butler, M., 2005. Conserving corals in Atlantic Canada: a historical perspective. In: A. Freiwald and J.M. Roberts (Editors), Cold-Water Corals and Ecosystems. Springer-Verlag, Berlin Heidelberg, pp. 1199-1209.

Colman, J.G., Gordon, D.M., Lane, A.P., Forde, M.J. and Fitzpatrick, J.J., 2005. Carbonate mounds off Mauritania, Northwest Africa: status of deep-water corals and implications for management of fishing and oil exploration activities. In: A. Freiwald and J.M. Roberts (Editors), Cold-Water Corals and Ecosystems. Springer-Verlag, Berlin Heidelberg, pp. 417-441.

Comas, M. and Pinheiro, L., 2007. Discovery of carbonate mounds in the Alboran Sea: The Melilla Mound Field, The First MAPG International Convention. MAPG-AAPG, Marrakech, pp. 96-97.

Cordes, E.E., McGinley, M.P., Podowski, E.L., Becker, E.L., Lessard-Pilon, S., Viada, S.T. and Fisher, C.R., 2008. Coral communities of the deep Gulf of Mexico. Deep-Sea Research Part I-Oceanographic Research Papers, 55(6), 777-787.

Davies, A.J., Duineveld, G.C.A., Lavaleye, M.S.S., Bergman, M.J.N., van Haren, H. and Roberts, J.M., 2009. Downwelling and deep-water bottom currents as food supply mechanisms to the cold-water coral *Lophelia pertusa* (Scleractinia) at the Mingulay Reef complex. Limnology and Oceanography, 54(2), 620-629.

De Cock, K., 2005. 3D-seismische studie van koraalbanken aan de oostelijke rand van het Porcupine bekken. MSc Thesis, Ghent University, Ghent, 135 pp.

de Haas, H., Mienis, F., Frank, N., Richter, T.O., Steinacher, R., De Stigter, H., van der Land, C. and Van Weering, T.C.E., 2009. Morphology and sedimentology of (clustered) cold-water coral mounds at the south Rockall Trough margins, NE Atlantic Ocean. Facies, 55, 1-26.

De Mol, B., 2002. Development of coral banks in Porcupine Seabight (SW Ireland): A multidisciplinary approach. Ph.D. thesis Thesis, Ghent University, Gent, 363 pp.

De Mol, B., Henriet, J.-P. and Canals, M., 2005. Development of coral banks in Porcupine Seabight: do they have Mediterranean ancestors? In: A. Freiwald and J. Murray Roberts (Editors), Cold-Water Corals and Ecosystems. Springer-Verlag, Berlin Heidelberg, pp. 515-533.

De Mol, B., Kozachenko, M., Wheeler, A.J., Alvares, H., Henriet, J.-P. and Olu-Le Roy, K., 2007. Thérèse Mound: a case study of coral bank development in the Belgica Mound Province, Porcupine Seabight. International Journal of Earth Sciences, 96, 103-120.

De Mol, B., Van Rensbergen, P., Pillen, S., Van Herreweghe, K., Van Rooij, D., McDonnell, A., Huvenne, V., Ivanov, M., Swennen, R. and Henriet, J.-P., 2002. Large deep-water coral banks in the Porcupine Basin, southwest of Ireland. Marine Geology, 188, 193-231.

De Mol, L., Van Rooij, D., Pirlet, H., Greinert, J., Frank, N., Quemmerais, F. and Henriet, J.P., 2010. Cold-water coral habitats in the Penmarc'h and Guilvinec Canyons (Bay of Biscay): Deep-water versus shallow-water settings Marine Geology, doi:10.1016/j.margeo.2010.04.011.

Dorschel, B., Hebbeln, D., Rüggeberg, A., Dullo, C. and Freiwald, A., 2005. Growth and erosion of a cold-

water coral covered carbonate mound in the Northeast Atlantic during the Late Pleistocene and Holocene. Earth and Planetary Science Letters, 233, 33-44.

Dorschel, B., Wheeler, A.J., Huvenne, V.A.I. and de Haas, H., 2009. Cold-water coral mounds in an erosive environmental setting: TOBI side-scan sonar data and ROV video footage from the northwest Porcupine Bank, NE Atlantic. Marine Geology, 264(3-4), 218-229.

Duineveld, G.C.A., Lavaleye, M.S.S. and Berghuis, E.M., 2004. Particle flux and food supply to a seamount cold-water coral community (Galicia Bank, NW Spain). Marine Ecology Progress Series, 277, 13-23.

Duineveld, G.C.A., Lavaleye, M.S.S., Bergman, M.I.N., De Stigter, H. and Mienis, F., 2007. Trophic structure of a cold-water coral mound community (Rockall Bank, NE Atlantic) in relation to the near-bottom particle supply and current regime. Bulletin of Marine Science, 81(3), 449-467.

Dullo, W.C., Flogel, S. and Rüggeberg, A., 2008. Cold-water coral growth in relation to the hydrography of the Celtic and Nordic European continental margin. Marine Ecology-Progress Series, 371, 165-176.

Eisele, M., Hebbeln, D. and Wienberg, C., 2008. Growth history of a cold-water coral covered carbonate mound - Galway Mound, Porcupine Seabight, NE-Atlantic. Marine Geology, 253(3-4), 160-169.

Etnoyer, P. and Morgan, L.E., 2005. Habitat-forming deep-sea corals in the Northeast Pacific Ocean. In: A. Freiwald and J.M. Roberts (Editors), Cold-Water Corals and Ecosystems. Springer-Verlag, Berlin Heidelberg, pp. 331-343.

Ferdelman, T.G., Kano, A., Williams, T., Henriet, J.P. and Scientists, I.E., 2006. IODP Expedition 307 drills cold-water coral mound along the Irish continental margin. Scientific Drilling, 2, 11-16.

Flügel, E., 2002. Triassic Reef Patterns. In: W. Kiessling, E. Flügel and J. Golonka (Editors), Phanerozoic Reef Patterns. SEPM Special Publication. Society for Sedimentary Geology, pp. 391-463.

Fossa, J.H., Lindberg, B., Christensen, O., Lundalv, T., Svellingen, I., Mortensen, P.B. and Alvsvag, J., 2005. Mapping of *Lophelia* reefs in Norway: experiences and survey methods. In: A. Freiwald and J.M. Roberts (Editors), Cold-Water Corals and Ecosystems. Springer-Verlag, Berlin Heidelberg, pp. 359-391.

Fossa, J.H., Mortensen, P.B. and Furevik, D.M., 2002. The deep-water coral *Lophelia pertusa* in Norwegian waters: distribution and fishery impacts. Hydrobiologia, 471, 1-12.

Foubert, A., Beck, T., Wheeler, A.J., Opderbecke, J., Grehan, A., Klages, M., Thiede, J., Henriet, J.-P. and the Polarstern ARK-XIX/3a shipboard party, 2005. New view of the Belgica Mounds, Porcupine Seabight, NE Atlantic: Preliminary Results from the Polarstern ARK-XIX/3a ROV cruise. In: A. Freiwald and J.M. Roberts (Editors), Deep-water Corals & Ecosystems. Springer-Verlag, Berlin Heidelberg, pp. 403-415.

Foubert, A., Depreiter, D., Beck, T., Maignien, L., Pannemans, B., Frank, N., Blamart, D. and Henriet, J.-P., 2008. Carbonate mounds in a mud volcano province off north-west Morocco: Key to processes and controls. Marine Geology, 248(1-2), 74-96.

Foubert, A. and Henriet, J.P., 2009. Nature and significance of the recent carbonate mound record: the Mound Challenger Code. Springer-Verlag, Heidelberg, 350 pp.

Foubert, A., Van Rooij, D., Blamart, D. and Henriet, J.-P., 2007. X-ray imagery and physical core logging as a proxy of the content sediment cores in cold-water coral mound provinces: a case study from Porcupine Seabight, SW of Ireland. International Journal of Earth Sciences, 96, 141-158.

Frederiksen, R., Jensen, A. and Westerberg, H., 1992. The distribution of the sleractinian coral *Lophelia pertusa* around the Fareo Islands and the relation to internal tidal mixing. Sarsia, 77, 157-171.

Freiwald, A., 1998. Geobiology of *Lophelia pertusa* (scleractinia) reefs in the North Atlantic. Habilitationsschrift Thesis, University Bremen.

Freiwald, A., 2002. Reef-forming cold-water corals. In: G. Wefer *et al.* (Editors), Ocean Margin Systems. Springer, Heidelberg, pp. 365-385.

Freiwald, A., Beuck, L., Rueggeberg, A., Taviani, M. and Hebbeln, D., 2009. The WHITE CORAL COMMUNITY in the Central Mediterranean Sea Revealed by ROV Surveys. Oceanography, 22(1), 58-74.

Freiwald, A., Fossa, J.H., Grehan, A., Koslow, T. and Roberts, J.M., 2004. Cold-water coral reefs. Biodiversity Series. UNEP-WCMC, Cambridge, 84 pp.

Freiwald, A., Henrich, R. and Patzold, J., 1997. Anatomy of a deep-water coral reef mound from

Stjernsund, west Finnmark, northern Norway. Cool-Water Carbonates(56), 141-162.

Freiwald, A., Wilson, J.B. and Henrich, R., 1999. Grounding Pleistocene icebergs shape recent deep-water coral reefs. Sedimentary Geology, 125, 1-8.

Gass, S.E. and Roberts, J.M., 2006. The occurrence of the cold-water coral *Lophelia pertusa* (Scleractinia) on oil and gas platforms in the North Sea: Colony growth, recruitment and environmental controls on distribution. Marine Pollution Bulletin, 52(5), 549-559.

Grasmueck, M., Eberli, G.P., Viggiano, D.A., Correa, T., Rathwell, G. and Luo, J.G., 2006. Autonomous underwater vehicle (AUV) mapping reveals coral mound distribution, morphology, and oceanography in deep water of the Straits of Florida. Geophysical Research Letters, 33(23), doi: 10.1029/2006gl027734.

Henriet, J.-P., De Mol, B., Pillen, S., Vanneste, M., Van Rooij, D., Versteeg, W., Croker, P.F., Shannon, P.M., Unnithan, V., Bouriak, S., Chachkine, P. and The Porcupine-Belgica 97 Shipboard Party, 1998. Gas hydrate crystals may help build reefs. Nature, 391, 648-649.

Hovland, M., Croker, P.F. and Martin, M., 1994. Fault-associated seabed mounds (carbonate knolls?) off western Ireland and north-west Australia. Marine and Petroleum Geology, 11(2), 232-246.

Hovland, M., Ottesen, D., Thorsnes, T., Fossa, J.H. and Bryn, P., 2005. Occurrence and implications of large *Lophelia*-reefs offshore Mid Norway. Onshore-Offshore Relationships on the North Atlantic Margin, 12, 265-270.

Hovland, M. and Risk, M., 2003. Do Norwegian deep-water coral reefs rely on seeping fluids? Marine Geology, 198(1-2), 83-96.

Huvenne, V., Beyer, A., de Haas, H., Dekindt, K., Henriet, J.P., Kozachenko, M., Olu-Le Roy, K., Wheeler, A. and the TOBI/Pelagia 197 and CARACOLE cruise participants, 2005. The seabed appearance of different coral bank provinces in the Porcupine Seabight, NE Atlantic: results from sidescan sonar and ROV seabed mapping. In: A. Freiwald and J.M. Roberts (Editors), Cold-water Corals and Ecosystems. Springer-Verlag, Berlin Heidelberg, pp. 535-569.

Huvenne, V.A.I., Bailey, W.R., Shannon, P.M., Naeth, J., di Primio, R., Henriet, J.-P., Horsfield, B., de Haas, H., Wheeler, A.J. and Olu-Le Roy, K., 2007. The Magellan mound province in the Porcupine Basin. International Journal of Earth Sciences, 96, 85-101.

Huvenne, V.A.I., De Mol, B. and Henriet, J.-P., 2003. A 3D seismic study of the morphology and spatial distribution of buried coral banks in the Porcupine Basin, SW of Ireland. Marine Geology, 198, 5-25.

Huvenne, V.A.I., Masson, D.G. and Wheeler, A.J., 2009. Sediment dynamics of a sandy contourite: the sedimentary context of the Darwin cold-water coral mounds, Northern Rockall Trough. International Journal of Earth Sciences, 98(4), 865-884.

IODP 307 Expedition Scientists, 2005. Modern carbonate mounds: Porcupine drilling, IODP Prel. Rept. doi: 10.2204/iodp.pr.307.2005.

James, N.P., Feary, D.A., Betzler, C., Bone, Y., Holbourn, A.E., Li, Q.Y., Machiyama, H., Simo, J.A.T. and Surlyk, F., 2004. Origin of late pleistocene bryozoan reef mounds; Great Australian Bight. Journal of Sedimentary Research, 74(1), 20-48.

James, N.P., Feary, D.A., Surlyk, F., Simo, J.A.T., Betzler, C., Holbourn, A.E., Li, Q.Y., Matsuda, H., Machiyama, H., Brooks, G.R., Andres, M.S., Hine, A.C., Malone, M.J. and Sci, O.D.P.L., 2000. Quaternary bryozoan reef mounds in cool-water, upper slope environments: Great Australian Bight. Geology, 28(7), 647-650.

Kano, A., Ferdelman, T.G., Williams, T., Henriet, J.P., Ishikawa, T., Kawagoe, N., Takashima, C., Kakizaki, Y., Abe, K., Sakai, S., Browning, E., Li, X. and the IODP Expedition 307 Scientists, 2007. Age constraints on the origin and growth history of a deep-water coral mound in northeast Atlantic drilled during Integrated Ocean Drilling Program Expedition 307. Geology, 35(11), 1051-1054.

Kenyon, N.H., Akhmetzhanov, A.M., Wheeler, A.J., van Weering, T.C.E., de Haas, H. and Ivanov, M.K., 2003. Giant carbonate mud mounds in the southern Rockall Trough. Marine Geology, 195, 5-30.

Kiriakoulakis, K., Freiwald, A., Fisher, E. and Wolff, G.A., 2007. Organic matter quality and supply to deep-water coral/mound systems of the NW European Continental Margin. International Journal of Earth Sciences, 96(1), 159-170.

Le Danois, E., 1948. Les profondeurs de la mer. Payot, Paris, 303 pp.

Le Goff-Vitry, M.C. and Rogers, A.D., 2005. Molecular ecology of *Lophelia pertusa* in the NE Atlantic. In: A. Freiwald and J.M. Roberts (Editors), Cold-Water Corals and Ecosystems. Springer-Verlag, Berlin Heidelberg, pp. 653-662.

Le Guilloux, E., Olu, K., Bourillet, J.F., Savoye, B., Iglesias, S.P. and Sibuet, M., 2009. First observations of deep-sea coral reefs along the Angola margin. Deep-Sea Research Part Ii-Topical Studies in Oceanography, 56(23), 2394-2403.

Lindberg, B., Berndt, C. and Mienert, J., 2007. The Fugloy Reef at 70°N; acoustic signature, geologic, geomorphologic and oceanographic setting. International Journal of Earth Sciences, 96, 201-213.

Masson, D.G., Bett, B.J., Billet, D.S.M., Jacobs, C.L., Wheeler, A.J. and Wynn, R.B., 2003. The origin of deep-water, coral-topped mounds in the northern Rockall Trough, Northeast Atlantic. Marine Geology, 194, 159-180.

Matsumoto, A.K., 2005. Recent observations on the distribution of deep-sea coral communities on the Shiribeshi Seamount, Sea of Japan. In: A. Freiwald and J.M. Roberts (Editors), Cold-Water Corals and Ecosystems. Springer-Verlag, Berlin Heidelberg, pp. 345-356.

Mienis, F., De Stigter, H., De Haas, H. and Van Weering, T.C.E., 2009. Near-bed particle deposition and resuspension in a cold-water coral mound area at the Southwest Rockall Trough margin, NE Atlantic. Deep Sea Research Part I: Oceanographic Research Papers, 56(6), 1026-1038.

Mienis, F., van Weering, T., de Haas, H., de Stigter, H., Huvenne, V. and Wheeler, A., 2006. Carbonate mound development at the SW Rockall Trough margin based on high resolution TOBI and seismic recording. Marine Geology, 233(1-4), 1-19.

Monty, C.L.V., 1995. The rise and nature of carbonate mud-mounds: an introductory actualistic approach. In: C.L.V. Monty, D.W.J. Bosence, P.H. Bridges and B.R. Pratt (Editors), Carbonate mud-mounds: Their origin and evolution. Blackwell, Oxford, pp. 11-48.

Mortensen, P.B., Hovland, M.T., Fossa, J.H. and Furevik, D.M., 2001. Distribution, abundance and size of *Lophelia pertusa* coral reefs in mid-Norway in relation to seabed characteristics. Journal of the Marine Biological Association of the United Kingdom, 81(4), 581-597.

Naeth, J., Di Primio, R., Horsfield, B., Schaefer, R.G. and Krooss, B.M., 2007. On the relationship between hydrocarbon migration pathways and carbonate mound occurence in the Porcupine Basin. International Journal of Earth Sciences, 96, 199-200.

Naeth, J., di Primio, R., Horsfield, B., Schaefer, R.G., Shannon, P.M., Bailey, W.R. and Henriet, J.P., 2005. Hydrocarbon seepage and carbonate mound formation: A basin modelling study from the porcupine basin (offshore Ireland). Journal of Petroleum Geology, 28(2), 147-165.

Nielsen, L., von Brockdorff, A.S., Bjerager, M. and Surlyk, F., 2009. Three-dimensional architecture and development of Danian bryozoan mounds at Limhamn, south-west Sweden, using ground-penetrating radar. Sedimentology, 56(3), 695-708.

O'Reilly, B.M., Readman, P.W., Shannon, P.M. and Jacob, A.W.B., 2003. A model for the development of a carbonate mound population in the Rockall Trough based on deep-towed sidescan sonar data. Marine Geology, 198(1-2), 55-66.

Paull, C.K., Neumann, A.C., Ende, B.A.A., Ussler, W. and Rodriguez, N.M., 2000. Lithoherms on the Florida-Hatteras slope. Marine Geology, 166(1-4), 83-101.

Reveillaud, J., Freiwald, A., Van Rooij, D., Le Guilloux, E., Altuna, A., Foubert, A., Vanreusel, A., Roy, K.O.L. and Henriet, J.P., 2008. The distribution of scleractinian corals in the Bay of Biscay, NE Atlantic. Facies, 54(3), 317-331.

Roberts, J.M., Brown, C.J., Long, D. and Bates, C.R., 2005. Acoustic mapping using a multibeam echosounder reveals cold-water coral reefs and surrounding habitats. Coral Reefs, 24(4), 654-669.

Roberts, J.M., Henry, L.A., Long, D. and Hartley, J.P., 2008. Cold-water coral reef frameworks, megafaunal communities and evidence for coral carbonate mounds on the Hatton Bank, north east Atlantic. Facies, 54(3), 297-316.

Roberts, J.M., Wheeler, A., Freiwald, A. and Cairns, S., 2009. Cold-water corals. The Biology and Geology of Deep-sea Coral Habitats. Cambridge University Press, Cambridge, 334 pp.

Roberts, J.M., Wheeler, A.J. and Freiwald, A., 2006. Reefs of the deep: The biology and geology of cold-water coral ecosystems. Science, 312(5773), 543-547.

Rogers, A.D., 1999. The biology of *Lophelia pertusa* (LINNAEUS 1758) and other deep-water reef-forming corals and impacts from human activities. International Reviews of Hydrobiology, 84(4), 315-406.

Rüggeberg, A., Dorschel, B., Dullo, W.C. and Hebbeln, D., 2005. Sedimentary patterns in the vicinity of a carbonate mound in the Hovland Mound Province, northern Porcupine Seabight. In: A. Freiwald and J.M. Roberts (Editors), Cold-Water Corals and Ecosystems. Springer-Verlag, Berlin Heidelberg, pp. 87-112.

Rüggeberg, A., Dullo, C., Dorschel, B. and Hebbeln, D., 2007. Environmental changes and growth history of a cold-water carbonate mound (Propeller Mound, Porcupine Seabight). International Journal of Earth Sciences, 96, 57-72.

Sakai, S., Kano, A. and Abe, K., 2009. Origin, glacial-interglacial responses, and controlling factors of a cold-water coral mound in NE Atlantic. Paleoceanography, 24, doi:10.1029/2008pa001695.

Schroeder, W.W., 2002. Observations of *Lophelia pertusa* and the surficial geology at a deep-water site in the northeastern Gulf of Mexico. Hydrobiologia, 471, 29-33.

Schroeder, W.W., 2007. Seabed characteristics and *Lophelia pertusa* distribution patterns at sites in the northern and eastern Gulf of Mexico. Conservation and Adaptive Management of Seamount and Deep-Sea Coral Ecosystems, 315-323.

Stanley, J., G.D., 2001. Introduction of Reef Ecosystems and Their Evolution. In: J. Stanley, G.D. (Editor), The History and Sedimentology of Ancient Reef Systems. Kluwer Academic/Plenum Publishers, New York, pp. 1-40.

Strømgren, T., 1971. Vertical and horizontal distribution of *Lophelia pertusa* (Linné) in Trondheimsfjorden on the West Coast of Norway. Det Kongelige Norske Videnskabers Selskabs Skrifter, 6, 1-9.

Sumida, P.Y.G., Yoshinaga, M.Y., Madureira, L.A.S.P. and Hovland, M., 2004. Seabed pockmarks associated with deepwater corals off SE Brazilian continental slope, Santos Basin. Marine Geology, 207(1-4), 159-167.

Surlyk, F., 1997. A cool-water carbonate ramp with bryozoan mounds: Late Cretaceous-Danian of the Danish basin. In: N.P. James and J.A.D. Clarke (Editors), Cool-Water Carbonates. Society for Sedimentary Geology, Tulsa, Oklahoma, pp. 293-307.

Surlyk, F., Damholt, T. and Bjerager, M., 2006. Stevns Klint, Denmark: Uppermost Maastrichtian chalk, Cretaceous-Tertiary boundary, and lower Danian bryozoan mound complex. Bulletin of the Geological Society of Denmark, 54, 1-46.

Taviani, M., Angeletti, L., Dimech, M., Mifsud, C., Freiwald, A., Harasewych, M.G. and Oliverio, M., 2009. Coralliophilinae (Gastropoda: Muricidae) associated with deep-water coral banks in the Mediterranean. Nautilus, 123(3), 106-112.

Taviani, M., Remia, A., Corselli, C., Freiwald, A., Malinverno, E., Mastrototaro, F., Savini, A. and Tursi, A., 2005. First geo-marine survey of living cold-water *Lophelia* reefs in the Ionian Sea (Mediterranean basin). Facies, 50(3-4), 409-417.

Titschack, J., Thierens, M., Dorschel, B., Schulbert, C., Freiwald, A., Kano, A., Takashima, C., Kawagoe, N., Li, X. and Scientists, I.E., 2009. Carbonate budget of a cold-water coral mound (Challenger Mound, IODP Exp. 307). Marine Geology, 259(1-4), 36-46.

Van Rensbergen, P., Depreiter, D., Pannemans, B., Moerkerke, G., Van Rooij, D., Marsset, B., Akhmanov, G., Blinova, V., Ivanov, M.K., Rachidi, M., Magalhaes, V., Pinheiro, L. and Henriet, J.-P., 2005. The El Arraiche mud volcano field at the Moroccan Atlantic slope, Gulf of Cadiz. Marine Geology, 219, 1-17.

Van Rooij, D., Blamart, D., Kozachenko, M. and Henriet, J.-P., 2007. Small mounded contourite drifts associated with deep-water coral banks, Porcupine Seabight, NE Atlantic Ocean. In: A.R. Viana and M. Rebesco (Editors), Economic and Palaeoceanographic Importance of Contourite Deposits. Special Publication. Geological Society, London, pp. 225-244.

Van Rooij, D., De Mol, B., Huvenne, V., Ivanov, M.K. and Henriet, J.-P., 2003. Seismic evidence of current-controlled sedimentation in the Belgica mound province, upper Porcupine slope, southwest of Ireland. Marine Geology, 195(1-4), 31-53.

Van Rooij, D., Huvenne, V.A.I., Blamart, D., Henriet, J.P., Wheeler, A. and de Haas, H., 2008. The Enya mounds: a lost mound-drift competition. International Journal of Earth Sciences, doi: 10.1007/s00531-007-0293-9.

van Weering, T.C.E., de Haas, H., Akhmetzhanov, A.M. and Kenyon, N.H., 2003a. Giant Carbonate Mounds along the Porcupine and SW Rockall Trough Margins. In: J. Mienert and P.P.E. Weaver (Editors), European margin sediment dynamics: side-scan sonar and seismic images. Springer-Verlag, Heidelberg, pp. 211-216.

van Weering, T.C.E., de Haas, H., de Stigter, H.C., Lykke-Andersen, H. and Kouvaev, I., 2003b. Structure and development of giant carbonate mounds at the SW and SE Rockall Trough margins, NE Atlantic Ocean. Marine Geology, 198, 67-81.

Von Allmen, 2006. Composition, growth dynamics and controlling factors of Carboniferous carbonate build-ups in the Puebla de Lillo area. PhD thesis, University of Fribourg, Switzerland, 166 pp.

Waller, R.G., 2005. Deep-water Scleractinia (Cnidaria : Anthozoa): current knowledge of reproductive processes. In: A. Freiwald and J.M. Roberts (Editors), Cold-Water Corals and Ecosystems. Springer-Verlag, Berlin Heidelberg, pp. 691-700.

Waller, R.G. and Tyler, P.A., 2005. The reproductive biology of two deep-water, reef-building scleractinians from the NE Atlantic Ocean. Coral Reefs, 24(3), 514-522.

Webster, G., Blazejak, A., Cragg, B.A., Schippers, A., Sass, H., Rinna, J., Tang, X., Mathes, F., Ferdelman, T.G., Fry, J.C., Weightman, A.J. and Parkes, R.J., 2008. Subsurface microbiology and biogeochemistry of a deep, cold-water carbonate mound from the Porcupine Seabight (IODP Expedtion 307). Environmental Microbiology, doi: 10.1111/j.1462-2920.2008.01759.x.

Wheeler, A.J., Kozachenko, M., Masson, D.G. and Huvenne, V.A.I., 2008. Influence of benthic sediment transport on cold-water coral bank morphology and growth: the example of the Darwin Mounds, north-east Atlantic. Sedimentology, 55(6), 1875-1887.

White, M., 2007. Benthic dynamics at the carbonate mound regions of the Porcupine Sea Bight continental margin. International Journal of Earth Sciences, 96, 1-9.

White, M., Mohn, C., de Stigter, H. and Mottram, G., 2005. Deep-water coral development as a function of hydrodynamics and surface productivity around the submarine banks of the Rockall Trough, NE Atlantic. In: A. Freiwald and J.M. Roberts (Editors), Cold-Water Corals and Ecosystems. Springer-Verlag, Berlin Heidelberg, pp. 503-514.

Wienberg, C., Beuck, L., Heidkamp, S., Hebbeln, D., Freiwald, A., Pfannkuche, O. and Monteys, X., 2008. Franken Mound: facies and biocoenoses on a newly-discovered “carbonate mound” on the western Rockall Bank, NE Atlantic. Facies, 54(1), 1-24.

Wienberg, C., Hebbeln, D., Fink, H.G., Mienis, F., Dorschel, B., Vertino, A., Correa, M.L. and Freiwald, A., 2009. Scleractinian cold-water corals in the Gulf of Cadiz-First clues about their spatial and temporal distribution. Deep-Sea Research Part I-Oceanographic Research Papers, 56(10), 1873-1893.

Williams, T., Kano, A., Ferdelman, T.G., Henriet, J.P., Abe, K., Andres, M.S., Bjerager, M., Browning, E., Cragg, B.A., De Mol, B., Dorschel, B., Foubert, A., Frank, T.D., Fuwa, Y., Gaillot, P., Gharib, J.J., Gregg, J.M., Huvenne, V., Léonide, P., Li, X., Mangelsdorf, K., Tanaka, A., Monteys, X., Novosel, I., Sakai, S., Samarkin, V.A., Sasaki, K., Spivack, A.J., Takashima, C. and Titschak, J., 2006. Cold-Water Coral Mounds Revealed. EOS Transactions, 87(47), 525-526.

Zibrowius, H., 1980. Les Scléractiniens de la Méditerranée et de l’Atlantique nord-oriental. Bulletin de l’Institut Océanographique de Monaco 11, 1-284.

Chapter 2 - Methodology

2.1 Geophysical Core Logging

Geophysical core logging comes upfront in the core analysis sequence and was usually carried out on board the vessel, straight after core recovery. Magnetic Susceptibility (MS), Gamma density and P-wave velocity were analyzed with a GEOTEK Multi Sensor Core Logger at a resolution of 2 cm (Fig. 2.1) (Foubert *et al.*, 2007; Van Rooij *et al.*, 2001). Magnetic susceptibility was measured using a Bartington loop sensor (Model MS2B). The sediment density was analyzed based on the gamma ray attenuation using a ^{137}Cs source (with energies principally at 0.662 MeV) in combination with a scintillation detector. For the P-wave velocity, P-wave piston transducers were used as a transmitter and receiver.

Magnetic susceptibility is the degree of magnetization of a material in response to an external magnetic field. Changes in MS are due to variations in the concentration and/or the composition of the magnetic minerals and grain-size (e.g. Stoner *et al.*, 1996). Therefore, MS records changes in carbonate productivity and Ice Rafting Events (IRE) which are characterized by the deposition of sandy, magnetite-rich ice-rafted debris (Foubert *et al.*, 2007; Richter *et al.*, 2001; Robinson *et al.*, 1995; Thouveny *et al.*, 1994; Thouveny *et al.*, 2000). MS also provides information about diagenetic conditions since the consumption of iron-(oxyhydr)oxides (ferro-

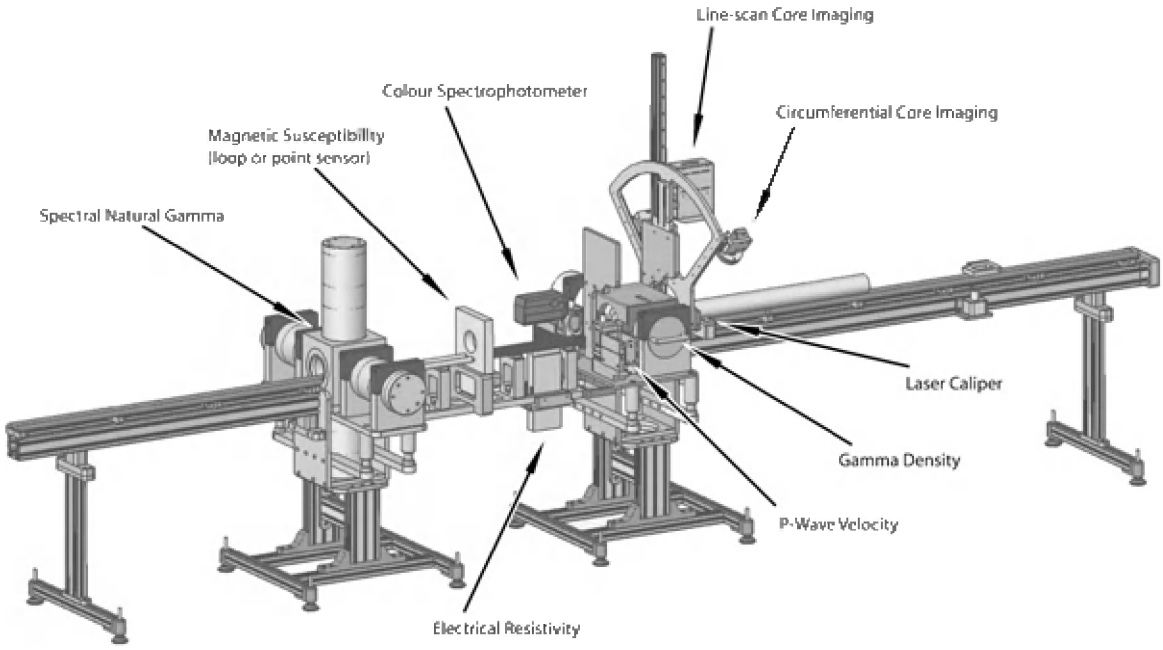

Fig. 2.1 *Schematic diagram of a GEOTEK Multi Sensor Core Logger (suitable for both whole and split lined sediment cores), illustrating the range of sensor systems available (St-Onge et al., 2007).*

magnetic) and the formation of pyrite (paramagnetic) during bacterial sulfate reduction is marked by a significant lowering of the MS signal. The effect of reductive diagenesis on the magnetic properties has already been described by several studies (Bloemendal *et al.*, 1992; Hayashida *et al.*, 2007; Karlin, 1990; Leslie *et al.*, 1990a; Leslie *et al.*, 1990b).
Gamma density is used to estimate the bulk density of sediments and serves as an indicator for porosity and lithological changes. P-wave velocity reflects variations in the lithology, porosity and density of the bulk sediment, state of stress, such as lithostatic pressure, and fabric or degree of fracturing (Foubert and Henriet, 2009). The gamma density and P-wave velocity may be interpreted in terms of diagenetic processes and/or changing oceanographic and paleoclimatic conditions (Foubert *et al.*, 2007).

2.2 Geochemical core logging

The major chemical element composition was analyzed using an AVAATECH XRF core scanner (Fig. 2.2) installed at the Royal Netherlands Institute for Sea Research (Royal NIOZ). X-ray fluorescence is a semi-quantitative non-destructive method which provides high-resolution records of chemical composition on split sediment cores (Jansen *et al.*, 1998; Richter *et al.*, 2006). An X-ray is emitted and ejects an electron from an inner shell of an atom. The resulting vacancy is subsequently filled by an electron falling back from an outer shell, and the energy between both shells is emitted as electromagnetic radiation. The wavelength of the emitted radiation is characteristic for each element and the amplitudes of peaks in the XRF-spectrum are proportional to the concentration of corresponding elements in the analyzed sample (Jenkins and De Vries, 1970).
Prior to scanning the sediment cores, the surface of the sediment is carefully flattened and irregularities from core slicing are removed. Subsequently, the sediment surface is covered with a thin (4 µm) Ultralene film in order to further diminish the surface roughness and prevent contamination of the prism unit during core logging (Richter *et al.*, 2006). Element intensities were recorded in two runs with a resolution of 1 cm. In a first run, element intensities were measured for the elements ranging from Al to Co using a computer controlled forced air cooled Oxford 50 Watt X-ray source operating at a current of 0.15 mA and 10 kV. In a second run, a higher energy was applied to measure the element intensities for the elements with higher atomic numbers ranging from Zn to Zr with the

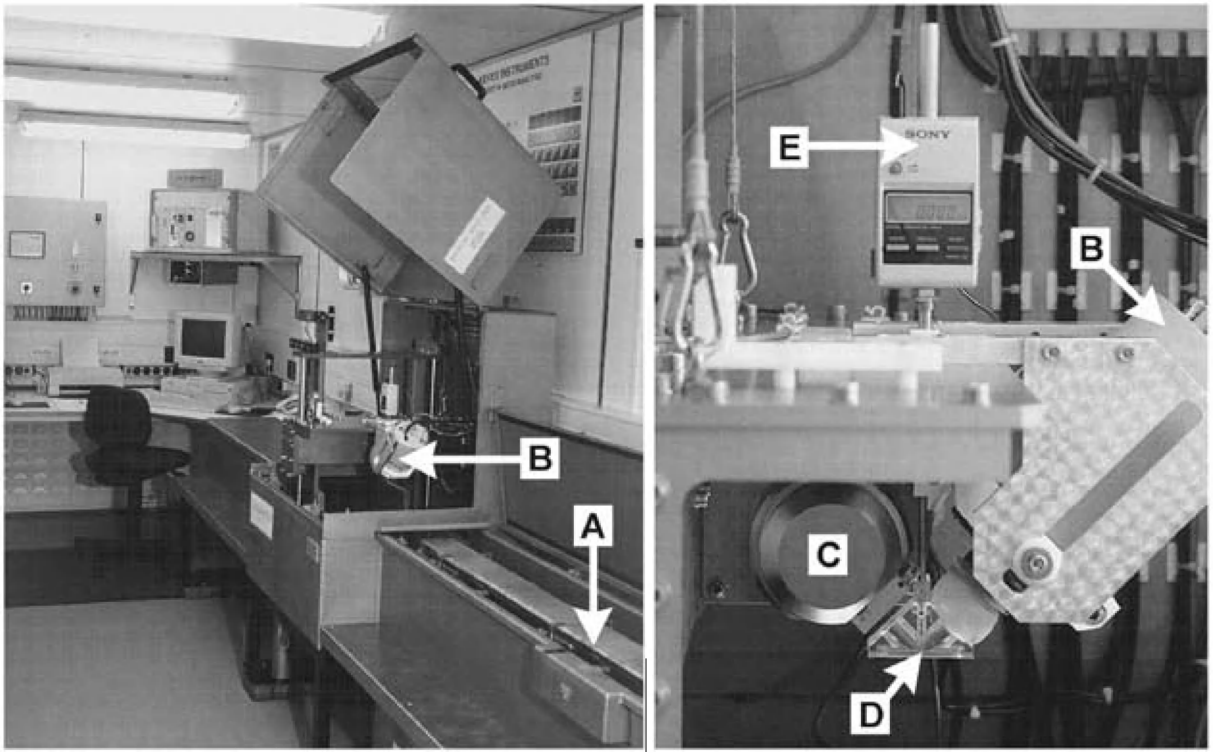

Fig. 2.2 *Picture of an XRF core scanner, modified after Jansen et al. (1998). A. Split-core surface, B. XRF detector, C. X-ray tube, D. Hollow helium-flushed prism, E. Sensor to control the lowering of the prism to the sediment surface.*

X-ray source operating at a current of 0.8 mA and 30 kV. In both runs the count time was 30 seconds (Foubert and Henriet, 2009).
In the domain of paleoceanography, XRF core scanning is used for two main purposes: (1) the study of sedimentation processes and (2) the study of forcing parameters affecting sedimentation (and thus the development of paleoclimatic proxies) (St-Onge *et al.*, 2007). XRF core scanning has been successfully applied on sediment cores from cold-water coral mounds in order to elucidate changes in the biogenic and or terrigenous sedimentation throughout glacial-interglacial cycles (Ca vs Fe/Ti counts) and characterize the coral content (Sr counts) (Eisele *et al.*, 2008; Foubert and Henriet, 2009; Richter *et al.*, 2006). Furthermore, XRF-core scanning has also been used to identify and characterize diagenetic features (e.g. coral dissolution, authigenic mineral formation, lithified carbonate layers,...) in cores from cold-water coral mounds (Foubert and Henriet, 2009; Pirlet *et al.*, 2010; Richter *et al.*, 2006; Van der Land *et al.*, 2010).

2.3 X-ray computed tomography

X-ray computed tomography (CT) investigates the external and internal structure of objects in 3 dimensions, without actually opening or cutting the object (Kak and Slaney, 1988). All transmission CT-devices are based on the same principle: the object is positioned in between and X-ray source and X-ray detector. CT requires a rotational motion of the sample relative to the source-detector system (Fig. 2.3). Digital radiographs of the sample are made from different rotation angles between 0 to 360 degrees. After the data collection, a computer algorithm is used to calculate the slices or cross-sections through the object. The stacking of these 2-dimensional slices results in a three dimensional image (Cnudde *et al.*, 2006).
The physical parameter, providing the structural information, is the (X-ray) attenuation coefficient μ (cm^{-1}). This coefficient is the product of the photon mass attenuation coefficient μ/ρ (cm^2/g) and the chemical density ρ (g/cm^3) of the sample. The attenuation coefficient μ depends on the local composition of the material of the sample and the energy of the X-rays: the higher the energy of the photon, the smaller the attenuation in the sample (for energies below 200 keV, where the photo-electric effect is the pre-dominant process of interaction). X-ray CT is based on the X-ray transmission information and follows the Lambert-Beer equation:

$$I = I_0 * \exp\left(-\int_L \mu(s) \cdot \rho(s) \cdot ds\right)$$

(I_0 = the X-ray intensity before passing through the sample, I = the intensity after passing through the sample and L = the path of the X-ray through

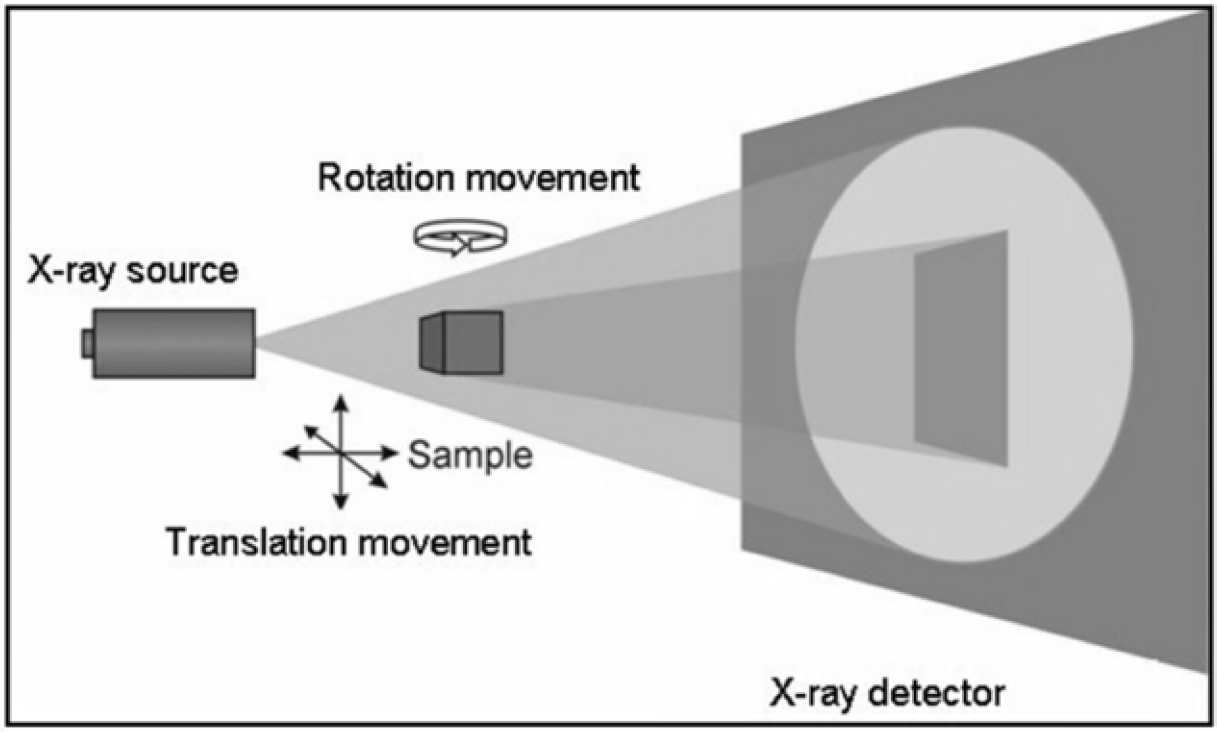

Fig. 2.3 *Schematic illustration of the set-up of an X-ray CT system (courtesy UGCT, University Ghent).*

Fig. 2.4 *The medical CT scanning of a sediment core in the Ghent University Hospital.*

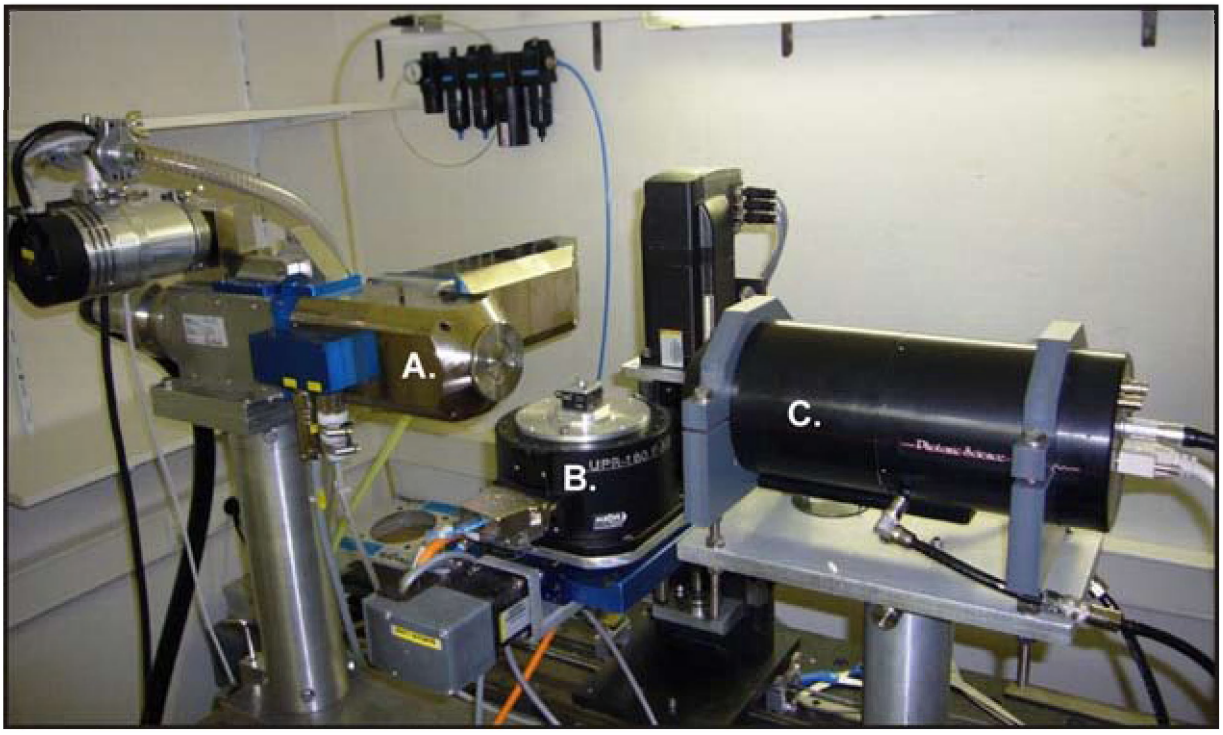

Fig. 2.5 *The set-up for micro-CT scanning at the Centre for X-ray CT at Ghent University, Belgium (UGCT). A. X-ray source, B. Sample on rotational stage, C. Detector.*

the sample (typically a line between the X-ray source and the detector pixel)).
The medical-CT scans were conducted on sediment cores (length: 75 cm, diameter: 10 cm) in the Ghent University Hospital (Fig. 2.4). Medical scanners use a rotating detector-source system that revolves around the object of interest. The cores were scanned with a Siemens medical CT with an X-ray tube operating at 120 kV and an output of 100 mAs. Slices were taken every 3 mm with an overlap of 1 mm. The table feet rotation amounted to 10 mm and the field of view was 150 mm.
Micro-CT scans were carried out at the Centre for X-ray CT at Ghent University, Belgium (UGCT) to study sediment cubes (8 cm^3) in high resolution. The set-up of the micro-CT scanner (Fig. 2.5) is described in detail by Masschaele *et al.* (2007). For this study, the high power directional head was used as X-ray source. The typical current of a micro-focus X-ray tube is 300 µA, which is about 1000 times less than in the medical scanner, resulting in longer scan time and thus higher resolution (Cnudde *et al.*, 2006). The samples were scanned at 130 kV with a thin Cu-filter, to minimize beam hardening effects. 800 projections were taken, each projection averaging 2 frames of 400 ms exposure time. The Varian 2520V Paxscan was used as X-ray detector. This detector consists of 2000 x 1600 pixels, with a pixel size of 127 µm by 127 µm. To enhance image statistics, a pixel averaging of 2 x 2 pixels was used, reducing the resolution.
The micro-CT data were processed with the reconstruction software Octopus which was developed at the UGCT. The raw projection data from the X-ray cameras were filtered by removing bright and dark spots. Subsequently they were normalized and regrouped in sinogram files which are finally used to calculate cross sections (Vlassenbroeck *et al.*, 2007). 3D morphological analysis of the medical and micro-CT scans was performed using Morpho+. This software, developed at the UGCT, is able to segment the volume using advanced tresholding. Furthermore it enables us to label, classify and separate different objects in the volume. VGStudioMax 1.2 from Volume Graphics (64 bit version) was used for 3D volume rendering.
X-ray computed tomography is used in a wide range of geological investigations: interior examination of fossils or meteorites, textural analysis of igneous and metamorphic rocks, geometric description and quantification of porosity and permeability in rocks and soils, the assessment of bulk density of marine sediment, sedimentary structures and any other application demanding three-dimensional data that formerly required physical serial sectioning (e.g. Cnudde *et al.*, 2006; Dierick *et al.*, 2007; Jacobs and Cnudde, 2008; Ketcham and Carlson, 2001; Long *et al.*, 2009; Orsi *et al.*, 1994; Speijer *et al.*, 2008; Van Geet *et al.*, 2001). Specifically for this study, CT scans will be used to describe and quantify the biogenic fragments, the porosity and the diagenetic minerals. Furthermore, CT scans will be used to assess the preservation state of the aragonitic corals.

2.4 Particle-size analysis

Prior to grain-size analysis, the carbonate fraction of the sediment was removed to eliminate biogenic fragments. One cm^3 of bulk sediment was transferred in a glass vial with 200 ml distilled water. Next, 10 ml of 2.7M HCl was added to decarbonate the sample via leaching along with 10 ml 2.9M H_2O_2 to remove the organic matter by oxidation. The water level was brought up to 250 ml using water and subsequently the sample was heated to a temperature between 70° and 90° C for 120 minutes on a hot plate. The temperature was checked regularly using alcohol filled thermometers. When the reaction was completed, the samples usually took on a straw colour. In case of incomplete reaction, extra heating was applied and/or extra H_2O_2/HCl was added. After 120 minutes, the sample was boiled for a period of 1 minute to remove excess H_2O_2. The sample was rinsed 2 or 3 times with distilled water to obtain a neutral pH. Next, the sample was decanted using a standard laboratory suction pump and transferred to sample pot. The samples were stored in a cold room in order to prevent the development of fungal colonies in the sediment.
Before measurement the sediment was treated with 0.05% Calgon (Sodium HexaMetaPhosphate) and sonicated for 10 s to reduce the effect of flocculation. Grain-size distribution measurements of siliciclastic sediments were carried out at the National Oceanography Centre Southampton (NOCS), with a Malvern Mastersizer 2000 with autosampler. The Malvern Mastersizer 2000 is based on the laser diffraction method. This method relies on the fact that particles passing through a laser beam will scatter light at an angle that is directly related to their size. An average measurement precision of 4.4% (on grain-size mode) was estimated for similar sediments by Thierens *et al.* (2010).
Studies of particle size shed light on many facets of deep-sea sediments, especially on depositional conditions. Because deep-sea sediments normally show few structures other than biological

disturbance, grain size parameters have been used as the best indicator of relative flow speed (McCave, 2007). However, in the specific setting of cold-water coral mounds and reefs, special care has to be taken when interpreting grain-size distributions since coral thickets create low-energy environments and baffle the sediment (de Haas *et al.*, 2009; Dorschel *et al.*, 2007; Mienis *et al.*, 2009; Thierens *et al.*, 2010).

2.5 Petrographic and mineralogical analyses

2.5.1 Petrographic microscope and cathodoluminescence (CL)

Standard thin sections were studied at the Department of Earth and Environmental Sciences, K.U. Leuven using conventional transmitted, reflected and UV light microscopy as well as cold cathodoluminescence (CL) microscopy. Cathodoluminescence is an optical and electrical phenomenon whereby a beam of electron is generated by a cathode ray tube and subsequently impacts on thin sections (Fig. 2.6). The impingement of a high energy electron beam onto the minerals will result in the excitation of electrons. Depending on the composition, the purity (extrinsic CL) and defect state (intrinsic CL) of the mineral, this excitation may result in the emission of a photon (light) with a characteristic energy (colour) (Boggs and Krinsley, 2006). The most abundant kind of luminescence centers are activators which emit luminescence whereas quenchers are impurities, suppressing the emission of CL by activator ions (Boggs and Krinsley, 2006). The efficiency of the activators may be enhanced by the presence of sensitizers which have the ability to absorb energy and transmit it to activator ions. The luminescence of the various minerals is recorded by a camera, mounted on the microscope using extended exposure times (around 90 sec). CL petrography was carried out with an in-house adapted (Technosyn) cold cathodoluminescence model 2800, Mark II. Operating conditions were around 10 kV gun potential, 200 mA current, 0.5 Torr vacuum and 5 mm beam width.

In carbonates CL is routinely used to distinguish chemical and crystallographic zonation, define paragenetic sequences, evaluate crystal growth histories and assess recrystallization of bioclasts and dolomites. It is generally accepted that Mn^{2+} and trivalent REE-ions are the most important activators of extrinsic CL in carbonate minerals, while Fe^{2+} is an important quencher of CL (e.g. Marshall, 1988; Richter *et al.*, 2003). Hence, carbonates which precipitated under oxic conditions will be non-luminescent while precipitation in a suboxic environment will result in bright-luminescent carbonates (mobilization of Mn^{2+}). Under reducing conditions, dull-luminescent carbonates will form (mobilization of Mn^{2+} and Fe^{2+}). In general, calcite is yellow-orange luminescent, while dolomites reveal yellow-red colours. Biogenic carbonate fragments will be typically non-luminescent unless they underwent recrystallization.

Besides the study of carbonates, CL can also be applied in siliciclastic petrology. Quartz grains reveal significant changes in CL depending on the origin. Blue, red, yellow and green CL-colours are most common. These are mainly caused by

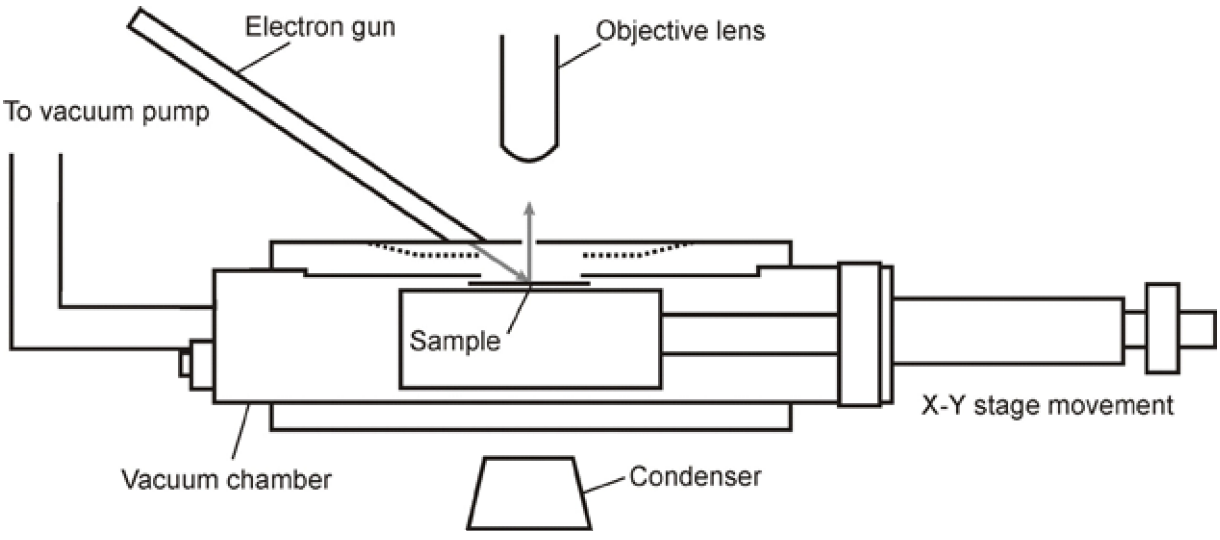

Fig. 2.6 *Schematic cross-section of the Technosyn cathodoluminescence stage. Modified after Barker and Wood (1986).*

structural defects (intrinsic CL) whereas activation of trace elements (e.g. Ti, Fe) plays a minor role (Götze *et al.*, 2001). The most recent general classification of detrital quartz distinguishes the following categories: blue to violet = plutonic quartz as well as high-grade metamorphic quartz and phenocrysts in volcanic rocks; red = matrix quartz in volcanic rocks; brown = quartz from regional metamorphic rocks; non or weakly luminescent = authigenic quartz; short-lived green or blue = hydrothermal and pegmatitic quartz (Götze and Zimmerle, 2000). However, Richter *et al.* (2003) pointed out that great care has to be taken when interpreting the luminescence of quartz grains as luminescence colours might change with increasing irradiation. According to Götte and Richter (2006), this colour shift depends on the defect structure of the quartz grains and may be used in provenance studies.
Blue CL is the most frequently observed colour in feldspars (Boggs and Krinsley, 2006). However, due to the presence of intrinsic and extrinsic defect centers other CL colours occur. (Marshall, 1988) reported that Fe^{3+} activates red CL in orthoclase while anorthite activated by Fe^{2+} has green luminescence and Ti^{4+} activates blue CL in K-feldspar. Authigenic feldspar is usually non-luminescent.

2.5.2 SEM-EDS analysis

The mineralogical composition of thin sections and bulk sediment was also studied in high resolution with a scanning electron microscope (SEM). Bulk sediment was first brought into suspension in distilled water and treated in an ultrasonic bath for 20 s. Subsequently, the solution was filtered and dried. The filters with the bulk sediment and the thin sections were gold-coated and studied with a JEOL 6400 SEM at Ghent University. The SEM is a type of electron microscope that images the sample surface by scanning it with a high-energy electron beam in a raster scan pattern. This method enables to study the sample surface in very high resolution, revealing details about 1 to 5 nm in size. The elemental composition of several points was measured using Energy Dispersive Spectroscopy (EDS).

2.5.3 X-ray diffraction of bulk sediment

The mineralogical composition of bulk sediment was identified and quantified using X-ray diffraction (XRD) at the department of Earth and Environmental Sciences, Geology, K.U. Leuven. First, a representative amount of sediment is dried (around 30 g) before crushing the sample by hand and passing it through a 500 µm sieve. Subsequently, 2.7 g of sample is mixed with 0.3 g ZnO which is added as an internal standard. This mixture is micronized for 5 minutes in a McCrone Micronizing mill using 4 ml of methanol as lubricating agent. The samples are recuperated in porcelain cups and dried under a fume hood (no extra heating is used). The dried samples are gently disaggregated in a mortar and passed through a 250 µm sieve to ensure good mixing of the sample with the internal standard. Around 0.5 g of powder is needed to fill the sample holders. In order to ensure good packing of the grains back loading is used.
X-ray diffraction is based in Bragg's Law ($n\lambda = 2d\sin\theta$). This law connects the wavelength of electromagnetic radiation (λ) to the diffraction angle (θ) and the lattice spacing in a crystalline sample (d). The samples are scanned through a range of 2θ angles and the diffracted X-rays are detected, processed and counted. Conversion of the diffraction peaks to d-spacing allows the identification of minerals present in the powder given that each mineral has its own set of unique d-spacing. X-ray data were collected on a Philips PW1830 diffractometer (Bragg-Bretano geometry) equipped with a CuK radiation source (Generator: 30 mA, 45 kV), graphite monochromator, receiving slit (width: 1 mm), divergence slit (width: 1 mm) and antiscatter slit (width: 0.1 mm). An angular range of 5 to 70° 2θ was measured with a step size of 0.02° and 2 s counting time, each step. For quantitative phase analysis the Rietveld refinement program Topas academic was used.

2.6 Clay mineralogy

2.6.1 Detrital clay in marine sediments

In the sedimentary clays two main groups can be distinguished based on their origin. Authigenic clays are the result of in situ precipitation from a concentrated solution in closed continental or marine sedimentary basins (Fagel, 2007). Hence, authigenic clays provide insight into the geochemical environment. However, authigenesis is a minor process which accounts for less than 10% of clay minerals, although it may be important locally (e.g. around hydrothermal vents) (Velde, 1995). Given that the study site is not located in a closed basin and no evidence was found for the seepage of concentrated solutions, authigenic clay minerals will not be regarded in the present study. A second group of clay minerals results from weathering processes on the continent

and are detrital clays (Fagel, 2007). In marine sediments, clays are mainly detrital (~90% according to Velde (1995)) and their assemblages are the result of differentiation processes during transport and deposition, the mineralogy of the source rock and the continental climate (Fig. 2.7) (Fagel, 2007).

Clay minerals are eroded from soils by rivers, wind or ice and carried into the adjacent marine environment (Fig. 2.7) (Fagel, 2007). Subsequently, different processes exert a control on the transport of sediment from shelves into the deep ocean basins (Fagel, 2007; Wahsner *et al.*, 1999): (1) suspension along different current systems which lead to the dispersion of clay minerals over large distances within the water column; (2) gravitational flows (turbidity currents and debris flows); (3) at high latitudes, iceberg transport and the sinking of suspended clay-rich cold and saline water masses formed on the shelf during ice formation. With increasing distance from the source areas, advection of fine-grained particles by deep-water currents becomes the most important mode of detrital sediment transport to the deep-sea (Biscaye, 1965; Petschick *et al.*, 1996). During transport, detrital clay assemblages may undergo differentiation processes (e.g. selective erosion of the soil

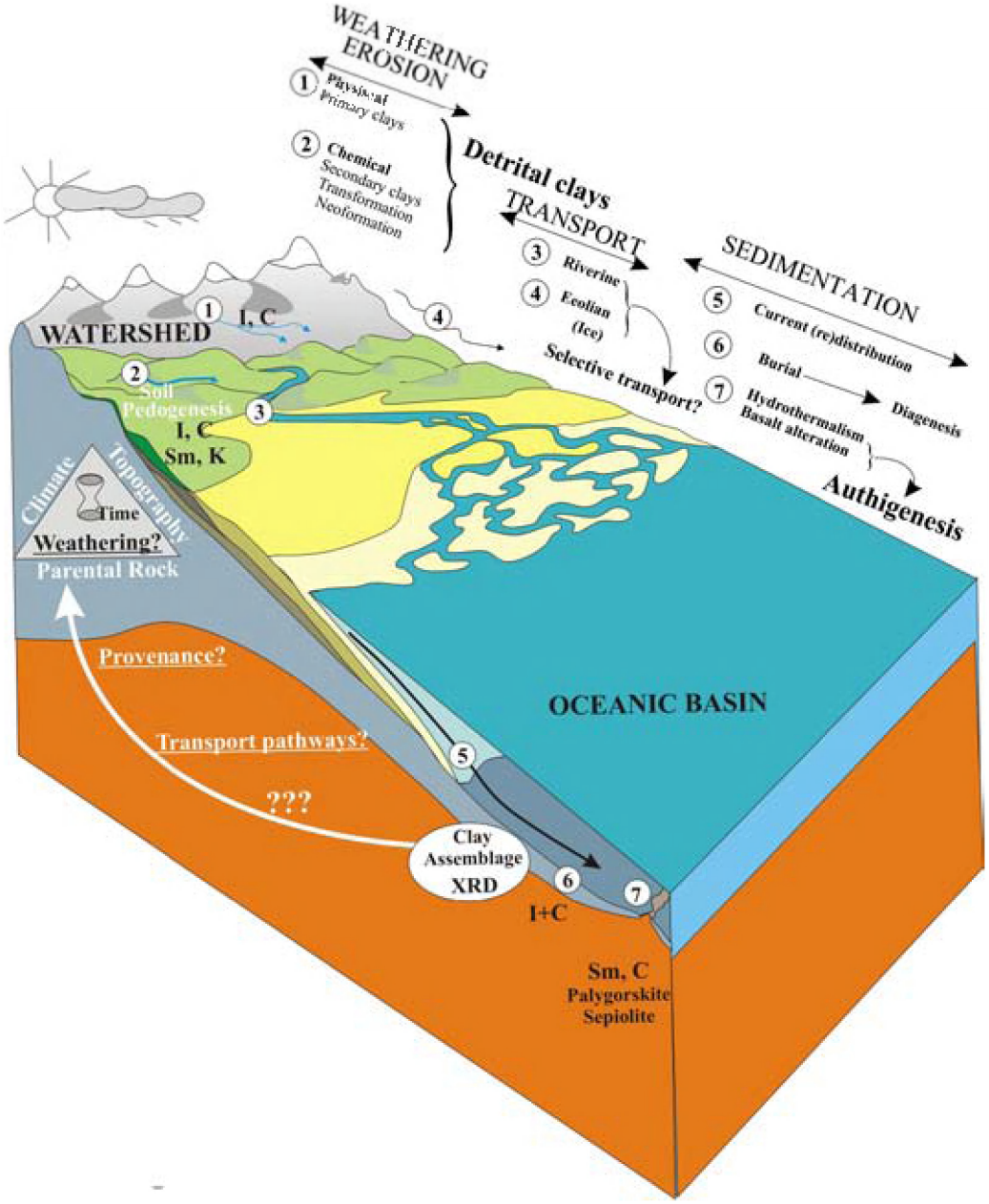

Fig. 2.7 *The "clay toolbox". Primary control on clay assemblage composition of deep-sea sediments. I: Illite, C: Chlorite, Sm: Smectite, K: Kaolinite, XRD: X-ray diffraction technique (Fagel, 2007).*

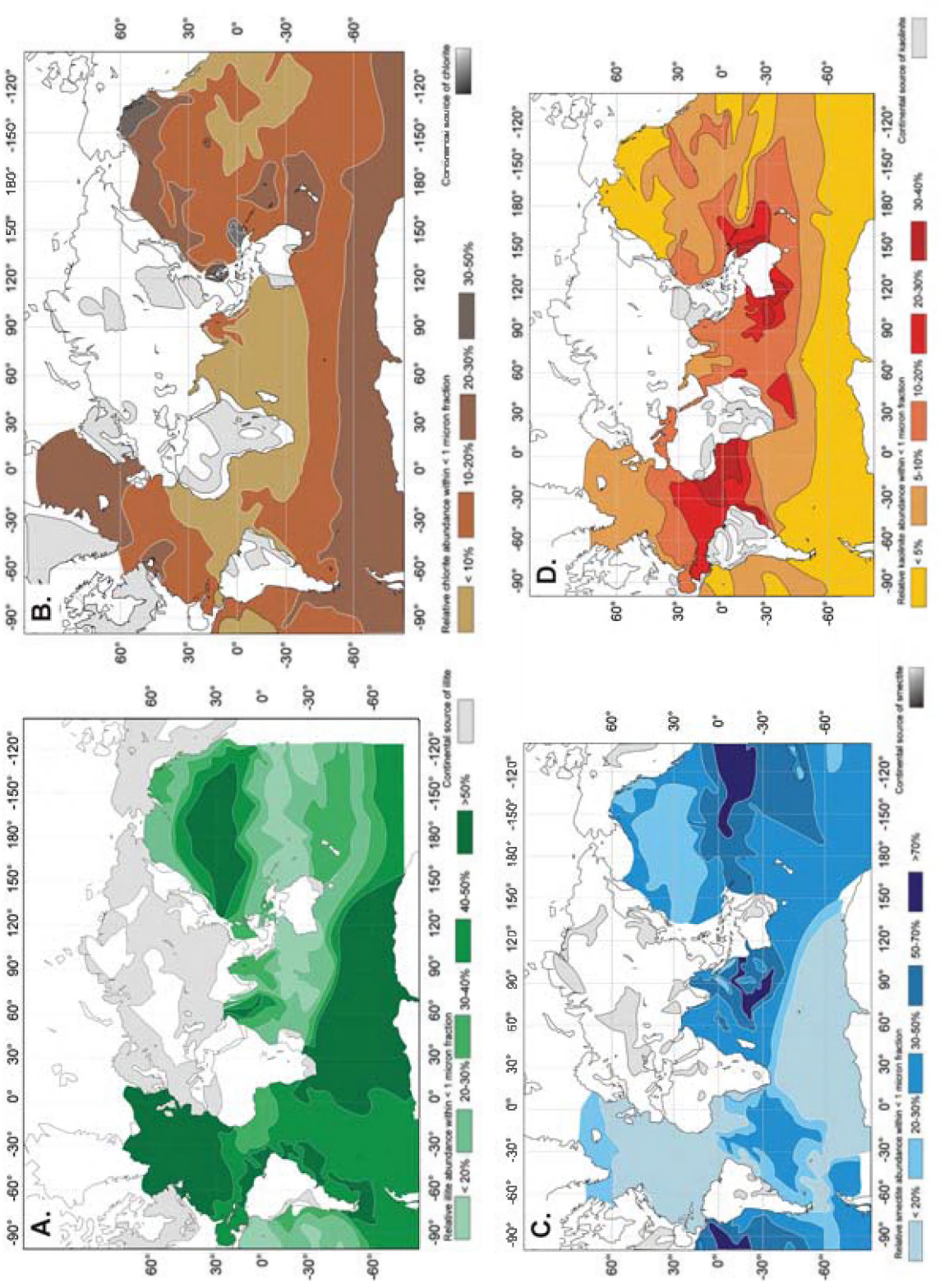

Fig. 2.8 *Distribution of Illite (A), Chlorite (B), Smectite (C) and Kaolinite (D) in the clay fraction (<1 µm) of surface marine sediments. The continental sources of the latter clay minerals are also shown (Fagel, 2007; Lisitzin, 1996).*

source) by size sorting or differential flocculation (Singer, 1984).

Detrital clay mineral assemblages in deep-sea sediments have been widely used to constrain the provenance of detrital inputs (e.g. Biscaye, 1965; Griffin *et al.*, 1968; Rateev *et al.*, 1969). In these studies, the clay mineralogy generally reflects the intensity of continental weathering in the source areas although the mineralogy of the source rock plays an important role as well

(Fig. 2.7) (Chamley, 1989). The use of radiogenic isotope measurements (Sr, Nd and/or Pb) provides further constraints on the identification of the source area (e.g. Fagel *et al.*, 1999; Grousset *et al.*, 1988; Innocent *et al.*, 2000). A thorough knowledge of the source areas also contributes to the identification of the potential transport routes and transport mechanisms of the sediment (e.g. Ballini *et al.*, 2006; Fagel *et al.*, 2001).

Given that clays are sensitive indicators of their environment, variations in down-core clay mineral distribution in deep-sea sediments may be interpreted in terms of changes in the climatic conditions prevailing in the continental source area (Chamley, 1989; Fagel, 2007). However, the paleoclimatic interpretation of clay mineral data requires knowledge of the potential source areas (Moriarty, 1977), as well as of the mode and strength of transport processes (Gingele *et al.*, 1999).

As discussed above, detrital clay assemblages reflect mainly the combined influences of land petrography and continental climate. This is systematically the case in temperate regions, where chemical weathering is weak enough to allow the recognition of geological susbstrates, and strong enough to permit the mineralogical expression of pedologic processes (Chamley, 1989). Kaolinite forms abundantly in soils of intertropical land masses characterized by a warm, humid climate. The distribution of kaolinite in marine sediments reflects this dominant climatic control. Therefore, the abundance of this clay mineral increases toward the equator in all oceanic basins and expresses a strong climatic dependence by the intensity of continental hydrolysis (Fig. 2.8) (Chamley, 1989). Detrital chlorite mainly results from the erosion of plutonic and metamorphic rocks preserved from noticeable chemical weathering. Such rocks crop out widely on continental shields from high latitudes, where soils hardly develop and physical weathering predominates. This is reflected in the abundance of chlorite in marine sediments which increases toward cold latitudinal zones parallel to the decrease of continental hydrolysis (Fig. 2.8) (Chamley, 1989). The relative abundance of illite tends to increase toward high latitudes parallel to chlorite, which reflects the decrease of hydrolytic processes and the increase of direct rock erosion under cold climatic conditions. This is particularly well expressed in the North Atlantic Ocean where illite commonly exceeds 50% of the clay fraction (Fig. 2.8) (Chamley, 1989). Smectite displays a distribution that does not entirely parallel the zonal distribution of weathering processes (Fig. 2.8), indicating the influence of other allochthonous and/or autothonous processes. Volcanic rocks weather preferentially into smectite, regardless of climatic conditions if there is sufficient water to allow hydrolytic processes. The increased amounts of marine smectite recorded off the temperate to subarid regions nevertheless suggest that the mineral partly reflects conditions intermediate between those of cold-dry and warm-humid climate (Chamley, 1989). Conclusively said, kaolinite and smectite are concentrated in the tropical-humid zone, and their abundances decrease to both the north and the south; this is called the equatorial-type distribution (Fagel, 2007). In contrast, chlorite and illite are concentrated at moderate and high latitudes, mainly within the cold, moderately humid and glacial zones; this is called the bipolar-type distribution (Fagel, 2007).

After burial, clay minerals may be subjected to diagenetic transformations. However, the present study only discusses the clay mineralogy in the upper 150 m of the sedimentary column, where clay minerals may be regarded as stable and largely unaffected by diagenetic processes.

2.6.2 Sample preparation and analysis

For the identification of the clay minerals, the method used by Colin *et al.* (1999) was followed. Prior to the separation of the clay fraction, the carbonate was removed. Some grams of sediment were put in distilled water and brought into suspension using a magnetic stirrer. Acetic acid (3.3 M) was added until the dissolution reaction was terminated and a pH around 3 was reached. The acidic environment promotes flocculation of the clay, therefore, the sample was rinsed 5 times with distilled water until a neutral pH was obtained and the clay particles remained in suspension.

The clay fraction (<2 µm) was separated using gravity settling, following Stokes' law: The sample was stirred and after settling for 90 minutes, the clays were isolated in the upper 2 cm of the suspension. The suspension containing the clay minerals was transferred to centrifuge tubes using a syringe. Next, the clay fraction was brought out of suspension by centrifuging the samples. The non-calcareous clay-sized particles were prepared for measurement on oriented mounts. Subsequently, the clay minerals were identified by standard X-ray diffraction (XRD) analysis using a PANalytical diffractometer at the IDES laboratory (University of Paris XI). Three XRD runs were performed, following air-drying, ethylene-glycol solvation for 24 hours, and heating at 490°C for two hours.

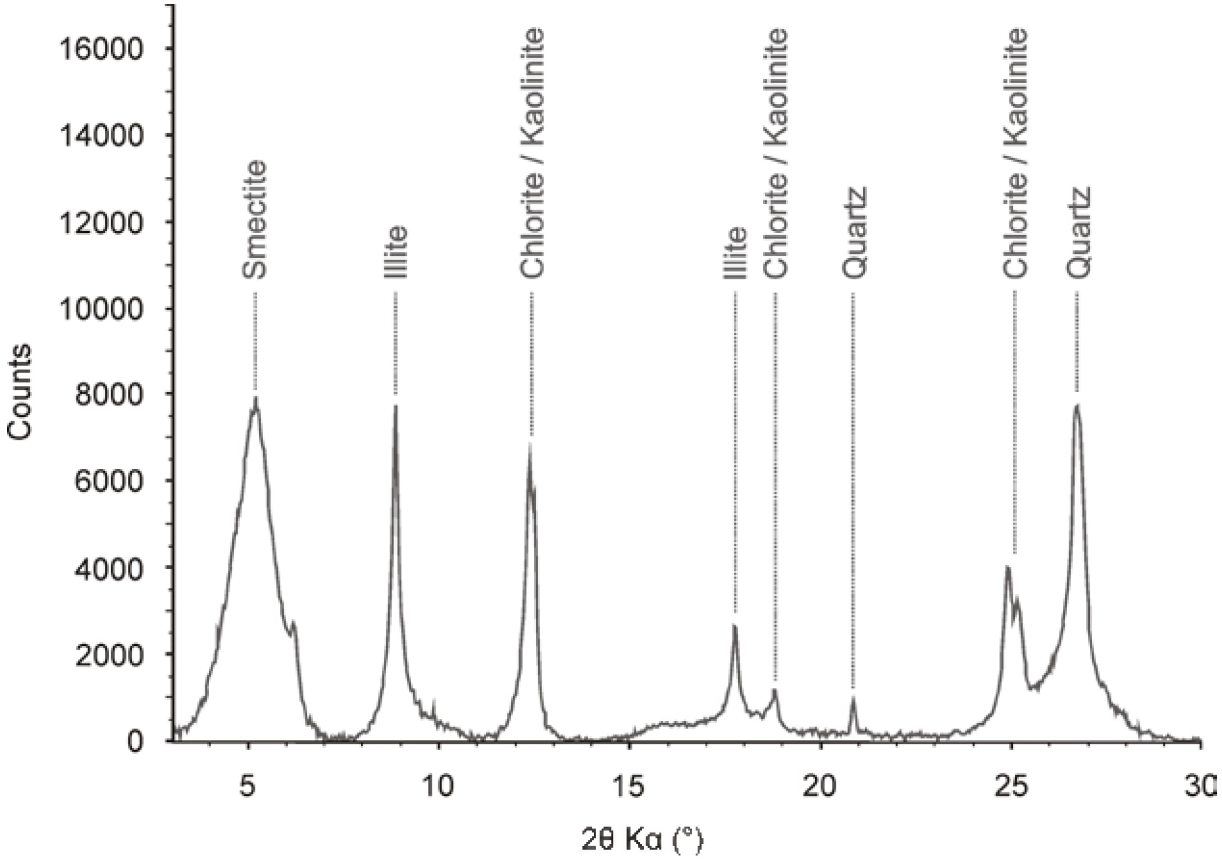

Fig. 2.9 *An example of the basal reflections of the main clay minerals on a glycolated diffractogram.*

The term 'clay mineral' refers to a mineral group rather than a specific mineralogical species. The mineralogy of the clay-sized fraction of the deep-sea sediment (<2 µm) comprises the common clay minerals smectite (or montmorillonite), illite, kaolinite and chlorite (Fagel, 2007). The various clay minerals are identified by their characteristic basal X-ray diffraction maxima (Fig. 2.9). Illites are characterized by a peak at 1.0 nm which is not affected by glyconation or heating. Illite crystallinity was obtained from the full width at half maximum (FWHM) of the 0.5 nm peak and 1.0 nm peak from the X-ray diffractograms (Chamley, 1989). Ratios lower than 0.5 represent Fe-Mg-rich illites, which are characteristic for low chemical weathering conditions; ratios higher than 0.5 are found in Al-rich illites, which are formed by strong hydrolysis. Any material which expands to 1.7 nm upon glyconation is assigned to the smectite group which consists of pure smectite but also smectite-illite mixed layers with variable abundances of smectite layers. Chlorites are defined by a 1.4 nm reflection which is affected neither by solvatation nor heating. Kaolinite is identified by a 0.7 nm peak which disappears above 500°C (Fagel, 2007).
Semi-quantitative estimates of peak areas of the basal reflections for the main clay mineral groups were carried out on the glycolated diffractogram using the MacDiff software (Petschick, 2000). On glycolated samples, kaolinite and chlorite both have a peak around 0.7 nm. Therefore, relative proportions of kaolinite and chlorite were determined based on the ratio of the 0.357/0.354 nm peak areas. Replicate analyses of selected samples gave a precision of ±2% (2σ). Based upon the XRD method, the semi-quantitative evaluation of each clay mineral has an accuracy of ~5%.

2.7 Neodymium and strontium isotope analysis

2.7.1 Neodymium and strontium isotope ratios as tracer for provenance studies

Neodymium (Nd) is a rare earth element (REE) with atomic number 60 and belongs to the Lanthanoid series. Naturally occurring, Nd is composed of 5 stable isotopes ^{142}Nd, ^{143}Nd, ^{145}Nd, ^{146}Nd and ^{148}Nd and 2 radio-isotopes ^{144}Nd and ^{150}Nd. However, given the very long half-life of the radio-isotopes ($2.29*10^{15}$ and $7*10^{18}$ yrs

Source Regions	[Sr] ppm	$^{87}Sr/^{86}Sr$	[Nd] ppm	$^{143}Nd/^{144}Nd$	$\varepsilon_{Nd}(0)$
Southeast Canada	286	0.722000		0.511354	-25
Baffin Bay area	208	0.73755	20.9	0.511124	-29.5
Scandinavia	141	0.728191	23	0.511644	-19.3
British Isles	97	0.734253	38	0.512019	-12.1
Bay of Biscaye	81	0.729611	25	0.512045	-11.6
Iceland (volcanic)	154	0.703040		0.513034	+7.8
East Greenland	366	0.712000	23	0.511457	-23

Table 2.1 *Mean values of Sr and Nd concentration and $^{87}Sr/^{86}Sr$ and $^{143}Nd/^{144}Nd$ isotope ratios for the main potential source areas in the North Atlantic region (Revel et al., 1996b).*

respectively) these isotopes may be regarded as stable. In paleoceanographic studies, the isotope ratio of $^{143}Nd/^{144}Nd$ is used as a proxy for the provenance of marine sediments (e.g. Revel *et al.*, 1996b). ^{143}Nd is a radiogenic isotope as it is the product of radio-active decay of ^{147}Sm. Therefore, the $^{143}Nd/^{144}Nd$ ratio will primarily reflect the age of the source rock and in a secondary way the original Sm-Nd ratio, and thus lithology of the rock. The $^{143}Nd/^{144}Nd$ ratio is usually expressed in ε-units, with:

$$\varepsilon_{Nd} = ((^{143}Nd/^{144}Nd)_{sample} - (^{143}Nd/^{144}Nd)_{CHUR}) / (^{143}Nd/^{144}Nd)_{CHUR})*10^4$$

where CHUR stands for Chondritic Uniform Reservoir (Goldstein *et al.*, 1984), i.e., the global mean isotopic composition deduced from measurements in chondrites ($(^{143}Nd/^{144}Nd)_{CHUR}$ = 0.512638) (Jacobsen and Wasserburg, 1980).
Strontium (Sr) is an alkaline earth element with atomic number 38. Strontium has four stable, naturally occurring isotopes: ^{84}Sr, ^{86}Sr, ^{87}Sr and ^{88}Sr. Only ^{87}Sr is radiogenic as it is the result of the radio-active decay of ^{87}Rb. The ratio $^{87}Sr/^{86}Sr$ is the parameter which is generally reported in sedimentological studies (e.g. Revel *et al.*, 1996b). The latter ratio is an expression of the age and orginial Rb-Sr ratio of the source rock. However, although Sr isotope ratios are good tracers of the geological origin of sediments, the results are influenced by the grain-size distribution of the samples analyzed: in the finest fraction of the sediment (e.g. < 2 µm), the $^{87}Sr/^{86}Sr$ ratio is generally higher compared to the ratio of the

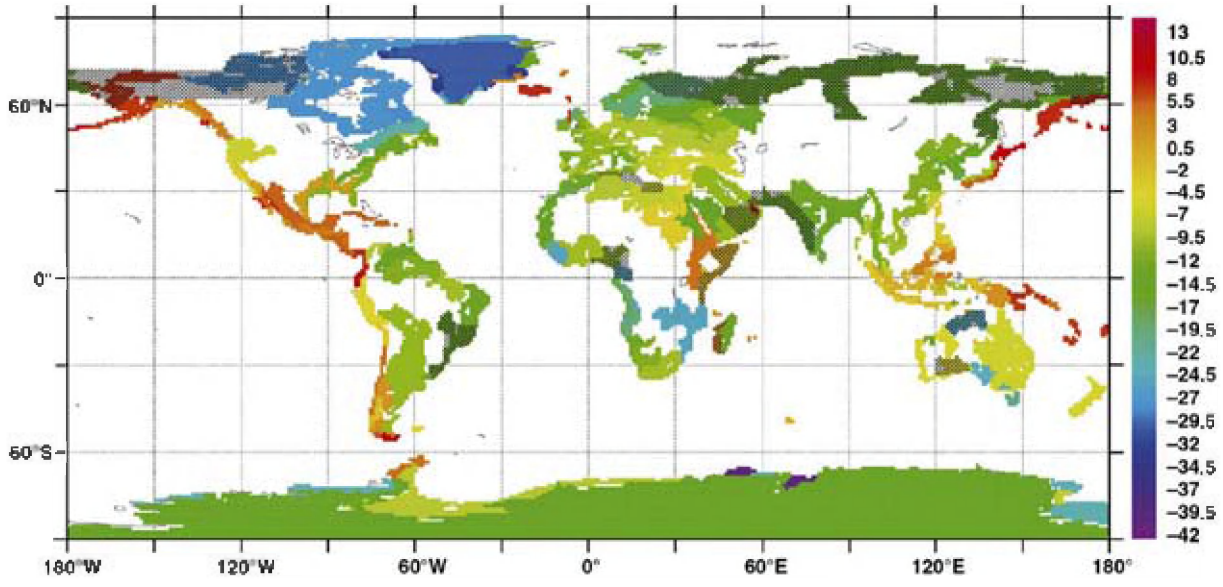

Fig. 2.10 *Extrapolated map providing a picture of the Nd signature of all the margins surrounding the ocean (Jeandel et al., 2007).*

bulk lithic sample and coarser fractions due to fractionation (Revel *et al.*, 1996a,b). In this regard, the Nd isotopic composition is more reliable as it is not, or less affected by grain-size variations (Goldstein *et al.*, 1984; Revel *et al.*, 1996b).

Over the last 30 years Nd and Sr isotope ratios became well established proxies to trace the provenance of detrital marine sediment (Fig. 2.10). Especially in the North Atlantic, numerous studies used Nd and Sr for isotopic fingerprinting of the terrigenous material (e.g. Farmer *et al.*, 2003; Grousset *et al.*, 1988; Grousset *et al.*, 2000; Hemming *et al.*, 1998; Innocent *et al.*, 1997; Peck *et al.*, 2007; Revel *et al.*, 1996b; Snoeckx *et al.*, 1999). The main potential source areas for the North Atlantic are: (1) the southeastern part of Canada and the Labrador/Hudson Bay Canadian region, dominated by the Superior and Grenville geological provinces; (2) the northeastern Canadian province mostly corresponding to the Churchill and Appalachian geological provinces; (3) the volcanic provinces consisting of Iceland, the Faeroe Islands and the eastern Greenlandic and the NW British-Irish volcanic provinces; (4) Scandinavia (mostly its Norwegian part); (5) the British-Irish Isles; (6) the Bay of Biscay and (7) East Greenland. For each source region a mean isotopic value from weighted values of all the available data from each region is listed in Table 2.1 (Jeandel *et al.*, 2007; Revel *et al.*, 1996b). It has to be noted that the reduction of these large and geologically diverse areas to a single isotopic value is a serious simplification. In most cases, the samples of a certain area will be located in an envelope with the mean isotopic value in its centre.

The heterogeneity of the continental ε_{Nd} composition (Fig. 2.10) is reflected to a certain extent in the oceanic ε_{Nd} values. Given that the residence time of Nd in the ocean is less than the ocean mixing time, different water masses will have distinct ε_{Nd} values, governed by sources and sinks alongside ocean circulation (Arsouze *et al.*, 2007; Claude and Hamelin, 2007; Jeandel *et al.*, 2007; Tachikawa *et al.*, 2003 and references therein). Therefore, the ε_{Nd} values incorporated in corals, foraminifera and iron-manganese crusts can be used as a tracer for water masses and ocean circulation (e.g. Burton *et al.*, 1999; Palmer and Elderfield, 1986; Vance and Burton, 1999; Vance *et al.*, 2004).

The present study will not address the ε_{Nd} of water masses given that the Nd isotope ratio is measured on the bulk detrital fraction of the sediment which is a reflection of the provenance and does not record the isotope ratio of the water masses. However, the identification of the source areas of the detrital material will also provide additional information about the potential transport routes and transport mechanisms of the sediment.

2.7.2 Sample preparation and analysis

For the analysis of the Sr and Nd isotope ratios of the detrital sediment, the procedure was followed described by Colin *et al.* (1999). In a first step, the carbonate of the sediment was removed using 3.3M acetic acid (CH_3COOH). After the removal of the carbonate, the sample was washed five times with Milli-Q water in order to remove all traces of the acid and dissolved carbonate. Subsequently, the sample was dried and transferred to savillex vials.

In a next step, the sediment was completely dissolved. A first acid-attack was carried out with a mixture of 2 ml HF and 0.2 ml $HClO_4$ on a hot plate (80°C). After the first attack, the sample was dried and a new acid-mixture was added containing 2 ml HNO_3 and 2 ml HCl. When a complete dissolution of the sediment was obtained, the samples were dried.

The actual isolation of the neodymium (Nd) and strontium (Sr) isotopes was carried out at the LSCE (Gif-sur-Yvette), using liquid chromatography. The first chemical separation utilizes Bio-Rad columns (length: 10 cm / diameter: 0.8 cm) packed with 10 ml AG50WX-8, 200-400 mesh cationic exchange resin to separate the Rare Earth Elements (REE) and Sr (Fig. 2.11). Prior to separation, the column was cleaned with 15 ml 6M HCl and Milli-Q water until a neutral pH was reached. After this treatment, 3 ml 1M HCl was passed onto the column. Meanwhile, the dried sample was dissolved again in 2 ml 1M HCl (Fig. 2.12 A). In order to remove the organic material which is still in suspension, the sample was centrifuged and the organic material was decanted (Fig. 2.12 B). After the sample was passed onto the column, 35 ml 2M HCl was added. The Sr fraction was eluted when the next 15 ml 2M HCl was put on the column. Subsequently, the column was washed with 35 ml 2.5M HNO_3. The next 24 ml 2.5M HNO_3 that runned through the column eluted the REE fraction. Both the Sr and the REE fraction were dried on the hot plate after this first separation (Fig. 2.13 A).

Prior to analysis, the fraction containing Sr isotopes needs to be purified. Therefore, this fraction was passed onto a 20 µl SrSpec® column, consisting of a polyethylene syringe with a 4 mm Ø millex® filter (Fig. 2.13 B). First, this column was washed with 2 ml Milli-Q water. Subsequently, 0.4 ml 4M HNO_3 was added. The dried Sr fraction (Fig 2.13A) was dissolved again using 0.15 ml 4M HNO_3

Fig. 2.11 *The columns containing AG50X8-resin that are used for the separation of strontium (Sr) and the rare earth elements (REE).*

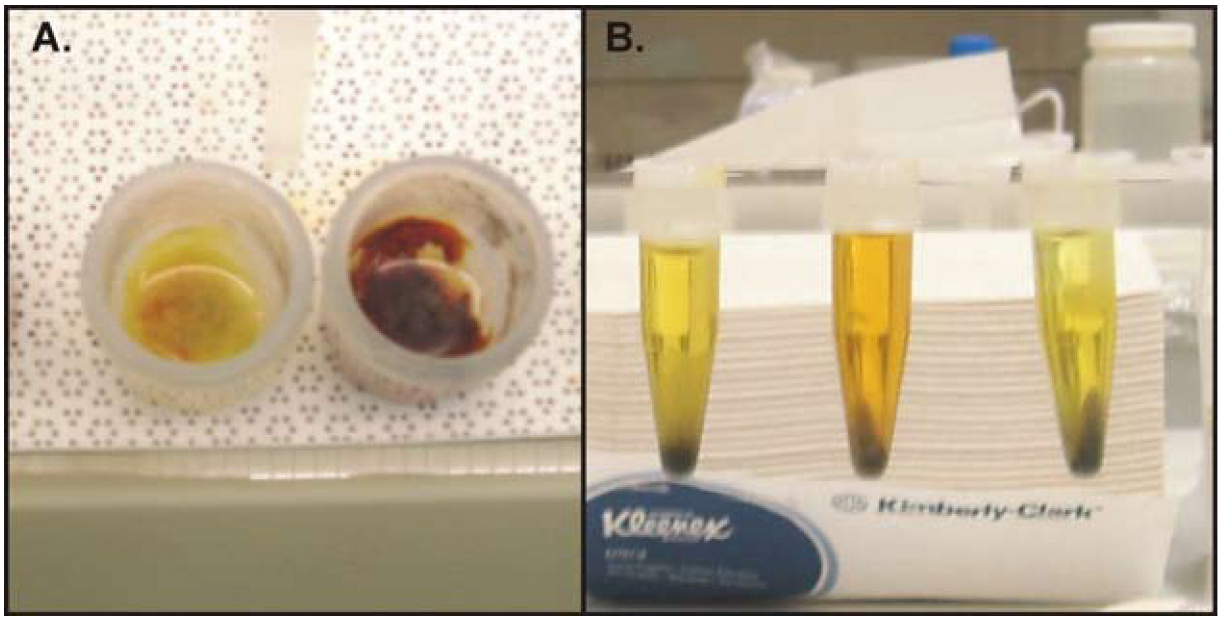

Fig. 2.12 A. *The dissolution of the dried samples using 2 ml 1M HCl before the separation on the AG50X8 column. B. The dissolved samples are centrifuged to decant the organic material.*

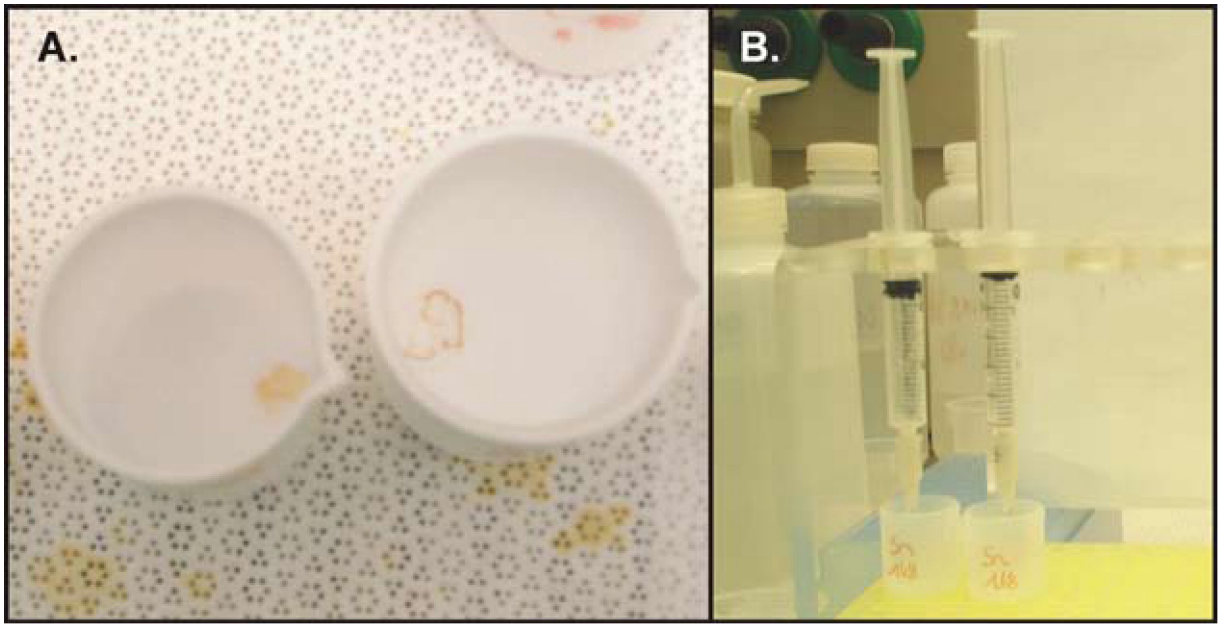

Fig. 2.13 *A. The Sr fraction that is dried on a hot plate after the separation from the rare earth elements on the AG50X8 column. B. The purification of the Sr fraction using a syringe containing Sr-spec resin.*

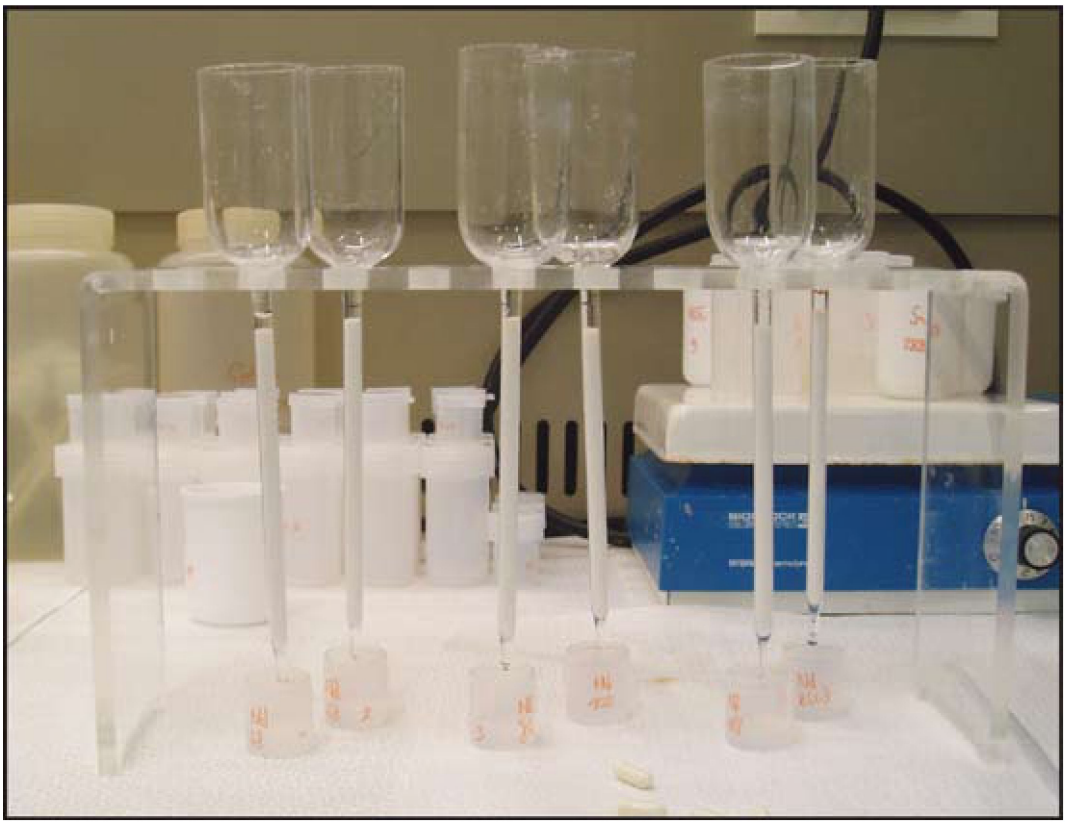

Fig. 2.14 *Separation of the Nd isotopes from the other REE on a column containing Voltalef-HDEHP resin.*

and put on the column. After washing the column with 1 ml 4M HNO_3, the purified Sr was eluted with 2 ml Milli-Q water. After this procedure, the Sr was ready for isotopic analysis.

The Nd was separated from the other REE by reverse-phase chromatography on HDEHP-coated Teflon powder (Fig. 2.14). The column was cleaned with 20 ml 6M HCl and 15 ml Milli-Q water. Next, 3 ml 0.27M HCl was added and the dried sample was passed onto the column in 0.2

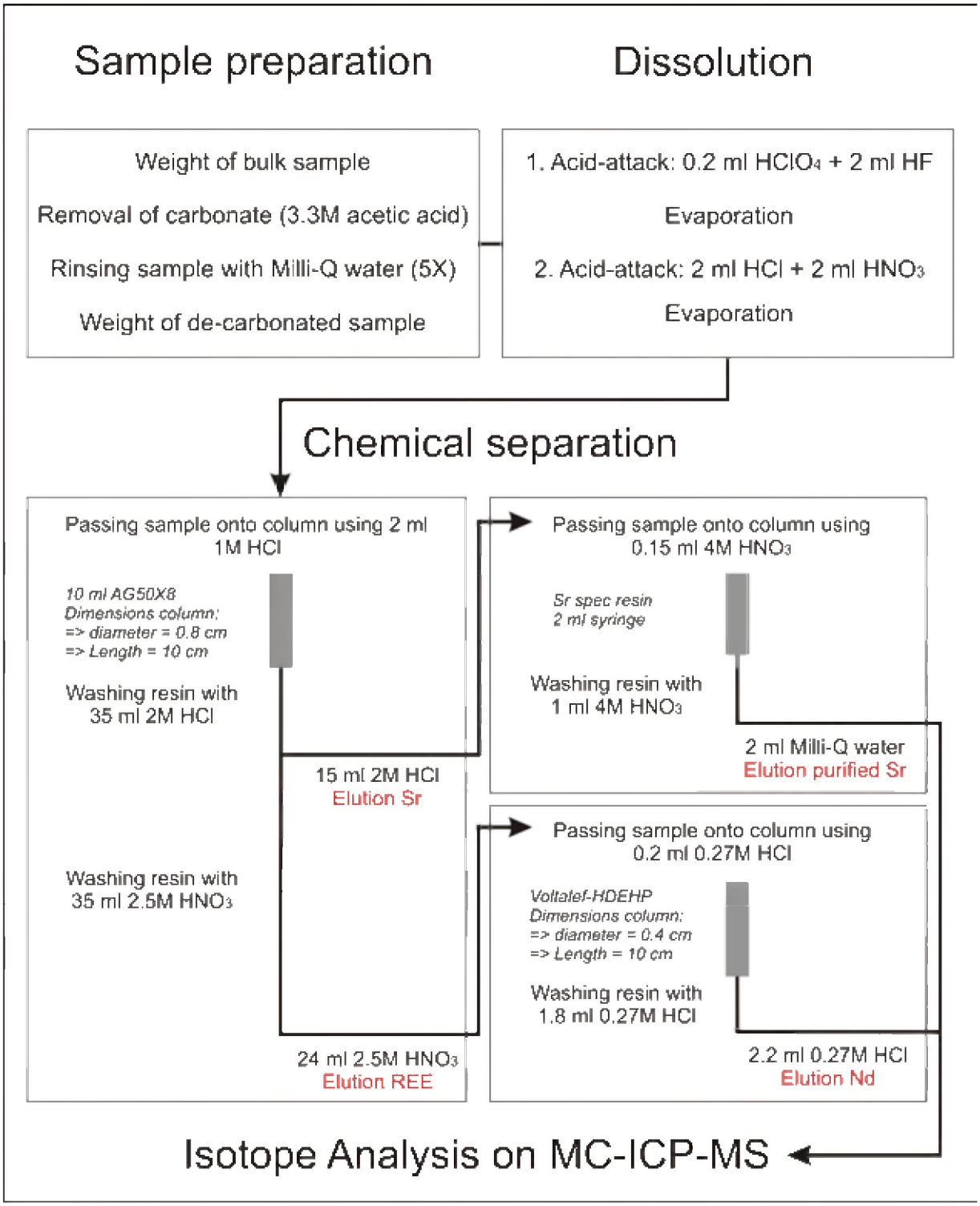

Fig. 2.15 *Schematic overview of sample preparation for neodymium and strontium isotope analysis of decarbonated sediment.*

ml 0.27M HCl. Subsequently, 1.8 ml 0.27M HCl was put on the column. The fraction containing Nd was eluted by adding another 2.2 ml 0.27M HCl. After this step, the Nd fraction was ready for isotopic analysis.

Prior to the isotopic analysis, the concentrations were measured with a Perkin Elmer Sciex Elan 5000, a traditional quadrupole-based ICP-MS, at the department of analytical chemistry, Ghent University. The Sr and Nd isotope ratios were determined using a Thermo Scientific Neptune MC-ICP-MS (multi-collector inductively coupled plasma mass spectrometer). The JNdi-1 standard was used as reference material for

neodymium ($^{143}Nd/^{144}Nd$ = 0.51215, $^{146}Nd/^{144}Nd$ = 0.7219) (Tanaka *et al.*, 2000) to correct for instrumental mass discrimination using external standardization (sample-standard bracketing). For the measurement of the Sr isotopes the NIST SRM 987 standard was used.
ICP-MS (Inductively coupled plasma mass spectrometry) is a method for separating and detecting ions by coupling together an inductively coupled plasma and a mass spectrometer. An inductively coupled plasma is a gas which contains a sufficient concentration of ions and electrons to make the gas electrically conductive. The sample is introduced using a nebulizer which aspirates the sample with high velocity argon, forming a fine mist. As a droplet of nebulized sample enters the central channel of the ICP, the hot plasma removes any remaining solvent and causes sample atomization followed by ionization. For coupling to mass spectrometry, the ions from the plasma are extracted through a series of cones into a mass spectrometer. Subsequently, the ions are separated on the basis of their mass-to-charge ratio and a detector receives an ion signal, proportional to the concentration.
An MC-ICP-MS instrument contains multiple collectors, allowing the measurement of different ion signals at the same time. This development improves the precision of the MC-ICP-MS compared to conventional ICP-MS which only allows single-collector analysis. Due to the inherent instability of the plasma, the precision of the signal intensities measured on a single collector ICP-MS with a quadrupole analyzer is limited to around 1%, although for isotope ratios a precision around 0.1% RSD (relative standard deviation) can be obtained.

2.8 Stable carbon (C) and oxygen (O) isotopes in carbonates

2.8.1 Stable C and O isotope composition of bulk carbonate

Prior to stable isotope analysis, bulk sediment samples were weighed in function of the carbonate content to ensure an adequate mass of carbonate for isotopic analysis (equivalent to 50 - 70 µg of pure carbonate). All samples were digested in 10M phosphoric acid at 90°C. Samples containing calcite and/or aragonite reacted 15 minutes in the acidic bath whereas those with dolomite reacted for a period of 45 minutes. All isotope analyses were carried out on a VG optima mass spectrometer coupled with an automated preparation line at the Laboratoire des Sciences du Climat et de l'Environnement (LSCE, Gif-sur-Yvette, France). All values are reported in per mil relative to Vienna Pee Dee Belemnite (V-PDB). Reproducibility is 0.04‰ and 0.05‰ respectively for the carbon and the oxygen isotope ratios.

2.8.2 Stable C and O isotope composition of extracted dolomite

For the present study, a partial extraction procedure was performed to separate the dolomite fraction from the calcite fraction in a sample taken at 181 cm in Alpha Mound. In a first phase, ammonium acetate (1M) buffered with acetic acid (pH 5) dissolved only calcium carbonate, and to a minor extent the non-stoichiometric dolomite. During a second phase, boiling hydrochloric acid dissolved the rest of the carbonate fraction (stoichiometric dolomite) and partly some other constituents (clay minerals). Subsequently, stable isotopic measurements were performed at the University of Erlangen (Germany) on the bulk fraction, as well as on separated calcite and dolomite fractions.
Carbonate powders were reacted with 10M phosphoric acid (density >1.9, (Wachter and Hayes, 1985)) at 75°C using a Kiel III online carbonate preparation line connected to a ThermoFinnigan 252 masspectrometer. All values are reported in per mil relative to V-PDB by assigning a $\delta^{13}C$ value of +1.95‰ and a $\delta^{18}O$ value of -2.20‰ to NBS19. Reproducibility was checked by replicate analysis of laboratory standards. Oxygen isotopic compositions of dolomite were corrected using the fractionation factors given by (Rosenbaum and Sheppard, 1986). Reproducibility was checked by replicate analysis of laboratory standards and was better than ± 0.02 for $\delta^{13}C$ (1σ) and ± 0.02 for $\delta^{18}O$ (1σ) during this study.

2.9 Sulfur (S) and oxygen (O) isotope ratios in sulfur-bearing minerals

The oxygen and sulfur isotopic composition of gypsum-bound sulfate was measured on hand-picked gypsum crystals at the Max Planck Institute for Marine Microbiology, Bremen and the Swiss Federal Institute of Technology (ETH) Zurich. The crystals were digested in a $NaCl_2$/ascorbic acid solution and subsequently precipitated in the form of $BaSO_4$ by addition of $BaCl_2$. To determine the sulfur isotopic composition of pyrite, sediment sub-samples were subjected to a two-step chromium-II reduction method (Fossing

and Jorgensen, 1989). This method separately traps acid volatile sulfide (AVS) and chromium reducible sulfur (CRS) as ZnS. The CRS fraction, which mainly consists of sulfur bound as pyrite, was converted into Ag_2S by treatment with $AgNO_3$. Precipitates were washed several times with deionized water and dried.

Sulfur isotope ratios were measured by adding 0.4 to 0.6 mg of $BaSO_4$ or 0.2 to 0.4 mg Ag_2S to 1 mg of V_2O_5 in a tin capsule and combusted at 1060°C in an elemental analyzer (EURO EA Elemental Analyzer®) to produce SO_2. The evolved SO_2 was carried by a helium stream through a GC column, Finnigan Conflo III®, and into a Finnigan Delta V® stable isotope ratio mass spectrometer to determine $\delta^{34}S$. The sulfur isotope measurements were calibrated with reference materials National Bureau Standards (NBS) 127 ($\delta^{34}S$ = +20.3‰) and IAEA-SO-6 ($\delta^{34}S$ = −34.1‰). The standard errors (σ1) of the measurements were less than 0.2‰ for $\delta^{34}S$.

For oxygen isotope analysis, approximately 0.16 mg of $BaSO_4$ was transferred to a silver capsule and thermochemically reduced at 1450°C in the presence of graphite and glassy carbon in the Finnigan Thermal Conversion/Elemental Analyzer (TC/EA®) to produce CO. The evolved CO was carried by a helium stream through a GC column, Finnigan Conflo III®, and into a Thermo Scientific MAT 253® stable isotope ratio mass spectrometer to measure $\delta^{18}O$. The oxygen isotope measurements were calibrated with NBS 127 ($\delta^{18}O$ = +8.6‰ (Boschetti and Iacumin, 2005)), IAEA-SO-5 ($\delta^{18}O$ = +12.0‰) and IAEA-SO-6 ($\delta^{18}O$ = -11.3‰ (Halas *et al.*, 2007)). The standard errors (σ1) of the measurements were less than 0.3‰ for $\delta^{18}O$.

The isotope measurements are reported with respect to the standards, Vienna Standard Mean Oceanic Water (V-SMOW) and Vienna Canyon Diablo Troilite (V-CDT).

2.10 Sulfur (S) and oxygen (O) isotope composition of carbonate associated sulfate (CAS) in dolomite

In order to determine the isotope composition of the carbonate associated sulfate (CAS) in the dolomite, a sequential leaching technique was used. First, the sample (6.7 g) was ground to a grain size smaller than 125 µm. Subsequently, the sample was leached in a 1M sodium chloride, 0.05M ascorbic acid solution for 48 hours. This leaching step removes easily soluble sulfates (e.g. gypsum), whereas the ascorbic acid inhibits iron oxidation, therefore suppressing oxidation of sulfides (e.g. pyrite). The treatment also induces limited dissolution of carbonate, which buffers the ascorbic acid. Next, the sample was centrifuged and the supernatant discarded. The sample was then exposed for 1 hour to acetic acid under a nitrogen atmosphere. This procedural step is assumed to dissolve calcium carbonate, while leaving dolomite intact. The residue of this leaching step was recovered by centrifugation, and exposed to concentrated hydrochloric acid for 15 minutes under a nitrogen atmosphere. The sulfate from the supernatant of this leaching step was recovered by precipitation with barium chloride. Finally, sulfur and oxygen isotopes were measured using a Finnigan Delta V® stable isotope ratio mass spectrometer. The sulfur isotope of CAS is reported with respect to Vienna Canyon Diablo Troilite (V-CDT), the oxygen isotope of CAS is reported with respect to Vienna Standard Mean Ocean Water (V-SMOW).

References

Arsouze, T., Dutay, J.C., Lacan, F. and Jeandel, C., 2007. Modeling the neodymium isotopic composition with a global ocean circulation model. Chemical Geology, 239(1-2), 165-177.

Ballini, M., Kissel, C., Colin, C. and Richter, T., 2006. Deep-water mass source and dynamic associated with rapid climatic variations during the last glacial stage in the North Atlantic: A multiproxy investigation of the detrital fraction of deep-sea sediments. Geochemistry Geophysics Geosystems, 7, doi: 10.1029/2005GC001070.

Barker, C.E. and Wood, T., 1986. A review of the Technosyn and Nuclide cathodoluminescence stages and their application to sedimentary geology. In: R.D. Hagni (Editor), Process Mineralogy, VI. The Metallurgical Society Inc., Warrendale, PA, pp. 137-158.

Biscaye, P.E., 1965. Mineralogy and Sedimentation of Recent Deep-Sea Clay in Atlantic Ocean and Adjacent Seas and Oceans. Geological Society of America Bulletin, 76(7), 803-832.

Bloemendal, J., King, J.W., Hall, F.R. and Doh, S.J., 1992. Rock Magnetism of Late Neogene and Pleistocene Deep-Sea Sediments - Relationship to Sediment Source, Diagenetic Processes, and Sediment Lithology. Journal of Geophysical Research-Solid Earth, 97(B4), 4361-4375.

Boggs, S.J. and Krinsley, D., 2006. Application of Cathodoluminescence Imaging of the Study of Sedimentary Rocks. Cambridge University Press, Cambridge, 165 pp.

Boschetti, T. and Iacumin, P., 2005. Continuous-flow delta O-18 measurements: new approach to standardization, high-temperature thermodynamic and sulfate analysis. Rapid Communications in Mass Spectrometry, 19(21), 3007-3014.

Burton, K.W., Lee, D.C., Christensen, J.N., Halliday, A.N. and Hein, J.R., 1999. Actual timing of neodymium isotopic variations recorded by Fe-Mn crusts in the western North Atlantic. Earth and Planetary Science Letters, 171(1), 149-156.

Chamley, H., 1989. Clay Sedimentology. Springer, Berlin, 623 pp.

Claude, C. and Hamelin, B., 2007. Isotopic Tracers of Water Masses and Deep Currents. In: C. Hillaire-Marcel and A. De Vernal (Editors), Proxies in Late Cenozoic Paleoceanography. Elsevier, Amsterdam, pp. 645-680.

Cnudde, V., Masschaele, B., Dierick, M., Vlassenbroeck, J., Van Hoorebeke, L. and Jacobs, P., 2006. Recent progress in X-ray CT as a geosciences tool. Applied Geochemistry, 21(5), 826-832.

Colin, C., Turpin, L., Bertaux, J., Desprairies, A. and Kissel, C., 1999. Erosional history of the Himalayan and Burman ranges during the last two glacial-interglacial cycles. Earth and Planetary Science Letters, 171(4), 647-660.

de Haas, H., Mienis, F., Frank, N., Richter, T.O., Steinacher, R., De Stigter, H., van der Land, C. and Van Weering, T.C.E., 2009. Morphology and sedimentology of (clustered) cold-water coral mounds at the south Rockall Trough margins, NE Atlantic Ocean. Facies, 55, 1-26.

Dierick, M., Cnudde, V., Masschaele, B., Vlassenbroeck, J., Van Hoorebeke, L. and Jacobs, P., 2007. Micro-CT of fossils preserved in amber. Nuclear Instruments & Methods in Physics Research Section a-Accelerators Spectrometers Detectors and Associated Equipment, 580(1), 641-643.

Dorschel, B., Hebbeln, D., Foubert, A., White, M. and Wheeler, A.J., 2007. Hydrodynamics and cold-water coral facies distribution related to recent sedimentary processes at Galway Mound west of Ireland. Marine Geology, 244(1-4), 184-195.

Eisele, M., Hebbeln, D. and Wienberg, C., 2008. Growth history of a cold-water coral covered carbonate mound - Galway Mound, Porcupine Seabight, NE-Atlantic. Marine Geology, 253(3-4), 160-169.

Fagel, N., 2007. Clay Minerals Deep Circulation and Climate. In: C. Hillaire-Marcel and A. De Vernal (Editors), Proxies in Late Cenozoic Paleoceanography. Elsevier, Amsterdam, pp. 139-184.

Fagel, N., Innocent, C., Stevenson, R.K. and Hillaire-Marcel, C., 1999. Deep circulation changes in the Labrador sea since the last glacial maximum: New constraints from Sm-Nd data on sediments. Paleoceanography, 14(6), 777-788.

Fagel, N., Robert, C., Preda, M. and Thorez, J., 2001. Smectite composition as a tracer of deep circulation: the case of the Northern North Atlantic. Marine Geology, 172(3-4), 309-330.

Farmer, G.L., Barber, D. and Andrews, J., 2003. Provenance of Late Quaternary ice-proximal sediments in the North Atlantic: Nd, Sr and Pb isotopic evidence. Earth and Planetary Science Letters, 209(1-2), 227-243.

Fossing, H. and Jorgensen, B.B., 1989. Measurement of Bacterial Sulfate Reduction in Sediments - Evaluation of a Single-Step Chromium Reduction Method. Biogeochemistry, 8(3), 205-222.

Foubert, A. and Henriet, J.P., 2009. Nature and significance of the recent carbonate mound record: the

Mound Challenger Code. Springer-Verlag, Heidelberg, 350 pp.
Foubert, A., Van Rooij, D., Blamart, D. and Henriet, J.-P., 2007. X-ray imagery and physical core logging as a proxy of the content sediment cores in cold-water coral mound provinces: a case study from Porcupine Seabight, SW of Ireland. International Journal of Earth Sciences, 96, 141-158.
Gingele, F.X., Schmieder, F., von Dobeneck, T., Petschick, R. and Ruhlemann, C., 1999. Terrigenous flux in the Rio Grande Rise area during the past 1500 ka: Evidence of deepwater advection or rapid response to continental rainfall patterns? Paleoceanography, 14(1), 84-95.
Goldstein, S.L., Onions, R.K. and Hamilton, P.J., 1984. A Sm-Nd Isotopic Study of Atmospheric Dusts and Particulates from Major River Systems. Earth and Planetary Science Letters, 70(2), 221-236.
Götte, T. and Richter, D.K., 2006. Cathodoluminescence characterization of quartz particles in mature arenites. Sedimentology, 53(6), 1347-1359.
Götze, J., Plötze, M. and Habermann, D., 2001. Cathodoluminescence of quartz: origin, spectral characteristics and practical applications. Contributions to Mineralogy and Petrology, 141, 225-250.
Götze, J. and Zimmerle, W., 2000. Quartz and silica as guide to provenance in sediments and sedimentary rocks. Contributions to Sedimentary Geology, 12, 91 pp.
Griffin, J.J., Windom, H. and Goldberg, E.D., 1968. Distribution of Clay Minerals in World Ocean. Deep-Sea Research, 15(4), 433-459.
Grousset, F.E., Biscaye, P.E., Zindler, A., Prospero, J. and Chester, R., 1988. Neodymium isotopes as tracers in marine sediments and aerosols: North Atlantic. Earth and Planetary Science Letters, 87, 367-378.
Grousset, F.E., Pujol, C., Labeyrie, L., Auffret, G.A. and Boelaert, A., 2000. Were the North Atlantic Heinrich events triggered by the behavior of the European ice sheets? Geology, 28(2), 123-126.
Halas, S., Szaran, J., Czarnacki, M. and Tanweer, A., 2007. Refinements in BaSO4 to CO2 preparation and delta O-18 calibration of the sulfate reference materials NBS-127, IAEA SO-5 and IAEA SO-6. Geostandards and Geoanalytical Research, 31(1), 61-68.
Hayashida, A., Hattoni, S. and Oda, H., 2007. Diagenetic modification of magnetic properties observed in a piston core (MD01-2407) from the Oki Ridge, Japan Sea. Palaeogeography Palaeoclimatology Palaeoecology, 247(1-2), 65-73.
Hemming, S.R., Broecker, W.S., Sharp, W.D., Bond, G., Gwiazda, R.H., McManus, J., Klas, M. and Hadjas, I., 1998. Provenance of Heinrich layers in core V28-82, northeastern Atlantic: $^{40}Ar/^{39}Ar$ ages of ice-rafted hornblende, Pb isotopes in feldspar grains, and Nd-Sr-Pb isotopes in the fine sediment fraction. Earth and Planetary Science Letters, 164, 317-333.
Innocent, C., Fagel, N. and Hillaire-Marcel, C., 2000. Sm-Nd isotope systematics in deep-sea sediments: clay-size versus coarser fractions. Marine Geology, 168(1-4), 79-87.
Innocent, C., Fagel, N., Stevenson, R.K. and Hillaire-Marcel, C., 1997. Sm-Nd signature of modern and late Quaternary sediments from the northwest North Atlantic: Implications for deep current changes since the Last Glacial Maximum. Earth and Planetary Science Letters, 146(3-4), 607-625.
Jacobs, P. and Cnudde, V., 2008. Applications of X-ray computed tomography in engineering geology. Engineering Geology, 103, 67-146.
Jacobsen, S.B. and Wasserburg, G.J., 1980. Sm-Nd isotopic evolution of chondrites. Earth and Planetary Science Letters, 50(1), 139-155.
Jansen, J.H.F., Van der Gaast, S.J., Koster, B. and Vaars, A.J., 1998. CORTEX, a shipboard XRF-scanner for element analyses in split sediment cores. Marine Geology, 151, 143-153.
Jeandel, C., Arsouze, T., Lacan, F., Techine, P. and Dutay, J.C., 2007. Isotopic Nd compositions and concentrations of the lithogenic inputs into the ocean: A compilation, with an emphasis on the margins. Chemical Geology, 239(1-2), 156-164.
Jenkins, R. and De Vries, J.L., 1970. Practical X-ray Spectrometry. MacMillan, London, 190 pp.
Kak, A.C. and Slaney, M., 1988. Principles of computerized tomographic imaging. IEEE press, New York, 344 pp.
Karlin, R., 1990. Magnetite Diagenesis in Marine-Sediments from the Oregon Continental-Margin. Journal of Geophysical Research-Solid Earth and Planets, 95(B4), 4405-4419.
Ketcham, R.A. and Carlson, W.D., 2001. Acquisition, optimization and interpretation of X-ray computed tomographic imagery: applications to the geosciences. Computers & Geosciences, 27(4), 381-400.
Leslie, B.W., Hammond, D.E., Berelson, W.M. and Lund, S.P., 1990a. Diagenesis in Anoxic Sediments from the California Continental Borderland and Its Influence on Iron, Sulfur, and Magnetite Behavior.

Journal of Geophysical Research-Solid Earth and Planets, 95(B4), 4453-4470.
Leslie, B.W., Lund, S.P. and Hammond, D.E., 1990b. Rock Magnetic Evidence for the Dissolution and Authigenic Growth of Magnetic Minerals within Anoxic Marine-Sediments of the California Continental Borderland. Journal of Geophysical Research-Solid Earth and Planets, 95(B4), 4437-4452.
Lisitzin, A.P., 1996. Oceanic Sedimentation. Lithology and Geochemistry. American Geophysical Union, Washington, 400 pp.
Long, H.L., Swennen, R., Foubert, A., Dierick, M. and Jacobs, P., 2009. 3D quantification of mineral components and porosity distribution in Westphalian C sandstone by microfocus X-ray computed tomography. Sedimentary Geology, 220(1-2), 116-125.
Marshall, J.D., 1988. Cathodoluminescence of geological materials. Unwin Hyman, Boston, 146 pp.
Masschaele, B.C., Cnudde, V., Dierick, M., Jacobs, P., Van Hoorebeke, L. and Vlassenbroeck, J., 2007. UGCT: New x-ray radiography and tomography facility. Nuclear Instruments & Methods in Physics Research Section a-Accelerators Spectrometers Detectors and Associated Equipment, 580(1), 266-269.
McCave, I.N., 2007. Deep-Sea Sediment Deposits and Properties Controlled by Currents. In: C. Hillaire-Marcel and A. De Vernal (Editors), Proxies in Late Cenozoic Paleoceanography. Elsevier, Amsterdam, pp. 19-62.
Mienis, F., De Stigter, H., De Haas, H. and Van Weering, T.C.E., 2009. Near-bed particle deposition and resuspension in a cold-water coral mound area at the Southwest Rockall Trough margin, NE Atlantic. Deep Sea Research Part I: Oceanographic Research Papers, 56(6), 1026-1038.
Moriarty, K.C., 1977. Clay-Minerals in Southeast Indian-Ocean Sediments, Transport Mechanisms and Depositional Environments. Marine Geology, 25(1-3), 149-174.
Orsi, T.H., Edwards, C.M. and Anderson, A.L., 1994. X-Ray Computed-Tomography - a Nondestructive Method for Quantitative-Analysis of Sediment Cores. Journal of Sedimentary Research Section a-Sedimentary Petrology and Processes, 64(3), 690-693.
Palmer, M.R. and Elderfield, H., 1986. Rare-Earth Elements and Neodymium Isotopes in Ferromanganese Oxide Coatings of Cenozoic Foraminifera from the Atlantic-Ocean. Geochimica et Cosmochimica Acta, 50(3), 409-417.
Peck, V.L., Hall, I.R., Zahn, R., Grousset, F., Hemming, S.R. and Scourse, J.D., 2007. The relationship of Heinrich events and their European precursors over the past 60 ka BP: a multi-proxy ice-rafted debris provenance study in the North East Atlantic. Quaternary Science Reviews, 26(7-8), 862-875.
Petschick, R., 2000. MacDiff 4.2.5 Manual, 61 pp.
Petschick, R., Kuhn, G. and Gingele, F., 1996. Clay mineral distribution in surface sediments of the South Atlantic: Sources, transport, and relation to oceanography. Marine Geology, 130(3-4), 203-229.
Pirlet, H., Wehrmann, L.M., Brunner, B., Frank, N., Dewanckele, J., Van Rooij, D., Foubert, A., Swennen, R., Naudts, L., Boone, M., Cnudde, V. and Henriet, J.P., 2010. Diagenetic formation of gypsum and dolomite in a cold-water coral mound in the Porcupine Seabight, off Ireland. Sedimentology, 57, 786-805.
Rateev, M.A., Gorbunov.Zn, Lisitzyn, A.P. and Nosov, G.L., 1969. Distribution of Clay Minerals in Oceans. Sedimentology, 13(1-2), 21-43.
Revel, M., Cremer, M., Grousset, F.E. and Labeyrie, L., 1996a. Grain-size and Sr-Nd isotopes as tracer of paleo-bottom current strength, Northeast Atlantic Ocean. Marine Geology, 131(3-4), 233-249.
Revel, M., Sinko, J.A. and Grousset, F.E., 1996b. Sr and Nd isotopes as tracers of North Atlantic lithic particles: Paleoclimatic implications. Paleoceanography, 11(1), 95-113.
Richter, D.K., Gotte, T., Gotze, J. and Neuser, R.D., 2003. Progress in application of cathodoluminescence (CL) in sedimentary petrology. Mineralogy and Petrology, 79(3-4), 127-166.
Richter, T.O., Lassen, S., van Weering, T.C.E. and de Haas, H., 2001. Magnetic susceptibility patterns and provenance of ice-rafted material at Feni Drift, Rockall Trough: implications for the history of the British-Irish ice sheet. Marine Geology, 173, 37-54.
Richter, T.O., van der Gaast, S., Koster, B., Vaars, A., Gieles, R., de Stigter, H.C., De Haas, H. and van Weering, T.C.E., 2006. The Avaatech XRF Core Scanner: technical description and applications to NE Atlantic sediments. In: R.G. Rothwell (Editor), New techniques in Sediment Core Analysis. Special Publications. Geological Society, London, pp. 39-50.
Robinson, S.G., Maslin, M.A. and McCave, I.N., 1995. Magnetic susceptibility variations in Upper Pleistocene deep-sea sediments of the NE Atlantic: Implications for ice rafting and paleocirculation

at the last glacial maximum. Paleoceanography, 10(2), 221-250.
Rosenbaum, J. and Sheppard, S.M.F., 1986. An Isotopic Study of Siderites, Dolomites and Ankerites at High-Temperatures. Geochimica et Cosmochimica Acta, 50(6), 1147-1150.
Singer, A., 1984. The paleoclimatic interpretation of clay minerals in sediments - a review. Earth Science Reviews, 21, 251-293.
Snoeckx, H., Grousset, F.E., Revel, M. and Boelaert, A., 1999. European contribution of ice-rafted sand to Heinrich layers H3 and H4. Marine Geology, 158, 197-208.
Speijer, R.P., Van Loo, D., Masschaele, B., Vlassenbroeck, J., Cnudde, V. and Jacobs, P., 2008. Quantifying foraminiferal growth with high-resolution X-ray computed tomography: New opportunities in foraminiferal ontogeny, phylogeny, and paleoceanographic applications. Geosphere, 4(4), 760-763.
St-Onge, G., Mulder, T., Francus, P. and Long, B., 2007. Continuous physical properties of cored marine sediments. In: C. Hillaire-Marcel and A. De Vernal (Editors), Proxies in Late Cenozoic Paleoceanography. Elsevier, Amsterdam, pp. 63-98.
Stoner, J.S., Channell, J.E.T. and HillaireMarcel, C., 1996. The magnetic signature of rapidly deposited detrital layers from the deep Labrador Sea: Relationship to North Atlantic Heinrich layers. Paleoceanography, 11(3), 309-325.
Tachikawa, K., Athias, V. and Jeandel, C., 2003. Neodymium budget in the modern ocean and paleo-oceanographic implications. Journal of Geophysical Research-Oceans, 108, doi: 10.1029/1999jc000285.
Tanaka, T., Togashi, S., Kamioka, H., Amakawa, H., Kagami, H., Hamamoto, T., Yuhara, M., Orihashi, Y., Yoneda, S., Shimizu, H., Kunimaru, T., Takahashi, K., Yanagi, T., Nakano, T., Fujimaki, H., Shinjo, R., Asahara, Y., Tanimizu, M. and Dragusanu, C., 2000. JNdi-1: a neodymium isotopic reference in consistency with LaJolla neodymium. Chemical Geology, 168(3-4), 279-281.
Thierens, M., Titschack, J., Dorschel, B., Huvenne, V., Wheeler, A., Stuut, J.B. and O´Donnell, R., 2010. The 2.6 Ma depositional sequence from the Challenger cold-water coral mound (IODP Exp. 307): sediment contributors and hydrodynamic environments. Marine Geology, 271, 260-277.
Thouveny, N., de Beaulieu, J.-L., Bonifay, E., Creer, K.M., Guiot, J., Icole, M., Johnsen, S., Jouzel, J., Reille, M., Williams, T. and Williamson, D., 1994. Climate variations in Europe over the past 140 kyr deduced from rock magnetism. Nature, 371, 503-506.
Thouveny, N., Moreno, E., Delanghe, D., Candon, L., Lancelot, Y. and Shackleton, N.J., 2000. Rock magnetic detection of distal ice-rafted debries: clue for the identification of Heinrich layers on the Portuguese margin. Earth and Planetary Science Letters, 180, 61-75.
Van der Land, C., Mienis, F., De Haas, H., Frank, N., Swennen, R. and Van Weering, T.C.E., 2010. Diagenetic processes in carbonate mound sediments at the southwest Rockall Trough margin. Sedimentology, 57, 912-931.
Van Geet, M., Swennen, R. and Wevers, M., 2001. Towards 3-D petrography: application of microfocus computer tomography in geological science. Computer & Geosciences, 27, 1091-1099.
Van Rooij, D., Blamart, D. and Unnithan, V., 2001. Cruise report MD123-Géosciences: Leg 2, part GEOMOUND, RCMG, Gent.
Vance, D. and Burton, K., 1999. Neodymium isotopes in planktonic foraminifera: a record of the response of continental weathering and ocean circulation rates to climate change. Earth and Planetary Science Letters, 173(4), 365-379.
Vance, D., Scrivner, A.E., Beney, P., Staubwasser, M., Henderson, G.M. and Slowey, N.C., 2004. The use of foraminifera as a record of the past neodymium isotope composition of seawater. Paleoceanography, 19(2), doi:10.1029/2003PA000957.
Velde, B., 1995. Origin and mineralogy of clays. Clays and the environment. Springer-Verlag, Berlin, 356 pp.
Vlassenbroeck, J., Cnudde, V., Masschaele, B., Dierick, M., Van Hoorebeke, L. and Jacobs, P., 2007. A comparative and critical study of X-ray CT and neutron CT as non-destructive material evaluation techniques. Building Stone Decay: From Diagnosis to Conservation(271), 277-285.
Wachter, E.A. and Hayes, J.M., 1985. Exchange of Oxygen Isotopes in Carbon Dioxide-Phosphoric Acid Systems. Chemical Geology, 52(3-4), 365-374.
Wahsner, M., Muller, C., Stein, R., Ivanov, G., Levitan, M., Shelekhova, E. and Tarasov, G., 1999. Clay-mineral distribution in surface sediments of the Eurasian Arctic Ocean and continental margin as indicator for source areas and transport pathways - a synthesis. Boreas, 28(1), 215-233.

Part 2

The terrigenous fraction in Challenger Mound

Chapter 3 - The importance of the terrigenous fraction within a cold-water coral mound: a case study.

Abstract

In the nineties, cold-water coral mounds were discovered in the Porcupine Seabight (NE Atlantic, west of Ireland). A decade later, this discovery led to the drilling of the entire Challenger cold-water coral mound (Eastern slope, Porcupine Seabight) during IODP Expedition 307. As more than 50 percent of the sediment within Challenger Mound consists of terrigenous material, the terrigenous component is equally important for the build-up of the mound as the framework-building corals. Moreover, the terrigenous fraction contains important information on the dynamics and the conditions of the depositional environment during mound development. In this study, the first in-depth investigation of the terrigenous sediment fraction of a cold-water coral mound is performed, combining clay mineralogy, sedimentology, petrography and Sr-Nd-isotope analysis on a gravity core (MD01-2451G) collected at the top of Challenger Mound.

Sr- and Nd-isotopic fingerprinting identifies Ireland as the main contributor of terrigenous material in Challenger Mound. Besides this, a variable input of volcanic material from the northern volcanic provinces (Iceland and/or the NW British Isles) is recognized in most of the samples. This volcanic material was most likely transported to Challenger Mound during cold climatic stages. In three samples, the isotope ratios indicate a minor contribution of sediment deriving from the old cratons on Greenland, Scandinavia or Canada. The grain-size distributions of glacial sediments demonstrate that ice-rafted debris was deposited with little or no sorting, indicating a slow bottom-current regime. In contrast, interglacial intervals contain strongly current-sorted sediments, including reworked glacio-marine grains. The micro textures of the quartz-sand grains confirm the presence of grains transported by icebergs in interglacial intervals. These observations highlight the role of ice-rafting as an important transport mechanism of terrigenous material towards the mound during the Late Quaternary.

Furthermore, elevated smectite content in the siliciclastic, glaciomarine sediment intervals is linked to the deglaciation history of the British-Irish Ice Sheet (BIIS). The increase of smectite is attributed to the initial stage of chemical weathering processes, which became activated following glacial retreat and the onset of warmer climatic conditions. During these deglaciations a significant change in the signature of the detrital fraction and a lack of coral growth is observed. Therefore, we postulate that the deglaciation of the BIIS has an important effect on mound growth. It can seriously alter the hydrography, nutrient supply and sedimentation processes, thereby affecting both sediment input and coral growth and hence, coral mound development.

This chapter is based on Pirlet, H., Colin, C., Thierens, M., Latruwe, K., Van Rooij, D., Foubert, A., Frank, N., Blamart, D., Huvenne, V.A.I., Swennen, R., Vanhaecke, F. and Henriet, J.-P. (in press) The importance of the terrigenous fraction within a cold-water coral mound: A case study. Marine Geology, doi: 10.1016/j.margeo.2010.05.008 (COCARDE special issue).

3.1 Introduction

Cold-water corals have been observed along the northeastern Atlantic margin from Norway (Freiwald *et al.*, 1999; Lindberg *et al.*, 2007) to the Gulf of Cadiz (Foubert *et al.*, 2008; Wienberg *et al.*, 2009) and even as far south as Mauritania (Colman *et al.*, 2005). In the Porcupine Seabight, southwest of Ireland (Fig. 3.1), these cold-water corals built large mound structures up to a height of 250 m and with a diameter of several kilometers (De Mol *et al.*, 2002). One of these carbonate mounds constitutes Challenger Mound, located on the eastern flank of the Porcupine Seabight (Fig. 3.1). Challenger Mound is the first, and so far only, cold-water coral mound that was drilled down to its base during IODP (Integrated Ocean Drilling Program) Expedition Leg 307. This drilling revealed the presence of well-preserved cold-water corals (mainly *Lophelia pertusa* and *Madrepora oculata*) throughout the entire mound sequence (IODP 307 Expedition Scientists, 2005). Strontium-dating of the corals indicate that mound growth started 2.7 Ma (Kano *et al.*, 2007) and the mound grew rapidly to a height of 130 m before growth was interrupted at ca. 1.7 Ma BP. A second coral growth phase lasted from ca. 1.0 Ma to 0.5 Ma (top ~23 m) (Kano *et al.*, 2007).
The mound sediments, that accumulate between the cold-water coral framework consist for more than 50 percent of terrigenous material (Titschack *et al.*, 2009). However, until now, no in-depth study of this fraction has been conducted. It has been suggested that the alternation of carbonate-rich and siliciclastic sediment is steered by climate changes, with an increased siliciclastic influx and/or reduced production of biogenic carbonate during glacial intervals (Frank

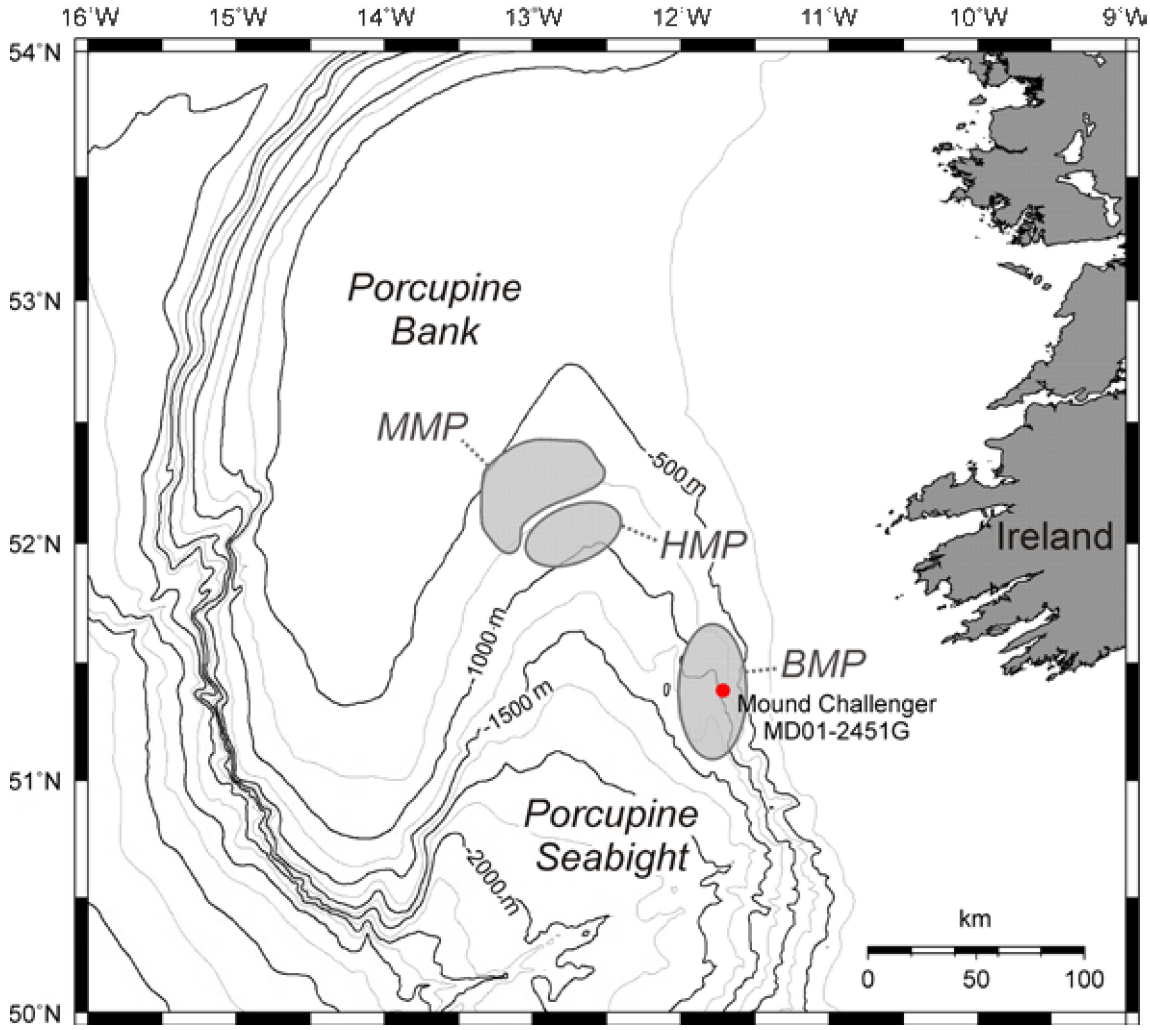

Fig. 3.1 *Location of the study area. The three main cold-water coral mound provinces of the Porcupine Seabight and Mound Challenger are indicated. (MMP = Magellan mound province, HMP = Hovland mound province, BMP = Belgica mound province).*

et al., 2009; Titschack *et al.*, 2009). A thorough characterization of the terrigenous fraction is also crucial given that it plays an important role in diagenetic processes. Ferdelman *et al.* (2006) and Wehrmann *et al.* (2009) already concluded that the reactive iron of the siliciclastic fraction buffers the pore-water carbonate system whereas Larmagnat and Neuweiler (in review) stated that an argillaceous sediment matrix will act as an inhibitor for organomineralisation. Furthermore, the analysis of the siliciclastic sediment fraction, and the clay minerals in particular, is important to understand the magnetic signal which is recorded in the mound (Foubert and Henriet, 2009). Moreover, the terrigenous sediment also provides crucial information on the hydrodynamics in the study site, weathering intensity on the near-by continents (Colin *et al.*, 2006) and sedimentary processes such as ice-rafting, turbidity flows and current reworking (Huvenne *et al.*, 2009; Revel *et al.*, 1996a), which transport and/or erode sediments to and from the mound. The present paper aims to constrain for the first time the source areas of the siliciclastic sediment fraction in Challenger Mound as well as its mode of transport and the timing of deposition. Furthermore, changes in the terrigenous sediment are linked to climatic variations and the influence of the proximal British-Irish Ice Sheet and their effects on cold-water coral mound growth are discussed.

3.2 Regional setting

Cold-water coral mounds occur in three well-delineated provinces in the Porcupine Seabight (De Mol *et al.*, 2002). Challenger Mound is situated in the Belgica Mound Province on the eastern slope of the Seabight (Fig. 3.1). This province comprises 66 mounds, with heights up to 190 m above the present-day seabed, and 17 buried mounds in water depths ranging from 550 to 1025 m (De Mol *et al.*, 2002; Foubert and Henriet, 2009). The mounds have conical, circular to NNE-SSW elongated shapes and seem to be aligned along the bathymetric contours, parallel to the continental margin (Beyer *et al.*, 2003). Challenger Mound is a typical conical, asymmetrical buried mound, with a more buried upslope side and a well-exposed basin-ward side (Fig. 3.2), which is subjected to strong bottom currents and active sediment transport as indicated by numerous bedforms (Foubert *et al.*, 2005). The basin-ward side of Challenger still protrudes 120 m above the surrounding seabed, while the upslope side

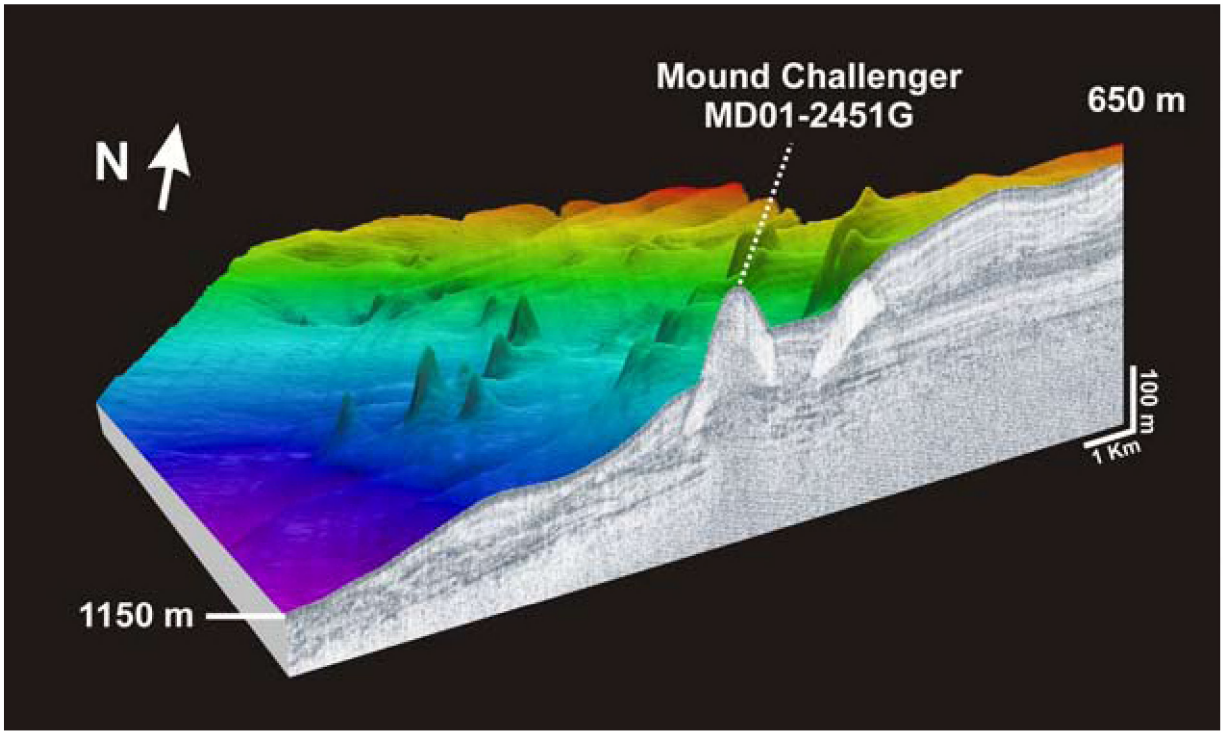

Fig. 3.2 *Geomound Multibeam bathymetry (courtesy AWI Bremerhaven) (Beyer et al., 2003) in combination with a single channel seismic reflection profile (courtesy RCMG, Gent) of the Belgica mound province (51°10'N – 51°40'N / 11°30'W – 11°50'W).*

is only 30-40 m exposed. The height of Challenger Mound above its actual base is 155 m (IODP 307 Expedition Scientists, 2005). The slopes of the mound grade steeply at an angle varying between 21° and 33° (Foubert and Henriet, 2009). Surface observations and ROV video imagery reveal little to no live coral coverage on the mound (Foubert *et al.*, 2005).

The general hydrography of the Porcupine Basin is described in detail in several studies (Hargreaves, 1984; Rice *et al.*, 1991; White, 2007; White *et al.*, 2005). The depth range of the mound provinces in the Porcupine Seabight coincides with the upper boundary of the Mediterranean Outflow Water (MOW) (800-1000 m), which is overlain by Eastern North Atlantic Water (ENAW). Along the eastern slope of the Porcupine Seabight, strong internal waves and tides are recognized within the depth interval of the outcropping mounds (White, 2007). Current measurements indicate an annual mean northward current with a speed of 3-10 cm/s near the seafloor (Pingree and Le Cann, 1990; Rice *et al.*, 1991) although much stronger bottom currents have been inferred at the eastern margin of the Porcupine Seabight. Dorschel *et al.* (2007) measured bottom current speeds up to 51 cm/s on the summit of Galway Mound (Belgica Mound Province), while Roberts *et al.* (2005) recorded peak current speeds of 70 cm/s for the same mound.

3.3 MD01-2451G lithology and chronological framework

The lithology of this core has been earlier discussed by Foubert and Henriet (2009) and Foubert *et al.* (2007). Based on the X-Ray fluorescence (XRF) results, magnetic susceptibility (MS) and density, the core MD01-2451G was subdivided in two major units (Fig. 3.3) (Foubert and Henriet, 2009; Foubert *et al.*, 2007). Unit A (0-400 cm) is characterized by a high-frequent alternation of light-grey and dark layers. The light-grey layers are characterized by abundant cold-water coral fragments whereas in the dark layers, no

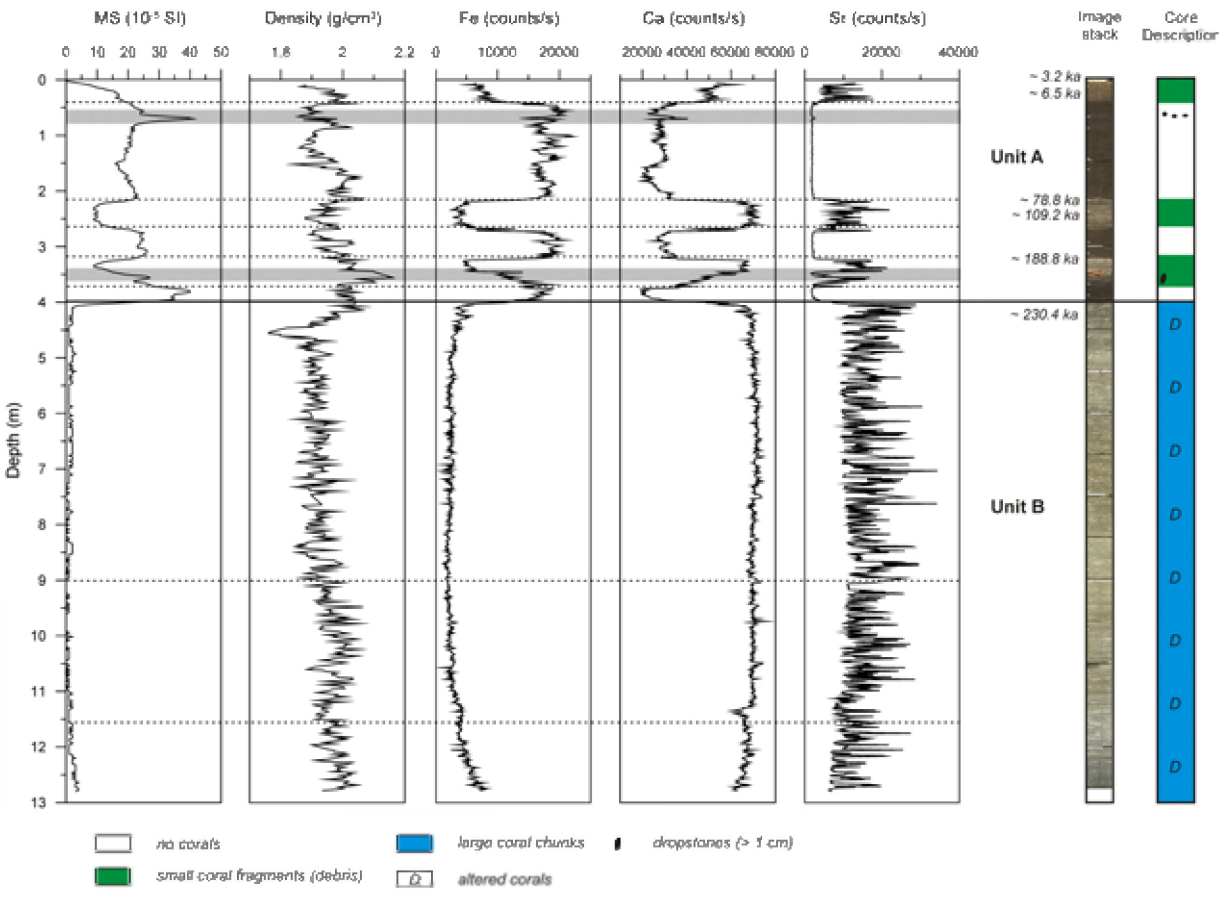

Fig. 3.3 *Overview of the stratigraphy of core MD01-2451G featuring the magnetic susceptibility (MS), density, X-ray fluorescence (XRF), image stack and a basic core log (Modified after Foubert and Henriet (2009)). U-Th ages of the corals are also noted (Frank et al., 2009).*

corals were observed. The XRF-scanning records high Ca content in the light-grey intervals (0-40 cm, 219-270 cm and 323-375 cm), while the dark layers correspond to an increased content of Fe (40-219 cm, 270-323 cm and 375-400 cm) (Fig. 3.3). The variable, but generally elevated Sr content in the light-grey zones is explained by the presence of small *Madrepora oculata* fragments and other aragonitic biogenic components (Foubert and Henriet, 2009). The presence of dropstones was observed at 60-70 cm and 350-356 cm (Foubert *et al.*, 2007). The transition from the dark, Fe-rich layers to the overlying light, coral-bearing intervals is gradual. The base of every dark layer, however, reveals a sharp boundary with the underlying layer (Foubert and Henriet, 2009). Unit B (400-1280 cm) reveals high Ca-values and low MS- and Fe-values. The high Sr values are due to the high concentration of big coral chunks, consisting mainly of *Lophelia pertusa*. In the lower part of unit B, dissolution of the corals was observed and is interpreted to be linked to extremely low values of the MS in unit B (Foubert and Henriet, 2009; Foubert *et al.*, 2007).
Six cold-water corals, collected in the light-grey layers, have been dated by ^{230}Th/U method by Frank *et al.* (2009) (Fig. 3.3). The deep-sea corals yield ^{230}Th/U ages ranging between 230.4 ± 2.9 ka and 3.2 ± 0.1 ka (Frank *et al.*, 2009). ^{230}Th/U dating of the corals indicates that coral growth in unit B ended abruptly around 230 ka ago (Marine Isotope Stage (MIS) 7). ^{230}Th/U dating indicates also that unit A represents a condensed record of three glacial-interglacial cycles during the last 200 ka (Fig. 3.3). The upper 40 cm of the core corresponds to the Holocene: at 6 cm depth, the coral has an age of 3.2 ± 0.1 ka, at 31 cm an age of 6.5 ± 0.1 ka. The interval between 219 and 270 cm reveals ages between 78.8 ± 0.5 and 109.2 ± 0.8 ka. At 326 cm depth, the coral dates 188.8 ± 2.3 ka. ^{230}Th/U dating demonstrates that these light-grey level layers (rich cold-water corals layers) were mainly deposited during interglacial periods (Foubert and Henriet, 2009).

3.4 Material and Methods

Core MD01-2451G was obtained with a gravity corer during the MD123-Geosciences campaign with the French R/V Marion Dufresne in September 2001. The core was retrieved from the top of Challenger Mound (51°22'47.99"N and 11°43'03.45"W) at a water depth of 762 m with a recovery of 1284 cm.

3.4.1 Grain-size analysis

Grain-size distribution measurements of siliciclastic sediments (section 2.4) were carried out at the National Oceanography Centre Southampton (NOCS), with a Malvern Mastersizer 2000 with autosampler. An average measurement precision of 4.4% (on grain-size mode) was estimated for similar sediments by Thierens *et al.* (2010). Samples were analyzed with a resolution of 10 cm in the first 5 m of the core and a resolution of 50 cm in the part below 5 m. For each sample the percentages of clay (<2 µm), silt (2-63 µm) and sand (63-2000 µm) were calculated.

3.4.2 Petrography and grain-surface microtextures

Thin sections for classic light microscopy and cold cathode luminescence (CL) (section 2.5.1) were manufactured and studied at the Department of Earth and Environmental Sciences (Leuven University). Cathode luminescence was carried out on an in-house built (Technosyn) cold cathodo-luminescence model 2800, Mark II in combination with a Zeiss microscope. In this paper, 5 thin sections of the upper 400 cm of the core were selected (9-11 cm, 59-61 cm, 230-232 cm, 275-277 cm and 399-401 cm).
Grain surfaces of sand-sized quartz grains of two samples (18-19 cm and 238-239 cm) were imaged and examined for microtextural evidence of their source/transport history. The subsamples were disaggregated (30 second sonication), dried, mounted on aluminium stubs and gold coated (Polaron E5150 Sputter Coating Unit). Scanning electron microscopic analysis of grain surface features took place at the Electron Microscopy Facility, University College Cork using a JEOL JSM 5510 Scanning Electron Microscope (acceleration voltage of 5 kV at 10 mm working distance) with attached INCA x-sight Energy Dispersive X-ray Spectroscopy Detector (Oxford Instruments), operating in secondary electron mode.
The combination of microtexture occurrence and dominance enables the identification of grain types which allow a differentiation of various sediment transport mechanisms, such as ice-rafting (Mahaney, 2002; Mahaney *et al.*, 2001;

Thierens *et al.*, 2010). A qualitative estimate of glacially versus non-glacially transported grains was aimed at in this study.

3.4.3 XRD analysis of the clay fraction

Clay minerals were identified within 68 samples by standard X-ray diffraction (XRD) analysis using a PANalytical diffractometer at the IDES laboratory (University of Paris XI) on oriented mounts of non-calcareous clay-sized (< 2 µm) particles. The oriented mounts were obtained following the methods described in section 2.6. Semi-quantitative estimates of peak areas of the basal reflections for the main clay mineral groups of smectite (including mixed-layers) (1.5–1.7 nm), illite (1.0 nm), and kaolinite/chlorite (0.7 nm) were carried out on the glycolated diffractograms using the MacDiff software (Petschick, 2000).

3.4.4 Neodymium and strontium isotope analysis

Nd and Sr isotope measurements were performed on the carbonate-free sediment fraction of 17 samples using a Multi-Collector ICPMS unit (Thermo Scientific Neptune) at the Department of Analytical Chemistry, Ghent University. The JNdi-1 standard was used as reference material for neodymium ($^{143}Nd/^{144}Nd$ = 0.51215, $^{146}Nd/^{144}Nd$ = 0.7219) (Tanaka *et al.*, 2000) to correct for instrumental mass discrimination using external standardization (sample-standard bracketing). For the measurement of the Sr isotopes the NIST SRM 987 standard was used. The standard deviation on these measurements were ≈ $80*10^{-6}$ for Nd and $50*10^{-6}$ for ≈ Sr. Samples were prepared for isotope analysis according to the method described in section 2.7.

3.5 Results

3.5.1 Siliciclastic grain-size distribution

Unit A reveals an alternation of bimodal grain-size distributions with a pronounced coarse mode in the light-grey, Ca-rich layers and an elevated contribution of the fine mode in the dark, Fe-rich intervals (Fig. 3.4). The grain-size distributions in the light-grey intervals (0-40 cm, 219-270 cm and 323-375 cm) represent fine-skewed, well-sorted medium to fine sands with a pronounced peak around 100 µm. The sand content (63-2000 µm) in the light-grey layers varies between 54 and 73 V%, the silt-percentage (2-63 µm) between 24 and 43 V%, whereas the clay (< 2 µm) ranges from 1 to 3 V%. The grain-size distributions in the dark intervals (40-219 cm, 270-323 cm and 375-400 cm) are coarse-skewed and poorly sorted with a fine mode around 5 µm and a coarse mode at about 100 µm. The sand-percentage in the dark layers varies between 18 and 30 V%, the silt-content between 65 and 74 V%, whereas the clay ranges from 4 to 7 V%.
The grain-size measurements of unit B reveal fine-skewed, poorly sorted coarse silts with a unimodal distribution (mode between 40 and 50 µm). The sand-percentage of unit B varies between 9 and 39 V%, the silt fraction between 65 and 85 V%, whereas the clay ranges from 2 to 5 V%. There was no clear grading upward cycles observed in any of the intervals mentioned above.

3.5.2 Petrography and surface microtextures of quartz grains

Thin sections of unit A reveal that the terrigenous sediment fraction of this core is mainly dominated by quartz grains (Fig. 3.5 A, B, D). However, feldspar and calcite are also observed abundantly while dolomite and pyrite occur as minor components in the matrix. In the light-grey layers of unit A, little fine matrix was noticed and embedded grains exhibit diameters of 200 µm (Fig. 3.5 B). In these zones, foraminifers and other biogenic fragments occur abundantly and are commonly broken (Fig. 3.5 C). The microtextures of the sand-sized quartz grains in the light layers of unit A (18-19 cm and 238-239 cm) are dominated by angular, sharp edges, conchoidal and linear fractures and linear and arc-shaped steps (Fig. 3.5 E, F). Furthermore quartz grains with predominantly rounded edges, dissolution etching and solution pits occur (Fig. 3.5 G). Occasionally more rounded quartz grains with frequent V-shaped percussion cracks, moderate fractures and/or steps are observed (Fig. 3.5 H).
In the dark intervals of unit A, the grains are embedded in a fine matrix (Fig. 3.5 A, D). In contrast to the light intervals of unit A, little or no foraminifers or biogenic fragments are observed.

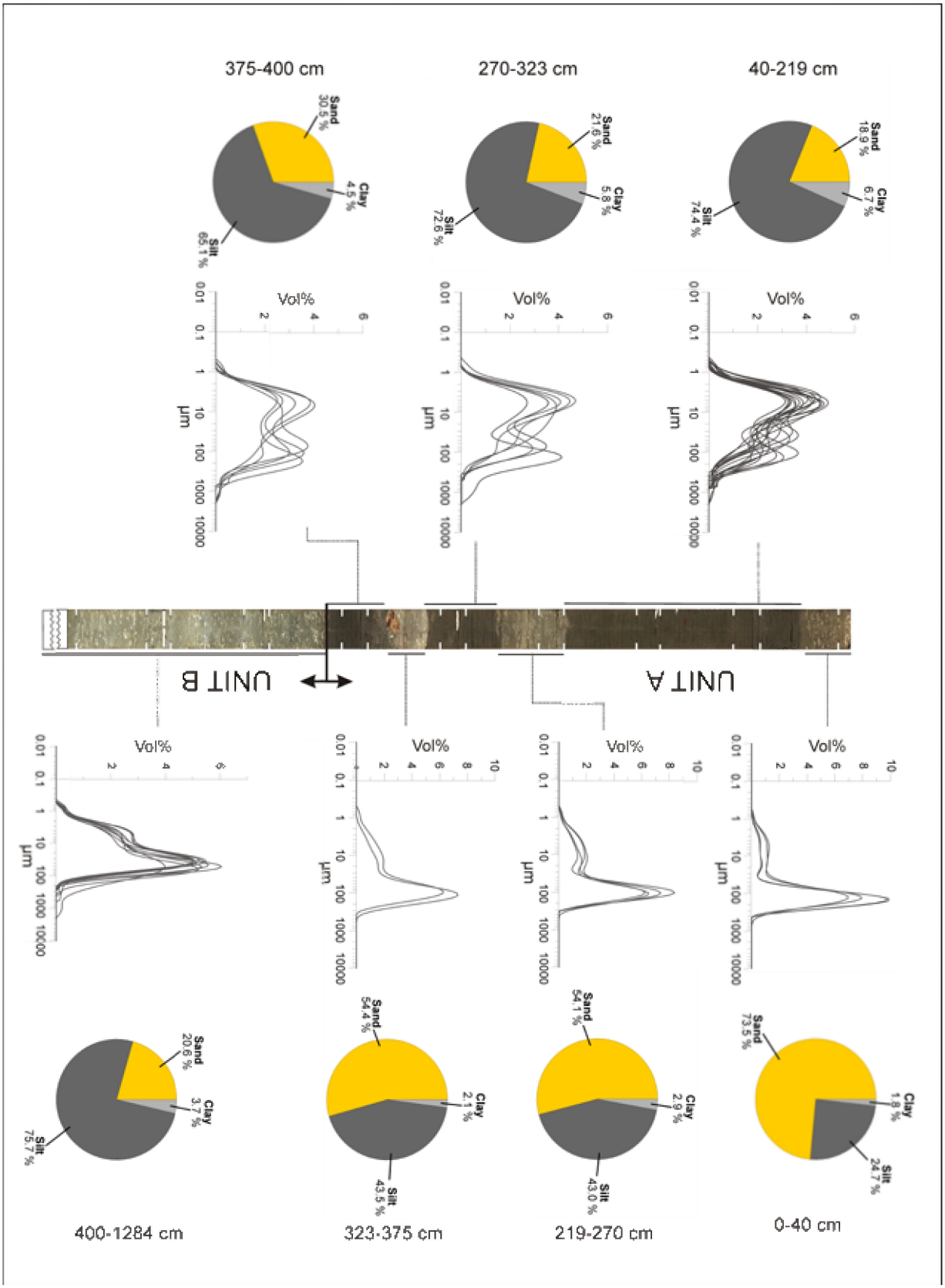

Fig. 3.4 *The results of the grainsize analysis of the carbonate-free sediment of core MD01-2451G.*

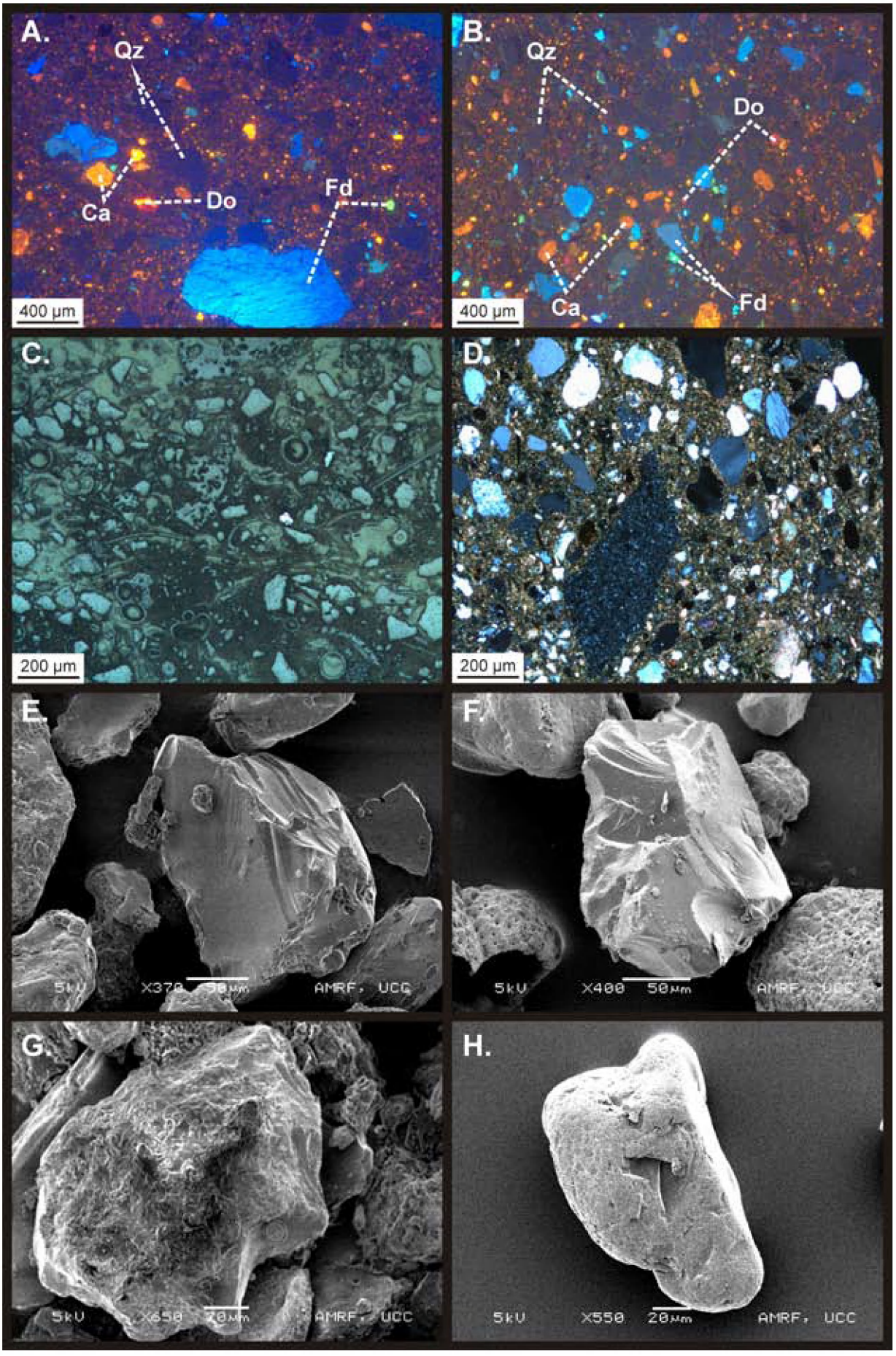
A.
Qz
Ca
Do
Fd
400 µm
B.
Qz
Do
Ca
Fd
400 µm
C.
200 µm
D.
200 µm
E.
5kV X370 50µm AMRF, UCC
F.
5kV X400 50µm AMRF, UCC
G.
5kV X650 20µm AMRF, UCC
H.
5kV X550 20µm AMRF, UCC

Fig. 3.5 (Left) *A. Cold cathode luminescence (CL) of the sediment from a Fe-rich interval in Unit A (59-61 cm) (Qz = quartz, Ca = calcite, Fd = Feldspar, Do = Dolomite). B. CL of the sediment from a Ca-rich interval in Unit A (9-11 cm). C. The presence of broken foraminifers shells and biogenic fragments in the Ca-rich layers (reflected light) (9-11 cm). D. Ice rafted debris embedded in a fine matrix (plane-polarized light) (398-400 cm). E. and F. Mechanically abraded quartz grains with surfaces dominated by angular, sharp edges, conchoidal and linear fractures and linear and arc-shaped steps. G. Quartz grains affected by chemical abrasion featuring rounded edges, dissolution etching and solution pits. H. Rounded quartz grain with frequent V-shaped percussion cracks, moderate fractures and/or steps and dissolution features.*

This is in line with the low Ca and Sr contents that were recorded in these zones (Fig. 3.3). The detrital grains in these dark layers have variable diameters up to 1 cm whereas the light layers reveal more uniform grain sizes (Fig. 3.5 A, D).
Cold cathode luminescence of the thin sections of unit A revealed the presence of dark brown to dark grey luminescent quartz grains (Fig. 3.5 A, B). Furthermore, green luminescent plagioclase and blue K-feldspar grains and red dolomite were observed. Also, a significant amount of bright-yellow calcite occurred in the samples. The dolomite and calcite observed in these thin sections most likely have a detrital origin since no well-formed, diagenetic crystals or cement sequences as described by Pirlet *et al.* (2010) were observed. It is important to note that these detrital carbonates were not taken into account in the analyses of the siliciclastic fraction since all samples were decalcified prior to analysis.

3.5.3 Clay mineralogy

Illite (18-43%) and smectite (14-65%) are the two dominant clay minerals in the core MD01-2451G sedimentary record (Fig. 3.6). Chlorite (6-24%) and kaolinite (10-21%) are less abundant. In general, the illite, chlorite and kaolinite content are inversely correlated to the smectite content. Variations in the kaolinite content are small throughout the record and are within the analytical limits of the method. Smectite is characterized by high amplitude fluctuations (14-65%) in unit A.

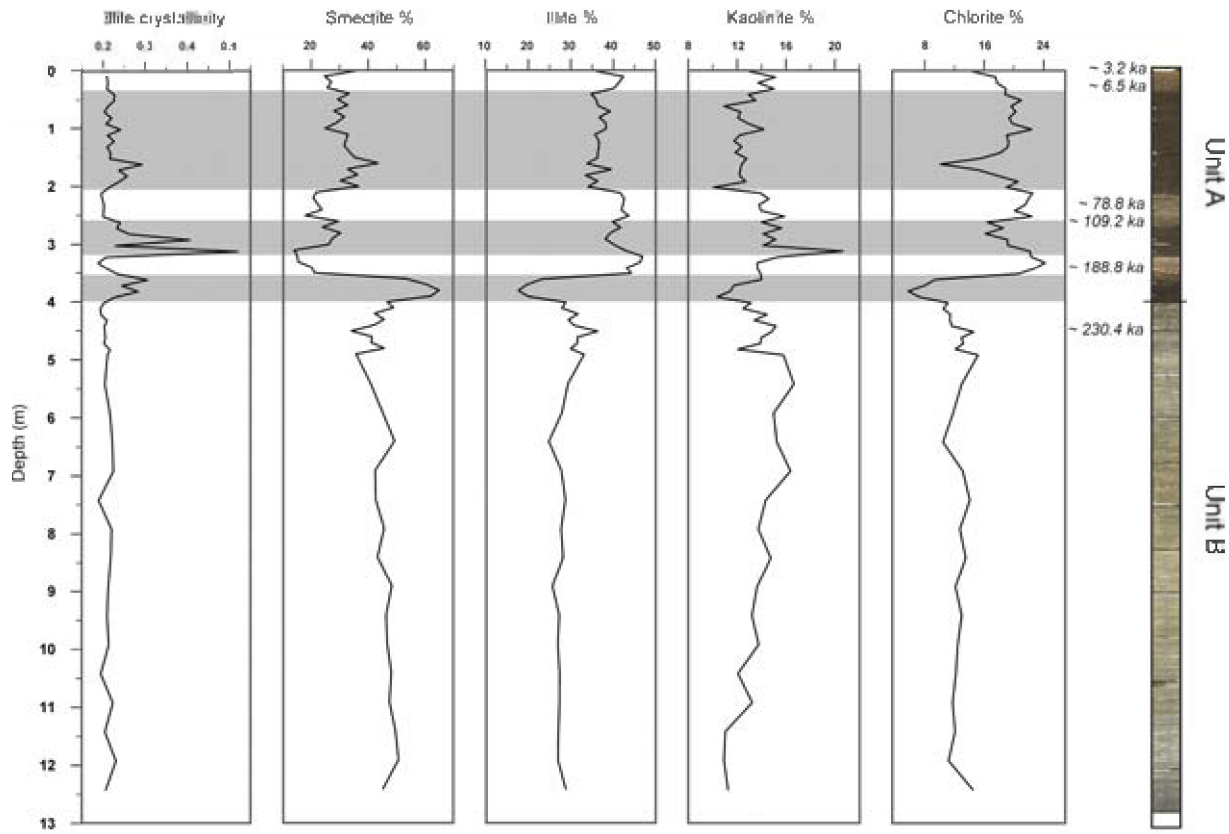

Fig. 3.6 *Illite crystallinity and the relative abundance of the clay minerals: illite, smectite, kaolinite and chlorite in core MD01-2451G. The grey bars correspond with the siliciclastic, glaciomarine intervals of the core.*

The light layers in unit A are characterized by a low smectite content whereas the dark layers reveal higher smectite values. Throughout unit B, the smectite content remains relatively stable with an average around 45%. Illite and chlorite proportions are lower in unit B (30% and 14% respectively) compared to unit A (40% and 22% respectively).
The illite crystallinity reveals 3 peaks in unit A, which are well correlated with the intervals characterized by an increased smectite content (Fig. 3.6).

3.5.4 Sr and Nd isotope results

The $^{87}Sr/^{86}Sr$ ratios and $\varepsilon_{Nd}(0)$ values measured on the carbonate-free fraction of core MD01-2451G are listed in table 3.1. The $^{87}Sr/^{86}Sr$ ratio and the ε_{Nd} (0) vary significantly between 0.73093 and 0.71512 and between -4.9 and -15.8, respectively (table 3.1). Generally, the $^{87}Sr/^{86}Sr$ ratio is higher in the dark layers of unit A compared to the values in the light-grey layers while the ε_{Nd} (0) values are more radiogenic in the light-grey layers. Care has to be taken when interpreting the $^{87}Sr/^{86}Sr$ isotope ratios of bulk sediment since they are influenced by the grain-size distribution (Revel *et al.*, 1996a). In this regard, the Nd isotopic composition is more reliable as it is not or less affected by grain-size variations (Goldstein *et al.*, 1984; Revel *et al.*, 1996b).

3.6 Discussion

3.6.1 Hydrodynamics

Grain-size distributions of the siliciclastic fraction are used to infer the hydrographic conditions at the time of deposition (Ballini *et al.*, 2006; McCave and Hall, 2006; Rüggeberg *et al.*, 2005). The grain-size measurements throughout unit B display a similar fine skewed, poorly sorted distribution with a mode around 40-50 µm, indicating stable hydrographic conditions during the deposition of these sediments (Fig.

Sample depth (cm)	$^{87}Sr/^{86}Sr$	$^{143}Nd/^{144}Nd$	$\varepsilon_{Nd}(0)$	Position in core
28	0.72801	0.511831	-15.7	Unit A: Light-grey level
48	0.72917	0.512100	-10.5	Unit A: Dark-grey level
68	0.72818	0.511894	-14.5	Unit A: Dark-grey level
88	0.72837	0.512119	-10.1	Unit A: Dark-grey level
108	0.72909	0.512147	-9.6	Unit A: Dark-grey level
128	0.72819	0.512090	-10.7	Unit A: Dark-grey level
148	0.72676	0.512109	-10.3	Unit A: Dark-grey level
168	0.72597	0.512114	-10.2	Unit A: Dark-grey level
188	0.72631	0.512111	-10.3	Unit A: Dark-grey level
208	0.72634	0.512099	-10.5	Unit A: Dark-grey level
228	0.71556	0.512259	-7.4	Unit A: Light-grey level
248	0.72169	0.512177	-9.0	Unit A: Light-grey level
328	0.72298	0.511928	-13.8	Unit A: Light-grey level
348	0.72412	0.512197	-8.6	Unit A: Light-grey level
389	0.73093	0.512096	-10.6	Unit A: Dark-grey level
428	0.71527	0.512388	-4.9	Unit B
488	0.72156	0.512093	-10.6	Unit B

Table 3.1 *Results of the Nd- and Sr-isotope measurements of the different samples and their position in the core MD01-2451G.*

3.4). However, caution has to be taken when interpreting these grain-size distributions as large coral fragments in unit B indicate the presence of a dense coral framework during the deposition of this layer. Major coral development may have baffled the bypassing sediment (de Haas *et al.*, 2009; Dorschel *et al.*, 2007) altering the original hydrographic signal. Mienis *et al.* (2009) already reported that less sediment is resuspended on a coral mound compared to the off-mound site. This might explain why the grain-size distributions are poorly-sorted.

The grain-size distribution in unit A reveals, in contrast to unit B, significant hydrodynamic changes. The dark intervals of unit A show a poorly-sorted bimodal grain-size distribution pointing towards ice-rafting as a likely sedimentation mechanism (Fig. 3.4). The presence of dropstones (up to several centimeters) and the absence of foraminifers or other biogenic fragments (Fig. 3.5 A, D) in these layers suggest that these sediments are of glaciomarine origin. Hereafter, these siliciclastic, glaciomarine sediments, deposited during or at the end of cold stages, will be referred to as 'glacial sediment'. The fact that little or no sediment sorting is evident suggests that bottom currents were reduced during glacial intervals. This is also supported by the fine lamination that was observed in these sediments. The abrupt change in grain-size, observed at the base of each of the glacial layers, might indicate the presence of an unconformity.

In contrast, the light-grey zones of unit A, which are mainly deposited during interglacial periods (Frank *et al.*, 2009), are characterized by identical, bimodal grain-size distributions with a pronounced coarse mode, indicating a strong sorting process (Fig. 3.4). The alternation of sluggish glacial currents and a significant increase of bottom-current speed during interglacials was previously reported (Dorschel *et al.*, 2005; Foubert *et al.*, 2007; Rüggeberg *et al.*, 2007; Van Rooij *et al.*, 2007). These authors attributed the increase in current speed in interglacials to the re-introduction of the northward flowing MOW. Generally, increased bottom currents are considered to be a prerequisite for cold-water coral growth since they prevent the corals from sediment burial and deliver nutrients to the coral polyps (Freiwald *et al.*, 2004). However, the increased bottom currents in the interglacial intervals of unit A did not lead to enhanced mound growth. On the contrary, these intervals are condensed sections with small coral fragments and broken foraminifers suggesting that these biogenic fragments were disintegrated and possibly reworked (Fig. 3.5C). Moreover, the corals might have been further fragmented by the enhanced activity of bio-eroders during the reduced sedimentation conditions (Beuck and Freiwald, 2005). The fragmentation of the corals can occur shortly after coral growth as evidenced by a fragmented coral of only 2 ka in the top of the core. Moreover, it is an ongoing process given that nowadays only coral debris is observed at the top of Challenger Mound (Foubert *et al.*, 2005). The subsequent burial of these coral fragments during interglacial periods is a slow process as indicated by the big time differences in the age of corals deriving from the same layer (e.g. 78.8 ka and 109.2 ka between 219 and 270 cm). Hence, the absence of a large coral framework in unit A is a fundamental difference with unit B where a dense framework was able to baffle the sediment, leading to faster burial which caused better coral preservation and increased mound growth.

Quartz grains within the interglacial sediments of unit A bear surface textures that can be attributed to mechanical, glacial abrasion (Fig. 3.5 E, F). Angular quartz-sands with abundant, deeply embedded and sharp mechanical abrasion features, such as conchoidal/linear fractures and arc-shaped/linear steps, are known from environments influenced by glacial erosion and/or transport (Mahaney (2002) and references therein). The occurrence of these glacially-transported grains suggests the reworking of glacial sediments during interglacial bottom current transport and deposition. This also indicates that an important part of the terrigenous fraction, even in interglacial intervals, was originally transported to Challenger Mound by icebergs during the Late Quaternary cold stages.

3.6.2 Sediment provenance

3.6.2.1 Sr-Nd isotopic composition

The average $^{87}Sr/^{86}Sr$ ratios (0.72521) and $\varepsilon_{Nd}(0)$ values (-10.4) reveal a dominant contribution of non-volcanogenic, continental crust-derived sediment throughout core MD01-2451G (Fig. 3.7). Given the proximity of Ireland to the study area, a continental input from the Irish mainland is a premise. The British-Irish Isles feature distinct $^{87}Sr/^{86}Sr$ and ε_{Nd} values of 0.734 and -12.1

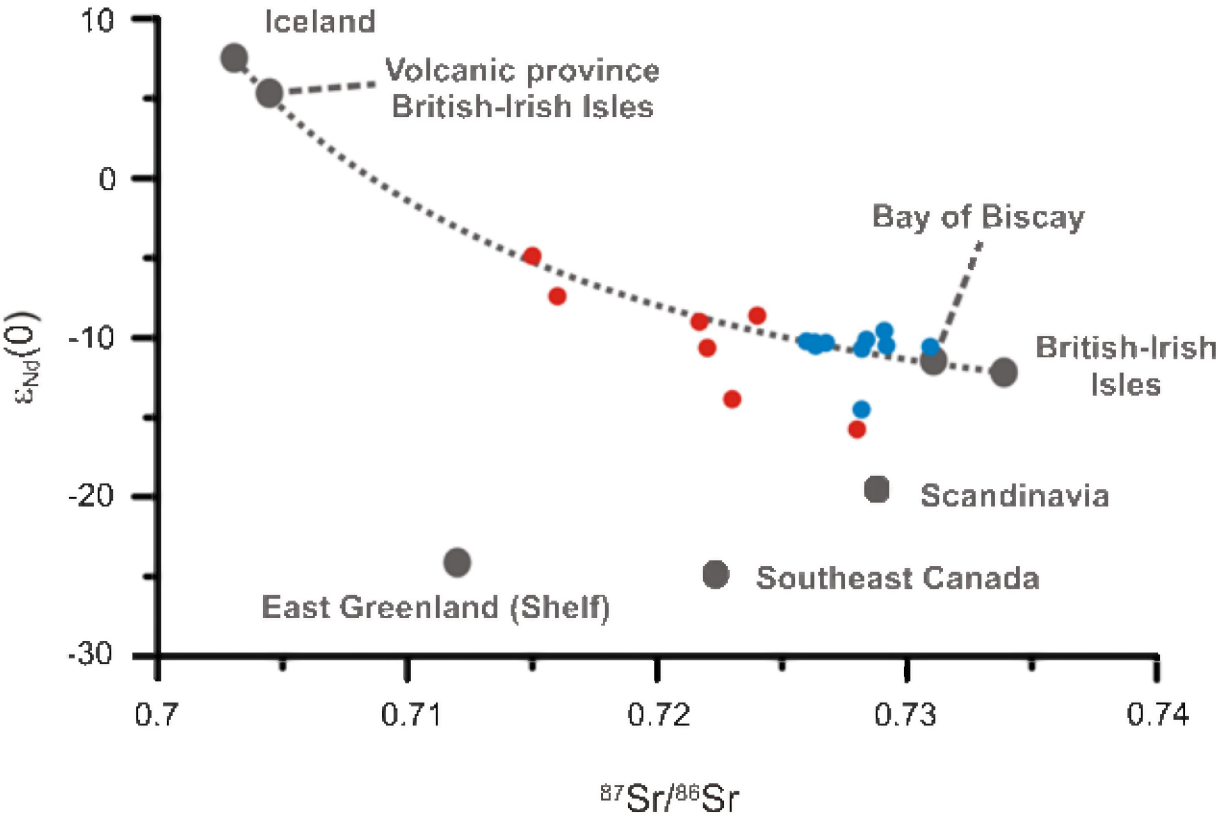

Fig. 3.7 *Sr-Nd isotopic composition of the carbonate-free sediment in core MD01-2451G. Also shown are the published data from potential sedimentary sources: Iceland, east Greenland shelf, southeast Canada, Scandinavia, Bay of Biscay and British-Irish Isles (Revel et al., 1996b). The dashed line represents a mixing hyperbole between the isotopic compositions of Iceland and the British-Irish Isles. The red dots are sediment samples deriving from unit B and the light-grey, interglacial layers of unit A, whereas the blue dots derive from the dark-grey glacial intervals of unit A.*

respectively (Revel *et al.*, 1996b). It is suspected that most of the detrital carbonates which were observed in the thin sections also derive from the Irish mainland since Carboniferous limestone deposits cover the entire central part of Ireland. However, most of the $^{87}Sr/^{86}Sr$ ratios and ε_{Nd} values in MD01-2451G, plot on a mixing hyperbole, indicating the presence of two source-areas: (1) the crustal rocks of the British-Irish Isles and (2) the northern volcanic provinces (Fig. 3.7). This mixing hyperbole is based on the isotopic composition and element concentration of both end-members sources (Faure, 1986). It also implies a significant contribution of volcanic material in the sediments of Challenger Mound. The presence of numerous blue to green luminescent plagioclase grains in the thin sections (Fig. 3.5 A, B) might indicate the influx of basaltic material (Andrews, 2008). Potential volcanic sources in the North Atlantic include Iceland, the NW British-Irish Isles and the Faeroe Islands (Jeandel *et al.*, 2007), with Iceland ($^{87}Sr/^{86}Sr \approx 0.703$; $\varepsilon_{Nd} \approx +8$) as the most important contributor of volcanic material in the North Atlantic (Revel *et al.*, 1996b) (Fig. 3.8). However, due to their proximity, it is also necessary to take into account the Tertiary volcanic provinces of the NW British Isles, whereas the Faeroe Islands are considered as a negligible source because of their limited size. Volcanic material from Iceland was most likely transported as ice-rafted debris (IRD) in drifting icebergs. The Porcupine Seabight is located between 40-55°N, within the zone of preferential IRD accumulation, i.e. the so-called Ruddiman-belt (Grousset *et al.*, 1993; Ruddiman, 1977) (Fig. 3.8). During cold stages, Iceland ice-sheet sourced icebergs (amongst others) may have become entrained in the cyclonic gyre of the central North Atlantic (Fig. 3.8) and in this way, they supplied IRD to the eastern Porcupine Seabight margin. Moreover, during cold stages, surface water movement reversed, flowing southwards as a coastal current west of Ireland (Sarnthein *et al.*, 1995). This southward flowing current likely acted as an

additional route for icebergs derived from the volcanic provinces in the NW British-Irish Isles, a hypothesis supported by the presence of north-south trending icebergs ploughmarks on Slyne Ridge (Games, 2001). Besides, Knutz *et al.* (2001) reported the influx of volcanic material from the Tertiary volcanic provinces of the NW British-Irish Isles during glacial sediment transport in the Rockall Trough. Another potential route for icebergs surges from Ireland and northern Britain which has to be considered is the Irish Sea ice stream, which drained the composite British and Irish Ice-sheet and transported icebergs to the south (Cofaigh and Evans, 2007; Roberts *et al.*, 2007).

All samples, except three (28 cm, 69 cm and 328 cm) have Sr and Nd isotope ratios which plot along the same elongated hyperbolic distribution (Fig. 3.7). Therefore, it is concluded that no major change of the sediment sources occurred. However, the relative contribution of each sedimentary source (end-member) varies significantly throughout the sedimentary record. Based on the mixing-hyperbola, it was inferred that between 3 and 60% of the terrigenous fraction in the samples may derive from a volcanic province. A shift in the isotope ratios can be recognized between the sediments from the interglacial light layers and the glacial dark layers from unit A (Fig. 3.7). The interglacial layers of unit A are generally characterized by an enhanced contribution of volcanic sediment compared to the glacial intervals, which show an increased contribution of the non-volcanic, continental crust end-member (Fig. 3.7). This distinction is attributed to the presence of enhanced bottom currents during interglacial periods, sorting and reworking sediment and hence, creating coarse lag deposits specifically enriched in sediment that was once transported as ice-rafted debris from a volcanic source region.

Three sediment samples (28 cm, 69 cm and 328

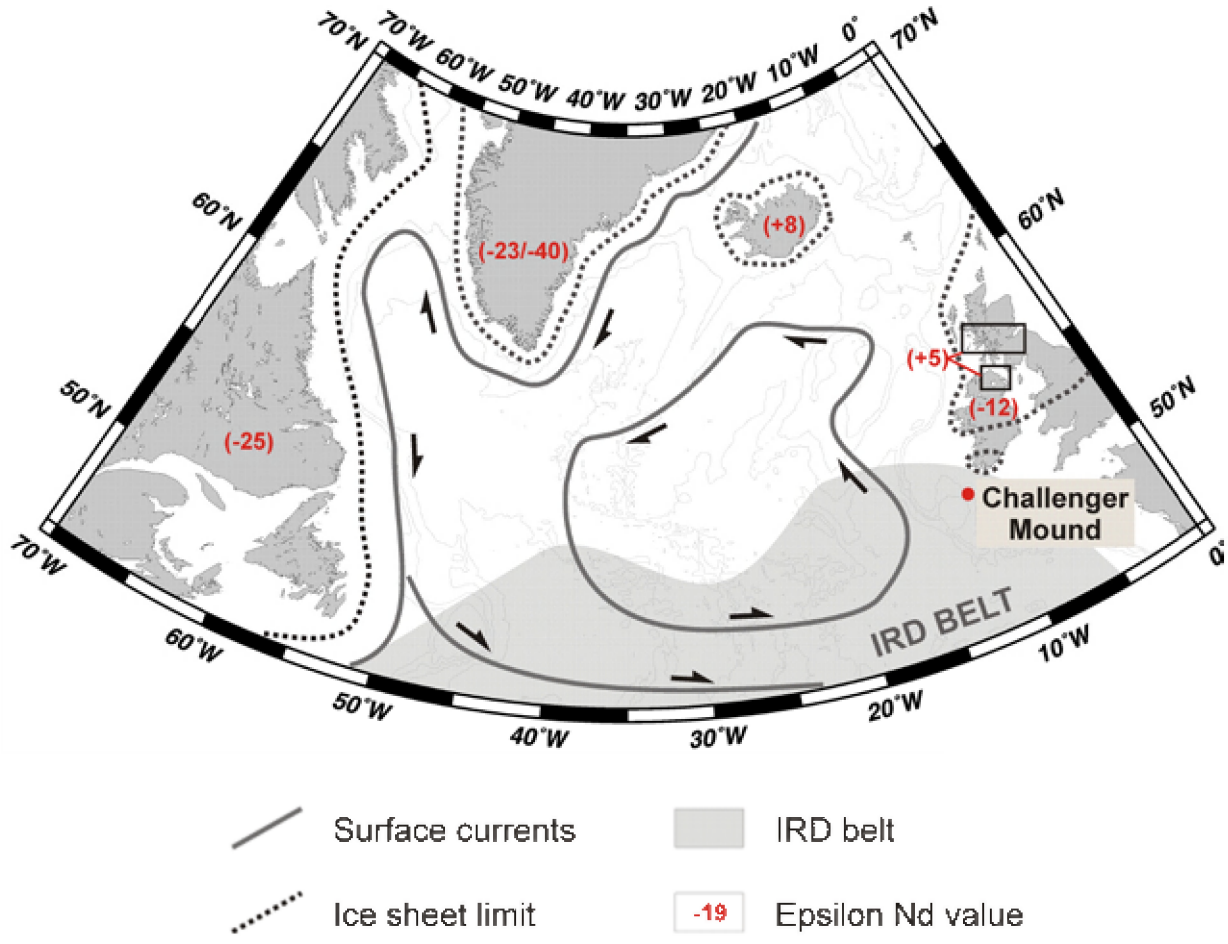

Fig. 3.8 *Reconstruction of the North Atlantic Ocean during the last glaciation with the location of the North Atlantic surface currents. The $\varepsilon_{Nd}(0)$ value of the different North Atlantic source-areas are indicated in red (Jeandel et al., 2007; Revel et al., 1996a). The grey-shaded zone corresponds to the Ruddiman belt. Modified after Ruddiman (1977), Bond et al. (1992), Grousset et al. (2001), Siegert (2001) and Auffret et al. (2002).*

cm) exhibit distinctly lower ε_{Nd} values compared to the British-Irish Isles, ranging between -13.8 and -15.7 (table 3.1 and Fig. 3.7). These lower values are related to a minor contribution of sediment derived from old continental crusts on e.g. Greenland ($^{87}Sr/^{86}Sr \approx 0.712$ to 0.730; $\varepsilon_{Nd}(0) \approx$ -23 to -40), Scandinavia ($^{87}Sr/^{86}Sr \approx 0.728$; $\varepsilon_{Nd}(0) \approx$ -19.3) and Canada ($^{87}Sr/^{86}Sr \approx 0.722$; $\varepsilon_{Nd}(0) \approx$ -25) (Revel *et al.*, 1996b). As described above, icebergs from these areas were possibly transported westward via the central North Atlantic gyre (Fig. 3.8). Ice-rafted debris, derived from the Laurentide Ice Sheet (Canada) and Greenland Ice Sheet, has already been reported in the Porcupine Seabight by Peck *et al.* (2007), supporting our interpretation.

3.6.2.2 Clay mineralogical evidence

The mineralogy of the clay fraction has the potential to provide information on the continental weathering processes in the source area (Colin *et al.*, 2006) and the type of source rock, i.e. weathering of volcanic rocks (Ballini *et al.*, 2006; Bout-Roumazeilles *et al.*, 1999). Throughout core MD01-2451G, significant changes are observed in the smectite content (Fig. 3.6). In the northern part of the North Atlantic Ocean smectite is often associated with the occurrence of basaltic rocks on Iceland, the Faeroe Islands and the eastern part of Greenland (Ballini *et al.*, 2006). However, in the case of core MD01-2451G, the elevated smectite content occurs in the glacial intervals where the Sr and Nd isotopic compositions indicate an enhanced contribution from the continental, Irish end-member. Therefore, a volcanic origin of the smectite is less likely for Challenger Mound and it is suggested that most of the smectites in core MD01-2451G are derived from the Irish mainland. Fagel *et al.* (2001) stated that smectites are common constituents of modern soils in Western Europe, where they are associated with vermiculite and linked to chemical weathering during warmer phases (Chamley, 1989).

The high smectite content observed throughout unit B (Fig. 3.6), likely indicates that this unit corresponds to a warm period of enhanced chemical weathering. The fact that the assemblage of clay minerals remains unchanged demonstrates that a stable terrigenous input occurred during the deposition of unit B. It is suggested that the abrupt smectite peaks in the glacial sediments of unit A (Fig. 3.6) point towards sedimentation during deglaciation episodes and associated melt-water pulses (Marinoni *et al.*, 2008; Vogt and Knies, 2008). In this scenario, the increase in smectite may be attributed to the initial stage of chemical weathering processes, which became activated following glacial retreat and the onset of warmer climatic conditions (Marinoni *et al.*, 2008; Vogt and Knies, 2008). This hypothesis is supported by the elevated illite crystallinity in the dark intervals of unit A which suggests strong hydrolysis conditions (Chamley, 1989). Besides, the rise in the smectite content may also be caused by the uncovering of the smectite-rich deposits on the Irish Isles (Fagel *et al.*, 2001) during glacial retreat.

The low smectite content in the light-grey, coral-rich levels of unit A might be surprising since these intervals are associated with warmer phases. However, a likely explanation is that this low content is possibly related to the strong currents during these intervals. Smectites are believed to flocculate less easily than illite, which has a greater surface-charge density (Hillier, 1995). Therefore, the high-energy conditions during interglacials would facilitate the deposition of illite rather than smectite. Chamley (1989) already emphasized that strong currents might severely alter the original clay signature induced by climate.

3.6.3 The role of the British-Irish Ice-Sheet

The grain-size analyses and the grain-surface textures of the terrigenous fraction in Challenger Mound indicate that an important part of the detrital material has a glacial origin. During cold stages, when most of Ireland was covered by the British-Irish Ice-Sheet (BIIS) (Bowen *et al.*, 2002; McCabe *et al.*, 2005; Scourse *et al.*, 2009; Sejrup *et al.*, 2005), an enhanced flux of terrigenous material was created offshore (Knutz *et al.*, 2002; Van Rooij *et al.*, 2007). This enhanced flux is supported by the elevated XRF Fe-counts in the glacial layers of unit A (Foubert and Henriet, 2009), indicating the dominance of the terrigenous material over the biogenic component (Richter *et al.*, 2006).

Gravity-driven processes such as low-density turbidity currents or hyperpycnal or density flows are possible processes transporting sediment

off-slope, as well as deposition from melting sea ice that drifted offshore (Auffret *et al.*, 2002). However, considering the position of the core on top of an elevated structure, most of the gravity processes can be excluded since these currents would bypass the mounds along the surrounding gullies (Van Rooij *et al.*, 2003). Thus, it is proposed that ice-rafting accounted for an important part of the terrigenous sediment supply to Challenger Mound, which is supported by the grain-size measurements, grain-surface micro-textures and Nd- and Sr-isotope ratios. This conclusion was also confirmed by the study of Thierens *et al.* (2010). However, the role of fall-out of fine-grained sediment plumes (Hesse and Khodabakhsh, 2006) derived from the BIIS, transport of fine-grained sediment by nepheloid layers and sediment transport by currents (especially during interglacial periods) play a significant role as well. All these observations indicate that the influx of glacial sediment is an important component in the infill of the coral framework and the build-up of cold-water coral mounds in the Porcupine Seabight. A different situation occurs in the Rockall Trough where coral mounds are much less affected by the influx of terrigenous sediment (Noé *et al.*, 2006).

A major control on the influx of terrigenous material from the Irish mainland into the study site seems to be the activity of the BIIS. The grain-size distributions, clay mineralogy and Nd and Sr isotopic compositions support that the dark, siliciclastic intervals of unit A are linked to deglaciations of the BIIS. The absence of corals or other biogenic fragments prohibits the dating of these glacial intervals. However, the dating of the corals within the interglacial layers provides a time-frame for the deposition of the glacial zones.

The two lowermost glacial intervals of unit A were deposited respectively between 230 ka - 189 ka and 189 ka - 109 ka ago (MIS 6-7). These time intervals correspond mainly with the Munsterian cold stage which lasted from ca. 302 ka to ca. 132 ka BP when an ice-sheet covered most of Ireland (McCabe, 2008). The presence of a glacial layer between 189 ka and 230 ka might indicate that ice-rafting also occurs in the cold periods during MIS 7 as already described by Desprat *et al.* (2006). The uppermost glacial layer of unit A was deposited after 78 ka (MIS 4). The deposition of the latter interval is attributed to ice-rafting of the Midlandian ice-sheet, which has already been described in detail (Bowen *et al.*, 2002; Cofaigh and Evans, 2007; McCabe, 2008; McCabe *et al.*, 2005). Scourse *et al.* (2009) and Bowen *et al.* (2002) reported repeated deglacial events between 40 and 12 ka.

During the deposition of these glacial sediments, no coral growth occurred. The change in hydrographic conditions during these deglaciations might have led to variations in the food supply to the cold-water corals and also the enhanced input of terrigenous material during BIIS ice-rafting or a combination of these factors, might explain the lack of coral fragments in the glacial layers. The close relation between cold-water coral growth and hydrography was already addressed by White (2007) and Dullo *et al.* (2008). Besides, the enhanced influx of terrigenous material might have a negative influence on coral growth (Freiwald *et al.*, 2004). Overall, less favorable conditions for coral growth seem associated with the deglaciation of the proximal BIIS.

3.7 Conclusion

The study of the terrigenous fraction of the Late Quaternary Challenger Mound reveals important changes in the hydrography, provenance and transport mechanism throughout the upper depositional sequence of this cold-water coral mound.

The Sr and Nd isotopic composition of the sediment in core MD01-2451G point towards Ireland as the dominant contributor of detrital material in Challenger Mound, with a variable contribution from a volcanic source. Two potential volcanic sources, i.e. Iceland and the Tertiary volcanic provinces of the NW British Isles are considered. Most likely, the southward transportation of volcanic material to the Porcupine Seabight was by drifting icebergs. A limited amount of samples indicate a potential third sedimentary source which is characterized by old continental crust Sr and Nd isotopic composition. Potential sources are the old cratons on Greenland, Scandinavia or Canada. Material from these regions was transported to the Porcupine Seabight during cold stages when icebergs got entrained in the cyclonic gyre of the central North Atlantic.

The glacial intervals in Challenger Mound are characterized by a bimodal grain-size distribution, typical for ice-rafting. The fact that little or no sorting occurred indicates that bottom currents were reduced during cold stages. On the

contrary, during interglacial times, enhanced bottom currents reworked biogenic fragments and ice-rafted material. This is supported by the surface microtextures of quartz grains in these interglacial layers, showing obvious signs of glacial abrasion. This paper highlights the role of ice-rafting as an important transport mechanism of terrigenous sediment towards the Late Quaternary Challenger Mound. An elevated smectite content indicates that the glacial layers of unit A were deposited during glacial retreat of the BIIS at the onset of warmer climatic conditions. The absence of coral fragments in these glacial intervals shows that coral growth was suppressed. It is put forward that the deglaciation of the BIIS seriously altered the hydrography and terrigenous input in the Porcupine Seabight and therefore affected coral growth. As such the role of the BIIS is ambiguous given that the influx of glacial sediments is an important factor for the infill of the coral framework and thus mound build-up, while deglaciations seem to suppress coral growth.

References

Andrews, J.T., 2008. The role of the Iceland Ice Sheet in the North Atlantic during the late Quaternary: a review and evidence from Denmark Strait. Journal of Quaternary Science, 23(1), 3-20.

Auffret, G.A., Zaragosi, S., Dennielou, B., Cortijo, E., Van Rooij, D., Grousset, F.E., Pujol, C., Eynaud, F. and Siegert, M., 2002. Terrigenous fluxes at the Celtic margin during the last glacial cycle. Marine Geology, 188, 79-108.

Ballini, M., Kissel, C., Colin, C. and Richter, T., 2006. Deep-water mass source and dynamic associated with rapid climatic variations during the last glacial stage in the North Atlantic: A multiproxy investigation of the detrital fraction of deep-sea sediments. Geochemistry Geophysics Geosystems, 7, doi: 10.1029/2005GC001070.

Beuck, L. and Freiwald, A., 2005. Bioerosion patterns in a deep-water *Lophelia pertusa* (Scleractinia) thicket (Propeller Mound, northern Porcupine Seabight). In: A. Freiwald and J.M. Roberts (Editors), Cold-Water Corals and Ecosystems. Springer-Verlag, Berlin Heidelberg, pp. 915-936.

Beyer, A., Schenke, H.W., Klenke, M. and Niederjasper, F., 2003. High resolution bathymetry of the eastern slope of the Porcupine Seabight. Marine Geology, 198, 27-54.

Bond, G., Heinrich, H., Broecker, W.S., Labeyrie, L.D., McManus, J., Andrews, J.T., Huon, S., Jantschik, R., Clasen, S., Simet, C., Tedesco, K., Klas, M., Bonani, G. and Ivy, S., 1992. Evidence for massive discharges of icebergs into the North Atlantic ocean during the last glacial period. Nature, 360, 245-249.

Bout-Roumazeilles, V., Cortijo, E., Labeyrie, L. and Debrabant, P., 1999. Clay mineral evidence of nepheloid layer contributions to the Heinrich layers in the northwest Atlantic. Palaeogeography Palaeoclimatology Palaeoecology, 146(1-4), 211-228.

Bowen, D.Q., Phillips, F.M., McCabe, A.M., Knutz, P.C. and Sykes, G.A., 2002. New data for the Last Glacial Maximum in Great Britain and Ireland. Quaternary Science Reviews, 21, 89-101.

Chamley, H., 1989. Clay Sedimentology. Springer, Berlin, 623 pp.

Cofaigh, C.O. and Evans, D.J.A., 2007. Radiocarbon constraints on the age of the maximum advance of the British-Irish Ice Sheet in the Celtic Sea. Quaternary Science Reviews, 26(9-10), 1197-1203.

Colin, C., Turpin, L., Blamart, D., Frank, N., Kissel, C. and Duchamp, S., 2006. Evolution of weathering patterns in the Indo-Burman Ranges over the last 280 kyr: Effects of sediment provenance on Sr-87/Sr-86 ratios tracer. Geochemistry Geophysics Geosystems, 7, doi: 10.1029/2005GC000962.

Colman, J.G., Gordon, D.M., Lane, A.P., Forde, M.J. and Fitzpatrick, J.J., 2005. Carbonate mounds off Mauritania, Northwest Africa: status of deep-water corals and implications for management of fishing and oil exploration activities. In: A. Freiwald and J.M. Roberts (Editors), Cold-Water Corals and Ecosystems. Springer-Verlag, Berlin Heidelberg, pp. 417-441.

de Haas, H., Mienis, F., Frank, N., Richter, T.O., Steinacher, R., De Stigter, H., van der Land, C. and Van Weering, T.C.E., 2009. Morphology and sedimentology of (clustered) cold-water coral mounds at the south Rockall Trough margins, NE Atlantic Ocean. Facies, 55, 1-26.

De Mol, B., Van Rensbergen, P., Pillen, S., Van Herreweghe, K., Van Rooij, D., McDonnell, A., Huvenne, V., Ivanov, M., Swennen, R. and Henriet, J.-P., 2002. Large deep-water coral banks in the Porcupine Basin, southwest of Ireland. Marine Geology, 188, 193-231.

Desprat, S., Goni, M.F.S., Turon, J.L., Duprat, J., Malaize, B. and Peypouquet, J.P., 2006. Climatic variability of Marine Isotope Stage 7: direct land-sea-ice correlation from a multiproxy analysis of a north-western Iberian margin deep-sea core. Quaternary Science Reviews, 25(9-10), 1010-1026.

Dorschel, B., Hebbeln, D., Foubert, A., White, M. and Wheeler, A.J., 2007. Hydrodynamics and cold-water coral facies distribution related to recent sedimentary processes at Galway Mound west of Ireland. Marine Geology, 244(1-4), 184-195.

Dorschel, B., Hebbeln, D., Rüggeberg, A., Dullo, C. and Freiwald, A., 2005. Growth and erosion of a cold-water coral covered carbonate mound in the Northeast Atlantic during the Late Pleistocene and Holocene. Earth and Planetary Science Letters, 233, 33-44.

Dullo, W.C., Flogel, S. and Rüggeberg, A., 2008. Cold-water coral growth in relation to the hydrography of the Celtic and Nordic European continental margin. Marine Ecology-Progress Series, 371,

165-176.
Fagel, N., Robert, C., Preda, M. and Thorez, J., 2001. Smectite composition as a tracer of deep circulation: the case of the Northern North Atlantic. Marine Geology, 172(3-4), 309-330.
Faure, G., 1986. Principles of Isotope Geology. J. Wiley, New York, 589 pp.
Ferdelman, T.G., Kano, A., Williams, T., Henriet, J.P. and Scientists, I.E., 2006. IODP Expedition 307 drills cold-water coral mound along the Irish continental margin. Scientific Drilling, 2, 11-16.
Foubert, A., Beck, T., Wheeler, A.J., Opderbecke, J., Grehan, A., Klages, M., Thiede, J., Henriet, J.-P. and the Polarstern ARK-XIX/3a shipboard party, 2005. New view of the Belgica Mounds, Porcupine Seabight, NE Atlantic: Preliminary Results from the Polarstern ARK-XIX/3a ROV cruise. In: A. Freiwald and J.M. Roberts (Editors), Deep-water Corals & Ecosystems. Springer-Verlag, Berlin Heidelberg, pp. 403-415.
Foubert, A., Depreiter, D., Beck, T., Maignien, L., Pannemans, B., Frank, N., Blamart, D. and Henriet, J.-P., 2008. Carbonate mounds in a mud volcano province off north-west Morocco: Key to processes and controls. Marine Geology, 248(1-2), 74-96.
Foubert, A. and Henriet, J.P., 2009. Nature and significance of the recent carbonate mound record: the Mound Challenger Code. Springer-Verlag, Heidelberg, 350 pp.
Foubert, A., Van Rooij, D., Blamart, D. and Henriet, J.-P., 2007. X-ray imagery and physical core logging as a proxy of the content sediment cores in cold-water coral mound provinces: a case study from Porcupine Seabight, SW of Ireland. International Journal of Earth Sciences, 96, 141-158.
Frank, N., Ricard, E., Paque, A., van der Land, C., Colin, C., Blamart, D., Foubert, A., Van Rooij, D., Henriet, J.P., De Haas, H. and Van Weering, T., 2009. The Holocene occurrence of cold-water corals in the NE Atlantic: Implications for coral carbonate mound evolution. Marine Geology, 266, 129-142.
Freiwald, A., Fossa, J.H., Grehan, A., Koslow, T. and Roberts, J.M., 2004. Cold-water coral reefs. Biodiversity Series. UNEP-WCMC, Cambridge, 84 pp.
Freiwald, A., Wilson, J.B. and Henrich, R., 1999. Grounding Pleistocene icebergs shape recent deep-water coral reefs. Sedimentary Geology, 125, 1-8.
Games, K.P., 2001. Evidence of shallow gas above the Connemara oil accumulation, Block 26/28, Porcupine Basin. In: P.M. Shannon, P. Haughton and D. Corcoran (Editors), The Petroleum Exploration of Ireland's Offshore Basins. Special Publication. Geological Society, London, pp. 361-373.
Goldstein, S.L., Onions, R.K. and Hamilton, P.J., 1984. A Sm-Nd Isotopic Study of Atmospheric Dusts and Particulates from Major River Systems. Earth and Planetary Science Letters, 70(2), 221-236.
Grousset, F.E., Cortijo, E., Huon, S., Hervé, L., Richter, T.O., Burdloff, D., Duprat, J. and Weber, O., 2001. Zooming in in Heinrich layers. Paleoceanography, 16(3), 240-259.
Grousset, F.E., Labeyrie, L.D., Sinko, J.A., Cremer, M., Bond, G., Duprat, J., Cortijo, E. and Huon, S., 1993. Patterns of ice-rafted detritus in the glacial North Atlantic. Paleoceanography, 8(2), 175-192.
Hargreaves, P.M., 1984. The distribution of Decapoda (Crustacea) in the open ocean and near-bottom over an adjacent slope in the northern North-East Atlantic Ocean during Autumn 1979. Journal of the Marine Biological Association of the United Kingdom, 64, 829-857.
Hesse, R. and Khodabakhsh, S., 2006. Significance of fine-grained sediment lofting from melt-water generated turbidity currents for the timing of glaciomarine sediment transport into the deep sea. Sedimentary Geology, 186(1-2), 1-11.
Hillier, S., 1995. Erosion, sedimentation and sedimentary origin of clays. In: B. Velde (Editor), Origin and Mineralogy of Clays. Springer, Berlin, pp. 162-219.
Huvenne, V.A.I., Van Rooij, D., De Mol, B., Thierens, M., O'Donnell, R. and Foubert, A., 2009. Sediment dynamics and palaeo-environmental context at key stages in the Challenger cold-water coral mound formation: Clues from sediment deposits at the mound base. Deep Sea Research Part I: Oceanographic Research Papers, 56, 2263-2280.
IODP 307 Expedition Scientists, 2005. Modern carbonate mounds: Porcupine drilling, IODP Prel. Rept. doi: 10.2204/iodp.pr.307.2005.
Jeandel, C., Arsouze, T., Lacan, F., Techine, P. and Dutay, J.C., 2007. Isotopic Nd compositions and concentrations of the lithogenic inputs into the ocean: A compilation, with an emphasis on the margins. Chemical Geology, 239(1-2), 156-164.
Kano, A., Ferdelman, T.G., Williams, T., Henriet, J.P., Ishikawa, T., Kawagoe, N., Takashima, C., Kakizaki,

Y., Abe, K., Sakai, S., Browning, E., Li, X. and the IODP Expedition 307 Scientists, 2007. Age constraints on the origin and growth history of a deep-water coral mound in northeast Atlantic drilled during Integrated Ocean Drilling Program Expedition 307. Geology, 35(11), 1051-1054.

Knutz, P.C., Austin, W.E.N. and Jones, E.J.W., 2001. Millenial-scaled depostional cycles related to British Ice Sheet variability and North Atlantic paleocirculation since 45 kyr B.P., Barra Fan, U.K. margin. Paleoceanography, 16(1), 53-64.

Knutz, P.C., Jones, E.J.W., Austin, W.E.N. and van Weering, T.C.E., 2002. Glacimarine slope sedimentation, contourite drifts and bottom current pathways on the Barra Fan, UK North Atlantic margin. Marine Geology, 188, 129-146.

Larmagnat, S. and Neuweiler, F., in review. Exploring a link between Atlantic coral mounds and Phanerozoic carbonate mudmounds: insights from pore water fluorescent dissolved organic matter (FDOM), Pen Duick mounds, offshore Morocco. Marine Geology.

Lindberg, B., Berndt, C. and Mienert, J., 2007. The Fugloy Reef at 70°N; acoustic signature, geologic, geomorphologic and oceanographic setting. International Journal of Earth Sciences, 96, 201-213.

Mahaney, W.C., 2002. Atlas of sand grain surface textures and applications. Oxford University Press, 237 pp.

Mahaney, W.C., Stewart, A. and Kalm, V., 2001. Quantification of SEM microtextures useful in sedimentary environmental discrimination. Boreas, 30, 165-171.

Marinoni, L., Setti, M., Salvi, C. and Lopez-Galindo, A., 2008. Clay minerals in late Quaternary sediments from the south Chilean margin as indicators of provenance and palaeoclimate. Clay Minerals, 43(2), 235-253.

McCabe, A.M., 2008. Glacial geology and geomorphology. The landscapes of Ireland. Dunedin Edinburgh, 274 pp.

McCabe, A.M., Clark, P.U. and Clark, J., 2005. AMS 14C dating of deglacial events in the Irish Sea Basin and other sectors of the British-Irish ice sheets. Quaternary Science Reviews, 24, 1673-1690.

McCave, I.N. and Hall, I.R., 2006. Size sorting in marine muds: Processes, pitfalls, and prospects for paleoflow-speed proxies, Geochemistry Geophysics Geosystems, doi: 10.1029/2006GC001284.

Mienis, F., De Stigter, H., De Haas, H. and Van Weering, T.C.E., 2009. Near-bed particle deposition and resuspension in a cold-water coral mound area at the Southwest Rockall Trough margin, NE Atlantic. Deep Sea Research Part I: Oceanographic Research Papers, 56(6), 1026-1038.

Noé, S., Titschack, J., Freiwald, A. and Dullo, W.C., 2006. From sediment to rock: diagenetic processes of hardground formation in deep-water carbonate mounds of the NE Atlantic. Facies, 52(2), 183-208.

Peck, V.L., Hall, I.R., Zahn, R., Grousset, F., Hemming, S.R. and Scourse, J.D., 2007. The relationship of Heinrich events and their European precursors over the past 60 ka BP: a multi-proxy ice-rafted debris provenance study in the North East Atlantic. Quaternary Science Reviews, 26(7-8), 862-875.

Petschick, R., 2000. MacDiff 4.2.5 Manual, 61 pp.

Pingree, R.D. and Le Cann, B., 1990. Structure, strength and seasonality of the slope currents in the Bay of Biscay region. Journal of the Marine Biological Association of the United Kingdom, 70, 857-885.

Pirlet, H., Wehrmann, L.M., Brunner, B., Frank, N., Dewanckele, J., Van Rooij, D., Foubert, A., Swennen, R., Naudts, L., Boone, M., Cnudde, V. and Henriet, J.P., 2010. Diagenetic formation of gypsum and dolomite in a cold-water coral mound in the Porcupine Seabight, off Ireland. Sedimentology, 57, 786-805.

Revel, M., Cremer, M., Grousset, F.E. and Labeyrie, L., 1996a. Grain-size and Sr-Nd isotopes as tracer of paleo-bottom current strength, Northeast Atlantic Ocean. Marine Geology, 131(3-4), 233-249.

Revel, M., Sinko, J.A. and Grousset, F.E., 1996b. Sr and Nd isotopes as tracers of North Atlantic lithic particles: Paleoclimatic implications. Paleoceanography, 11(1), 95-113.

Rice, A.L., Billet, D.S.M., Thurston, M.H. and Lampitt, R.S., 1991. The institute of oceanographic sciences biology programme in the Porcupine Seabight: background and general introduction. Journal of the Marine Biological Association of the United Kingdom, 71, 281-310.

Richter, T.O., van der Gaast, S., Koster, B., Vaars, A., Gieles, R., de Stigter, H.C., De Haas, H. and van

Weering, T.C.E., 2006. The Avaatech XRF Core Scanner: technical description and applications to NE Atlantic sediments. In: R.G. Rothwell (Editor), New techniques in Sediment Core Analysis. Special Publications. Geological Society, London, pp. 39-50.

Roberts, D.H., Dackombe, R.V. and Thomas, G.S.P., 2007. Palaeo-ice streaming in the central sector of the British-Irish Ice Sheet during the Last Glacial Maximum: evidence from the northern Irish Sea Basin. Boreas, 36(2), 115-129.

Roberts, J.M., Peppe, O.C., Dodds, L.A., Mercer, D.J., Thomson, W.T., Gage, J.D. and Mel-drum, D.T., 2005. Monitoring evironmental variability around cold-water reefs: the use of a benthic photolander and the potential of seafloor observatories. In: A. Freiwald and J.M. Roberts (Editors), Cold-water corals and ecosystems. Springer-Verlag, Berlin Heidelberg, pp. 483-502.

Ruddiman, W.F., 1977. Late Quaternary deposition of ice-rafted sand in the subpolar North Atlantic (lat 40° to 65°N). Geological Society of America Bulletin, 88, 1813-1827.

Rüggeberg, A., Dorschel, B., Dullo, W.C. and Hebbeln, D., 2005. Sedimentary patterns in the vicinity of a carbonate mound in the Hovland Mound Province, northern Porcupine Seabight. In: A. Freiwald and J.M. Roberts (Editors), Cold-Water Corals and Ecosystems. Springer-Verlag, Berlin Heidelberg, pp. 87-112.

Rüggeberg, A., Dullo, C., Dorschel, B. and Hebbeln, D., 2007. Environmental changes and growth history of a cold-water carbonate mound (Propeller Mound, Porcupine Seabight). International Journal of Earth Sciences, 96, 57-72.

Sarnthein, M., Jansen, E., Weinelt, M., Arnold, M., Duplessy, J.C., Erlenkeuser, H., Flatoy, A., Johannessen, G., Johannessen, T., Jung, S., Koc, N., Labeyrie, L., Maslin, M., Pflaumann, U. and Schulz, H., 1995. Variations in Atlantic surface ocean paleoceanography, 50-degrees-80-degrees-N - a time-slice record of the last 30,000 years. Paleoceanography, 10(6), 1063-1094.

Scourse, J.D., Haapaniemi, A.I., Colmenero-Hildago, E., Peck, V.L., Hall, I.R., Austin, W.E.N., Knutz, P.C. and Zahn, R., 2009. Growth, dynamics and deglaciation of the last British-Irish Ice Sheet: the deep-sea ice-rafted detritus record. Quaternary Science Reviews, 28(27-28), 3066-3084.

Sejrup, H.P., Hjelstuen, B.O., Dahlgren, K.I.T., Haflidason, H., Kuijpers, A., Nygard, A., Praeg, D., Stoker, M.S. and Vorren, T.O., 2005. Pleistocene glacial history of the NW European continental margin. Marine and Petroleum Geology, 22, 1111-1129.

Siegert, M., 2001. Ice Sheets and Late Quaternary Environmental Change. Wiley, Chichester, 231 pp.

Tanaka, T., Togashi, S., Kamioka, H., Amakawa, H., Kagami, H., Hamamoto, T., Yuhara, M., Orihashi, Y., Yoneda, S., Shimizu, H., Kunimaru, T., Takahashi, K., Yanagi, T., Nakano, T., Fujimaki, H., Shinjo, R., Asahara, Y., Tanimizu, M. and Dragusanu, C., 2000. JNdi-1: a neodymium isotopic reference in consistency with LaJolla neodymium. Chemical Geology, 168(3-4), 279-281.

Thierens, M., Titschack, J., Dorschel, B., Huvenne, V., Wheeler, A., Stuut, J.B. and O´Donnell, R., 2010. The 2.6 Ma depositional sequence from the Challenger cold-water coral mound (IODP Exp. 307): sediment contributors and hydrodynamic environments. Marine Geology, 271, 260-277.

Titschack, J., Thierens, M., Dorschel, B., Schulbert, C., Freiwald, A., Kano, A., Takashima, C., Kawagoe, N., Li, X. and Scientists, I.E., 2009. Carbonate budget of a cold-water coral mound (Challenger Mound, IODP Exp. 307). Marine Geology, 259(1-4), 36-46.

Van Rooij, D., Blamart, D., Richter, T.O., Wheeler, A.J., Kozachenko, M. and Henriet, J.-P., 2007. Quaternary sediment dynamics in the Belgica mounds province, Porcupine Seabight: Ice rafting events and contour current processes. International Journal of Earth Sciences, 96, 121-140.

Van Rooij, D., De Mol, B., Huvenne, V., Ivanov, M.K. and Henriet, J.-P., 2003. Seismic evidence of current-controlled sedimentation in the Belgica mound province, upper Porcupine slope, southwest of Ireland. Marine Geology, 195(1-4), 31-53.

Vogt, C. and Knies, J., 2008. Sediment dynamics in the Eurasian Arctic Ocean during the last deglaciation - The clay mineral group smectite perspective. Marine Geology, 250(3-4), 211-222.

Wehrmann, L.M., Knab, N.J., Pirlet, H., Unnithan, V., Wild, C. and Ferdelman, T.G., 2009. Carbon mineralization and carbonate preservation in modern cold-water coral reef sediments on the Norwegian shelf. Biogeosciences, 6(4), 663-680.

White, M., 2007. Benthic dynamics at the carbonate mound regions of the Porcupine Sea Bight continental margin. International Journal of Earth Sciences, 96, 1-9.

White, M., Mohn, C., de Stigter, H. and Mottram, G., 2005. Deep-water coral development as a function of hydrodynamics and surface productivity around the submarine banks of the Rockall Trough, NE Atlantic. In: A. Freiwald and J.M. Roberts (Editors), Cold-Water Corals and Ecosystems. Springer-Verlag, Berlin Heidelberg, pp. 503-514.

Wienberg, C., Hebbeln, D., Fink, H.G., Mienis, F., Dorschel, B., Vertino, A., Correa, M.L. and Freiwald, A., 2009. Scleractinian cold-water corals in the Gulf of Cadiz-First clues about their spatial and temporal distribution. Deep-Sea Research Part I-Oceanographic Research Papers, 56(10), 1873-1893.

Chapter 4 - The terrigenous fraction in Challenger Mound as paleo-environmental recorder

Abstract

IODP expedition 307 drilled for the first time a complete sequence through a cold-water coral mound (i.e. Challenger Mound, Porcupine Seabight). In this study, the provenance of the terrigenous fraction in Challenger Mound is determined using neodymium (Nd) and strontium (Sr) isotope ratios in combination with the identification of coarse lithic grains. The British-Irish Isles appeared to be the dominant sediment contributor in Challenger Mound with a variable amount of volcanic material. The Early Pleistocene ice-rafted horizons, which were identified throughout the mound sequence (Thierens *et al.*, 2010) can be linked with the British-Irish Isles as well. Therefore, it is concluded that a recurring, marine-based ice sheet was present on the British-Irish Isles during the Early Pleistocene since 2.7 Ma. Hence, for the first time, the existence of early and significant ice accumulation in mid-latitudinal regions, such as the British-Irish Isles is evidenced. In a next step, the clay mineralogy is analyzed throughout the entire mound sequence. After constraining the provenance of the terrigenous sediment and the sediment transport processes (Thierens *et al.*, 2010) it is concluded that the clay mineralogy is primarily controlled by the continental climate. Interglacial periods are characterized by enhanced smectite values indicating the presence of a temperate climate with sufficient water to allow hydrolysis. In contrast, glacial periods reveal increased illite concentrations which are attributed to the growing importance of direct rock erosion. During deglaciations, smectite peaks are recorded, caused by the initial chemical weathering after glacial retreat. A shift is observed in the chlorite and kaolinite content before and after the Mid-Pleistocene Transition (MPT). Enhanced chlorite concentrations and decreasing kaolinite values point towards an increase of the physical weathering processes after the MPT which may be attributed to the prolonged and more extensive glaciations.

This chapter is partly based on Thierens, M., Pirlet, H., Colin, C., Latruwe, K., Vanhaecke, F., Lee, J., Stuut, J.-B., Titschack, J., Huvenne, V., Dorschel, B., Wheeler, A., Henriet, J.-P. (in review) Ice-rafting from the British-Irish ice sheet since the earliest Pleistocene (2.6 million years ago): implications for long-term mid-latitudinal ice-sheet growth in the North Atlantic region. Quaternary Science Reviews. (Pirlet, H. prepared samples for radiogenic isotope measurement and assisted in data analysis and writing of the manuscript.)

4.1 Introduction

The discovery of cold-water coral mounds in the Porcupine Seabight (De Mol *et al.*, 2002; Henriet *et al.*, 1998; Hovland *et al.*, 1994) resulted in various (European) research programmes which culminated in the drilling of an entire coral mound. In May 2005, IODP Expedition 307 drilled Challenger Mound (Belgica mound province) in the Porcupine Seabight (Fig. 4.1) and recovered the first complete section through a deep-water coral mound (Foubert and Henriet, 2009; Williams *et al.*, 2006). The drilling revealed a 155 m long sequence of unlithified sediment, structurally supported by corals (Site U1317). The presence of cold-water corals (mainly *Lophelia pertusa*) throughout the entire mound sequence allowed to compile a stratigraphic framework based on the Sr isotope ratios of the corals (Kano *et al.*, 2007). This framework was further refined by the magnetostratigraphy of the mound sediment (Foubert and Henriet, 2009). Challenger Mound originated 2.7 Ma ago on top of a Miocene firmground (Louwye *et al.*, 2008) and grew almost continuously to a height of 132 m until mound growth was interrupted around 1.7 Ma (Foubert and Henriet, 2009; Kano *et al.*, 2007). Hence this first mound phase (M1) is characterized by an average growth rate of 15 cm/ka with rates up to 52.6 cm/ka. The sediment-stabilising capacities of a dense cold-water coral framework (Mienis *et al.*, 2009; Roberts *et al.*, 2009) appeared crucial for the successful build-up of the M1 Early-Pleistocene sequence. Generally, an erosive/non-depositional current-controlled environment was present along the NW European continental margin during this period (Laberg *et al.*, 2005; Thierens *et al.*, 2010). Therefore, M1 represents a unique record of the Early-Pleistocene on the NE Atlantic continental slope which is poorly or not preserved elsewhere. The sediment of M1 reveals a repetitive alternation of lighter and darker layers due to variations in the carbonate content of the background sediment suggesting the development of full interglacial-glacial cycles (Ferdelman *et al.*, 2006; Titschack *et al.*, 2009). This hypothesis was confirmed by the stable oxygen isotopes of the planktonic foraminifers which reveal alternations of warm and cold stages (Sakai *et al.*, 2009) and correlate nicely with the carbonate cycles. Moreover, the siliciclastic grain-size distributions of the mound sediments

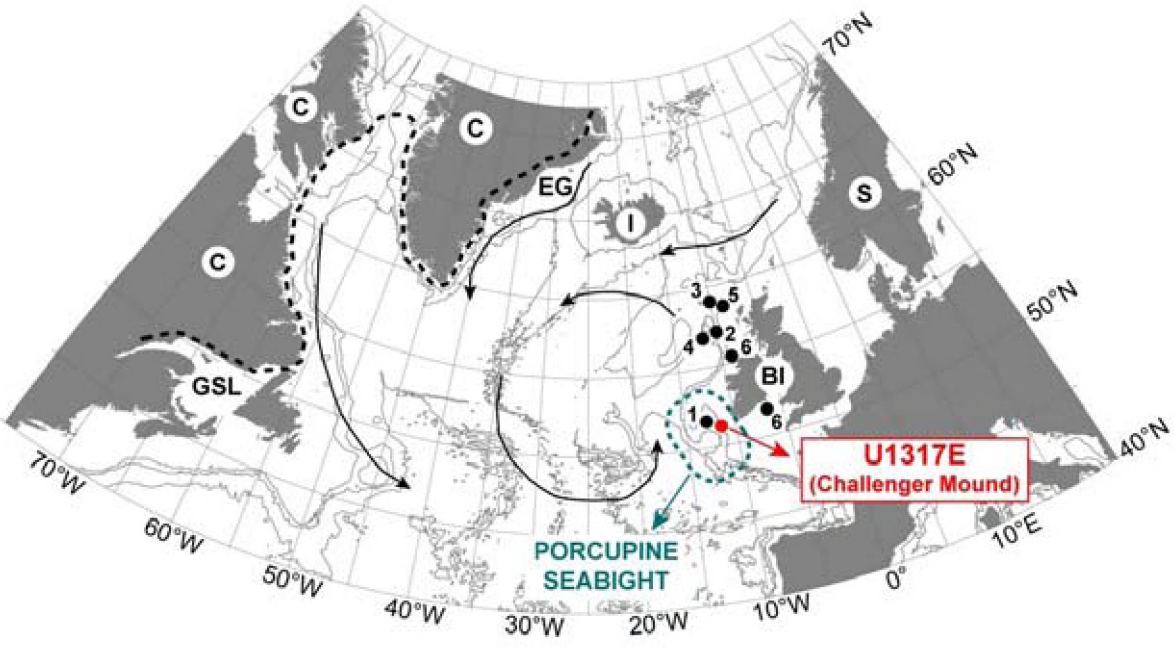

Fig. 4.1 *Location of IODP Exp. 307 site U1317E (Challenger Mound), eastern Porcupine Seabight continental margin, and additional sites cited in this study (black dots), with 1: Peck et al. (2007); 2: Knutz et al. (2001); 3: Knutz et al. (2007); 4: Hibbert et al. (2009); 5: Stoker et al. (1994); 6: Grousset et al. (2001). Potential source areas are indicated (more details in Fig. 4.5), with BI: British-Irish Isles; S: Scandinavia; I: Iceland; EG: East Greenland; C: Canadian Province (dashed line); GSL: Gulf of St Lawrence. Black arrows indicate likely iceberg drift trajectories in the glacial N Atlantic, adapted from Death et al. (2006). Bathymetry based on the GEBCO dataset.*

in M1 reveal a striking cyclicity as well which are attributed to variations of the governing contour current system (Thierens *et al.*, 2010).
Mound growth was interrupted between 1.7 Ma and 1 Ma ago, a period of non-deposition which is usually referred to as the "mound crisis" (Titschack *et al.*, 2009). A 23 m thick sediment sequence was deposited between 1 Ma and 1.5 ka ago, i.e. the upper mound phase (M2) (Foubert and Henriet, 2009; Kano *et al.*, 2007; Thierens *et al.*, 2010). The upper mound phase (M2) reveals significantly reduced growth rates (ca. 2 cm/ka (Foubert and Henriet, 2009; Thierens *et al.*, 2010)) and contains indications for several periods of non-deposition (Thierens *et al.*, 2010). The carbonate content (Titschack *et al.*, 2009), $\delta^{18}O$ values of the foraminifers (Sakai *et al.*, 2009) and grain-size distributions (Thierens *et al.*, 2010) reveal a much more chaotic pattern in M2. Hence, the potential of Challenger Mound as an oceanographic and climatic recorder is significantly reduced during M2. The difference in mound growth between M1 and M2 may be attributed to the more intense and prolonged glacial periods after the Mid-Pleistocene Transition (MPT) (Foubert and Henriet, 2009).
In the present study, a multiproxy provenance study, combining sediment neodymium (Nd) and strontium (Sr) isotopic source-fingerprinting and coarse (>150 µm) lithic species data, is performed on selected samples throughout Challenger Mound (both M1 and M2). Special attention is paid to the ice-rafted layers which were identified in the Early-Pleistocene lower mound phase (M1) (Thierens *et al.*, 2010). Evidence is presented which links these ice-rafted layers to the presence of a recurrent Early-Pleistocene ice-sheet on the British-Irish Isles which was capable of releasing iceberg into the marine domain.
In a second phase, the clay mineralogy of the complete Challenger Mound sequence is presented in combination with the provenance data, the carbonate content (Titschack *et al.*, 2009), $\delta^{18}O$ values of the planktonic foraminifers (Sakai *et al.*, 2009) and particle size analysis (Thierens *et al.*, 2010). The main parameters which affect the clay mineralogy in Challenger Mound are elucidated. It is proposed that the mineralogy of the clay fraction holds information about the weathering processes on the near-by British-Irish Isles and thus provides a record of the continental climate.

4.2 Material and methods

Neodymium (Nd) and strontium (Sr) isotope ratio measurements were carried out on the total carbonate-free (hereafter termed "siliciclastic") sediment fraction of 16 IODP Exp. 307 hole U1317E samples (drilled at 51°22.8'N, 11°43.1'W; 792.2 m water depth). Material from both ice-rafted and background-sediment layers, as identified by Thierens *et al.* (2010) (see also Fig. 4.4, Table 4.1), was isotopically analysed to constrain the sediment provenance throughout the depositional sequence (Grousset *et al.*, 2001; Peck *et al.*, 2007; Revel *et al.*, 1996b). The chemical separation and measurement of the Nd and Sr was conducted following the procedures, described in section 2.7. On average, isotope ratios are measured with a standard deviation (2σ) of 0.000051 ($^{87}Sr/^{86}Sr$; RSD: 0.0035%) and 0.000074 ($^{143}Nd/^{144}Nd$; RSD: 0.0072%). To independently ground-truth the Nd-Sr isotope data, coarse lithic grains (> 150 µm; bulk sediment) from the isotopically-analysed layers were lithologically classified using a binocular and light microscope. The identification of (pale) dolomitic carbonate, dark-grey carbonate, haematite-coated grains and volcanic debris is diagnostic in provenance studies along the NE Atlantic continental margin (Knutz *et al.*, 2001; Knutz *et al.*, 2007; Peck *et al.*, 2007). The absence or presence of these and additional lithic species is therefore systematically recorded for all samples in this study. Furthermore, the clay mineralogy of 147 sediment samples (hole U1317E) was identified using standard X-ray diffraction (PANalytical diffractometer) at the IDES laboratory (University of Paris XI) on oriented mounds of decarbonated clay-sized particles (< 2 µm). The methodology of the identification of the clay minerals is described in detail in section 2.6.

4.3 Results

The $\varepsilon_{Nd}(0)$ and $^{87}Sr/^{86}Sr$ values of the siliciclastic sediment are listed in table 4.1. The $^{87}Sr/^{86}Sr$ ration and $\varepsilon_{Nd}(0)$ value vary significantly between 0.706212 and 0.730139 and between -11.1 and +0.3, respectively. The results of the identification of the coarse lithic grains are given in table 4.2.
Overall, smectite is the dominant clay mineral in Challenger Mound with an average content of

n°	depth (mbsf)	sedimentological interpretation		clay (vol.%)	$^{87}Sr/^{86}Sr$	± 2 σ (10^{-5})	$^{143}Nd/^{144}Nd$	± 2 σ (10^{-5})	$\varepsilon_{Nd}(0)$
1	0.23	IRD	lag sediment?	2	0.728170	8.2	0.512203	5.9	-8.5
2	6.92	B	current deposit (coarse)	3	0.722575	6.4	0.512122	13.8	-10.1
3	8.44	B	current deposit (medium)	3	0.724805	3.0	0.512138	6.0	-9.8
4	14.92	IRD	lag sediment?	5	0.724875	7.7	0.512069	5.0	-11.1
5	22.65	IRD	lag sediment?	3	0.725935	8.2	0.512173	5.1	-9.1
6	23.72	B	aggregate deposit (fine)	5	0.730139	5.6	0.512170	3.3	-9.1
7	26.88	IRD		4	0.723179	2.8	0.512070	13.4	-11.1
8	31.58	IRD		5	0.712031	4.1	0.512236	7.7	-7.8
9	46.03	B	aggregate deposit (fine)	8	0.720158	3.5	0.512404	14.4	-4.6
10	63.26	B	current deposit (coarse)	3	0.723157	5.9	0.512175	12.1	-9.0
11	68.73	IRD		6	0.706212	6.1	0.512651	0.4	0.3
12	76.87	B	aggregate deposit (fine)	6	0.721426	3.2	0.512329	10.0	-6.0
13	107.74	IRD		4	0.7214032	2.4	0.512144	4.8	-9.6
14	118.95	B	current deposit (coarse)	3	0.720243	5.7	0.512095	7.1	-10.6
15	144.84	IRD		4	0.723728	7.3	0.512116	6.1	-10.2
16	154.93	B	current deposit (coarse)	4	0.723010	1.7	0.512131	2.8	-9.9

Table 4.1 *Characterization of IODP Exp. 307 U1317E samples selected for Nd-Sr isotopic provenance analysis. All depths are in compaction-corrected metre below seafloor (mbsf). Sedimentological interpretation and clay-size (vol.% < 2 µm) as determined by Thierens et al. (2010), with IRD: ice-rafted detritus layer; B: background-sediment layer.* $^{87}Sr/^{86}Sr$ *and* $^{143}Nd/^{144}Nd$ *(*$\varepsilon_{Nd}(0)$*) ratios were measured on the total siliciclastic sediment fraction.*

41.4% (Fig. 4.2). Illite is the second most important clay mineral with an average contribution of 30.6% followed by kaolinite (18.1%) and chlorite (9.9%) (Fig. 4.2). The smectite content reveals important variations between 23 and 64%. In the upper part of Challenger Mound (M2), a chaotic pattern is observed in the smectite distribution. In contrast, in M1 clear cycles occur in the smectite content which correlate closely to the oxygen isotopes of the planktonic foraminifers (Sakai *et al.*, 2009) and carbonate content (Titschack *et al.*, 2009). The lower part of Challenger Mound

n°	Depth (mbsf)	(pale) dolomitic carbonate	dark-grey carbonate	haematite-coated grains	volcanic debris	quartz - feldspars	rock fragments
1	0.23		X	X		X	X
2	6.92		X			X	X
3	8.44					X	X
4	14.92					X	X
5	22.65		X	X		X	X
6	23.72					X	X
7	26.88					X	X
8	31.58		X	X		X	X
9	46.03					X	X
10	63.26					X	
11	68.73					X	X
12	76.87	NA	NA	NA	NA	NA	NA
13	107.74					X	X
14	118.95					X	X
15	144.84					X	X
16	154.93					X	X

Table 4.2 *U1317E coarse (> 150 µm) lithic species data. Presence (minimum of 1%) of six lithic groups is recorded and the dominant species highlighted (bold x). NA: not analysed.*

marks an increase in the smectite content with the highest values below the mound base. The illite content varies between 17 and 41%. In general, illite correlates inversely to smectite. Similar to smectite, illite reveals a cyclic pattern in the lower part of the mound (M1) whereas the upper part (M2) is rather chaotic. The lower part of the mound is characterized by a significant decrease in the illite content with the lowest values below the mound base. Given that kaolinite and chlorite represent a minority in the clay fraction, they are clearly imprinted by the variations of smectite and illite. Nevertheless, some important trends are observed in their distribution. Kaolinite varies between 10 and 26% and M1 is characterized by a clear increase in kaolinite compared to M2. The chlorite content ranges between 3 and 19%. The highest values are observed in M2 whereas the lowest chlorite content is recorded in the lower part of M1 and below the mound base.

4.4 Discussion

4.4.1 Evidence for an ice-rafting British-Irish ice sheet since the earliest Pleistocene (2.6 million years ago)

4.4.1.1 Early-Pleistocene glaciations

The Early Pleistocene intensification of Northern Hemisphere glaciation, with the first large-scale

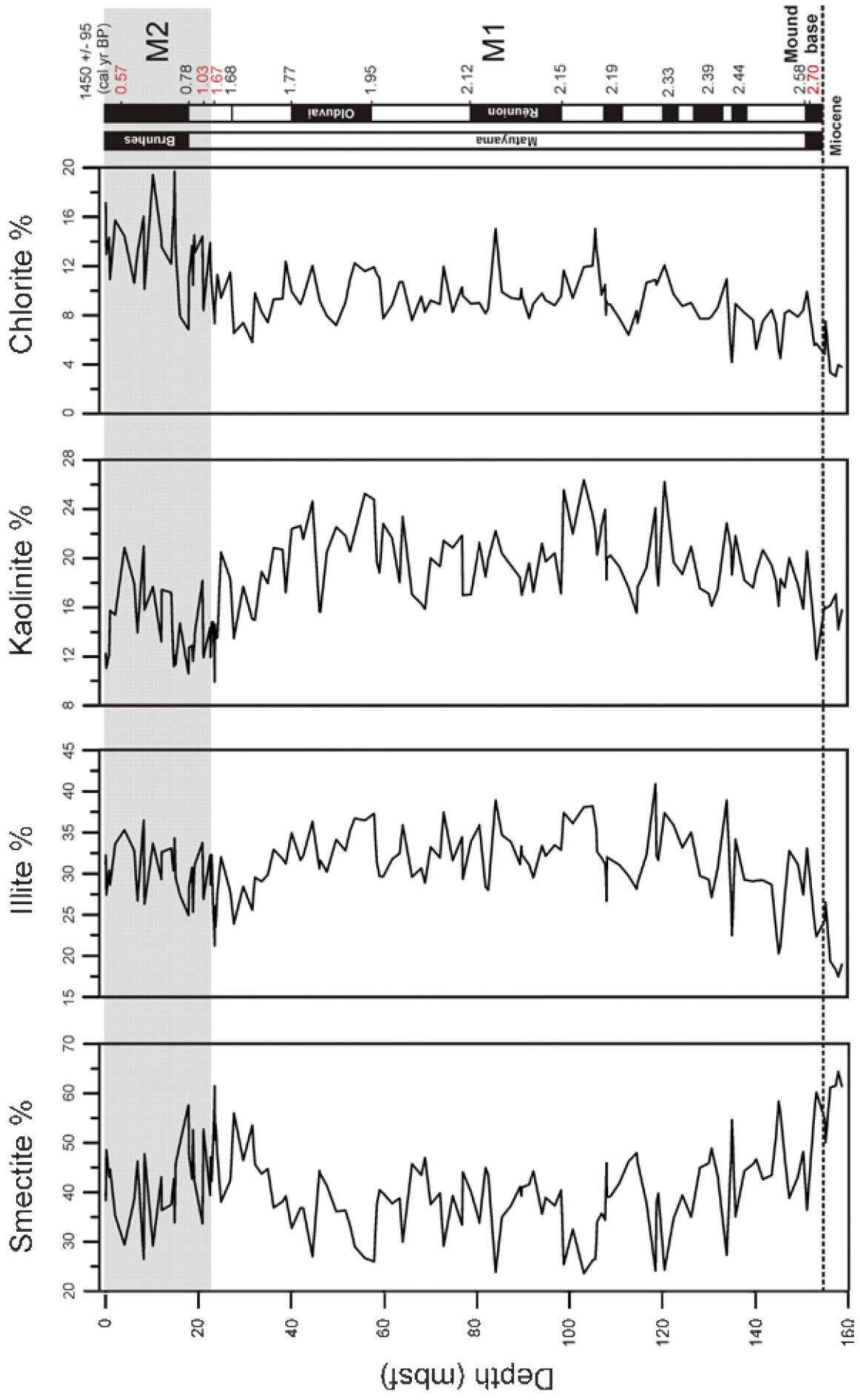
1450 +/- 95 (cal yr BP)
0.57
M2
0.78
1.03
1.67
1.68
1.77
1.95
2.12
M1
2.15
2.19
2.33
2.39
2.44
2.58
2.70
Mound base
Miocene
Brunhes
Matuyama
Réunion
Olduvai
Chlorite %
Kaolinite %
Illite %
Smectite %
Depth (mbsf)

Fig. 4.2 (Left) *The clay mineralogy of Challenger Mound. The stratigraphic framework is based on the Sr isotope ratios of the corals (ages indicated in red) (Kano et al., 2007), the magnetostratigraphy (ages indicated in black) (Foubert and Henriet, 2009) and one ^{14}C date of the surface sediment (Thierens et al., 2010). M1 = mound phase 1, M2 = mound phase 2. All depths in corrected metre below seafloor (mbsf).*

development of continental ice sheets at ca. 2.75 - 2.55 million years (Ma) ago (e.g. Maslin *et al.*, 1998), marks an important threshold in Earth's climate system. Unravelling the extent and dynamics of early ice-sheet development is crucial to our understanding of its response to, and amplification of, Quaternary climate forcing and its overall impact on global climate variability (e.g. Maslin *et al.*, 1998; Raymo and Huybers, 2008). On-land evidence of these early glaciations is rather limited, due to erosion and overprinting during later glacial phases. As the build-up of considerable ice volumes also strongly affects oceanic circulation and sedimentation (e.g.Raymo *et al.*, 1992; Ruddiman *et al.*, 1989), records of continental ice-sheet expansion are however widely preserved in the marine environment. In the North Atlantic Ocean, ice-rafted deposits evidence the first widespread discharge, and melting, of sediment-loaded icebergs into the ocean around ca. 2.7 – 2.4 Ma (e.g. Flesche Kleiven *et al.*, 2002; Shackleton *et al.*, 1984). By that time, all major ice sheets located at high northern latitudes (on Canada, Greenland, Iceland and Scandinavia) are assumed to have developed marine margins, generating North-Atlantic iceberg-surges, which deposit ice-rafted detritus (IRD) onto the seabed (Ehlers and Gibbard, 2007; Flesche Kleiven *et al.*, 2002; Sejrup *et al.*, 2005). Provenance data linking this Early-Pleistocene IRD to the glaciation of specific continental areas is, however, largely absent. In addition, the role of any significant Early-Pleistocene ice build-up in more temperate mid-latitudinal regions, such as the British-Irish Isles (BI), especially to an extent that allows ice-rafting, is still undocumented (Ehlers and Gibbard, 2007; Raymo and Huybers, 2008; Sejrup *et al.*, 2005).

4.4.1.2 Early-Pleistocene ice-rafted detritus in Challenger Mound

In the North Atlantic, sediments enriched in coarse (>150 µm) lithic particles are generally regarded as ice-rafted deposits (e.g. Bond and Lotti, 1995; Hemming, 2004 and references therein). However, in continental margin settings this definition is challenged as processes other than ice-rafting, such as bottom-current reworking and turbidity currents, can also concentrate coarser-grained material (e.g. Laberg *et al.*, 2005). Consequently, a rigorous identification and ground-truthing procedure was designed to screen the U1317E sediments for ice-rafted detritus (IRD), as published in Thierens *et al.* (2010). Siliciclastic particle-size end-member modelling (Weltje, 1997) and quartz grain-surface microtextural analysis were thereby combined, defining IRD layers as deposits with a poorly-sorted, often bimodal, siliciclastic particle-size signature, distinctly enriched in the coarser size-fractions ("IRD_{EM} -dominated samples"; Fig. 4.3). Microtextural analysis of sand-sized quartz grain-surfaces validated ice as the dominant mode of transport for these sediments (Fig. 4.3). No evidence for mass sediment transport (e.g. turbidites) or high-energy contour-current action is found in the IRD_{EM}-dominated layers (Thierens *et al.*, 2010). The presence of fresh, glacially-abraded grains implies deposition from icebergs rather than sea ice, since sediment entrainment into sea ice does not commonly inflict intense mechanical grain-abrasion (e.g. Dethleff and Kuhlmann, 2009; St. John, 2008). Moreover, the poorly-sorted and coarse nature of the U1317E ice-rafted deposits, often associated with mm- to cm-sized clasts (dropstones), does not comply with the preferential incorporation of silt-sized particles into sea ice (Dethleff and Kuhlmann, 2009). Non-size-selective transport via land-derived icebergs is therefore proposed as the main depositional mechanism for the U1317E IRD layers (Thierens *et al.*, 2010).

Through this procedure, a total of 27 IRD intervals have been identified throughout the U1317E sequence (Fig. 4.4; Thierens *et al.*, 2010). Considering the condensed and fragmented nature of the ca. 23 m-long upper record (unit M2: 1 Ma – 1450 cal years BP) (Fig. 4.4; Thierens *et al.*, 2010; Titschack *et al.*, 2009), IRD layers in this part of the sequence may be complex composites of multiple depositional and/or erosional events and therefore will not be discussed in detail. In contrast, the fast-accumulated (14 cm ka-

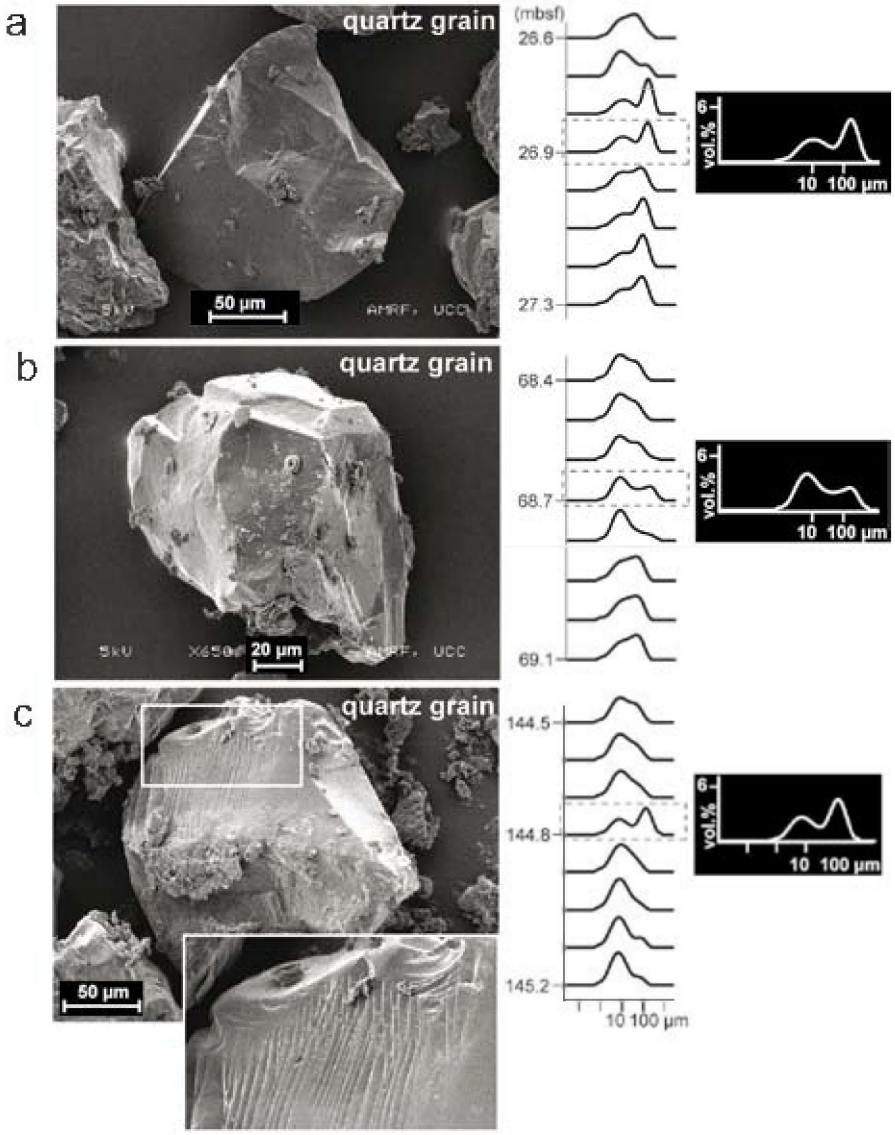

Fig. 4.3 *Ground-truthing of Early-Pleistocene ice-rafted detritus (IRD) layers within U1317E. Examples of glacial-abrasion features (scanning electron microscope images; Thierens, M., unpublished data) on sand-sized quartz grain-surfaces from sample 7 (26.9 mbsf; A.), 11 (68.7 mbsf; B.) and 15 (144.8 mbsf; C.). Sample numbers as indicated in (Fig. 4.4) and Table 4.1; all depths in corrected metre below seafloor (mbsf). Microtextural analysis (Thierens et al., 2010) clearly shows angular and fresh grains, with sharp edges and deeply embedded mechanical abrasion features (inset in image C: conchoidal and linear fractures, step features). Silicilastic particle-size spectra (0.01 – 2000 µm, on a logarithmic x-axis) of the three IRD samples in comparison to neighbouring background-sediment layers in the sequence.*

1; Foubert and Henriet, 2009) and semi-continuous M1 record reveals a series of 16 distinct IRD horizons; the oldest deposited around 2.6 Ma (Fig. 4.4). Moreover, these Early-Pleistocene ice-rafting events, typically associated with episodes of raised siliciclastic versus biogenic-carbonate input, appear mainly in glacial climatic intervals (Fig. 4.4).

4.4.1.3 Sediment provenance

To fully comprehend the impact of Early-Pleistocene iceberg-rafting, recorded as far southeast as the eastern Porcupine Seabight continental margin, it is crucial to identify the continental source area(s) of the calving icebergs. Multi-proxy provenance analyses, including the Nd-Sr isotopic fingerprinting of lithic particles, have proven successful in relating N Atlantic (ice-rafted) deposits to distinct circum-Atlantic source

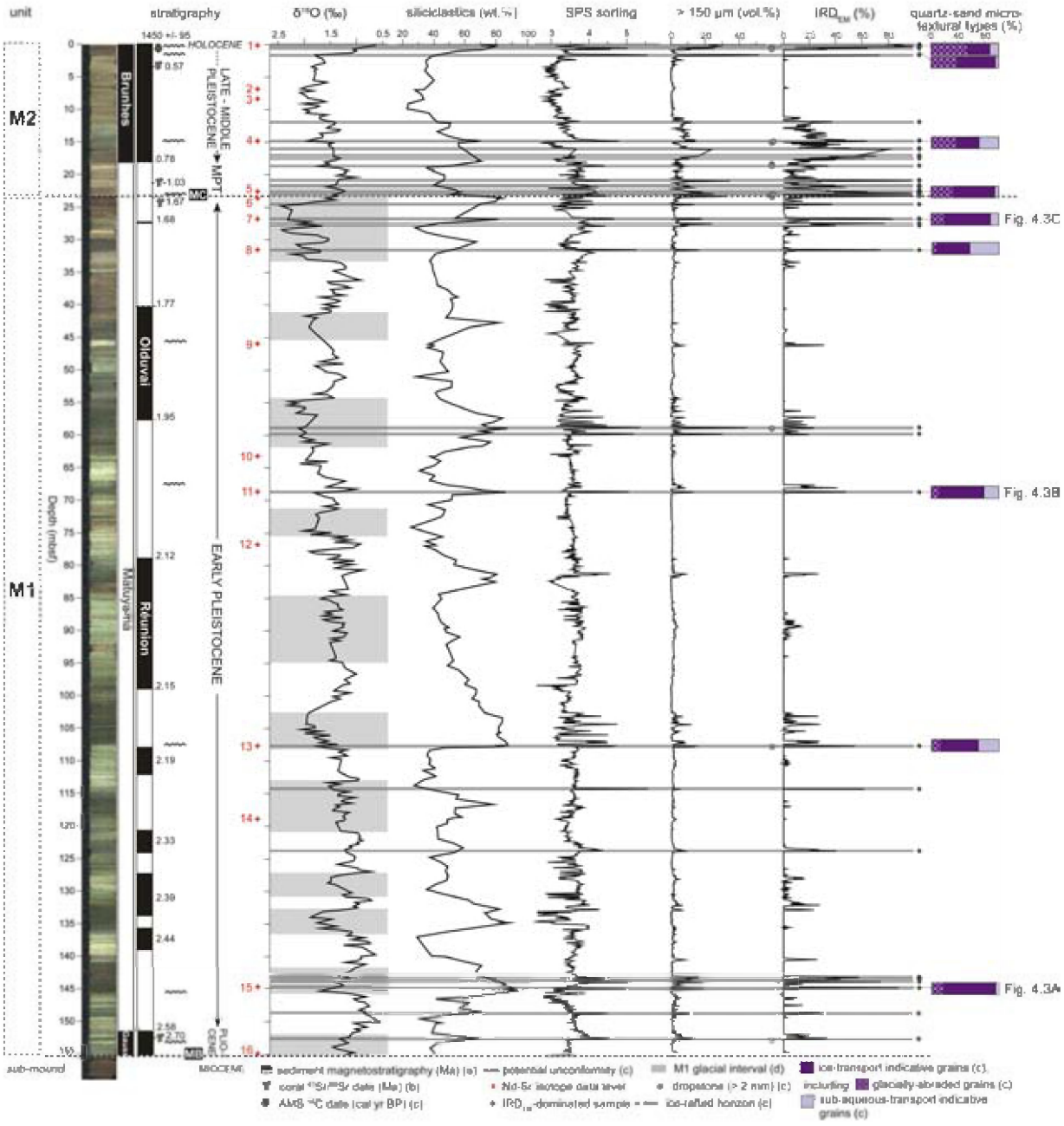

Fig. 4.4 *Identification and ground-truthing of ice-rafted detritus (IRD) layers within U1317E. IRD is defined as dominated by the "IRD$_{EM}$ siliciclastic particle-size (SPS)" signature (Thierens et al., 2010): poorly-sorted sediments, enriched in the coarser size-fractions (> 150 µm and dropstones). Quartz-sand microtextural analysis indicates a dominance of ice-transported grains in IRD$_{EM}$-dominated layers (Thierens et al., 2010) (see also Fig. 4.3). IRD occurs mainly in glacial $\delta^{18}O$ intervals (G. bulloides $\delta^{18}O$ curve; Sakai et al., 2009), rich in siliciclastic matrix-sediment (wt.% versus pelagic matrix-carbonate; Titschack et al., 2009). Core stratigraphy, defining two mound units (M1: 2.6 – 1.7 Ma; M2: 1 Ma – 1450 cal year BP) separated by a hiatus (MC) (Foubert and Henriet, 2009; Kano et al., 2007; Thierens et al., 2010), for reference. MB = Challenger Mound base; MPT = mid-Pleistocene climate transition. All depths in corrected metre below seafloor (mbsf). Core levels analysed in this provenance study are marked for further reference (see Table 4.1 for details). (a): ref. Foubert and Henriet (2009); (b):ref. Kano et al. (2007); (c): ref. Thierens et al. (2010); (d): ref. Sakai et al. (2009).*

terrains (e.g. Farmer *et al.*, 2003; Grousset *et al.*, 2000; Peck *et al.*, 2007; Revel *et al.*, 1996b). On an $\varepsilon_{Nd}(0)$ – $^{87}Sr/^{86}Sr$ plot, these potential source regions (Fig. 1) delineate three isotope fields (I to III), characterised predominantly by significantly differing $\varepsilon_{Nd}(0)$ and $^{87}Sr/^{86}Sr$ values (Fig. 4.5A).
All measurements (unit M1 and M2), except one (sample 11) clearly cluster together within iso-

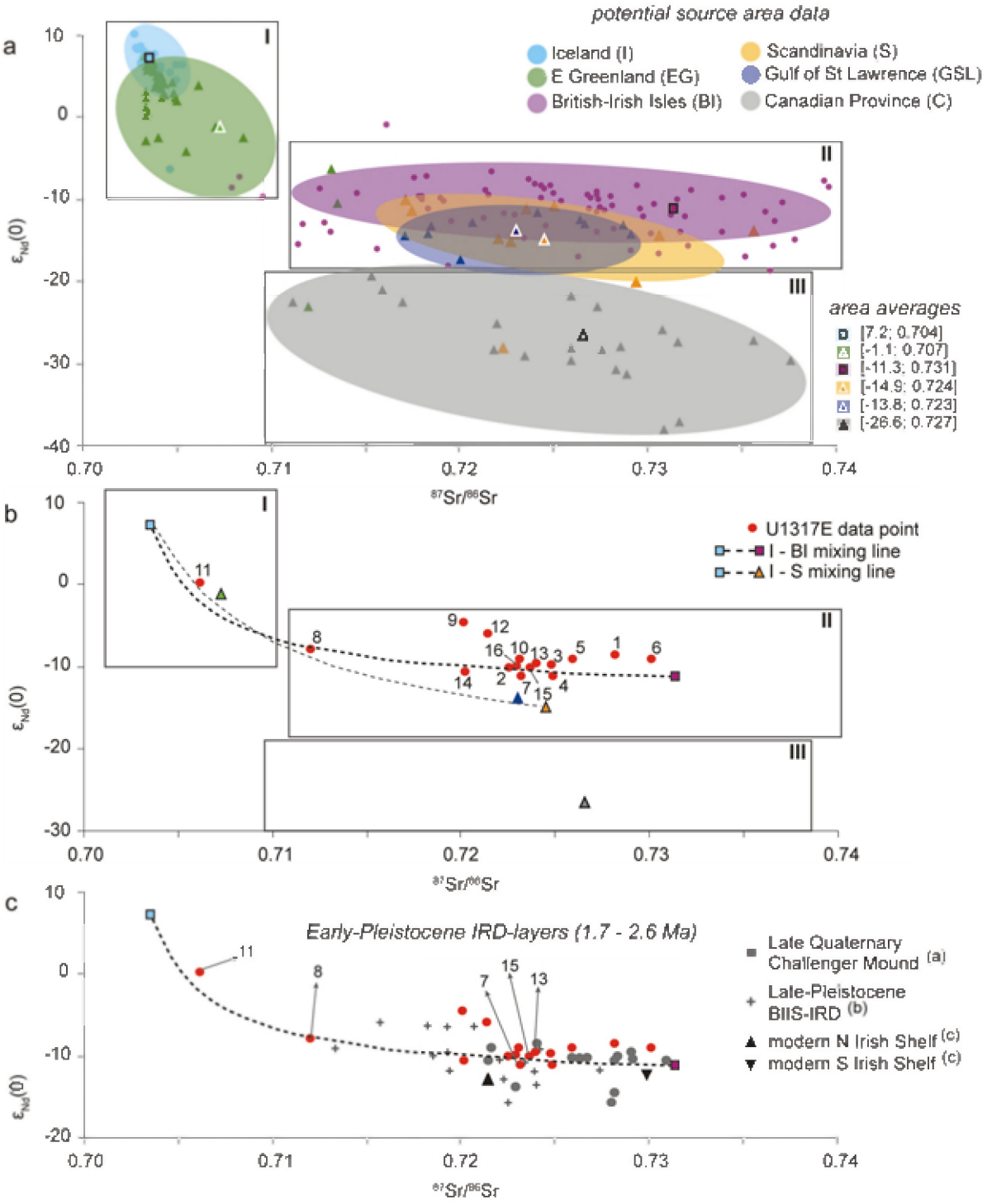

Fig. 4.5 *Provenance isotopic fingerprinting ($\varepsilon_{Nd}(0)$ versus $^{87}Sr/^{86}Sr$) of 16 U1317E horizons. Note the differences in scale of the vertical axis across panels. A: Potential source area isotope compositions delineate three $\varepsilon_{Nd}(0)$ - $^{87}Sr/^{86}Sr$ fields (boxes I to III), with (I) the young, Tertiary- recent, volcanic rocks from Iceland (including the Faeroe Islands) and E Greenland; (II) the Palaeozoic, radiogenic formations of the NW European continent (British-Irish Isles and Scandinavia – mostly Norway) and the Gulf of St Lawrence; (III) rocks of the old, Precambrian shields on Canada and Greenland (termed "Canadian Province"), including the Labrador, Hudson and Baffin Bay areas (locations as on Fig. 4.1). Weighted area averages are indicated as [$\varepsilon_{Nd}(0)$; $^{87}Sr/^{86}Sr$]. All data from the following literature: Bernstein et al., 1998; Brueckner et al., 1998; Davies et al., 1985; Farmer et al., 2003; Grousset et al., 2001; Hansen and Nielsen, 1999; Holm et al., 2001; Leng et al., 1999; Revel et al., 1996b; Weis et al., 1997. B: U1317E $\varepsilon_{Nd}(0)$ - $^{87}Sr/^{86}Sr$ isotope signatures. Error bars are smaller than symbols. Sample numbers as indicated in Fig. 4.4 and Table 4.1; $\varepsilon_{Nd}(0)$ - $^{87}Sr/^{86}Sr$ fields and area averages as defined in panel A. Isotopic mixing lines (cf.*

Faure, 1986) are calculated between the main potential source areas in field I and II. C. U1317E isotope values of Early-Pleistocene IRD layers compared to local "modern analogues": (a) late Quaternary BI-derived sediments from Challenger Mound from Pirlet et al. (2010); (b) late Pleistocene IRD sourced from the British-Irish Ice Sheet (BIIS) from Peck et al. (2007); (c) modern Irish Shelf sediments from Grousset et al. (2001). U1317E isotope ratio results as in panel B; sample numbers as indicated in Fig. 4.4 and Table 4.1; $\varepsilon_{Nd}(0)$ - $^{87}Sr/^{86}Sr$ area averages as defined in panel A.

tope field II (Fig. 4.5B). In this cluster, IRD isotope ratios cannot be differentiated from background-sediment isotope signatures, implying a common source area for both IRD and background-sediment siliciclastics. The two anomalous isotope signatures indicate the influence of a volcanic source (field I) besides the more dominant, crustal one (field II). These volcanic isotope compositions are considered to reflect a genuine provenance signal, as grain-size variability does not correlate with $^{87}Sr/^{86}Sr$ variation in the U1317E dataset (Table 4.1). Therefore, grain-size effects (Revel *et al.*, 1996a) are not thought to strongly overprint the Sr provenance signal.

As shown on Figure 4.5 B, none of the analysed sediments (IRD and background-sediment) are isotopically compatible with an origin in the Canadian Province (field III), as a contribution of this source would shift $\varepsilon_{Nd}(0)$ to lower values (cf. Grousset *et al.*, 2001; Peck *et al.*, 2007). This statement is further supported by the lithic species data (Table 4.2). Pale dolomitic carbonate grains, typically associated with ice surges from the Canadian Province (Hudson Strait ice-rafting; Bond *et al.*, 1992), are not observed in the coarse lithic fraction. As a consequence, U1317E IRD horizons should not be classified as Heinrich layers (sensu strictu; see review by Hemming (2004)), linked to glaciological instabilities of the Laurentide Ice Sheet (LIS) (Hemming, 2004; MacAyeal, 1993). Although the Gulf of St Lawrence (GSL), at the south-eastern LIS margin (Fig. 4.1, is isotopically similar to the NW European source terrains (field II; Fig. 4.5), it is not considered to be an important sediment supplier. In addition, the U1317E coarse lithic assemblage does not insist on a GSL-contribution. Haematite-rich lithologies are not unique to the GSL area, although GSL-sourced IRD is characteristically enriched in haematite-coated particles (Bond and Lotti, 1995). U1317E assemblages, however, do not contain diagnostic amounts of this lithic type (< 2% of fraction, if present). In all samples (IRD and background-sediment), quartz and feldspar grains make up the majority of the coarse fraction (> 80% of fraction), while rock fragments (mainly of metamorphic and sedimentary origin) appear ubiquitous, though in lesser quantities (< 20% of fraction; Table 4.2). Besides (mainly) schist, quartzite and shale clasts, small amounts of dark-grey carbonates have been identified in several IRD layers (Table 4.2). In this part of the NE Atlantic, the combination of these lithologies has been associated particularly with a sediment provenance from the nearby British-Irish Isles (BI), rather than with more distal source regions, such as the GSL area (Knutz *et al.*, 2001; Knutz *et al.*, 2007; Peck *et al.*, 2007).

Strengthening this point, the U1317E Nd-Sr isotope ratio distribution clearly supports the BI as crustal source. As shown in Figure 4.5 B, U1317E isotope values spread out along an Iceland/ East Greenland (volcanic end-member, field I) – British-Irish (crustal end-member, field II) mixing hyperbola, rather than fitting one between field I and the GSL or Scandinavia (field II). Although discriminating Scandinavian from British-Irish sourced particles is complex, our data thus seem to favor a dominant British-Irish input. The general provenance similarity between IRD and background-sediment layers would thereby be simply explained by a common sediment source in the nearby BI. The hyperbolic isotope distribution, furthermore, implies a two-end-member provenance system for the entire U1317E sequence (unit M1 and M2), with all samples (both IRD and background sediment) containing specific mixtures of the same end-member sources. Except for the most volcanogenic samples, all assemblages are dominated heavily by input from the British-Irish crustal terrains (> 80% source contribution). Potentially, the Tertiary volcanic provinces of the BI could also be contributing particles to the sedimentary system (Hibbert *et al.*, 2009; Knutz *et al.*, 2001), besides the larger Icelandic and East Greenland provinces. Lithic tracers, such as basalt or volcanic glass, could help to differentiate between volcanic sources (cf. Hibbert *et al.*, 2009; Knutz *et al.*, 2001; Knutz *et al.*, 2007; Peck *et al.*, 2007). However, no volcanic particles can be discerned in the coarse U1317E lithic assemblage (Table 4.2), as the most volcanogenic

samples seem to concentrate this signal mainly in their finer fraction (higher $\varepsilon_{Nd}(0)$ values correlate distinctly with higher abundance of clay-sized particles; Table 4.1). Additional analyses would, therefore, be needed to ground-truth the volcanic end-member of this provenance system.

4.4.1.3 An early, ice-rafting British-Irish Ice sheet

Overall, this study strongly indicates a dominant sediment input from the adjacent BI, rather than a more complex, across-Atlantic sediment pathway. Moreover, this local, British-Irish sediment source is inferred for several ice-rafting events throughout the sequence (unit M1 and M2). This clearly implies the recurrent existence of an ice sheet (i.e. ice mass of unspecified dimensions) located on the BI, capable of releasing sediment-loaded icebergs into the marine domain. For the Middle-Late Pleistocene (MIS 6 and onwards), multiple IRD records along the British-Irish Atlantic margin have been linked to ice surges from the proximal British-Irish Ice Sheet (BIIS; see review by Scourse *et al.* (2009)). However, the U1317E sequence extends this BIIS-IRD record into the Early Pleistocene, where several ice-rafted layers are found with isotope signatures analogous to their Late Pleistocene equivalents and within the range of modern Irish Shelf signatures (Fig. 4.5C). Consequently, this study evidences, for the first time, the presence of an Early Pleistocene British-Irish ice cap, which repeatedly expanded onto the continental shelf.

Delimiting the position and dimensions of an early BIIS is not straightforward, as any terrestrial evidence is unlikely to have survived subsequent glacial erosion phases. The marine environment can preserve records of successive continental glaciations (if they reach sea-level), but the generally erosive, Early-Pleistocene setting along the NE Atlantic margin (Laberg *et al.*, 2005), reduces their reconstructive potential for this time interval. To our knowledge, the north British-Irish continental margin off the Hebrides (Fig. 4.1 location 5), contains the only other report of local, Early-Pleistocene ice-rafting. There, clasts from a condensed Early-Pleistocene sequence are taken as indication of a (localised) ice centre on the adjacent Scottish mainland (Stoker *et al.*, 1994). Considering the position of the U1317E site southwest of Ireland, on the east flank of the enclosed Porcupine Seabight (Fig. 4.1), and with the presence of ice-rafted lithics typical for the Irish Carboniferous (e.g. shale and dark-grey carbonates), the restriction of significant ice build-up solely to Scotland now seems debatable. Although tentative without additional analyses, the early existence of one extended ice mass or even multiple ice centres of considerable size on the BI is here proposed.

The Early-Pleistocene development of higher-latitude ice sheets (e.g. on Greenland, Iceland and Scandinavia) and, specifically, their marine advances are taken to be (partly) documented in the North Atlantic IRD sequences (e.g. Flesche Kleiven *et al.*, 2002; Jansen *et al.*, 2000; Sejrup *et al.*, 2005). In this study, contemporaneous and repeated ice build-up on the mid-latitudinal BI is evidenced in addition. It therefore seems that the first sustained episodes of climate deterioration, from ca. 2.6 – 2.4 Ma onwards (cf. Lisiecki and Raymo, 2005), were able to force significant, circum-Atlantic ice accumulation and ice-rafting, and this as far south as the 57° - 52°N BI (cf. timing and glacial character of U1317E unit M1 IRD peaks; Fig. 4.4). Hence, even prior to the mid-Pleistocene transition to a higher amplitude, 100-ka orbital cyclicity (e.g. Mudelsee and Schulz, 1997), the BIIS appears to have been a considerable and dynamic ice mass, sensitively responding to (orbitally-induced) climate fluctuations. The extreme maritime position of the BI favours this climatic sensitivity, as changes in oceanic circulation (due to e.g. latitudinal migrations of the polar front) can directly influence ice accumulation through the availability of heat and moisture. In this way, significant south-ward excursions of the polar front during colder orbital stages may have promoted BIIS formation and variability throughout the Pleistocene (cf. Scourse *et al.* (2009) for the later stage BIIS). To which degree the early BIIS was affected by external and/or internal destabilisation processes (cf. Hubbard *et al.* (2009) for the later stage BIIS) has to be further constrained.

For the first time, the long-term existence of an ice-rafting BIIS is argued for in this study. The regionally unique continental margin record from the Challenger coral carbonate mound, thereby identifies the BIIS as a dynamic and persistent feature of the Pleistocene climate system. Not only in the more intensively glaciated, post "mid-Pleistocene Transition" world (e.g. Mudelsee and Schulz, 1997), but even in the early stages of Northern Hemisphere glacial expansion, an

ice-rafting BIIS repeatedly appears during glacial intervals. Therefore, early and significant ice accumulation in mid-latitudinal regions, such as the British-Irish Isles, should be accounted for in reconstructions and modelling studies addressing the mechanisms that steer Northern Hemisphere ice sheet development and their impact on Quaternary climate variability.

4.4.2 The clay mineralogy of Challenger Mound: A unique archive of the continental climate on the British-Irish Isles

As discussed in chapter 3, the clay assemblage is the result of the complex interplay between (1) the petrography of the source rock, (2) differentiation processes during transport and deposition and (3) the continental climate (Fagel, 2007). In order to accurately interpret the clay mineralogy, a rigorous control of these parameters is necessary (Fagel, 2007; Gingele *et al.*, 1999; Moriarty, 1977).

(1) The provenance of the detrital material was constrained using Nd and Sr isotopes (see also chapter 3). The Nd and Sr isotope ratios identify the British-Irish Isles as the main contributor of terrigenous sediment in Challenger Mound with a varying contribution of volcanic material. Given that most isotope ratios cluster together (Fig. 4.5C), it is assumed that no significant change in the provenance of the detrital material occurred. Hence, the variations in the clay mineralogy cannot be attributed to changes in provenance of the source rock.

(2) Thierens *et al.* (2010) constrained the depositional processes which affected Challenger Mound by analyzing the siliciclastic grain-size of the entire mound sequence with a resolution of 10 cm. The lower mound fase (M1) seems to attest to a rather continuous, steadily changing current-controlled depositional environment (Thierens *et al.*, 2010). The fast and semi-continuous sediment build-up during this first mound development stage (Foubert and Henriet, 2009; Kano *et al.*, 2007) is attributed to the presence of a dense coral cover which is able to trap fine-grained sediment and prevents reworking (Thierens *et al.*, 2010). Moreover, with increasing distance from the pedogenic sources, the influence of differential settling processes during transport decreases and the clay assemblage seems to be more and more steered by climate (Chamley, 1989). Hence, the effect of differentiation processes on the clay mineralogy in M1 will be significantly reduced. In contrast, the upper mound phase (M2) reveals several unconformities and generally coarser deposits are observed (Thierens *et al.*, 2010). This is attributed to a reduced coral density, resulting in a decreasing capacity to deposit and/or preserve finer-grained material (Thierens *et al.*, 2010). Therefore, great care has to be taken when interpreting the clay mineralogy in M2 as differentiation processes may have significantly altered the clay assemblage. The influence of reworking and/or strong sorting processes on the clay mineralogy was already discussed in chapter 3.

(3) Given the small variations in the provenance of the source rock and the limited influence of differentiation processes, the cyclic patterns observed in the clay mineralogy of M1 may be interpreted in terms of changing conditions of continental weathering (Fagel, 2007). In general, interglacial periods, characterized by increased carbonate content (Titschack *et al.*, 2009) and low $\delta^{18}O$ values (Sakai *et al.*, 2009), reveal enhanced values for the smectite content (Fig. 4.6). This indicates that a temperate climate was present on the British-Irish Isles with sufficient precipitation (50-100 cm/year) to allow hydrolysis (Chamley, 1989). Under these climatic conditions, chemical weathering processes will lead to a pedogenic transformation of illite to smectite. In contrast, glacial intervals in M1, characterized by an increased siliciclastic content (Titschack *et al.*, 2009) and higher $\delta^{18}O$ values (Sakai *et al.*, 2009), reveal enhanced illite values (Fig. 4.6). The increase of the illite content is attributed to the decrease of hydrolytic processes and the increase of direct rock erosion (Chamley, 1989). This is in accordance with the presence of an Early Pleistocene ice sheet on the BI which results in enhanced physical weathering while the absence of free water inhibits chemical weathering processes. A remarkable feature is the occurrence of abrupt smectite peaks which are superimposed on the cyclic glacial-interglacial pattern (Fig. 4.6). These smectite peaks correspond to ice-rafted horizons occurring throughout the entire mound sequence (Thierens *et al.*, 2010). Similar observations were made by Marinoni *et al.* (2008) and Vogt and Knies (2008) which attributed the smectite peaks to the initial stage of chemical weathering during deglaciations. Below the mound base, the strong increase of smectite and

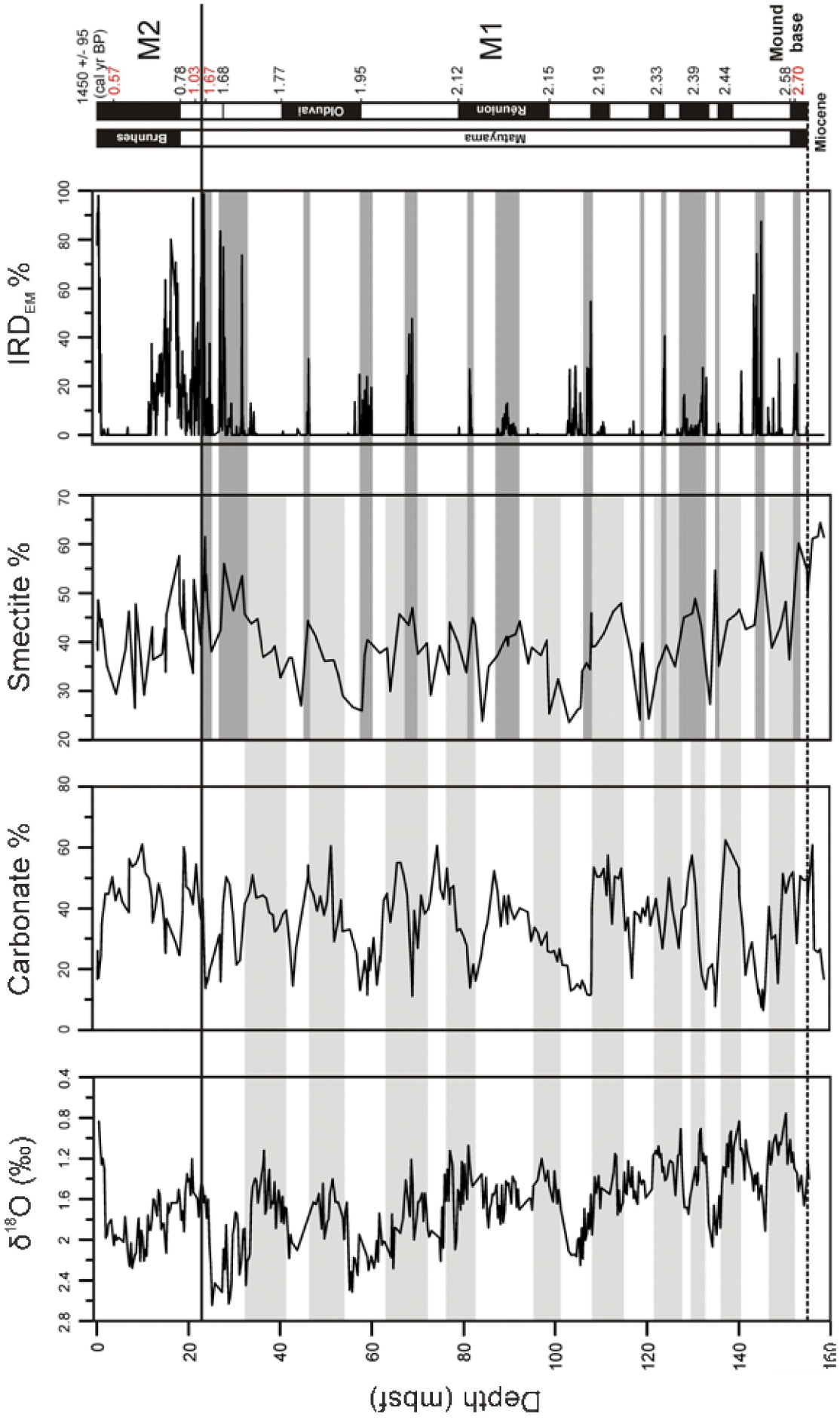
1450 +/- 95 (cal yr BP)
0.57
M2
0.78
1.03
1.67
1.68
1.77
1.95
2.12
M1
2.15
2.19
2.33
2.39
2.44
2.58
2.70
Mound base
Miocene
Brunhes
Matuyama
Olduvai
Réunion
IRD$_{EM}$ %
Smectite %
Carbonate %
$\delta^{18}O$ (‰)
Depth (mbsf)

Fig. 4.6 (Left) *The $\delta^{18}O$ values of the planktonic foraminifers (Sakai et al., 2009), the carbonate content (Titschack et al., 2009), the smectite content and the particle-size analysis with the percentage of the coarse, bimodal end-member (EM) which was interpreted to be linked with ice-rafted debris (IRD) (Thierens et al., 2010). The stratigraphic framework is based on Thierens et al. (2010), Kano et al. (2007) and Foubert and Henriet (2009). The grey zones in mound phase 1 (M1) are interglacial intervals (Sakai et al., 2009), the dark grey zones are linked with ice-rafting events. All depths in corrected metre below seafloor (mbsf).*

the decrease of illite (Fig. 4.6) mark the increased importance of chemical weathering under warm and humid conditions (Chamley, 1989). This is in accordance with the higher temperatures which are recorded during the Miocene, compared to the Pleistocene.

The clay mineralogy in the upper mound phase (M2) is harder to interpret in terms of glacial-interglacial cycles as the increasing importance of differentiation processes and the presence of numerous unconformities (Thierens *et al.*, 2010) result in a more chaotic pattern (Fig. 4.6). Nevertheless, a clear shift is observed in the kaolinite and chlorite content of M2 compared to M1. The upper mound fase (M2) is characterized by an enhanced content of chlorite and a decrease of the kaolinite values (Fig. 4.6). This observation indicates the increased importance of physical weathering during M2 compared to M1. In this regard, the change in periodicity of the glacial-interglacial cycles from 41 ka to 100 ka during the Mid-Pleistocene Transition (MPT) (Lisiecki and Raymo, 2005) may be of great importance. After the MPT, the prolonged and more extensive glaciations resulted in increased physical weathering and thus chlorite formation whereas the formation of kaolinite through chemical weathering was reduced.

4.5 Conclusions

Provenance data, based on sediment neodymium (Nd) and strontium (Sr) isotopic source-fingerprinting and coarse (>150 µm) lithic species identification, identifies the British-Irish Isles as the main sediment contributor throughout the entire Challenger Mound record. Moreover, the Early-Pleistocene ice-rafted horizons which occur in the lower mound phase (M1) are linked with the British-Irish Isles as well. Hence, for the first time, evidence is presented for the presence of a recurring, marine-based ice sheet on the British-Irish Isles since the earliest Pleistocene, implying significant mid-latitudinal glaciations, even in the earliest stages of Northern Hemisphere glacial expansion. Therefore, early and significant ice accumulation in mid-latitudinal regions, such as the British-Irish Isles, should be accounted for in reconstructions and modelling studies addressing the mechanisms that steer Northern Hemisphere ice sheet development and their impact on Quaternary climate variability.

The clay mineralogy of the lower mound phase (M1) of Challenger Mound provides an excellent record of the Early-Pleistocene continental climate on the nearby British-Irish Isles. Interglacial periods are characterized by an enhanced smectite content indicating the presence of a temperate climate with sufficient precipitation to allow hydrolysis. Glacial periods record an increase in illite due to the decrease of hydrolytic processes and the increase of direct rock erosion. Abrupt smectite peaks are superimposed on this cyclic glacial-interglacial pattern and are linked to the initial stage of chemical weathering during deglaciations. Below the mound base, the increased smectite content attests of the increased temperature and hence, increased chemical weathering during the Miocene. The clay mineralogy of the upper mound phase (M2) of Challenger reveals a more chaotic pattern due to the absence of a dense coral framework which results in the increased influence of differentiation processes and the presence of numerous unconformities. Nevertheless an increase is observed in the chlorite content compared to M1, while kaolinite reveals a decrease. This is attributed to the prolonged and more extensive glaciations after the MPT, which result in an increase of the physical weathering processes.

References

Bernstein, S., Kelemen, P.B., Tegner, C., Kurz, M.D., Blusztajn, J. and Brooks, C.K., 1998. Post-breakup basaltic magmatism along the East Greenland Tertiary rifted margin. Earth and Planetary Science Letters, 160, 845-862.

Bond, G., Heinrich, H., Broecker, W.S., Labeyrie, L.D., McManus, J., Andrews, J.T., Huon, S., Jantschik, R., Clasen, S., Simet, C., Tedesco, K., Klas, M., Bonani, G. and Ivy, S., 1992. Evidence for massive discharges of icebergs into the North Atlantic ocean during the last glacial period. Nature, 360, 245-249.

Bond, G. and Lotti, R., 1995. Iceberg Discharges into the North Atlantic on Millenial Time Scales During the Last Glaciation. Science, 267, 1005-1010.

Brueckner, H.K., Gilotti, J.A. and Nutman, A.P., 1998. Caledonian eclogite-facies metamorphism of Early Proterozoic protoliths from the North-East Greenland Eclogite Province. Contributions to Mineralogy and Petrology, 130, 103-120.

Chamley, H., 1989. Clay Sedimentology. Springer, Berlin, 623 pp.

Davies, G., Gledhill, A. and Hawkesworth, C., 1985. Upper Crustal Recycling in Southern Britain - Evidence from Nd-Isotopes and Sr-Isotopes. Earth and Planetary Science Letters, 75(1), 1-12.

De Mol, B., Van Rensbergen, P., Pillen, S., Van Herreweghe, K., Van Rooij, D., McDonnell, A., Huvenne, V., Ivanov, M., Swennen, R. and Henriet, J.-P., 2002. Large deep-water coral banks in the Porcupine Basin, southwest of Ireland. Marine Geology, 188, 193-231.

Death, R., Siegert, M.J., Bigg, G.R. and Wadley, M.R., 2006. Modelling iceberg trajectories, sedimentation rates and meltwater input to the ocean from the Eurasian Ice Sheet at the Last Glacial Maximum. Palaeogeography Palaeoclimatology Palaeoecology, 236(1-2), 135-150.

Dethleff, D. and Kuhlmann, G., 2009. Entrainment of fine-grained surface deposits into new ice in the southwestern Kara Sea, Siberian Arctic. Continental Shelf Research, 29(4), 691-701.

Ehlers, J. and Gibbard, P.L., 2007. The extent and chronology of Cenozoic Global Glaciation. Quaternary International, 164-165, 6-20.

Fagel, N., 2007. Clay Minerals Deep Circulation and Climate. In: C. Hillaire-Marcel and A. De Vernal (Editors), Proxies in Late Cenozoic Paleoceanography. Elsevier, Amsterdam, pp. 139-184.

Farmer, G.L., Barber, D. and Andrews, J., 2003. Provenance of Late Quaternary ice-proximal sediments in the North Atlantic: Nd, Sr and Pb isotopic evidence. Earth and Planetary Science Letters, 209(1-2), 227-243.

Faure, G., 1986. Principles of Isotope Geology. J. Wiley, New York, 589 pp.

Ferdelman, T.G., Kano, A., Williams, T., Henriet, J.P. and Scientists, I.E., 2006. IODP Expedition 307 drills cold-water coral mound along the Irish continental margin. Scientific Drilling, 2, 11-16.

Flesche Kleiven, H.F., Jansen, E., Fronval, T. and Smith, T.M., 2002. Intensification of Northern Hemisphere glaciations in the circum Atlantic region (3.5-2.4 Ma) - ice-rafted detritus evidence. Palaeogeography, Palaeoclimatology, Palaeoecology, 184, 213-223.

Foubert, A. and Henriet, J.P., 2009. Nature and significance of the recent carbonate mound record: the Mound Challenger Code. Springer-Verlag, Heidelberg, 350 pp.

Gingele, F.X., Schmieder, F., von Dobeneck, T., Petschick, R. and Ruhlemann, C., 1999. Terrigenous flux in the Rio Grande Rise area during the past 1500 ka: Evidence of deepwater advection or rapid response to continental rainfall patterns? Paleoceanography, 14(1), 84-95.

Grousset, F.E., Cortijo, E., Huon, S., Hervé, L., Richter, T.O., Burdloff, D., Duprat, J. and Weber, O., 2001. Zooming in in Heinrich layers. Paleoceanography, 16(3), 240-259.

Grousset, F.E., Pujol, C., Labeyrie, L., Auffret, G.A. and Boelaert, A., 2000. Were the North Atlantic Heinrich events triggered by the behavior of the European ice sheets? Geology, 28(2), 123-126.

Hansen, H. and Nielsen, T.F.D., 1999. Crustal contamination in Palaeogene East Greenland flood basalts: plumbing system evolution during continental rifting. Chemical Geology, 157(1-2), 89-118.

Hemming, S.R., 2004. Heinrich events: Massive late pleistocene detritus layers of the North Atlantic and their global climate imprint. Reviews of Geophysics, 42(1), doi: 10.1029/2003rg000128.

Henriet, J.-P., De Mol, B., Pillen, S., Vanneste, M., Van Rooij, D., Versteeg, W., Croker, P.F., Shannon, P.M., Unnithan, V., Bouriak, S., Chachkine, P. and The Porcupine-Belgica 97 Shipboard Party, 1998.

Gas hydrate crystals may help build reefs. Nature, 391, 648-649.
Hibbert, F.D., Austin, W.E.N., Leng, M.J. and Gatliff, R.W., 2009. British Ice Sheet dynamics inferred from North Atlantic ice-rafted debris records spanning the last 175 000 years. Journal of Quaternary Science, doi:10.1002/jqs.1331.
Holm, P.M., Hald, N. and Waagstein, R., 2001. Geochemical and Pb-Sr-Nd isotopic evidence for separate hot depleted and Iceland plume mantle sources for the Paleogene basalts of the Faroe Islands. Chemical Geology, 178(1-4), 95-125.
Hovland, M., Croker, P.F. and Martin, M., 1994. Fault-associated seabed mounds (carbonate knolls?) off western Ireland and north-west Australia. Marine and Petroleum Geology, 11(2), 232-246.
Hubbard, A., Bradwell, T., Golledge, N., Hall, A., Patton, H., Sugden, D., Cooper, R. and Stoker, M., 2009. Dynamic cycles, ice streams and their impact on the extent, chronology and deglaciation of the British-Irish ice sheet. Quaternary Science Reviews, 28(7-8), 758-776.
Jansen, E., Fronval, T., Rack, F.R. and Channell, J.E.T., 2000. Pliocene-Pleistocene ice rafting history and cyclicity in the Nordic Seas during the last 3.5 Myr. Paleoceanography, 15(6), 709-721.
Kano, A., Ferdelman, T.G., Williams, T., Henriet, J.P., Ishikawa, T., Kawagoe, N., Takashima, C., Kakizaki, Y., Abe, K., Sakai, S., Browning, E., Li, X. and the IODP Expedition 307 Scientists, 2007. Age constraints on the origin and growth history of a deep-water coral mound in northeast Atlantic drilled during Integrated Ocean Drilling Program Expedition 307. Geology, 35(11), 1051-1054.
Knutz, P.C., Austin, W.E.N. and Jones, E.J.W., 2001. Millenial-scaled depostional cycles related to British Ice Sheet variability and North Atlantic paleocirculation since 45 kyr B.P., Barra Fan, U.K. margin. Paleoceanography, 16(1), 53-64.
Knutz, P.C., Zahn, R. and Hall, I.R., 2007. Centennial-scale variability of the British Ice Sheet: Implications for climate forcing and Atlantic meridional overturning circulation during the last deglaciation. Paleoceanography, 22(1), doi: 10.1029/2006pa001298.
Laberg, J.S., Stoker, M.S., Dahlgren, K.I.T., de Haas, H., Haflidason, H., Hjelstuen, B.O., Nielsen, T., Shannon, P.M., Vorren, T.O., van Weering, T.C.E. and Ceramicola, S., 2005. Cenozoic alongslope processes and sedimentation on the NW European Atlantic margin. Marine and Petroleum Geology, 22, 1069-1088.
Leng, M.J., Glover, B.W. and Chisholm, J.I., 1999. Nd and Sr isotopes as elastic provenance indicators in the Upper Carboniferous of Britain. Petroleum Geoscience, 5(3), 293-301.
Lisiecki, L.E. and Raymo, M.E., 2005. A Pliocene-Pleistocene stack of 57 globally distributed benthic delta O-18 records Paleoceanography, 20(2), doi:10.1029/2004PA001071.
Louwye, S., Foubert, A., Mertens, K., Van Rooij, D. and the IODP Exp. 307 Scientific Party, 2008. Integrated stratigraphy and palaeoecology of the Lower and Middle Miocene of Porcupine Basin. Geological Magazine, 145(3), 321-344.
MacAyeal, D.R., 1993. Binge/purge oscillations of the Laurentide ice sheets as a cause of the North Atlantic's Heinrich Events. Paleoceanography, 8, 775-784.
Marinoni, L., Setti, M., Salvi, C. and Lopez-Galindo, A., 2008. Clay minerals in late Quaternary sediments from the south Chilean margin as indicators of provenance and palaeoclimate. Clay Minerals, 43(2), 235-253.
Maslin, M.A., Li, X.S., Loutre, M.F. and Berger, A., 1998. The contribution of orbital forcing to the progressive intensification of Northern Hemisphere glaciation. Quaternary Science Reviews, 17(4-5), 411-426.
Mienis, F., De Stigter, H., De Haas, H. and Van Weering, T.C.E., 2009. Near-bed particle deposition and resuspension in a cold-water coral mound area at the Southwest Rockall Trough margin, NE Atlantic. Deep Sea Research Part I: Oceanographic Research Papers, 56(6), 1026-1038.
Moriarty, K.C., 1977. Clay-Minerals in Southeast Indian-Ocean Sediments, Transport Mechanisms and Depositional Environments. Marine Geology, 25(1-3), 149-174.
Mudelsee, M. and Schulz, M., 1997. The Mid-Pleistocene climate transition: onset of 100 ka cycle lags ice volume build-up by 280 ka. Earth and Planetary Science Letters, 151(1-2), 117-123.
Peck, V.L., Hall, I.R., Zahn, R., Grousset, F., Hemming, S.R. and Scourse, J.D., 2007. The relationship of Heinrich events and their European precursors over the past 60 ka BP: a multi-proxy ice-rafted debris provenance study in the North East Atlantic. Quaternary Science Reviews, 26(7-8), 862-

875.

Pirlet, H., Colin, C., Thierens, M., Latruwe, K., Van Rooij, D., Foubert, A., Frank, N., Blamart, D., Huvenne, V.A.I., Vanhaecke, F. and Henriet, J.P., 2010. The importance of the terrigenous fraction within a cold-water coral mound: A case study. Marine Geology, doi: 10.1016/j.margeo.2010.05.008.

Raymo, M.E., Hodell, D.A. and Jansen, E., 1992. Response of deep ocean circulation to initiation of Northern Hemisphere glaciation (3-2 Ma). Paleoceanography, 7, 645-672.

Raymo, M.E. and Huybers, P., 2008. Unlocking the mysteries of the ice ages. Nature, 451(7176), 284-285.

Revel, M., Cremer, M., Grousset, F.E. and Labeyrie, L., 1996a. Grain-size and Sr-Nd isotopes as tracer of paleo-bottom current strength, Northeast Atlantic Ocean. Marine Geology, 131(3-4), 233-249.

Revel, M., Sinko, J.A. and Grousset, F.E., 1996b. Sr and Nd isotopes as tracers of North Atlantic lithic particles: Paleoclimatic implications. Paleoceanography, 11(1), 95-113.

Roberts, J.M., Wheeler, A., Freiwald, A. and Cairns, S., 2009. Cold-water corals. The Biology and Geology of Deep-sea Coral Habitats. Cambridge University Press, Cambridge, 334 pp.

Ruddiman, W.F., Raymo, M.E., Martinson, D.G., Clement, B.M. and Backman, J., 1989. Pleistocene evolution: Northern Hemisphere ice sheets and North Atlantic Ocean. Paleoceanography, 4, 353-412.

Sakai, S., Kano, A. and Abe, K., 2009. Origin, glacial-interglacial responses, and controlling factors of a cold-water coral mound in NE Atlantic. Paleoceanography, 24, doi:10.1029/2008pa001695.

Scourse, J.D., Haapaniemi, A.I., Colmenero-Hildago, E., Peck, V.L., Hall, I.R., Austin, W.E.N., Knutz, P.C. and Zahn, R., 2009. Growth, dynamics and deglaciation of the last British-Irish Ice Sheet: the deep-sea ice-rafted detritus record. Quaternary Science Reviews, 28(27-28), 3066-3084.

Sejrup, H.P., Hjelstuen, B.O., Dahlgren, K.I.T., Haflidason, H., Kuijpers, A., Nygard, A., Praeg, D., Stoker, M.S. and Vorren, T.O., 2005. Pleistocene glacial history of the NW European continental margin. Marine and Petroleum Geology, 22, 1111-1129.

Shackleton, N.J., Backman, J., Zimmerman, H., Kent, D.V., Hall, M.A., Roberts, D.G., Schnitker, D., Baldauf, J.G., Desprairies, A., Homrighausen, R., Huddlestun, P., Keene, J.B., Kaltenback, A.J., Krumsiek, K.A.O., Morton, A.C., Murray, J.W. and Westbergsmith, J., 1984. Oxygen Isotope Calibration of the Onset of Ice-Rafting and History of Glaciation in the North-Atlantic Region. Nature, 307(5952), 620-623.

St. John, K., 2008. Cenozoic ice-rafting history of the central Arctic Ocean: Terrigenous sands on the Lomonosov Ridge. Paleoceanography, 23, doi:10.1029/2007PA001483.

Stoker, M.S., Leslie, A.B., Scott, W.D., Briden, J.C., Hine, N.M., Harland, R., Wilkinson, I.P., Evans, D. and Ardus, D.A., 1994. A Record of Late Cenozoic Stratigraphy, Sedimentation and Climate-Change from the Hebrides Slope, Ne Atlantic-Ocean. Journal of the Geological Society, 151, 235-249.

Thierens, M., Titschack, J., Dorschel, B., Huvenne, V., Wheeler, A., Stuut, J.B. and O´Donnell, R., 2010. The 2.6 Ma depositional sequence from the Challenger cold-water coral mound (IODP Exp. 307): sediment contributors and hydrodynamic environments. Marine Geology, 271, 260-277.

Titschack, J., Thierens, M., Dorschel, B., Schulbert, C., Freiwald, A., Kano, A., Takashima, C., Kawagoe, N., Li, X. and Scientists, I.E., 2009. Carbonate budget of a cold-water coral mound (Challenger Mound, IODP Exp. 307). Marine Geology, 259(1-4), 36-46.

Vogt, C. and Knies, J., 2008. Sediment dynamics in the Eurasian Arctic Ocean during the last deglaciation - The clay mineral group smectite perspective. Marine Geology, 250(3-4), 211-222.

Weis, D., Demaiffe, D., Souchez, R., Gow, A.J. and Meese, D.A., 1997. Ice sheet development in central Greenland, implications from the Nd, Sr and pH isotopic compositions of basal material. Earth and Planetary Science Letters, 150(1-2), 161-169.

Weltje, G.J., 1997. End-member modeling of compositional data: Numerical-statistical algorithms for solving the explicit mixing problem. Mathematical Geology, 29(4), 503-549.

Williams, T., Kano, A., Ferdelman, T.G., Henriet, J.P., Abe, K., Andres, M.S., Bjerager, M., Browning, E., Cragg, B.A., De Mol, B., Dorschel, B., Foubert, A., Frank, T.D., Fuwa, Y., Gaillot, P., Gharib, J.J., Gregg, J.M., Huvenne, V., Léonide, P., Li, X., Mangelsdorf, K., Tanaka, A., Monteys, X., Novosel, I., Sakai, S., Samarkin, V.A., Sasaki, K., Spivack, A.J., Takashima, C. and Titschak, J., 2006. Cold-Water Coral Mounds Revealed. EOS Transactions, 87(47), 525-526.

Part 3

Early-diagenetic processes in cold-water coral mounds

Chapter 5 - Early diagenesis in cold-water coral mounds: Introduction and general concepts

In part 3 of this study, the early-diagenetic processes in cold-water coral mounds will be examined with a special focus on carbonate diagenesis. The term diagenesis encompasses all the processes which affect the sediments after deposition until the realms of incipient metamorphism at elevated temperatures and pressures. Carbonate diagenesis comprises obvious processes such as cementation and dissolution but also more subtle processes such as the development of microporosity and changes in trace element and isotopic signatures (Tucker and Wright, 1990). The precipitation or dissolution of calcium carbonate depends on the saturation state Ω of the ambient solution. The saturation state of a solution with respect to a given mineral is simply the ratio of the ion activity or concentration product to the thermodynamic or stoichiometric solubility product.

$$\Omega_{calcite} = (a(Ca^{2+})*a(CO_3^{2-}))/K_{calcite}$$

If Ω = 1 the solid and solution are in equilibrium; if Ω < 1, the solution is undersaturated and mineral dissolution may occur; if Ω > 1, the solution is supersaturated and precipitation might occur. Hence, parameters affecting carbonate ion activity such as pH, pCO_2 and total alkalinity must be considered when discussing carbonate dissolution or cementation (Morse and Arvidson, 2002; Morse *et al.*, 2007).

Three principal diagenetic environments can be distinguished: the near-surface meteoric, marine and burial environment (Fig. 5.1) (Tucker and Wright, 1990). The meteoric diagenetic environment is characterized by exposure to subaerial conditions and the presence of relatively dilute waters that generally exhibit a wide range of carbonate mineral saturation states (Moore, 2001). In the meteoric environment a distinction is made between the vadose zone, which is located above the water table and the phreatic zone, below the water table. The marine environment, in which most carbonate sediments originate today, is characterized by normal or modified marine pore fluids generally supersaturated with respect to most carbonate mineral species (Moore, 2001). Hence, the marine environment is potentially a site of extensive porosity destruction. In the shallow subsurface a mixing zone occurs at the interface of the marine and meteoric environment. Upon burial, the marine and meteoric environments pass vertically into the burial diagenetic environment. Choquette and Pray (1970) distinguished three stages during sediment burial: eogenetic, mesogenetic and telogenetic. The eogenetic stage is the time interval between initial sediment deposition and burial to the point that meteoric or normal marine waters cease to actively circulate by gravity or convection. The mesogenetic stage is the interval during which the sediments are buried at depth below the major influence of surficial diagenetic processes. During the telogenetic stage, sediments which have been in the mesogenetic zone are exhumed and occur in association with unconformities.

The present research will focus on the early-diagenetic processes which occur in the eogenetic, deep-marine realm (Fig. 5.1). A thorough knowledge of these processes is crucial as the early-diagenetic changes might form a template for later burial diagenesis. Moreover, it enables to better distinguish and identify early-diagenetic features in old rocks which have been subjected to

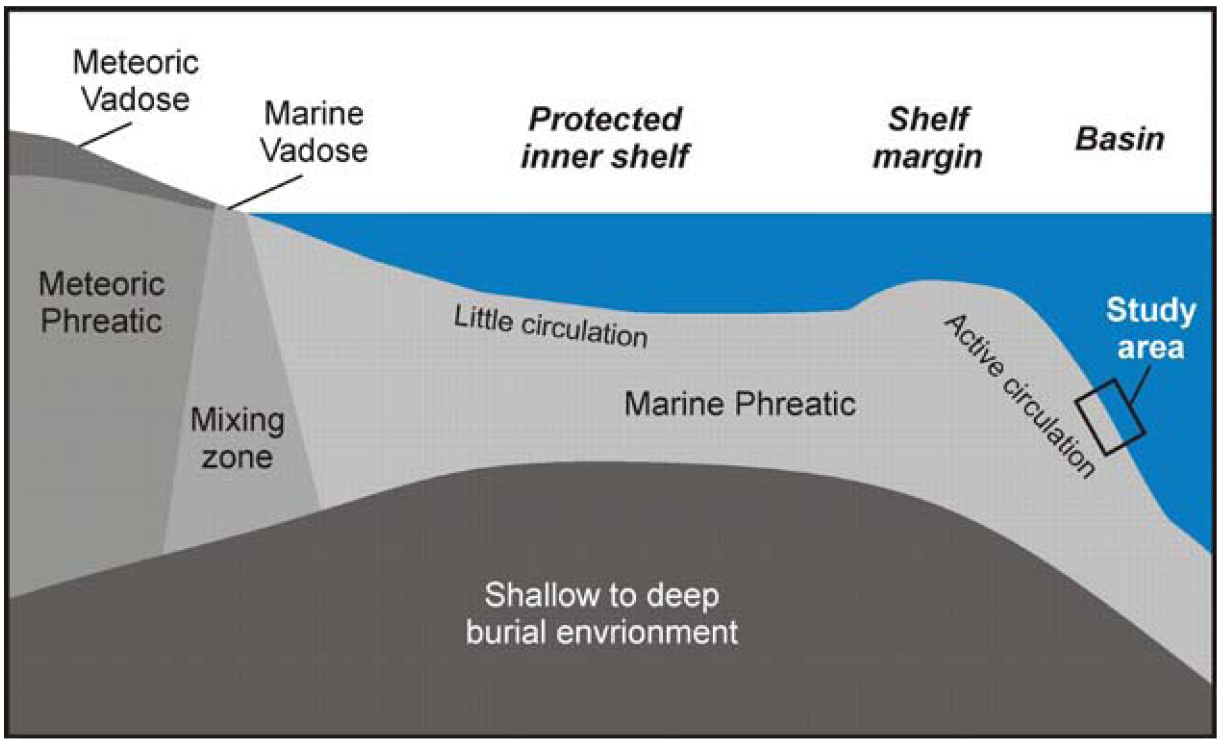

Fig. 5.1 *Schematic representation of the different carbonate diagenetic environments with indication of the present study area. Modified after Tucker and Wright (1990).*

burial diagenesis. The main driver for carbonate diagenesis in the surficial, marine environment is the microbial degradation of organic matter (e.g. Ferdelman *et al.*, 2006; Ku *et al.*, 1999; Sanders, 2003; Schulz and Zabel, 2000; Tribble, 1993; Walter *et al.*, 1993; Walter and Burton, 1990; Wehrmann *et al.*, 2009; Wehrmann *et al.*, 2010). During organic matter mineralization, bacteria will reduce electron acceptors to support their metabolism. The general depth sequence of oxidants used in the degradation of organic matter is O_2 -> NO_3^- -> Mn(IV) -> Fe(III) -> SO_4^{2-} -> CO_2 (Fig. 5.2). This sequence corresponds to a gradual decrease in redox potential of the oxidant and thus to a decrease in the free energy available by respiration with the different electron acceptors (Jørgensen, 2000). The biogeochemical processes associated with organic matter mineralization affect the alkalinity and pH of the interstitial water and therefore steer carbonate dissolution and precipitation (Fig. 5.2) (Soetaert *et al.*, 2007). Furthermore, the (re-) oxidation of reaction (by-) products of organic matter degradation might affect the saturation state of the porewater with respect to carbonate (Fig. 5.2). Hence, the degree of openness of the system is of major importance for diagenesis (Boudreau and Canfield, 1993; Sanders, 2003). In the following, the general concept of the biogeochemical processes which affect diagenesis in cold-water coral mounds will be discussed. In chapter 6 and 7, these processes will be studied in more detail. During organic matter degradation, the electron acceptors: O_2, NO_3^-, Mn(IV) and Fe(III) are rapidly consumed in the upper (tens of) centimeters of the sediment (Jørgensen, 2000). Therefore, they play a minor role in the diagenetic processes which affect the sediments in cold-water coral mounds. In contrast, the sulfate reduction zone extends several to even more than 100 meters in the sediment. The high concentration of sulfate in seawater (28 mmol/l) makes sulfate a dominant electron acceptor in the anaerobic degradation of organic matter (Kasten and Jørgensen, 2000). The sedimentary sulfur cycle starts with the bacterial reduction of seawater sulfate to hydrogen sulfide (H_2S), resulting in a decrease in the concentration of pore-water sulfate in a closed system (Fig. 5.2). Two types of sulfate reduction can be distinguished: (1) assimilatory sulfate reduction which serves for the biosynthesis of organic–sulfur compounds, and (2) dissimilatory sulfate reduction from which microorganisms conserve energy. We will focus here on the latter process.

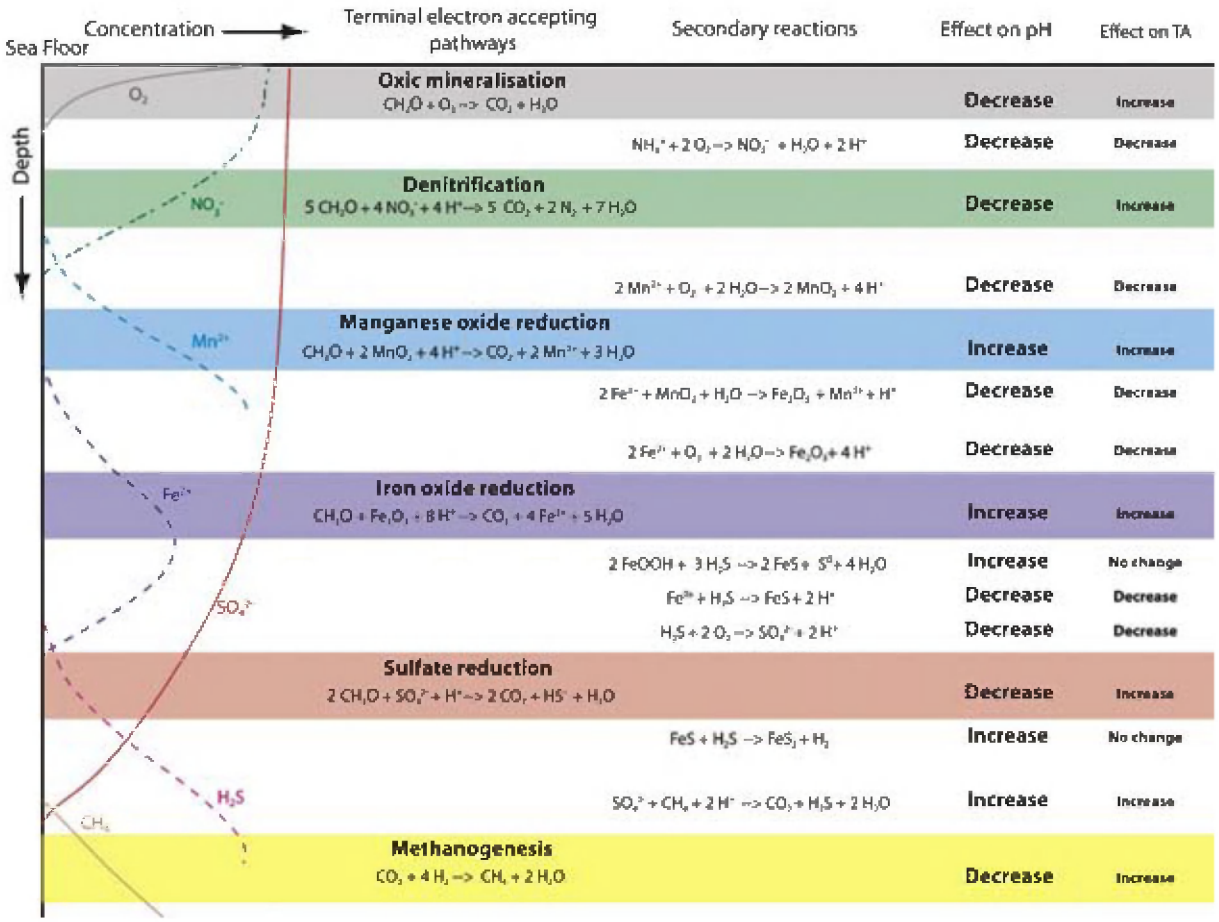

Fig. 5.2 *Schematic presentation of the terminal electron accepting pathways in marine sediments following the typical succession with depth (Froelich et al., 1979). At the overlapping intervals the reactions of the by-products are shown as well as the most important reactions of these products with solid-phase mineral phases. Also shown is the effect of the individual reactions on pore-water pH and total alkalinity (TA) for an initial pH close to seawater values (pH=8.2) based on Soetaert et al. (2007). Picture taken from Wehrmann (2010).*

Dissimilatory sulfate reduction can be described by the following net equation (e.g. Coleman and Raiswell, 1995):

$$2CH_2O + SO_4^{2-} \rightarrow 2HCO_3^- + H_2S$$

The sulfur isotopic composition of hydrogen sulfide, produced during bacterial sulfate reduction, will be depleted with respect to sea water which has a $\delta^{34}S$ value of 20.3‰ (Longinelli, 1989). This is the result of the preferential utilization of the lighter ^{32}S isotope by sulfate reducing bacteria such as *Desulfovibrio desulfuricans*. The depletion can go up to 46‰ (Kaplan and Rittenberg, 1964), however, larger fractionation values are reported due to re-oxidation of sulfide followed by disproportionation of thiosulfate and/or elemental sulfur (e.g. Böttcher *et al.*, 2001; Jørgensen, 1990). Due to the preferential removal of the lighter S isotope, the $\delta^{34}S$ value of both the remaining sulfate and the produced hydrogen sulfide will increase with depth in a closed system. However, the difference between the $\delta^{34}S$ values of both reactants will remain the same (Bickert, 2000). Hydrogen sulfide, produced during sulfate reduction, may react with reactive iron minerals (iron-(oxyhydr)oxides) or dissolved iron, resulting in the precipitation of pyrite. Hence, the $\delta^{34}S$ values of sedimentary pyrite might yield information about the biogeochemical processes which occurred at the time of pyrite formation and are therefore of major importance for the reconstruction of the diagenetic environment. The spectrum of reactions of sulfate reduction (and associated reactions involving the reaction byproducts) may in one case lead to precipitation and in another to dissolution of calcium carbonate (Sanders, 2003). In that respect, the degree of mechanical and chemical openness of the system plays an important role (Sanders, 2003) as

well as the pool of reactive iron present in the sediment (Ferdelman *et al.*, 2006; Wehrmann *et al.*, 2009).
Sulfate is also reduced in connection to anaerobic methane oxidation (AOM) (Kasten and Jørgensen, 2000). Methane is generated below the sulfate zone in the sediment as the end-product of anaerobic degradation of organic matter or is derived from seepage of thermogenic hydrocarbons. In marine sediments, microorganisms mediating AOM indeed consume methane at the expense of sulfate according to the equation (Hoehler *et al.*, 1994; Nauhaus *et al.*, 2002; Valentine and Reeburgh, 2000):

$$CH_4 + SO_4^{2-} \rightarrow HCO_3^- + HS^- + H_2O$$

The latter process is mediated by a consortium of anaerobic methane-oxidizing archaea and sulfate-reducing bacteria (Boetius *et al.*, 2000; Valentine and Reeburgh, 2000). AOM typically occurs one to several meters below the sediment surface in a zone referred to as the sulfate-methane transition zone (SMTZ), a cm- to m-scale interval of low pore-water sulfate and methane concentrations (Borowski *et al.*, 1999). Due to the increase in alkalinity (production of HCO_3^-), AOM favours the precipitation of authigenic carbonates (e.g. Aloisi *et al.*, 2002; Aloisi *et al.*, 2000). These carbonates are characterized by depleted $\delta^{13}C$ values due to the incorporation of carbon enriched in ^{12}C deriving from methane. The carbonates which precipitate below the SMTZ, in the zone where methanogenesis occurs, are characterized by increasing and even positive $\delta^{13}C$ values (Mozley and Burns, 1993). When present, AOM exerts a strong control on the diagenetic processes and the overall geochemistry (Maignien *et al.*, 2010).

References

Aloisi, G., Bouloubassi, I., Heijs, S.K., Pancost, R.D., Pierre, C., Damste, J.S.S., Gottschal, J.C., Forney, L.J. and Rouchy, J.M., 2002. CH4-consuming microorganisms and the formation of carbonate crusts at cold seeps. Earth and Planetary Science Letters, 203(1), 195-203.

Aloisi, G., Pierre, C., Rouchy, J.M., Foucher, J.P., Woodside, J. and party, M.s., 2000. Methane-related authigenic carbonates of eastern Mediterranean Sea mud volcanoes and their possible relation to gas hydrate destabilisation. Earth and Planetary Science Letters, 184, 321-338.

Bickert, T., 2000. Influence of Geochemical Processes on Stable Isotope Distribution in Marine Sediments. In: H.D. Schulz and M. Zabel (Editors), Marine Geochemistry. Springer-Verlag, Berlin Heidelberg, pp. 309-333.

Boetius, A., Ravenschlag, K., Schubert, C.J., Rickert, D., Widdel, F., Gieseke, A., Amann, R., Jorgensen, B.B., Witte, U. and Pfannkuche, O., 2000. A marine microbial consortium apparently mediating anaerobic oxidation of methane. Nature, 407, 623-626.

Borowski, W.S., Paull, C.K. and Ussler, W., 1999. Global and local variations of interstitial sulfate gradients in deep-water, continental margin sediments: Sensitivity to underlying methane and gas hydrates. Marine Geology, 159(1-4), 131-154.

Böttcher, M.E., Thamdrup, B. and Vennemann, T.W., 2001. Oxygen and sulfur isotope fractionation during anaerobic bacterial disproportionation of elemental sulfur. Geochimica et Cosmochimica Acta, 65(10), 1601-1609.

Boudreau, B.P. and Canfield, D.E., 1993. A Comparison of Closed-System and Open-System Models for Porewater Ph and Calcite-Saturation State. Geochimica et Cosmochimica Acta, 57(2), 317-334.

Choquette, P.W. and Pray, L.C., 1970. Geological nomenclature and classification of porosity in sedimentary carbonates. American Association of Petroleum Geologists Bulletin, 54, 207-250.

Coleman, M.L. and Raiswell, R., 1995. Source of Carbonate and Origin of Zonation in Pyritiferous Carbonate Concretions - Evaluation of a Dynamic-Model. American Journal of Science, 295(3), 282-308.

Ferdelman, T.G., Kano, A., Williams, T., Henriet, J.P. and Scientists, I.E., 2006. IODP Expedition 307 drills cold-water coral mound along the Irish continental margin. Scientific Drilling, 2, 11-16.

Froelich, P.N., Klinkhammer, G.P., Bender, M.L., Luedtke, N.A., Heath, G.R., Cullen, D., Dauphin, P., Hammond, D., Hartman, B. and Maynard, V., 1979. Early Oxidation of Organic-Matter in Pelagic Sediments of the Eastern Equatorial Atlantic - Suboxic Diagenesis. Geochimica et Cosmochimica Acta, 43(7), 1075-1090.

Hoehler, T.M., Alperin, M.J., Albert, D.B. and Martens, C.S., 1994. Field and Laboratory Studies of Methane Oxidation in an Anoxic Marine Sediment - Evidence for a Methanogen-Sulfate Reducer Consortium. Global Biogeochemical Cycles, 8(4), 451-463.

Jørgensen, B.B., 1990. A Thiosulfate Shunt in the Sulfur Cycle of Marine-Sediments. Science, 249(4965), 152-154.

Jørgensen, B.B., 2000. Bacteria and Marine Biogeochemistry. In: H.D. Schulz and M. Zabel (Editors), Marine Geochemistry. Springer-Verlag, Berlin Heidelberg, pp. 173-208.

Kaplan, I.R. and Rittenberg, S.C., 1964. Microbiological fractionation of sulphur isotopes. Journal of General Microbiology, 34, 195-212.

Kasten, S. and Jørgensen, B.B., 2000. Sulfate Reduction in Marine Sediments. In: H.D. Schulz and M. Zabel (Editors), Marine Geochemistry. Springer-Verlag, Berlin Heidelberg, pp. 263-282.

Ku, T.C.W., Walter, L.M., Coleman, M.L., Blake, R.E. and Martini, A.M., 1999. Coupling between sulfur recycling and syndepositional carbonate dissolution: Evidence from oxygen and sulfur isotope composition of pore water sulfate, South Florida Platform, USA. Geochimica Et Cosmochimica Acta, 63(17), 2529-2546.

Longinelli, A., 1989. Oxygen-18 and sulphur-34 in dissolved oceanic sulphate and phosphate. In: P. Fritz and J.C. Fontes (Editors), Handbook of Environmental Isotope Geochemistry. Elsevier, Amsterdam, pp. 219-255.

Maignien, L., Depreiter, D., Foubert, A., Reveillaud, J., De Mol, L., Boeckx, P., Blamart, D., Henriet, J.P. and Boon, N., 2010. Anaerobic oxidation of methane in a cold-water coral carbonate mound from

the Gulf of Cadiz. International Journal of Earth Sciences, doi: 10.1007/s00531-010-0528-z.
Moore, C.H., 2001. Carbonate Reservoirs: Porosity evolution and diagenesis in a sequence stratigraphic framework. Developments in sedimentology, 55. Elsevier, 444 pp.
Morse, J.W. and Arvidson, R.S., 2002. The dissolution kinetics of major sedimentary carbonate minerals. Earth-Science Reviews, 58(1-2), 51-84.
Morse, J.W., Arvidson, R.S. and Luttge, A., 2007. Calcium carbonate formation and dissolution. Chemical Reviews, 107(2), 342-381.
Mozley, P.S. and Burns, S.J., 1993. Oxygen and Carbon Isotopic Composition of Marine Carbonate Concretions - an Overview - Reply. Journal of Sedimentary Petrology, 63(5), 1008-1008.
Nauhaus, K., Boetius, A., Kruger, M. and Widdel, F., 2002. In vitro demonstration of anaerobic oxidation of methane coupled to sulphate reduction in sediment from a marine gas hydrate area. Environmental Microbiology, 4(5), 296-305.
Sanders, D., 2003. Syndepositional dissolution of calcium carbonate in neritic carbonate environments: geological recognition, processes, potential significance. Journal of African Earth Sciences, 36(3), 99-134.
Schulz, H.D. and Zabel, M., 2000. Marine Geochemistry. Springer-Verlag, Berlin Heidelberg, 455 pp.
Soetaert, K., Hofmann, A.F., Middelburg, J.J., Meysman, F.J.R. and Greenwood, J., 2007. The effect of biogeochemical processes on pH. Marine Chemistry, 105(1-2), 30-51.
Tribble, G.W., 1993. Organic-Matter Oxidation and Aragonite Diagenesis in a Coral-Reef. Journal of Sedimentary Petrology, 63(3), 523-527.
Tucker, M.E. and Wright, V.P., 1990. Carbonate sedimentology. Blackwell, Oxford.
Valentine, D.L. and Reeburgh, W.S., 2000. New perspectives on anaerobic methane oxidation. Environmental Microbiology, 2(5), 477-484.
Walter, L.M., Bischof, S.A., Patterson, W.P. and Lyons, T.W., 1993. Dissolution and Recrystallization in Modern Shelf Carbonates - Evidence from Pore-Water and Solid-Phase Chemistry. Philosophical Transactions of the Royal Society of London Series a-Mathematical Physical and Engineering Sciences, 344(1670), 27-36.
Walter, L.M. and Burton, E.A., 1990. Dissolution of Recent Platform Carbonate Sediments in Marine Pore Fluids. American Journal of Science, 290(6), 601-643.
Wehrmann, L.M., 2010. Biogeochemical processes in sediments associated to cold-water coral ecosystems, University Bremen, Bremen, 233 pp.
Wehrmann, L.M., Knab, N.J., Pirlet, H., Unnithan, V., Wild, C. and Ferdelman, T.G., 2009. Carbon mineralization and carbonate preservation in modern cold-water coral reef sediments on the Norwegian shelf. Biogeosciences, 6(4), 663-680.
Wehrmann, L.M., Templer, S.P., Brunner, B., Bernasconi, S.M., Maignien, L. and Ferdelman, T.G., 2010. The imprint of methane seepage on the geochemical record and early diagenetic processes in cold-water coral mounds on Pen Duick Escarpment, Gulf of Cadiz. Marine Geology, doi:10.1016/j.margeo.2010.08.005.

Chapter 6 - Diagenetic formation of gypsum and dolomite in a cold-water coral mound in the Porcupine Seabight, off Ireland

Abstract

Authigenic gypsum was found in a gravity core, retrieved from the top of Perseverance Mound, a giant cold-water coral mound in the Porcupine Basin, off Ireland. The occurrence of gypsum in such an environment is intriguing, since gypsum, a classic evaporitic mineral, is undersaturated with respect to sea water. Sedimentological, petrographic and isotopic evidence point to diagenetic formation of the gypsum, tied to oxidation of sedimentary sulfide minerals (i.e. pyrite). This oxidation is attributed to a phase of increased bottom currents which caused erosion and enhanced inflow of oxidizing fluids into the mound sediments. The oxidation of pyrite produced acidity, causing carbonate dissolution and subsequently leading to pore-water oversaturation with respect to gypsum and dolomite. Calculations based on the isotopic compositions of gypsum and pyrite reveal that between 21.6% and 28.6% of the sulfate incorporated into the gypsum derived from pyrite oxidation. Thus, authigenic gypsum can serve as a signature for diagenetic oxidation events in carbonate-rich sediments. The dissolution of carbonate increased the porosity in the affected sediment layer but promoted lithification of the sediments at the sediment-water interface. This lithified carbonate layer was subsequently buried by Holocene sediments which resulted in a new phase of bacterial sulfate reduction. The produced hydrogen sulfide, which acts as a weak acid, was not buffered in the lithified carbonate layer due to the limited pool of reactive iron. This led to the dissolution of aragonitic biogenic fragments, creating a moldic porosity in the lithified horizon.
These observations demonstrate that fluid flow, steered by environmental factors, has an important effect on the diagenesis of coral mounds.

This chapter is mostly based on Pirlet, H. Wehrmann, L.M., Brunner, B., Frank, N., Dewanckele, J., Van Rooij, D., Foubert, A., Swennen, R., Naudts, L., Boone, M., Cnudde, V., Henriet, J.-P. (2010) Diagenetic formation of gypsum and dolomite in a cold-water coral mound in the Porcupine Seabight, off Ireland. Sedimentology, 57: 786-805.

6.1 Introduction

The occurrence of cold-water corals has been reported all along the Atlantic European margin over a wide bathymetric and hydrographical range (Freiwald and Roberts, 2005; Roberts *et al.*, 2006). The framework-building cold-water corals, *Lophelia pertusa* and *Madrepora oculata* are found from northern Norway, where they form elongated reefs (Lindberg *et al.*, 2007; Wheeler *et al.*, 2007), to the Gulf of Cadiz where they occur in the vicinity of mud volcanoes (Foubert *et al.*, 2008). In the Porcupine Seabight, located southwest of Ireland, *Lophelia* and *Madrepora* have built mounds up to 200 m high (De Mol *et al.*, 2002; Henriet *et al.*, 1998; Huvenne *et al.*, 2002). In the latter area, the mounds occur in three well-delineated provinces (Fig. 6.1): the Belgica Mound Province, on the eastern slope of the Porcupine Seabight, the Hovland Mound Province, on the northern slope of the basin and the Magellan Mound Province which flanks the Hovland Mounds to the north. The mounds in each of these provinces feature distinct morphologies (De Mol *et al.*, 2002; Van Rooij *et al.*, 2003).
Until now, little attention has been paid to the diagenetic processes that occur within these cold-water coral mounds (Noé *et al.*, 2006). This paper focuses on the diagenetic changes observed within a gravity core (MD01-2459G) which was retrieved close to the top of Perseverance Mound (Magellan Mound Province, northern slope of the Porcupine Seabight). The aim of this study is to explore the process that led to the alteration of the corals and the formation of gypsum and dolomite crystals in the sediment. It is proposed that the presence of authigenic gypsum in carbonate-dominated sediments serves as an indicator for early diagenetic oxidation events. Furthermore the formation of a lithified carbonate layer overlying the interval containing gypsum crystals will be investigated.

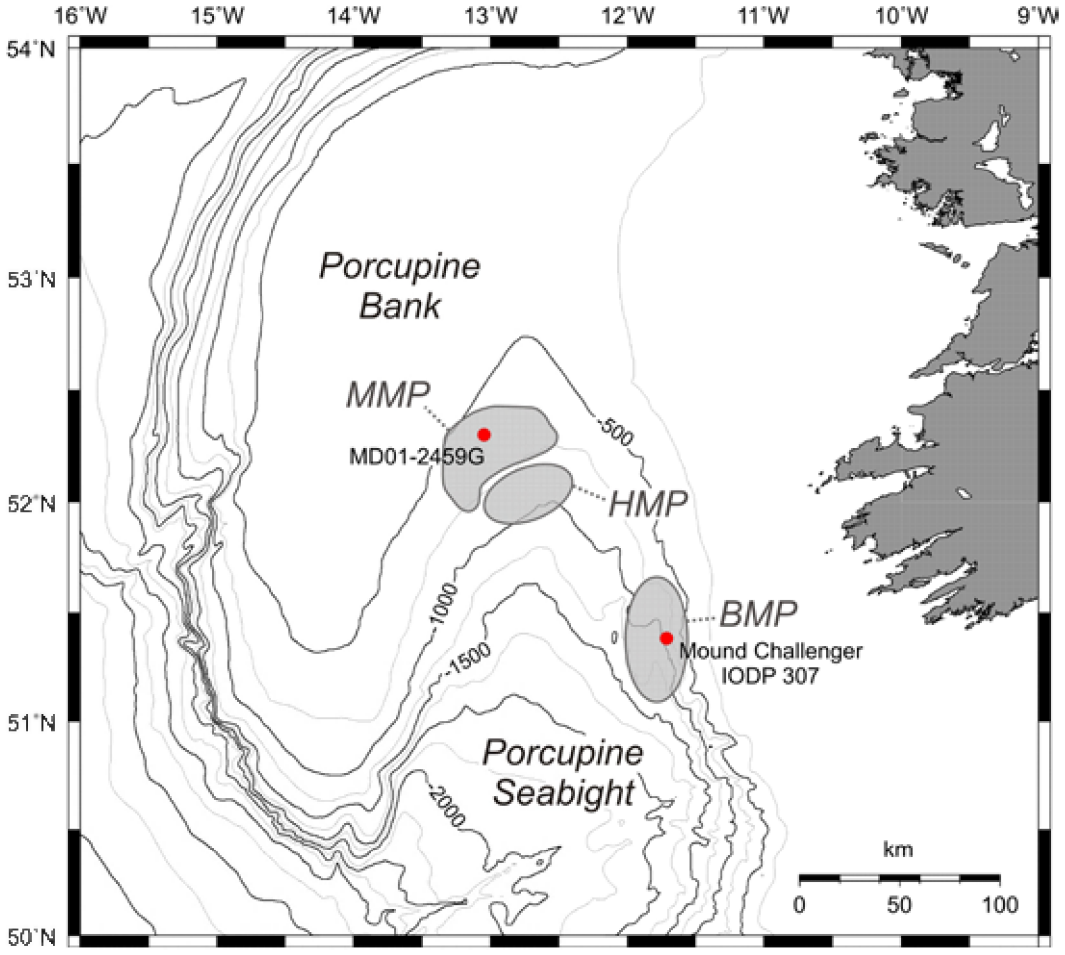

Fig. 6.1 *Overview map of the Porcupine Seabight, SW of Ireland, including main morphological features and localization of core MD01-2459G. The three main mound provinces: Belgica Mound Province (BMP), Hovland Mound Province (HMP) and Magellan Mound Province (MMP) are indicated.*

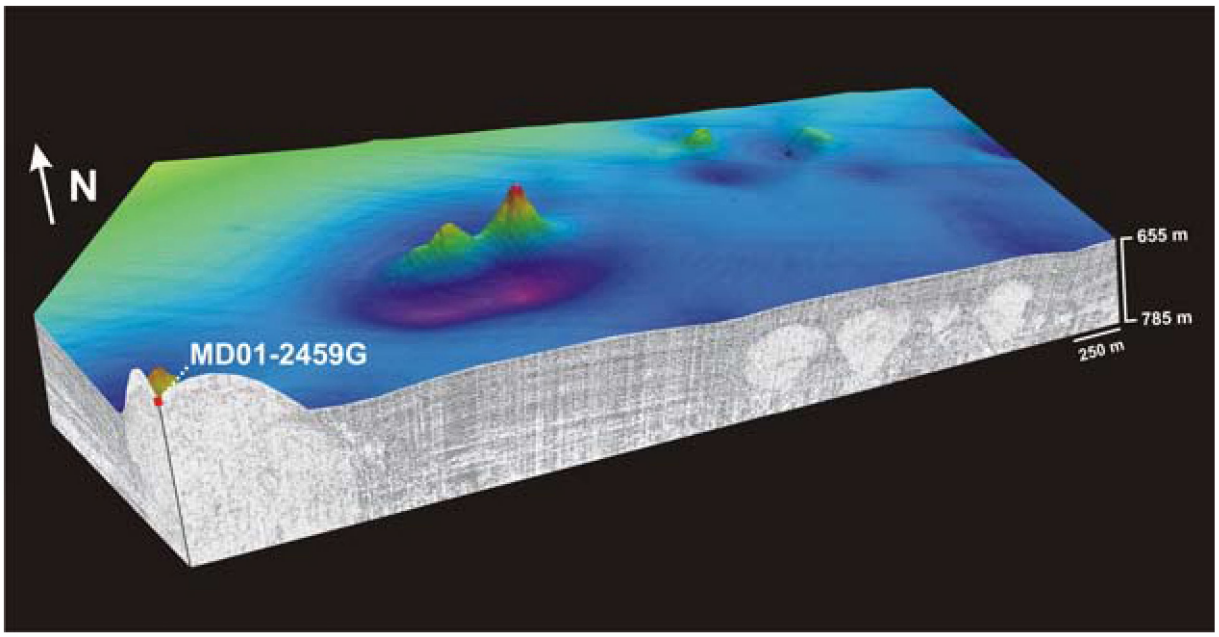

Fig. 6.2 *Location of core MD01-2459G, close to the top of Perseverance Mound. The bathymetry, derived from 3D seismic data, is used in combination with single channel reflection seismic profiles. East of Perseverance, buried mounds are observed on the seismic line.*

6.1.1 Regional setting

Perseverance Mound is situated in the Magellan Mound Province, where more than 1000 mounds occur with a spatial density of approximately 1 mound/km² (Fig. 6.2) (Huvenne *et al.*, 2007). The growth of these mounds was influenced and shaped by north-south oscillating palaeocurrents. All mounds root on one seismic horizon, indicating a sudden start-up event (Huvenne *et al.*, 2007). According to the results of the Integrated Ocean Drilling Program (IODP) Expedition 307, the start-up event of Challenger Mound, located in the Belgica Mound Province, is dated at 2.7 Ma (Kano *et al.*, 2007).

In contrast to the Belgica Mounds, which have a broad base, most Magellan Mounds have an ovoid shape, suggesting growth in competition with concurrent sedimentation (De Mol *et al.*, 2002; Huvenne *et al.*, 2007). Nowadays, most mounds in the Magellan Mound Province are buried. Based on the coccolith assemblage and the stratigraphy of a core taken on top of one of the buried mounds, it was concluded that the mounds were buried before Marine Isotope Stage (MIS) 6 (Foubert *et al.*, 2007). Unfortunately, this core did not penetrate the buried mound, so no exact timing of the burial is known. Perseverance Mound is one of few Magellan Mounds which are still outcropping at the sea bed (Fig. 6.2). The top of this mound is situated at a water depth of 610 m and its height above the actual mound base is ca 160 m. The mound is elevated 50 m above the present-day sea bed and shows a NNE-SSW elongation. Video footage that was taken during the Caracole cruise in 2001 with ROV Victor 6000 showed the presence of living corals on the flanks of Perseverance Mound (Huvenne *et al.*, 2007).

The water-mass stratification within the Porcupine Seabight has been reviewed by Hargreaves (1984), Rice *et al.* (1991) and White (2001). The depth range of the mounds in this area (600 to 1000 m) marks the upper boundary of the Mediterranean Outflow Water (MOW) which is overlain by the Eastern North Atlantic Water (ENAW). Both water masses are carried northwards by the eastern boundary slope current (White, 2007). At the northern end of the seabight, where the Magellan Mounds are located, currents are relatively weaker with some evidence of topographic steering of the mean flow cyclonically around the slope of the Porcupine Basin (Huvenne *et al.*, 2002; White, 2001; White, 2007).

6.1.2 Diagenesis in cold-water coral mounds

It is important to understand how early diagenetic processes alter the original sedimentary

record of mound sediments in order to decipher their geological history. The imprint on the sediment thereby provides information about the microbial and geochemical processes that occur within cold-water coral mounds.
Until recently, limited attention has been paid to these diagenetic processes. The most prominent diagenetic feature in cold-water coral mounds is the dissolution of the aragonitic corals (Foubert *et al.*, 2007). The latter authors described the dissolution of coral fragments and precipitation of carbonate in mounds in the Porcupine Seabight. They attributed the coral alteration to oxidation of organic matter, affecting the saturation state of aragonite. Geochemical processes controlling the preservation of corals in cold-water coral mounds have been described in detail by (Ferdelman *et al.*, 2006; Wehrmann *et al.*, 2009). Both studies suggest a coupling between microbial-mediated organic matter degradation and carbonate-mineral diagenesis and link sediment composition and coral skeleton preservation by showing that the availability of reactive iron leads to an effective buffering of the pore-water carbonate system.

6.2 Material and Methods

Core MD01-2459G was obtained with a gravity corer during the MD123-Geosciences campaign with R/V Marion Dufresne in September 2001. The core was retrieved close to the top of Perseverance Mound at a water depth of 610 m with a recovery of 1079 cm (52°18'00.60"N 13°02'51.00"W) (Fig. 6.2). After retrieval, the core was analyzed on board with the GEOTEK Multi Sensor Core Logger with a resolution of 2 cm, measuring magnetic susceptibility, gamma-ray density and P-wave velocity (Foubert *et al.*, 2007; Van Rooij *et al.*, 2001) (section 2.1).

6.2.1 Sedimentological and mineralogical analyses

The major chemical element composition was analyzed using an AVAATECH XRF core scanner installed at the Royal Netherlands Institute for Sea Research (Royal NIOZ) (section 2.2). Next, the different mineralogical phases of the sediment matrix of 14 samples were identified and quantified using X-ray diffraction (XRD) at the department of Earth and Environmental Sciences, Geology, K.U. Leuven (section 2.5.3). Grain-size analysis of the bulk sediment was carried out at Ghent University with a Malvern Mastersizer 2000 (section 2.4). The samples of this core were analyzed with a resolution of 50 cm. The clay minerals of 31 samples were identified using standard X-ray diffraction (PANalytical diffractometer) at the IDES laboratory (University of Paris XI) on oriented mounts of carbonate-free, clay-sized (< 2 µm) particles (section 2.6). Furthermore, micro-CT scans were carried out at the Centre for X-ray CT at Ghent University (UGCT). In total, 11 plastic cubes of 8 cm^3 filled with sediment were scanned according to the method described in section 2.3.
Standard thin sections were studied using conventional transmitted, reflected and UV light microscopy (section 2.5.1). For further investigation of diagenetic features, cold cathode luminescence (CL) was used (section 2.5.1). Individual gypsum crystals were embedded in epoxy. After polishing and carbon-coating they were studied with a JSM 6400 scanning electron microscope (SEM) at Ghent University. Bulk sediment was gold-coated and studied with a SEM. The composition of several points was measured using Energy Dispersive Spectroscopy (EDS) (section 2.5.2).

6.2.2 Isotope measurements

The oxygen and sulfur isotopic composition of gypsum-bound sulfate was measured on hand-picked gypsum crystals at the Max Planck Institute for Marine Microbiology Bremen and the Swiss Federal Institute of Technology (ETH) Zurich according to the method described in section 2.9. Furthermore, the sulfur isotopic composition of the sedimentary pyrite was determined as well (section 2.9).
Stable oxygen (O) and carbon (C) isotopes of the bulk sediment of 11 samples between 540 and 630 cm were measured at the LSCE (Gif-sur-Yvette) according to the method described in section 2.8.1. The O and C isotopes are reported with respect to Vienna Peedee Belemnite (V-PDB).

6.3 Results

6.3.1 Core stratigraphy

Based on the magnetic susceptibility, gamma ray density, XRF, XRD and X-ray imagery, core MD01-

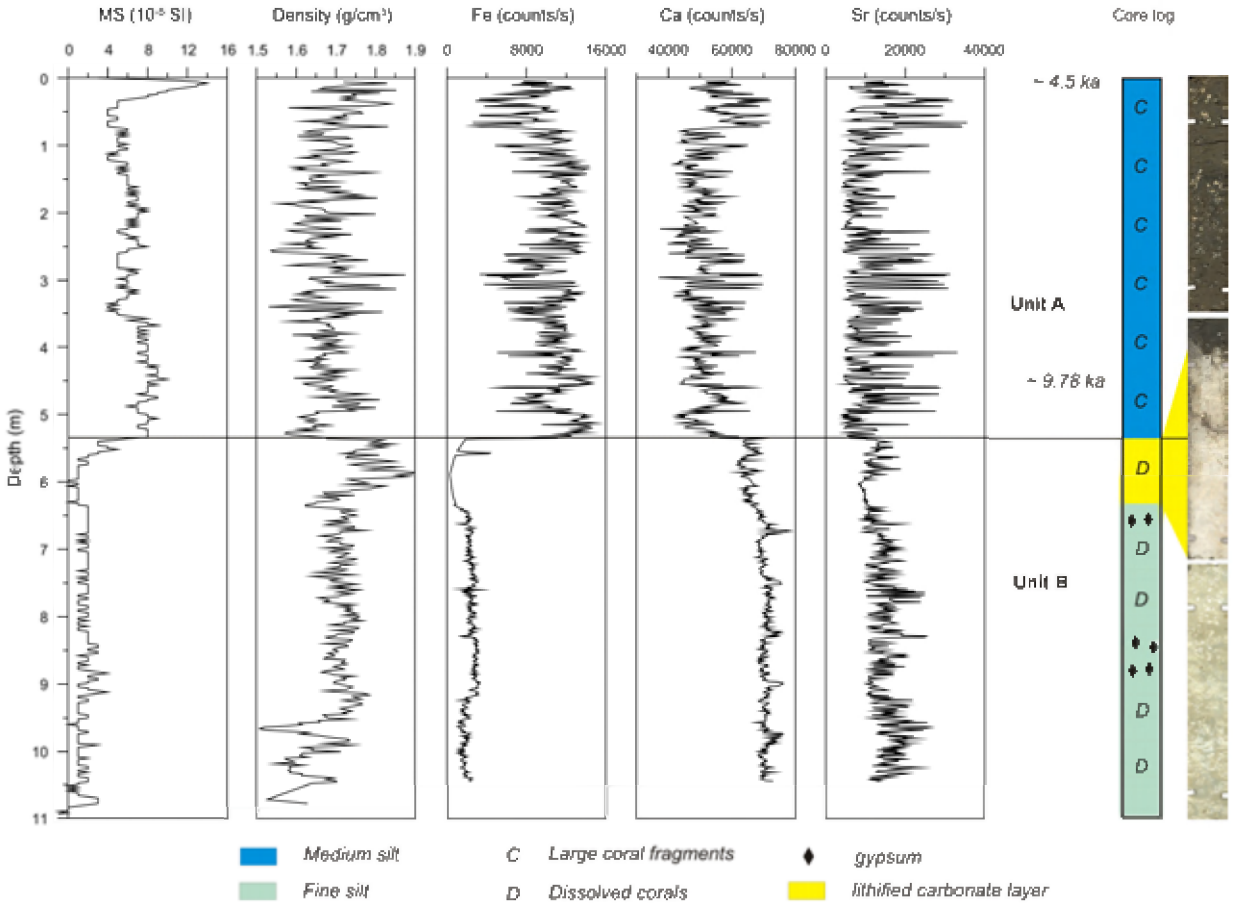

Fig. 6.3 *Overview of the stratigraphy of core MD01-2459G featuring the Magnetic Susceptibility (MS), Density, X-Ray Fluorescence (XRF), a basic core log. Images of core sections 300-375, 525-600 and 750-825 cm are given. U-Th dating of the corals of unit A are also noted (Frank et al., 2009). Gypsum crystals were discovered in two intervals in unit B: i.e. at a depth of 658-671 and 840-891 cm (modified after Foubert and Henriet (2009)).*

2459G was subdivided into two units. Unit A comprises the top 535 cm of the core and unit B comprises the lower 544 cm (Fig. 6.3) (Foubert and Henriet, 2009). Unit A is composed of olive-gray medium grained silt (5Y 4/2) and contains large coral fragments. Grain-size analysis reveals poorly sorted, unimodal distributions with an average mode around 10 µm. In some cases a coarser mode around 500 µm is present which can be attributed to the presence of biogenic fragments. In general, the calcium and strontium values are high, but lower than those of unit B. Except for a peak in the top 50 cm, the magnetic susceptibility values of this unit are rather low, averaging around 5 SI. The XRF iron intensities are high compared to unit B, averaging around 12K counts/sec. XRD analysis shows that the sediment matrix of unit A is dominated by quartz (25.6%), calcite (26.7%) and clay minerals (23.7%). Feldspar (7.3%) and aragonite (2.7%) appear in minor quantities (Fig. 6.4). The dominant clay minerals in unit A are smectite (38.8%) and illite (33.8%) whereas kaolonite (12.8%) and chlorite (14.6) are of subordinate importance (Fig. 6.5). Overall, the clay mineralogy reveals a little variation throughout this unit. The age of the corals in unit A have been dated to correspond to the Holocene (Frank *et al.*, 2009).

Unit B consists of light-gray fine grained silt (7.5Y 6/1). Grain-size analysis displays very poorly sorted, unimodal distributions with an average mode around 3 µm. Throughout the entire unit diagenetically altered corals are observed, characterized by fragile skeleton walls. The corals are hardly recognizable on X-ray images, indicating little density contrast between the corals and the surrounding sediment. The alteration of the corals prevented uranium-thorium dating in unit B. The magnetic susceptibility records extremely low values for unit B which can be explained by the presence of carbonate-rich sediments. This is also reflected in the high XRF calcium values,

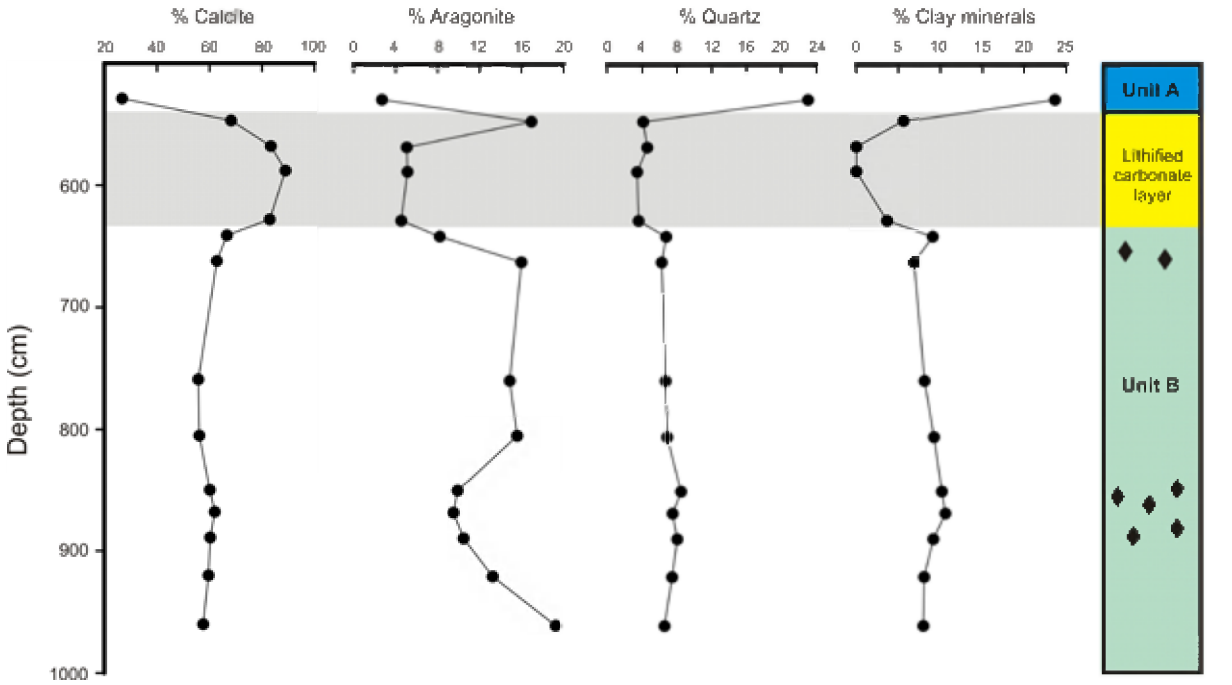

Fig. 6.4 *XRD-data of the bulk sediment. The percentages of calcite, aragonite, quartz and clay minerals are presented.*

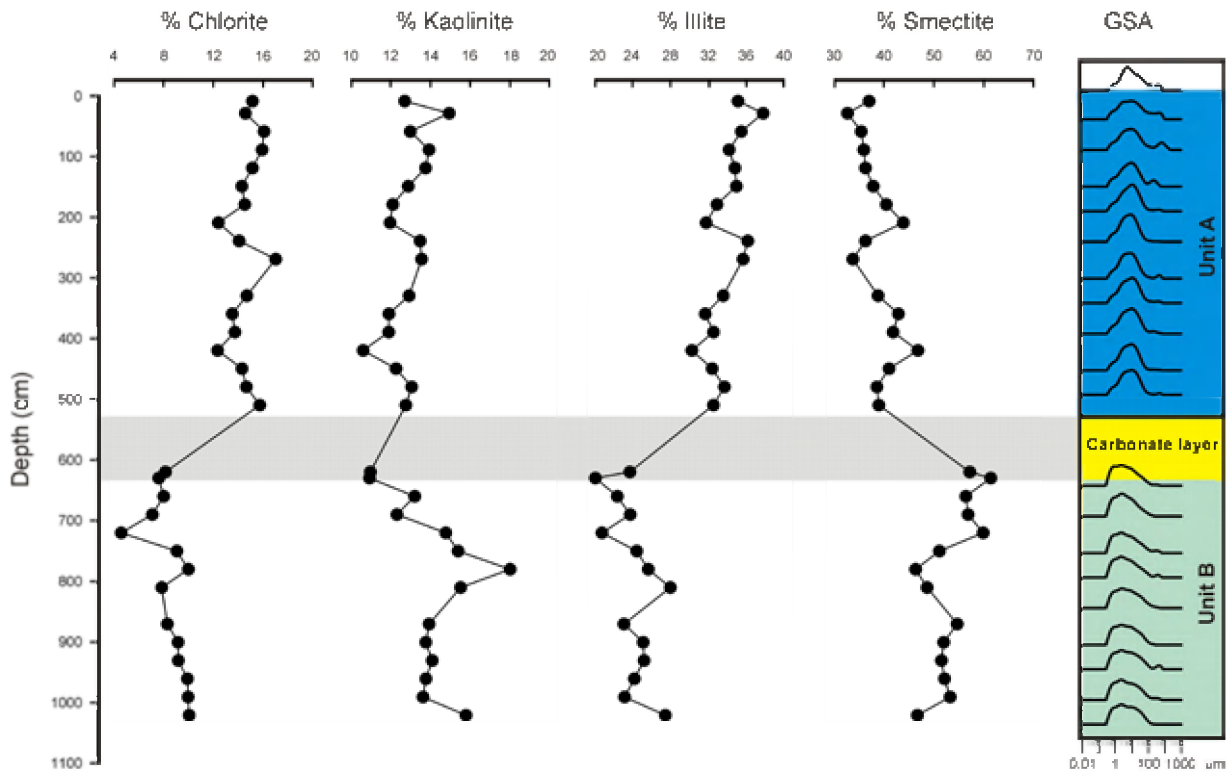

Fig. 6.5 *Clay mineralogy and grain-size analysis (GSA) of core MD01-2459G.*

Fig. 6.6 *Euhedral, tabular gypsum crystals with a size between 1.5 and 4 mm. Often, the crystals occur as twins.*

averaging around 70K counts/s (Fig. 6.3). The strontium values increase in unit B compared to unit A, while there is a significant decrease in the iron intensities. A remarkable feature in unit B is a lithified carbonate layer between 535 and 630 cm, which is reflected in the high density values (Fig. 6.3). The coral fragments in this layer are (almost) completely dissolved. Between 555 and 560 cm, a horizon of dark, siliciclastic sediment occurs, characterized by a peak in the XRF iron counts (Fig. 6.3). Some lithified carbonate fragments are embedded in the siliciclastic sediment. At 630 cm, there is a sharp boundary to the unlithified sediment below.

XRD analysis shows significantly more calcite in unit B than in unit A (Fig. 6.4). The lithified carbonate layer contains between 68 and 90% calcite with an average of 81%. The sediments of unit B below the lithified layer show lower percentages of calcite, ranging between 55 and 66% (average: 60.1%). The aragonite content of unit B fluctuates strongly. The lithified carbonate layer contains approximately 5% aragonite while the lower part of unit B contains 8 to 19% aragonite (Fig. 6.4). Quartz (3 to 8%) and clay minerals (3 to 10%) occur in minor abundances. Gypsum, pyrite and dolomite were detected in some samples in very low quantities at the limit of the resolution of XRD analysis (< 2%). XRD-analysis of the clay fraction indicates that smectite is the dominant clay mineral in unit B (53.4%) while illite (24.1%), kaolinite (14.0%) and chlorite (8.5%) are of secondary importance (Fig. 6.5). The clay mineralogy remains relatively stable throughout the entire unit.

Gypsum crystals were discovered in two intervals in unit B: at a depth of 658 to 671 cm and 840 to 891 cm. The gypsum occurs as euhedral, tabular crystals with a size between 1.5 and 4 mm, in a matrix of fine grained silt. The crystals are transparent white to beige and often twinned (Fig. 6.6).

6.3.2 Micro-CT scans of unit B

The micro-CT scans enable visualization and quantification of diagenetic features (Fig. 6.7). Scans of corals from unit B show signs of strong dissolution which created a secondary moldic porosity (Fig. 6.7 A). Only the most robust parts of the corals, where the septae meet the outer rim of the calyx, are preserved. The scanned sections have a porosity up to 0.43% pores which is almost entirely related to the dissolution of the corals. Micropores could not be visualized in this sample using micro-CT, because the scans were performed with a resolution of 20 µm.

The visualization of the gypsum crystals in unit B clearly shows that the crystals have no preferential orientation and are randomly scattered in the sediment (Fig. 6.7 B). Quantification of the scans indicates that the samples contain between 0.18 and 0.34 volume% gypsum. There is no apparent spatial correlation between the gypsum crystals and the occurrence of coral relics (Fig. 6.7 C).

In the micro-CT scans of the lithified carbonate layer, a discrepancy can be observed between the state of preservation of calcitic and aragonitic bioclasts. Throughout the entire lithified layer aragonitic biogenic fragments (e.g. corals and gastropods) are dissolved and moldic porosity is created (Fig. 6.8 A, B) whereas calcitic fragments (e.g. foraminifera and echinoid spines) are dense and thus well preserved (Fig. 6.8 C, D). In sample 555-557 cm a brecciated facies occurs with denser lithified carbonate fragments incorporated in the soft terrigenous sediment (Fig. 6.8 E, F).

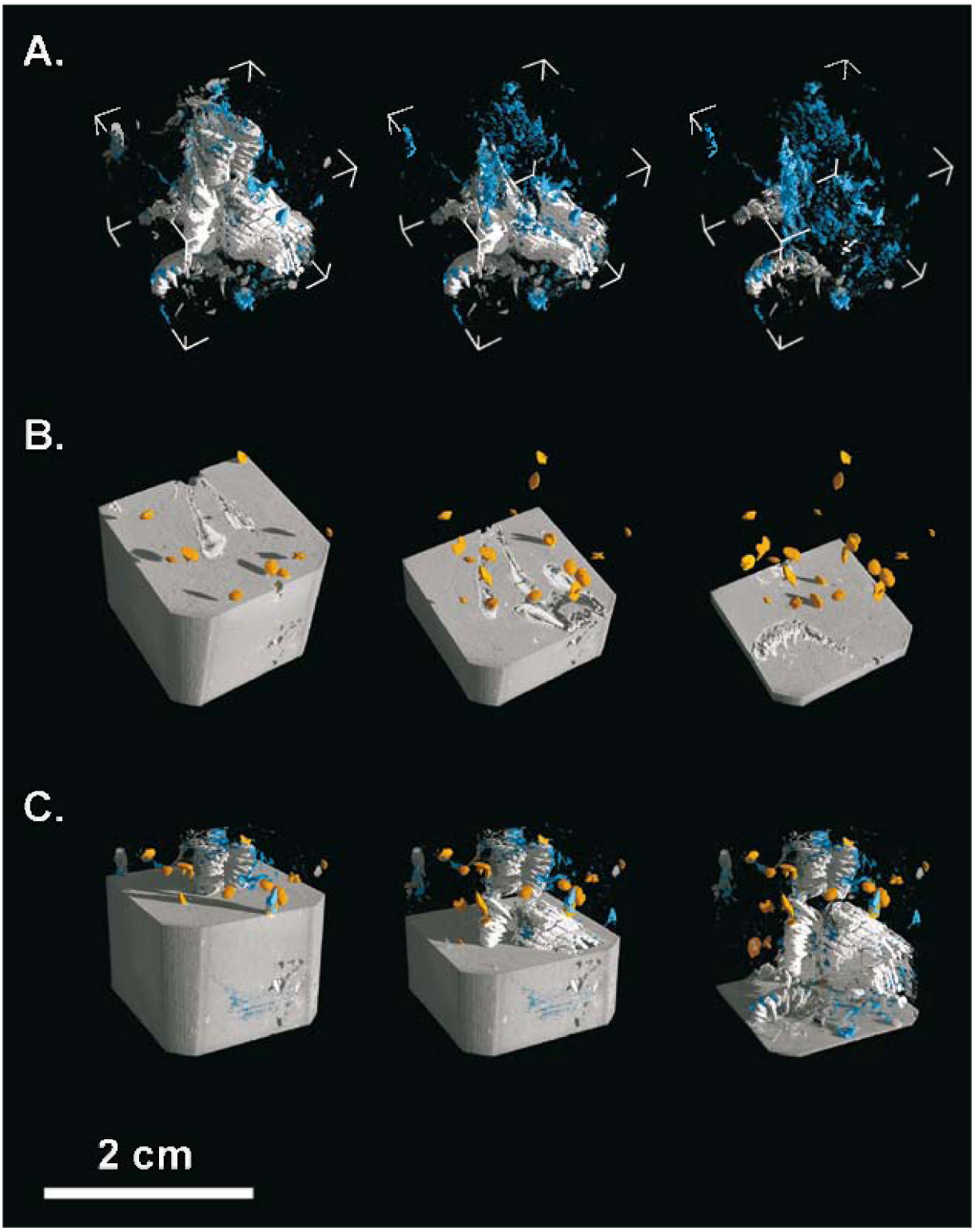

Fig. 6.7 *Micro-CT scans of sediment sampled at a depth of 889-891 cm. A. Micro-CT scans visualizing the dissolution of the corals (white) and subsequent creation of a secondary porosity (blue). B. Micro-CT scans showing the occurrence of gypsum crystals (yellow) in the sediment. C. Overview of the combined occurrence of gypsum (yellow), coral (white) and porosity (blue) in the sediment.*

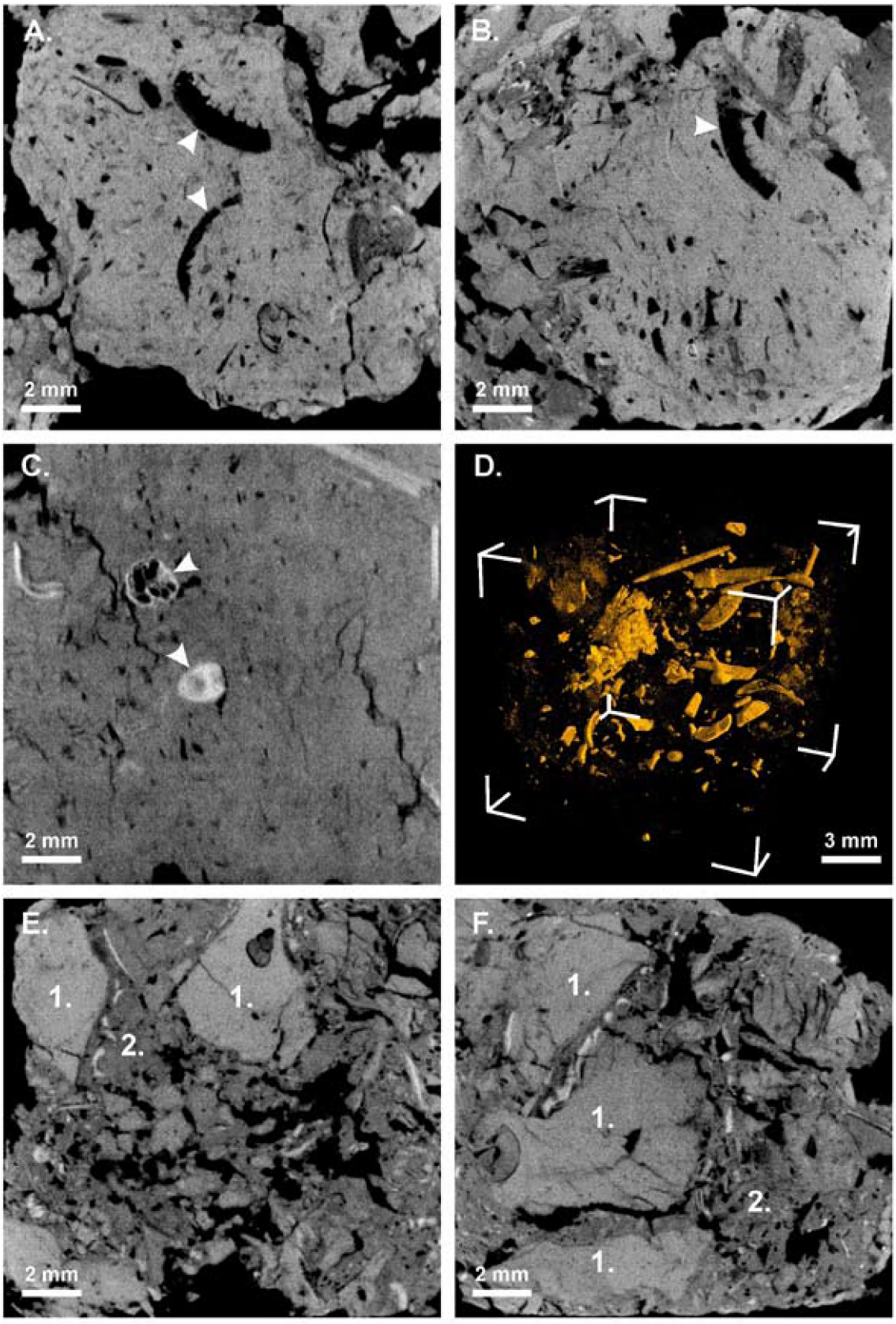

Fig. 6.8 *Micro-CT scans of samples from the lithified carbonate layer. A. and B. Moldic pores of aragonitic corals. C. Nicely preserved calcitic biogenic fragments. D. 3D visualization of well preserved echinoid spines and other calcitic bioclasts. E. and F. Micro-CT scan of brecciated layer (555-557 cm) with denser carbonate fragments (1.) embedded in a matrix of terrigenous sediment (2.).*

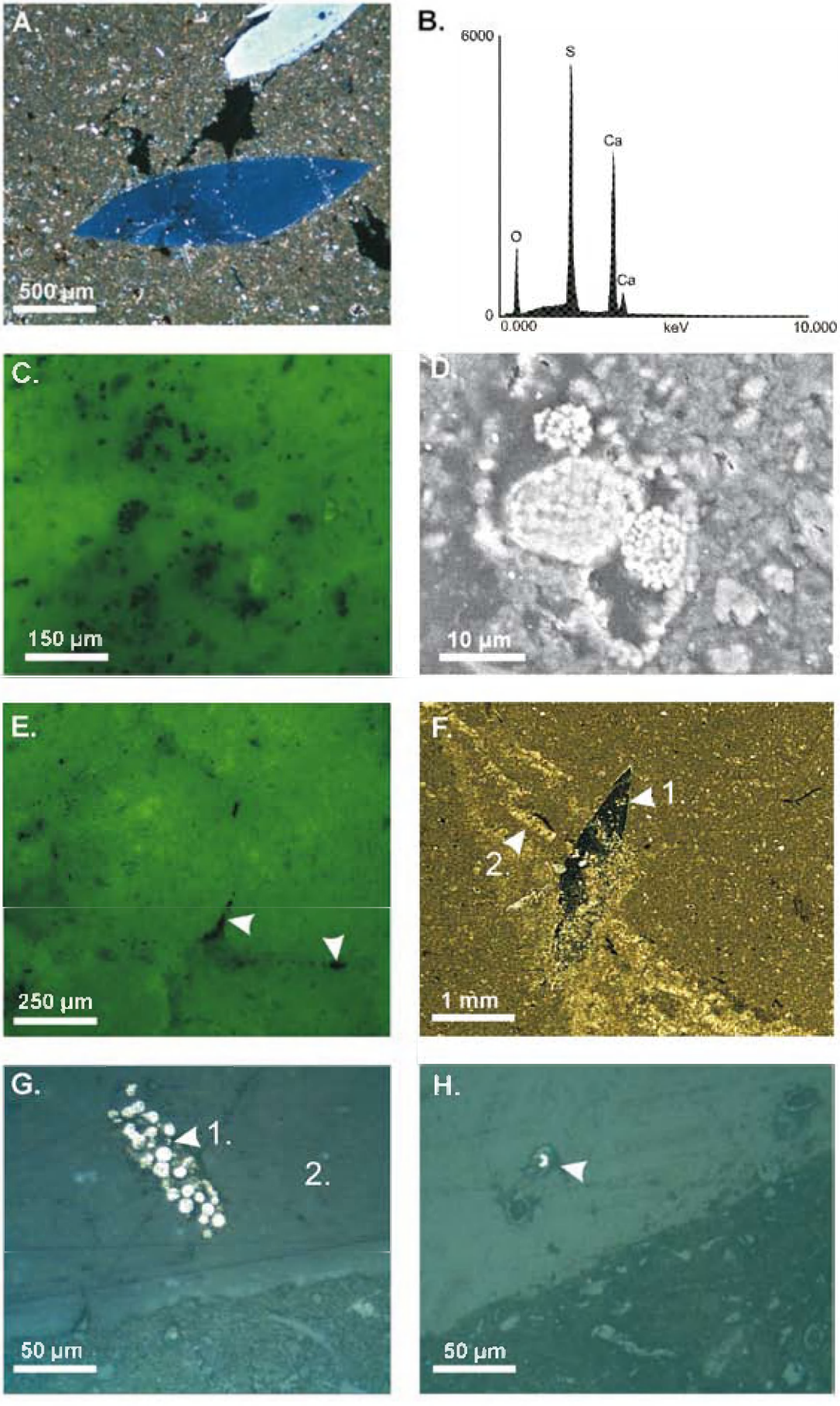
A.
500 µm
B.
6000
S
Ca
O
Ca
0
0.000
keV
10.000
C.
150 µm
D.
10 µm
E.
250 µm
F.
1.
2.
1 mm
G.
1.
2.
50 µm
H.
50 µm

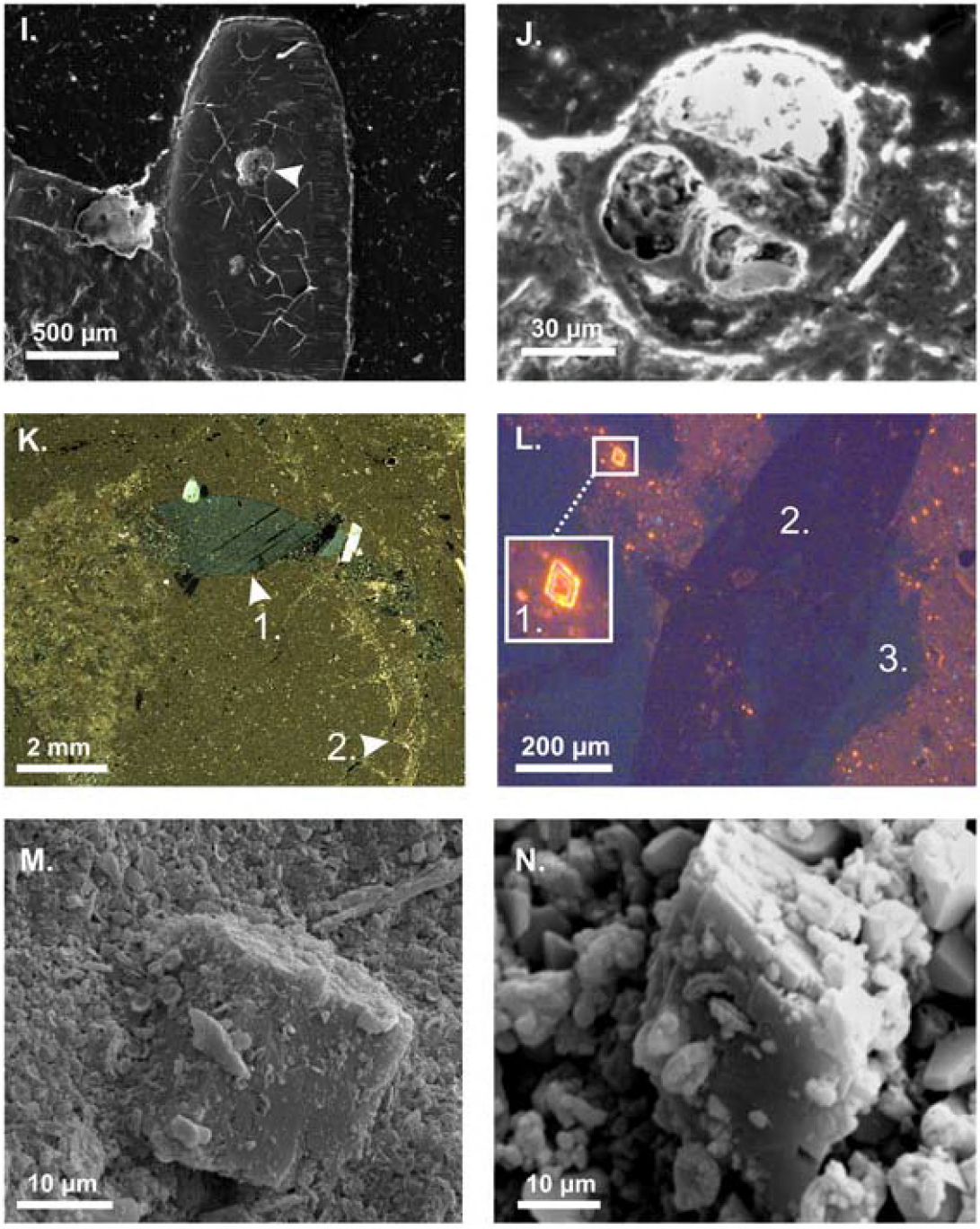

Fig. 6.9 *A. The occurrence of gypsum crystals in a micritic matrix containing some biogenic fragments (Plane-polarized light). B. An EDS-profile of one of the gypsum crystals. C. Framboidal pyrite (black spheres) in the sediment associated with the gypsum crystals (UV-light). D. A detail of a foraminifera containing intraparticular framboidal pyrite (SEM). E. Clusters of framboidal pyrite on the outer rim of the fecal pellets (UV-light). F. The incorporation of an altered coral (1.) in a gypsum crystal (2.) (Plane-polarized light). G. The occurrence of framboidal pyrite (1.) incorporated in a gypsum crystal (2.) (reflected light). H. A foraminifera containing intraparticular framboidal pyrite incorporated in a gypsum crystal (reflected light). I. and J. SEM images of foraminifera incorporated in gypsum crystals. K. A twinned gypsum crystal (1.) that was broken and displaced in different crystallographic orientations (Plane-polarized light). Strongly dissolved coral (2.) L. Cold Cathode Luminescence (CL) of a luminescent dolomite crystal (1.) in association with a non-luminescent gypsum crystal (2.) and non-luminescent coral (3.). M. and N. SEM images of dolomite crystals associated with the gypsum crystals. Note the incorporation of coccoliths into the dolomite crystals in picture N.*

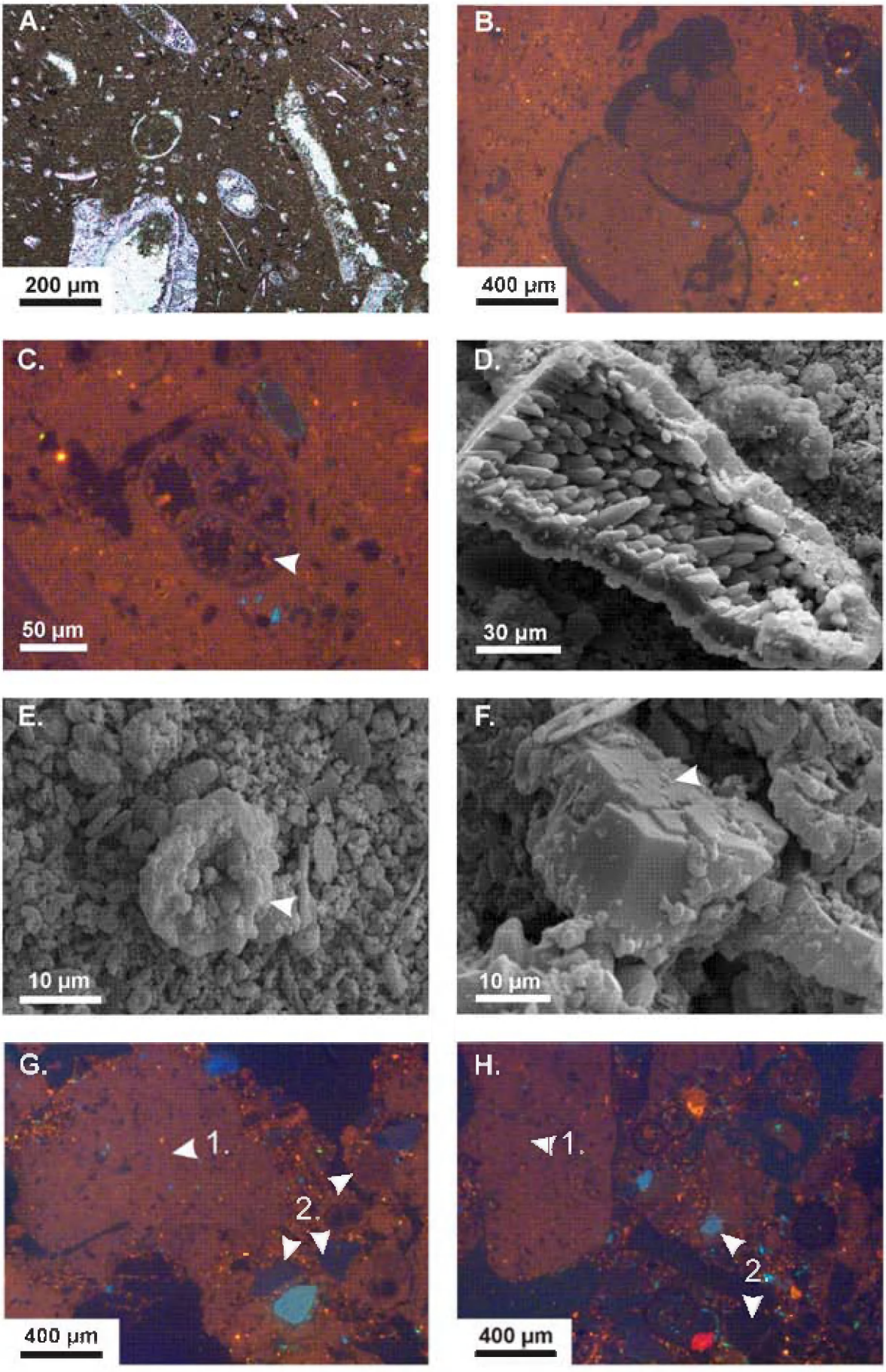
A.
200 µm
B.
400 µm
C.
50 µm
D.
30 µm
E.
10 µm
F.
10 µm
G.
1.
2.
400 µm
H.
1.
2.
400 µm

Fig. 6.10 (Left) *A. Biogenic fragments incorporated in a sediment matrix of micritic carbonate mud. B. Moldic pore of a dissolved gastropod. C. Cold CL reveals yellow luminescent calcite crystals inside the biogenic fragments. D. Biogenic fragment with intraparticular calcite crystals (SEM). E. Calcitic overgrowths on coccoliths (SEM). F. Dolomite rhomb encrusting coccolith. G. and H. Carbonate fragment (1.) in a matrix of terrigenous sediment (2.) containing feldspar (blue-green luminescent), quartz (Brown-dark blue luminescent) and carbonate grains (yellow-red luminescent).*

6.3.3 Petrography of intervals containing gypsum crystals

The gypsum crystals are embedded in a fine matrix of micritic mud with many biogenic fragments (i.e. corals, foraminifera, bivalve shells, etc.) (Fig. 6.9 A, B). Framboidal pyrite is scattered in the matrix (Fig. 6.9 C). The corals show obvious signs of dissolution whereas the foraminifera are better preserved. Some foraminifera are (partially) filled with the embedding sediment and a few foraminifera contain framboidal pyrite (Fig. 6.9 D).
In two thin sections, faecal pellets were observed in the vicinity of the gypsum crystals, indicating the presence of benthic feeders. There are clusters of framboidal pyrite on the outer rim of the pellets (Fig. 6.9 E).
The gypsum crystals are lens-shaped (Fig. 6.9 A) and often twinned. All crystals contain biogenic fragments such as foraminifera, corals (Fig. 6.9 F) and shell-fragments. Some of the investigated gypsum crystals revealed the presence of framboidal pyrite inside the gypsum (Fig. 6.9 G). A few crystals encase foraminifera containing intraparticular framboidal pyrite (Fig. 6.9 H). These findings were confirmed with SEM-EDS by which calcitic and siliceous biogenic fragments and iron sulfide crystals were indentified within the gypsum crystals (Fig. 6.9 I, J). Sometimes, the inclusions in the gypsum are aligned according to the cleavage of the crystals but in most cases, they appear randomly. A striking feature is the occurrence of broken and even displaced crystals, with displacement occurring along different crystallographic orientations (Fig. 6.9 K). However, it is unclear if this is the result of sample preparation (i.e. sediment sampling, thin section preparation) or a genuine feature.
With the exception of some inclusions, the gypsum crystals are non-luminescent in cold cathode CL. The biogenic fragments are also non-luminescent.
The matrix contains some bright yellow-red luminescent, rhombohedral crystals up to 50 µm with clear zonation (Fig. 6.9 L). These crystals were identified using SEM-EDS as dolomite ($CaMg(CO_3)_2$). The SEM-images reveal the incorporation of coccoliths in the dolomite crystals (Fig. 6.9 M, N).

6.3.4 Petrography of the lithified carbonate layer

The sediment matrix of the lithified carbonate layer consists of micritic carbonate mud with biogenic fragments such as corals, foraminifera, echinoids and bivalves (Fig. 6.10 A). Some of the biogenic fragments in the sediment matrix are partially or completely dissolved (Fig. 6.10 B). No extensive cementation can be observed when using a petrographic microscope, although in some of the biogenic fragments intraparticular calcite precipitation is noticed. Cold CL reveals the presence of bright-yellow to orange luminescent dolomite crystals up to 30 micrometer (Fig. 6.10 C). No framboidal pyrite was noticed in the samples of the lithified carbonate layer. Calcite overgrowths on coccoliths and calcite crystals on biogenic fragments were observed on SEM images (Fig. 6.10 D, E). Also, in some samples dolomite rhombs containing coccoliths occur (Fig. 6.10 F). In sample 555-557 cm a brecciated facies was observed with pieces of lithified carbonate surrounded by terrigenous sediment. In the terrigenous sediment quartz (dark blue to dark brown luminescent) and feldspar (blue to green luminescent) grains occur up to 400 micrometer (Fig. 6.10 G, H).

6.3.5 Isotope measurements

The sulfur isotopic composition of gypsum ($\delta^{34}S$), found at a depth of 890 cm in this core, is +11.0‰ V-CDT, the oxygen isotopic composition ($\delta^{18}O$) is +8.9‰ V-SMOW. The $\delta^{34}S$ values for pyrite, sampled at different depths, are reported in Table 6.1.
The $\delta^{13}C$ values of the lithified carbonate layer (535-630 cm) vary between -2.45 and -4.23‰ whereas the $\delta^{18}O$ values range between +2.87 and +3.79‰. The $\delta^{13}C$ values become less de-

pleted in the less lithified, lower part of the carbonate layer (612-630 cm) (Table 6.2).

Sample depth (cm)	$\delta^{34}S_{pyrite}$ (‰)
870	-22.88
880	-18.89
890	-21.14
900	-17.59
910	-12.30

Table 6.1 *Sulfur isotopic composition of pyrite, with respect to V-CDT, occurring adjacent to the gypsum crystals except sample 910 which was sampled 9 cm below the interval containing gypsum crystals.*

Sample depth (cm)	$\delta^{18}O$	$\delta^{13}C$
540	+2.87	-4.23
550	+3.47	-3.92
557	+3.61	-3.85
560	+3.60	-3.80
570	+3.47	-3.97
580	+3.59	-3.83
590	+3.79	-3.73
600	+3.60	-3.74
610	+3.26	-3.08
620	+3.21	-2.54
630	+3.52	-2.45

Table 6.2 *Stable C and O isotopes of bulk carbonate samples of the lithified layer in core MD01-2459G. The C and O isotopes are reported with respect to Pee Dee Belemnite (V-PDB).*

6.4 Discussion

Gypsum and its dehydrated form anhydrite are relatively common in sedimentary deposits throughout the world and throughout the geologic record (Bain, 1990). In general, the formation of these gypsum crystals is attributed to evaporation processes, i.e. in hypersaline basins, sabkhas and playas.

An evaporative nature, however, can be excluded for the gypsum crystals in Perseverance Mound. The fact that biogenic fragments and even coral pieces (Fig. 6.9 F) are incorporated into the gypsum indicates that the crystals precipitated in situ, due to a diagenetic process. Gypsum occurs only if extraordinary high sulfate and calcium concentrations cause oversaturation of this mineral. Therefore, reports of non-evaporitic gypsum are limited as this mineral is strongly undersaturated with respect to sea water. Gontharet *et al.* (2007) attributed the precipitation of gypsum in carbonate crusts associated with mud volcanoes to the presence of rising sulfate-rich fluids originating from the dissolution of underlying Messinian evaporites. Gypsum precipitation associated with the formation of sulfate-rich brines in the Bannock Basin was reported by Corselli and Aghib (1987). Bain (1990) attributed the formation of non-evaporitic gypsum to oxidizing calcium-rich groundwater. Similarly, Siesser and Rogers (1976) described gypsum crystals in calcareous plankton-rich sediments on the South West African continental slope in association with authigenic pyrite. The authors propose that pyrite first formed due to the production of sulfide during microbial sulfate reduction which reacted with sedimentary iron phases. Subsequently, a drop in the pH induced the dissolution of calcareous organisms, liberating high concentrations of calcium. Briskin and Schreiber (1978) attributed the occurrence of gypsum in carbonate deep-sea ooze to the influx of oxygen-rich, undersaturated Antarctic Bottom Water, which actively dissolved the foraminiferal ooze, supplying the necessary calcium for gypsum precipitation at the sediment/water interface. Xavier and Klemm (1979) described the occurrence of authigenic gypsum in deep-sea manganese nodules in the Central Pacific Ocean. Wang *et al.* (2004) reported the occurrence of authigenic gypsum crystals associated with gas hydrates at Hydrate Ridge in the Eastern North Pacific. They propose that the crystals precipitated at the interface between downward advecting sulfate-rich sea water and gas hydrates, where calcium concentrations are high due to hydrate formation. Similarly, Zhong *et al.* (2007) described the formation of gypsum and pyrite in association with gas venting in the Nansha Trough.

Gypsum crystals are also sometimes observed on the surface of cores due to the pore water drying-out after core retrieval. In the present study,

CT scans allowed the amount of gypsum crystals in the matrix to be quantified. Based on a mean value of 0.26 vol%, it was calculated that 33.8 g of gypsum is present in the core in the interval between 840 to 891 cm, using a gypsum-density of 2.3 g/cm³. Gypsum solubility in sea water is up to 3.8 g/l (Kopittke *et al.*, 2004). Consequently, 8.9 l of sea water would need to evaporate completely in order to obtain this amount of gypsum. The volume of this core-section is only 8.5 l, therefore, it is impossible to create this quantity of gypsum after coring. Moreover the core was stored under stable conditions (6° C), showing no signs of drying out.

In order to assess the exact timing of gypsum precipitation, uranium-thorium dating was applied to the gypsum crystals. However, the uranium (0.035 ppm) and thorium (0.028 ppm) concentrations in the gypsum are extremely low. Given these low concentrations and the small amount of sample material (0.2 g), the uranium and thorium isotopic values were impossible to determine with sufficient precision. Therefore, the dating of the crystals was not successful.

In this study, the oxygen and sulfur isotopic composition of gypsum and the sulfur isotopic composition of pyrite are used to reconstruct the diagenetic setting during gypsum formation and elucidate the mechanism for the formation of the authigenic gypsum crystals. Based on these findings, a mechanism is proposed that links the formation of gypsum to a phase of increased bottom currents which caused erosion and enhanced inflow of oxidizing fluids into previously anoxic sediments. This induced the oxidation of pyrite, carbonate dissolution and subsequent gypsum precipitation.

6.4.1 Potential sources of the sulfate in gypsum

The oxygen and sulfur isotopic composition of gypsum can be used to estimate the isotopic composition of the pore-water sulfate from which the gypsum originated. In an open system and at chemical equilibrium, gypsum is enriched in ^{34}S by +1.65‰ and in ^{18}O by +3.5‰ compared to dissolved sulfate (Holser and Kaplan, 1966; Thode

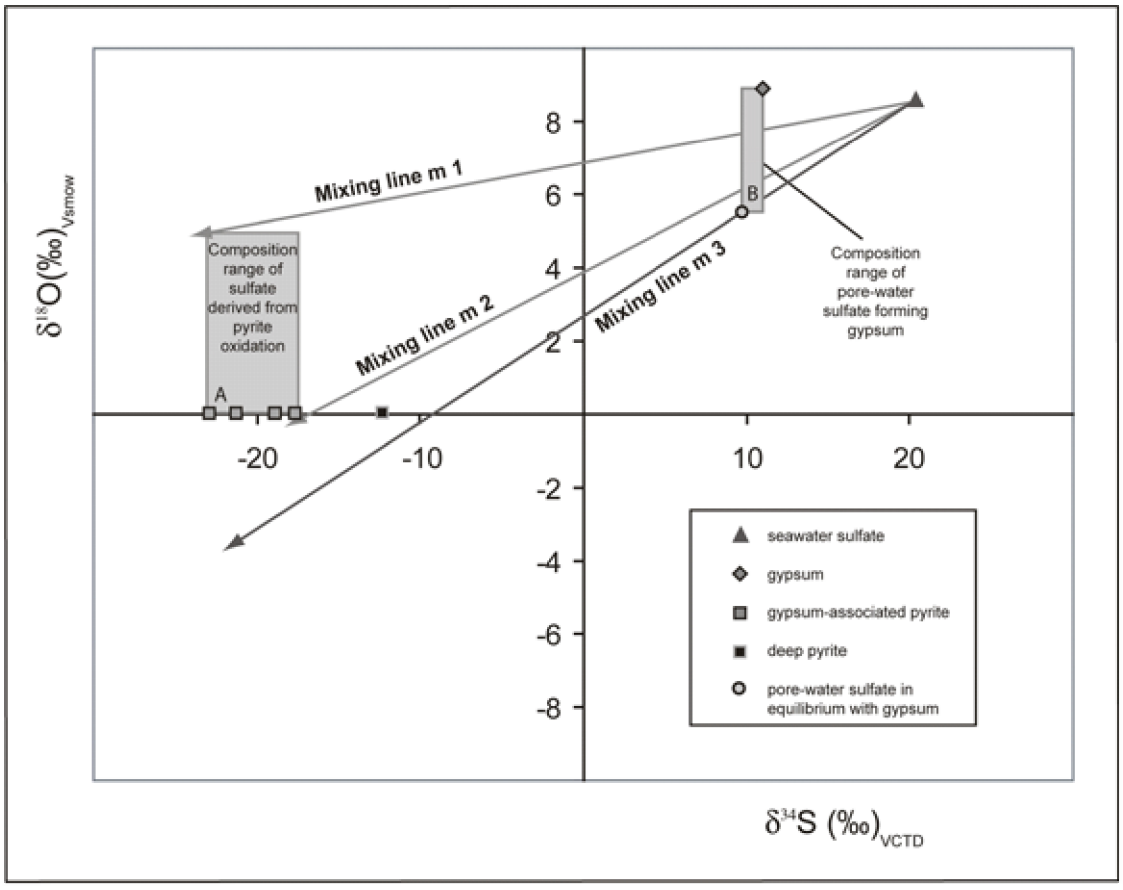

Fig. 6.11 *$\delta^{18}O$ versus $\delta^{34}S$ isotope plot showing the composition for seawater sulfate, gypsum and pyrite.*

and Monster, 1965). However, rapid precipitation of gypsum (i.e. precipitation in disequilibrium) or closed system conditions could suppress this isotope effect. Consequently, the isotopic composition of dissolved pore-water sulfate likely fell between +9.3 and +11.0‰ V-CDT for sulfur and +5.4 and +8.9‰ V-SMOW for oxygen (Fig. 6.11, Area B). Compared to sea-water sulfate with a sulfur isotopic composition of +20.3‰ (Longinelli, 1989), the pore-water sulfate from which the gypsum originated was depleted in ^{34}S. Depending on the assumed oxygen isotope fractionation for gypsum precipitation (0 to 3.5‰), the pore-water sulfate had the same oxygen isotopic composition as sea water (8.6‰ V-SMOW (Boschetti and Iacumin, 2005)) or was depleted in ^{18}O.
These observations indicate that apart from sea-water sulfate, which is a very likely sulfate source for gypsum in marine sediment, another source depleted in ^{34}S relative to sea-water sulfate must have contributed to the pore-water sulfate. A potential sulfate source is the oxidation of hydrogen sulfide-rich fluids. At Perseverance Mound, this process is most likely of minor importance. Pore-water profiles from Challenger Mound (IODP expedition 307) located in the close vicinity of Perseverance Mound show no accumulation of hydrogen sulfide within the mound sequence (Ferdelman *et al.*, 2006). Low sulfide concentrations are the result of extremely low rates of anaerobic carbon mineralization (organoclastic sulfate reduction) in cold-water coral bearing sediments (Wehrmann *et al.*, 2009) and a large pool of reactive iron-(oxyhydr)oxides that traps sulfide. The oxidation of such accumulated iron sulfide minerals (i.e. pyrite) is the more likely source of sulfate depleted in ^{34}S. Eventually, a mixture of sea-water sulfate and sulfate derived from the oxidation of pyrite precipitated as gypsum. This hypothesis is supported by the occurrence of framboidal pyrite within the gypsum crystals in some thin sections which indicates that gypsum precipitated after pyrite formation (Fig. 6.9 G, H).

6.4.2 Estimation of the $\delta^{18}O$ and $\delta^{34}S$ of sulfate derived from pyrite oxidation

Sulfate derived from pyrite oxidation has almost the same sulfur isotopic composition as the original sulfide because sulfur isotope fractionation during this process is smaller than 1‰ (Balci *et al.*, 2007). The sulfur isotopic composition of pyrite within the zone where gypsum was formed varies between - 22.9 to -17.9‰. Therefore it can be assumed that sulfate, derived from partial oxidation of these pyrites, would possess a sulfur isotopic composition covering the same range. The oxygen isotopic composition of sulfate derived from pyrite oxidation depends on the oxygen source (i.e. water and dissolved oxygen) and the oxidation mechanism (Balci *et al.*, 2007; Brunner *et al.*, 2008; Taylor *et al.*, 1984; Toran and Harris, 1989). According to Balci *et al.* (2007), water-derived oxygen accounts for around 90% of oxygen incorporated into sulfate during pyrite oxidation while 10% is derived from dissolved oxygen. Both sources are characterized by very different isotopic compositions: $\delta^{18}O_{H2O} \approx \delta^{18}O_{SMOW} = 0‰$ for sea water and $\delta^{18}O_{O2} = +23.5‰$ for oxygen (Kroopnick and Craig, 1972). In aquatic environments, oxidation of pyrite with oxygen derived from water is associated with a positive oxygen isotope fractionation effect of roughly 0 to 4‰ (Balci *et al.*, 2007; Brunner *et al.*, 2008; Taylor *et al.*, 1984). Oxidation of pyrite with oxygen derived from dissolved oxygen is associated with a negative oxygen isotope fractionation effect of around -10‰ (Balci *et al.*, 2007; Kroopnick and Craig, 1972). Consequently, it can be expected that sulfate derived from pyrite oxidation would have a sulfur isotopic composition of -22.9 to -17.9‰ and an oxygen isotopic composition of 0 to +5‰ (Fig. 6.11, Area A).

6.4.3 Estimation of the relative contribution of sulfate from pyrite oxidation versus sea-water sulfate

Mixing of sulfate from pyrite oxidation with sea-water sulfate could have produced the pore-water sulfate the gypsum precipitated from (Fig. 6.11). Based on this hypothesis, a sulfur isotope mass balance can be used to assess the contribution of sulfate derived from pyrite oxidation relative to the contribution of sea-water sulfate:

$$a*\delta^{34}S_{pyrite} + b*\delta^{34}S_{sea\text{-}water} = (a+b) * (\delta^{34}S_{gypsum} - \Delta^{34}S_{pore\text{-}water\_gypsum}) \quad \textbf{(Eq-1)}$$

The parameters a and b denote the contribution of sulfate from pyrite oxidation and sea-water sulfate, respectively. $\delta^{34}S_{pyrite}$ denotes the sulfur isotopic composition of sulfate derived from

pyrite oxidation and $\delta^{34}S_{sea\text{-}water}$ denotes the sulfur isotopic composition of sea-water sulfate. $\delta^{34}S_{gypsum}$ denotes the sulfur isotopic composition of gypsum, and $\Delta^{34}S_{pore\text{-}water\_gypsum}$ the sulfur isotope fractionation for the precipitation of gypsum from pore-water sulfate.
The rearrangement of equation 1 allows the introduction of the relative ratio (x), the contribution of sulfate from pyrite oxidation and sulfate from sea water.

$$a/b^* \delta^{34}S_{pyrite} + \delta^{34}S_{sea\text{-}water} = [(a+b)/b]^* (\delta^{34}S_{gypsum} - \Delta^{34}S_{pore\text{-}water\_gypsum})$$

$$x^* \delta^{34}S_{pyrite} + \delta^{34}S_{sea\text{-}water} = [x+1]^* (\delta^{34}S_{gypsum} - \Delta^{34}S_{pore\text{-}water\_gypsum})$$

$$x^*(\delta^{34}S_{pyrite} - (\delta^{34}S_{gypsum} - \Delta^{34}S_{pore\text{-}water\_gypsum})) = \delta^{34}S_{gypsum} - \Delta^{34}S_{pore\text{-}water\_gypsum} - \delta^{34}S_{sea\text{-}water}$$

$$x = (\delta^{34}S_{sea\text{-}water} - \delta^{34}S_{gypsum} + \Delta^{34}S_{pore\text{-}water\_gypsum}) / (\delta^{34}S_{gypsum} - \Delta^{34}S_{pore\text{-}water\_gypsum} - \delta^{34}S_{pyrite}) \quad \textbf{(Eq-2)}$$

The estimates for $\delta^{34}S_{sea\text{-}water}$ (+20.3‰), $\delta^{34}S_{gypsum}$ (+11.0‰), $\Delta^{34}S_{pore\text{-}water\_gypsum}$ (0 to +1.65‰), and $\delta^{34}S_{pyrite}$ (-17.9 to -22.9‰) can be used to calculate the contribution of sulfate from pyrite oxidation relative to the contribution of sea-water sulfate. The calculations show that about 22% to 29% of sulfate in gypsum could have been derived from pyrite oxidation. Using the graphical combination of sulfur and oxygen isotope mixing, the relative contribution from pyrite oxidation can be even better constrained. About 23% to 26% of sulfate in gypsum was derived from pyrite oxidation (Fig. 6.11, mixing line m 1 and m 2). Assuming that the concentration of sea-water sulfate was 28 mM, the calculated values would correspond to a sulfate contribution from sulfide oxidation to the pore-water sulfate pool of 7.7 to 11.2 mM sulfate. To produce the latter amount of sulfate, an oxidation of around 0.1 to 0.2 wt.% wet weight pyrite would have been required. Given the amount of pyrite that was observed in the thin-sections (Fig. 6.9 C), this estimate is reasonable.

6.4.4 Two pyrite generations?

The mixing lines in the oxygen-sulfur isotope plot in Figure 8 do not only allow the calculation of the contribution of sulfate from pyrite oxidation to gypsum (lines m 1 and m 2), but also provide information about the isotope fractionation related to gypsum precipitation. The intercepts between m 1, respectively m 2 and the composition range of pore-water sulfate forming gypsum (Fig. 6.11, Area B) indicate that the isotope fractionation (1.2 to 2.8‰ for $\Delta^{34}S_{pore\text{-}water\_gypsum}$ and 0.6 to 1.2‰ for $\Delta^{18}O_{pore\text{-}water\_gypsum}$) is smaller than the reported equilibrium isotope fractionation (1.65‰ for sulfur and 3.5‰ for oxygen (Holser and Kaplan, 1966; Thode and Monster, 1965). Such a suppression of the isotope fractionation effect could be due to closed-system or non-equilibrium conditions, e.g. rapid precipitation of gypsum. However, the alternative hypothesis that gypsum formed under isotopic equilibrium, can also be tested. In this case, the sulfur isotopic composition of sulfate derived from pyrite oxidation is estimated using a mixing line through the isotopic composition of sea-water sulfate and pore-water sulfate at isotopic equilibrium (Fig. 6.11, mixing line m 3). It is assumed that the lowest oxygen isotopic composition of sulfate derived from pyrite oxidation is equal to the oxygen isotopic composition of sea water, thus 0‰ V-SMOW. Therefore, the sulfur composition of the pyrite that was oxidized would be around -9‰ (intercept of m 3 with $\delta^{18}O_{SMOW}$ = 0‰). This scenario is possible under the assumption that the pyrite associated with gypsum, featuring sulfur isotope values around -20‰ V-CDT, formed after gypsum precipitation. In the latter case, an earlier pyrite generation, with sulfur isotope values around -9‰ V-CDT, was to a great extent removed by pyrite oxidation. A sulfur isotopic composition of -12.3‰ V-CDT of pyrite found in the layer 10 cm below the zone of gypsum formation supports this hypothesis. Under this assumption (i.e. oxidation of pyrite with $\delta^{34}S$ around -9‰ V-CDT), the relative contribution of sulfate from pyrite oxidation would be around 34% (Fig. 6.11, mixing line m 3).

6.4.5 Proposed mechanism of gypsum and dolomite formation

6.4.5.1 Initial setting

In marine sediments, oxic to sub-oxic conditions are usually restricted to the top few centimetres while sediments below are anoxic. In cold-water coral bearing sediments anaerobic carbon mineralization is extremely slow (Wehrmann *et al.*, 2009). Sulfate profiles from Challenger Mound suggest decomposition of organic matter by sulfate reduction within the top 50 m of the mound sequence while sulfate reduction coupled to anaerobic oxidation of methane is constrained to the underlying Miocene sediments (Ferdelman *et al.*, 2006). Sulfide produced during sulfate reduction in the mound sediments reacts with ferric iron minerals in the siliciclastic fraction and precipitates as framboidal pyrite (Berner, 1970).

6.4.5.2 The oxidation event

The oxygen and sulfur isotope values of the gypsum crystals indicate oxidation of pyrite as driver of the diagenetic alterations in the sediment of Perseverance Mound. It is proposed that oxidizing fluids enter previously anoxic sediments and induce the oxidation of pyrite. Pyrite oxidation with oxygen or ferric iron (Fe^{3+}) as oxidants produces sulfate and protons (H^+) (reaction R-1, R-2). To maintain reaction R-2 the produced ferrous iron (Fe^{2+}) needs to be oxidized to ferric iron, most likely by oxygen (reaction R-3).

$FeS_2 + 15/4\ O_2 + 1/2\ H_2O \rightarrow Fe^{3+} + 2\ SO_4^{2-} + H^+$ (**R-1**)

$FeS_2 + 14\ Fe^{3+} + 8\ H_2O \rightarrow 15\ Fe^{2+} + 2\ SO_4^{2-} + 16\ H^+$ (**R-2**)

$15\ Fe^{2+} + 15\ H^+ + 15/4\ O_2 \rightarrow 15\ Fe^{3+} + 15/2\ H_2O$ (**R-3**)

Dissolved ferric iron also reacts with H_2O to form iron-(oxyhdydr)oxides (reaction R-4).

$Fe^{3+} + 2\ H_2O \rightarrow FeOOH + 3\ H^+$ (**R-4**)

The oxidation event may have been initiated by increasing bottom currents. Van Rooij *et al.* (2007) described significant variations of bottom currents in the Porcupine Seabight throughout glacial-interglacial cycles. The intensification of the bottom currents enhances the pore-water transport from the bottom water into the sediment, bringing oxidizing fluids into intervals where pyrite previously formed (Fig. 6.12). This hypothesis is supported by the occurrence of framboidal pyrite within the gypsum (Fig. 6.9 G, H). Increasing currents can induce sediment erosion of a cold-water coral mound (Dorschel *et al.*, 2005), lowering the redox zones in the sediment column. The alternation of reducing and oxidizing conditions might be recorded in the zonation of the dolomites associated with the gypsum crystals (Fig. 6.9 L). The appearance of bright luminescent and non-luminescent layers in the dolomite, points toward crystallization under changing pore-water chemistry conditions (Richter *et al.*, 2003).
The influx of electron acceptors into the upper part of the sediment is favoured by the shape of a mound. This elevated structure promotes lateral inflow of oxidizing fluids. The presence of a coral framework in the mound potentially yields a higher hydraulic conductivity which allows oxidizing sea water to penetrate deep into the sediment. Depreiter (2009) modeled that increased bottom currents will push down the sulfate methane transition zone (SMTZ) significantly in an elevated structure on the sea bed, due to the strong lateral inflow of fluids advecting sulfate. Moreover, the organic matter turnover in cold-water coral reef sediments is low because the organic matter is already altered by aerobic and anaerobic microbial-mediated oxidation, leaving very refractory organic material (Wehrmann *et al.*, 2009). This also allows a deeper penetration of oxidizing fluids into the mound sediments compared to other surface sediments as oxygen consumption by aerobic carbon mineralization is lower.

6.4.5.3 Buffering of pyrite oxidation by carbonate dissolution

Pyrite oxidation strongly decreases the pore-water pH. Both oxidation pathways (R1 and R2) produce a similar amount of protons. The production of H^+ (drop in pH) leads to a decrease in the pore-water saturation state for carbonate phases (e.g. high-Mg calcite and aragonite) and hence induces dissolution of these minerals (reaction R-5) (Ku *et al.*, 1999). This process is enhanced by

the precipitation of iron-(oxyhydr)oxides (R-4).

$4\ CaCO_3 + 4\ H^+ \rightarrow 4\ Ca^{2+} + 4\ HCO_3^-$ (**R-5**)

This acidification process explains why the coral fragments in unit B are significantly altered, resulting in a secondary porosity (Fig. 6.8 A). In conjunction, XRD-data indicates the preferential dissolution of aragonite in the sediment containing gypsum. The zones of gypsum crystal occurrence are characterized by a decrease of aragonite in the sediment matrix (9.6%) compared to other zones in unit B (below the lithified layer) (average 15.7%) while the calcite content remains stable around 60% (Fig. 6.4). Brachert and Dullo (2000) and James *et al.* (2005) already discussed the preferential dissolution of aragonite during early marine diagenesis in cool-water carbonates.

6.4.5.4 Gypsum formation

The described mechanism of carbonate-buffered pyrite oxidation leads to the addition of dissolved sulfate and calcium. This results in oversaturation of the pore water with respect to gypsum and subsequent gypsum precipitation (reaction R-6):

$2\ SO_4^{2-} + 2\ Ca^{2+} + 4H_2O \rightarrow 2\ CaSO_4.2H_2O$ (**R-6**)

The net total reaction of carbonate-buffered pyrite oxidation can be written as follows:

$FeS_2 + 15/4\ O_2 + 9/2\ H_2O + 4\ CaCO_3 \rightarrow$

$4\ Ca^{2+} + 4\ HCO_3^- + 2\ SO_4^{2-} + FeOOH + 2\ H_2O$

$\rightarrow 2\ CaSO_4.2H_2O\ (s) + 2\ Ca^{2+} + 4\ HCO_3^- + FeOOH$

(**R-7**)

In the following, the mass balance calculation (Eq-2) will be used to test the proposed mechanism under the assumed conditions. The mass balance shows that 23% to 26% (or even 34%) of sulfate in the gypsum crystals derived from pyrite oxidation. For further calculations, a mean value of 25% is used. Assuming a sea-water sulfate concentration of 28 mM, pyrite oxidation contributed 7 mM sulfate. Consequently, the pore-water sulfate concentration during gypsum

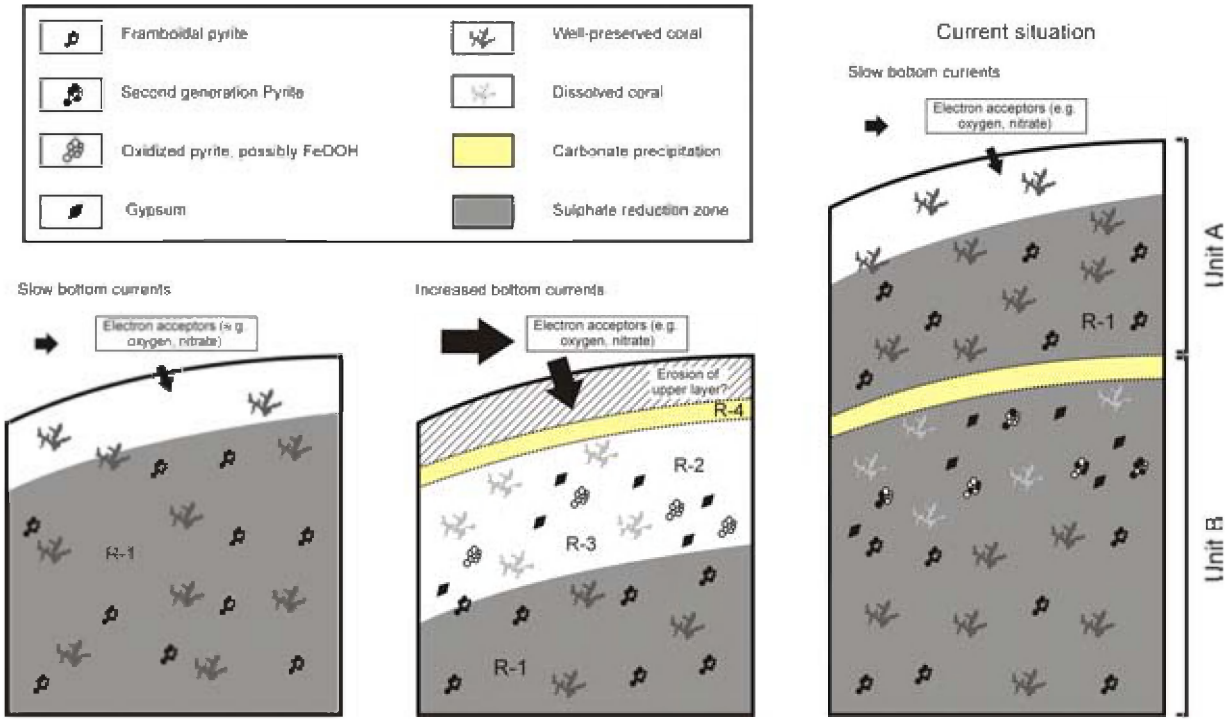

Fig. 6.12 *Schematic representation showing the increase of bottom current enhances the (sideward) inflow of electron acceptors in the upper layer of the sediment, oxidizing framboidal pyrite. The oxidation of pyrite produces sulfate and acidity, which induces dissolution of aragonitic corals. Subsequently the produced sulfate and calcium precipitate as gypsum. Erosion of the upper sediment layers, due to the increase of the bottom currents, might have triggered this oxidation process. R-1: formation of framboidal pyrite, R-2: sulfide oxidation buffered by aragonite dissolution, R-3: gypsum precipitation, R-4: precipitation of carbonate near the seabed.*

precipitation is approximately 35 mM. In order to produce 7 mM sulfate, an equivalent of 3.5 mM pyrite is oxidized. Oxidation of 3.5 mM pyrite (R-1, R-2) and subsequent precipitation of iron-(oxyhydr)oxides (R-4) result in the production of 14 mM H^+. This reaction is buffered by the dissolution of carbonates (R-4) which produces an equivalent of 14 mM Ca^{2+}. Given that sea water contains 10 mM calcium, the pore-water concentration of calcium during the oxidation event reaches approximately 24 mM. A sulfate concentration of 35 mM and a calcium concentration of 24 mM results in an ion product of:

$35*10^{-3} * 24*10^{-3} = 8.4*10^{-4}$ mol^2/l

The gypsum solubility product in sea water is in the order of $1.52*10^{-3}$ mol^2/l (assuming a seawater density of 1030 kg/m^3) (Shaffer, 1967) and $4.88*10^{-4}$ mol^2/l (Kopittke *et al.*, 2004). The calculated value of the ion product of calcium and sulfate is within the range of these values. Thus, gypsum precipitation related to oxidation of pyrite is a feasible process. Gypsum precipitation is even more likely if the possibility is considered that up to 35% of the gypsum may have been derived from pyrite oxidation, which corresponds to an ion product of $1.1*10^{-3}$ mol^2/l ($37.8*10^{-3} * 29.6*10^{-3}$).
The calculations show that the concentrations of sulfate and calcium in the pore water must be considerably higher than sea water in order to reach saturation with respect to gypsum. A semi-closed system is required to allow for the accumulation of calcium and sulfate. Consequently, the oxidant for sulfide oxidation may have been predominantely supplied by diffusive and not advective fluxes.

6.4.5.5 Dolomite precipitation

Pyrite oxidation and subsequent precipitation of gypsum favours the formation of dolomite (Fig. 6.9 L). The incorporation of coccoliths in the dolomite crystals clearly indicates that these crystals have a diagenetic origin (Fig. 6.9 M, N). Moreira *et al.* (2004) highlighted the role of sulfide oxidation in dolomitization in a lagoon system. The oxidation of sulfide provides acid that decreases the pore-water saturation state for high-magnesium calcite and aragonite, favouring the precipitation of dolomite. Carbonate phases such as calcite and high-magnesium calcite have been found to precipitate competitively with dolomite (Arvidson and Mackenzie, 1999). If auxiliary carbonate phases are prevented from precipitating, dolomite may be the preferred phase. Moreover, the formation of gypsum contributes significantly to dolomitization via incorporation of calcium ions into the gypsum crystals, resulting in an increase of the magnesium/calcium ratio in the associated fluids (Moore, 2001). This process has been described in evaporative marine diagenetic environments (Moore, 2001; Moreira *et al.*, 2004). There are however no reports of a similar process under deep-sea conditions.

6.4.5.6 Return to initial conditions

During the Holocene, unit A is deposited which causes a return to anoxic conditions in the sediments of unit B (Fig. 6.12). Microbial sulfate reduction recommences, leading to the formation of a second pyrite generation and the removal of the iron-(oxyhydr)oxides. The presence of two pyrite generations was already hypothesized, based on the sulfur isotopes composition of pyrite in unit B (Table 1).

6.4.6 Formation and characterization of a lithified carbonate layer

In core MD01-2459G, the layer containing gypsum is overlain by a lithified carbonate layer (Fig. 6.3). This suggests a link between the formation of this layer and gypsum precipitation. Most likely, excess calcium and bicarbonate produced during carbonate dissolution diffuse upwards from sites where pyrite oxidation occurs. Close to the sea bed, the pH increases and saturation of the pore water with respect to carbonate occurred which resulted in the precipitation of calcite (Fig. 6.12). The formation of calcite led to the lithification of the sediment at the top of unit B. Calcite precipitation is observed on a micrometer scale as calcite overgrowths on coccoliths and in biogenic fragments (Fig. 6.10 C, D, E). This is also expressed in the XRD-results with calcite values higher than 80% (Fig. 6.4).
The stable C and O isotopes of the bulk carbonate (Table 6.2, Fig. 6.13) reveal similar values as the isotopes reported by Takashima and Kano (2008) in a lithified layer in Challenger Mound. The $\delta^{13}C$ values of the bulk sediment become more depleted when the sediment becomes

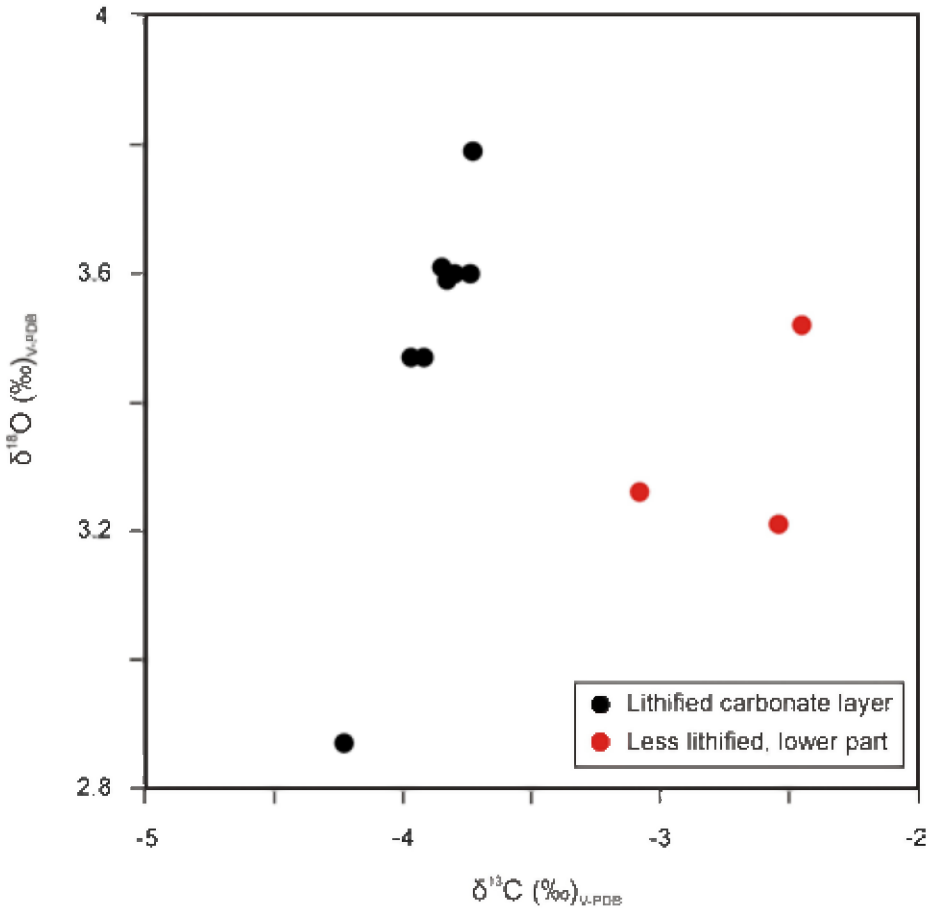

Fig. 6.13 *$\delta^{18}O$ versus $\delta^{13}C$ isotope plot of bulk carbonate samples of the lithified carbonate layer in core MD01-2459G.*

more lithified (Fig. 6.13). This might indicate that the cement is characterized by a slightly depleted $\delta^{13}C$ and enhanced $\delta^{18}O$ signature. Similar decreases in $\delta^{13}C$ and increases in $\delta^{18}O$ of the lithified sediment compared to their less lithified counterparts are reported in hardgrounds (e.g. Dickson *et al.*, 2008; Malone *et al.*, 2001; Mutti and Bernoulli, 2003). Dickson *et al.* (2008) and Mutti and Bernoulli (2003) attributed the 1‰ to 2‰ decrease in the $\delta^{13}C$ values of a hardground compared to the unlithified bulk sample to a cementation phase associated with microbial activity during organic matter decomposition. The oxygen isotope composition of authigenic carbonates is controlled by several factors including the carbonate mineralogy, temperature of formation and the oxygen isotopic composition of the porewater. Under present-day conditions (T = 10°C, $\delta^{18}O$ of the bottom water = 0.45‰ (Flögel *et al.*, in prep.)), calcite which precipitates in equilibrium with seawater will have a $\delta^{18}O$ value of +1.5‰ if we use the paleothermometer of O'Neil *et al.* (1969) and +2.3‰ according to Friedman and O'Neil (1977) and Tarutani *et al.* (1969) for high-Mg calcite. Hence, the increased $\delta^{18}O$ values might indicate that calcite precipitation occurred during glacial periods when cool bottom waters were present, resulting in an enrichment of ^{18}O. Alternatively, Takashima and Kano (2008) argued that the depletion of the $\delta^{13}C$ isotopes and the enrichment of the $\delta^{18}O$ values in a lithified layer in Challenger Mound may be attributed to the presence of *Lophelia pertusa*, characterized by $\delta^{18}O$ and $\delta^{13}C$ values which are far lower than the equilibrium values (Adkins *et al.*, 2003; Blamart *et al.*, 2005).

The widely distributed moldic porosity in the lithified layer indicates that a new phase of dissolution occurred during or after lithification (Fig. 6.8 A, B and 6.10 B). If dissolution would have occurred before lithification, the molds of the biogenic fragments would not have been preserved. Also, no calcite precipitation was observed in the moldic pores (Fig. 6.10 B). The selective dissolution of the aragonitic bioclasts is expressed in the low aragonite values of the XRD-results in

the lithified carbonate layer (Fig. 6.4). The preferential dissolution of aragonite over calcite is also described in other studies on cool-water carbonates (e.g. Brachert and Dullo, 2000; James *et al.*, 2005). This dissolution of aragonitic biogenic fragments may be attributed to the production of hydrogen sulfide during microbial sulfate reduction during the deposition of unit A. If there is a sufficient pool of iron-(oxyhydr)oxides, the hydrogen sulfide will react with the reactive iron and form iron sulfides (Ferdelman *et al.*, 2006; Wehrmann *et al.*, 2009). This process will prevent coral dissolution and might even lead to carbonate precipitation (Wehrmann *et al.*, 2010). However, in the lithified carbonate layer, only a small amount of terrigenous material is present resulting in a limited pool of reactive iron. Hence, little or no iron sulfides were observed in this layer. In the latter case, hydrogen sulfide will act as a weak acid (Soetaert *et al.*, 2007) and react with the carbonate ions (CO_3^{2-}) in the solubility equilibrium of calcium carbonate to form bicarbonate (HCO_3^-) and HS^-. This results in the further dissolution of calcium carbonate to sustain the solubility product equilibrium (Wehrmann *et al.*, 2010).
The brecciated facies which occurs between 555 and 560 cm indicates that brecciation may occur as an early-diagenetic process in cold-water coral mounds (Fig. 6.8 E, F and 6.10 G, H). The exact origin of the brecciated layer remains uncertain. A likely scenario is that the terrigenous material between 555 and 560 cm (Fig. 6.3) was not cemented during the lithification of the carbonate layer and acted as a 'basal shear surface'. When unit A was deposited, the weight of the overlying sediment might have caused sediment creep or even translational sliding (Blendinger, 2001) which resulted in a brecciated facies between 555 and 560 cm. This scenario is most likely on a coral-mound since the steep flanks might promote these creep and sliding processes.

6.4.7 A change in the sedimentary regime?

The appearance of lithified carbonate layers at the sea bed is usually associated with increased currents and a reduced sedimentation rate or even erosion (Allouc, 1990; Mutti and Bernoulli, 2003; Noé *et al.*, 2006). In this study, a clear change in grain-size distribution and clay mineralogy between the sediment of unit A and B also indicates a shift in the sedimentary regime (Fig. 6.5). Moreover, this adds to the hypothesis that increased bottom currents are responsible for the influx of electron acceptors which leads to pyrite oxidation and subsequent gypsum and dolomite precipitation in Perseverance Mound.
The elevated values of kaolinite and smectite in unit B point towards weathering under humid and warm conditions (Fig. 6.5). This is consistent with the high XRF Ca-values in unit B which are attributed to the biogenic sedimentation in interglacial periods (Fig. 6.3) (Foubert and Henriet, 2009; Titschack *et al.*, 2009). In contrast unit A is characterized by the fast deposition (0.5 m/ka) of Fe-rich, terrigenous sediment (Fig. 6.3). This unit displays enhanced concentration of illite and chlorite which are indicative for erosion under cold and dry climatic conditions (Fig. 6.5). Given that unit A was deposited during the Holocene it is proposed that the sediment of the latter unit is siliciclastic sediment of glacial origin which was reworked during the increase of bottom currents after the last glacial period (Rüggeberg *et al.*, 2005; Rüggeberg *et al.*, 2007; Van Rooij *et al.*, 2007). On the eastern flank of the Porcupine Seabight active reworking of glacial sediment occurs during the Holocene due to the high bottom currents (cf. Chapter 3). In the Magellan Mound Province currents are weaker (Huvenne *et al.*, 2005) and the sediment which is eroded from the eastern flank the Porcupine Seabight and subsequently transported northwards (Van Rooij *et al.*, 2007) gets deposited in this area.

6.5 Conclusions

In this study sedimentological, mineralogical and geochemical evidence is presented for a major diagenetic oxidation event in sediments from a cold-water coral mound. It is hypothesized that increased currents caused partial erosion and enhanced inflow of sea water in the mound. This led to penetration of oxygenated fluids into formerly anoxic sediments. Oxidation of sulfide minerals caused dissolution of aragonite and increased sulfate and calcium concentration, triggering the precipitation of gypsum and dolomite. Near the surface, upward diffusing bicarbonate was reprecipitated as carbonate, leading to a lithification of the sediment. This lithified carbonate layer was buried by Holocene sediments (Fig. 6.12) which resulted in a new phase of bacterial sulfate

reduction. The production of hydrogen sulfide, which acts as a weak acid, was not buffered in the lithified carbonate layer due to the limited pool of reactive iron and led to the dissolution of aragonitic biogenic fragments, creating a moldic porosity in the lithified horizon.

If the hypothesis that increased currents led to an oxidation of anoxic sediments in Perseverance Mound is correct, it can be expected that other cold-water coral mounds in the same region might have undergone similar events of pyrite oxidation. However, layers containing gypsum, that would be diagnostic for such oxidation events, have not been reported in other coral mounds as yet. One possibility is that the oxidation in Perseverance was a local process. The other possibility is that, so far, gypsum crystals went undetected in previous studies. This scenario is not unlikely given that the maximum amount of gypsum found in the gravity core from Perseverance Mound was 0.34 vol%. This quantity is not detectable by XRD analysis and is easily overlooked in visual core description. Therefore, it is concluded that the detection of diagenetic gypsum needs to be a target in studies investigating the diagenesis of coral mounds and carbonate sediments in general.

This study demonstrates the importance of environmental factors that affect fluid flow in cold-water coral mounds. It shows how changes in the flow regime impact the (early) diagenesis of these structures. In the future, the occurrence gypsum in marine sediments could be a powerful tool to indentify oxidation processes in carbonate sediments.

References

Adkins, J.F., Boyle, E.A., Curry, W.B. and Lutringer, A., 2003. Stable isotopes in deep-sea corals and a new mechanism for "vital effects". Geochimica et Cosmochimica Acta, 67(6), 1129-1143.

Arvidson, R.S. and Mackenzie, F.T., 1999. The dolomite problem: Control of precipitation kinetics by temperature and saturation state. American Journal of Science, 299(4), 257-288.

Bain, R.J., 1990. Diagenetic, nonevaporative origin for gypsum. Geology, 18(5), 447-450.

Balci, N., Shanks, W.C., Mayer, B. and Mandernack, K.W., 2007. Oxygen and sulfur isotope systematics of sulfate produced by bacterial and abiotic oxidation of pyrite. Geochimica Et Cosmochimica Acta, 71(15), 3796-3811.

Berner, R.A., 1970. Sedimentary pyrite formation. American Journal of Science, 268(1), 1-23.

Blamart, D., Rollion-Bard, C., Cuif, J.P., Juillet-Leclerc, A., Lutringer, A., van Weering, T.C.E. and Henriet, J.P., 2005. C and O isotopes in a deep-sea coral (*Lophelia pertusa*) related to skeletal microstructure. Cold-Water Corals and Ecosystems, 1005-1020.

Blendinger, W., 2001. Triassic carbonate buildup flanks in the Dolomites, northern Italy: breccias, boulder fabric and the importance of early diagenesis. Sedimentology, 48(5), 919-933.

Boschetti, T. and Iacumin, P., 2005. Continuous-flow delta O-18 measurements: new approach to standardization, high-temperature thermodynamic and sulfate analysis. Rapid Communications in Mass Spectrometry, 19(21), 3007-3014.

Brachert, T.C. and Dullo, W.C., 2000. Shallow burial diagenesis of skeletal carbonates: selective loss of aragonite shell material (Miocene to Recent, Queensland Plateau and Queensland Trough, NE Australia) - implications for shallow cool-water carbonates. Sedimentary Geology, 136(3-4), 169-187.

Briskin, M. and Schreiber, B.C., 1978. Authigenic gypsum in marine sediments. Marine Geology, 28(1-2), 37-49.

Brunner, B., Yu, J.Y., Mielke, R.E., MacAskill, J.A., Madzunkov, S., McGenity, T.J. and Coleman, M., 2008. Different isotope and chemical patterns of pyrite oxidation related to lag and exponential growth phases of Acidithiobacillus ferrooxidans reveal a microbial growth strategy. Earth and Planetary Science Letters, 270(1-2), 63-72.

Corselli, C. and Aghib, F.S., 1987. Brine formation and gypsum precipitation in the Bannock Basin, Eastern Mediterranean. Marine Geology, 75(1-4), 185-199.

De Mol, B., Van Rensbergen, P., Pillen, S., Van Herreweghe, K., Van Rooij, D., McDonnell, A., Huvenne, V., Ivanov, M., Swennen, R. and Henriet, J.-P., 2002. Large deep-water coral banks in the Porcupine Basin, southwest of Ireland. Marine Geology, 188, 193-231.

Depreiter, D., 2009. Sources, modes and effects of seabed fluid flow. PhD Thesis, Ghent University, Ghent, 207 pp.

Dickson, J.A.D., Wood, R.A., Al Rougha, H.B. and Shebl, H., 2008. Sulphate reduction associated with hardgrounds: Lithification afterburn! Sedimentary Geology, 205(1-2), 34-39.

Dorschel, B., Hebbeln, D., Rüggeberg, A., Dullo, C. and Freiwald, A., 2005. Growth and erosion of a cold-water coral covered carbonate mound in the Northeast Atlantic during the Late Pleistocene and Holocene. Earth and Planetary Science Letters, 233, 33-44.

Ferdelman, T.G., Kano, A., Williams, T., Henriet, J.P. and Scientists, I.E., 2006. IODP Expedition 307 drills cold-water coral mound along the Irish continental margin. Scientific Drilling, 2, 11-16.

Flögel, S., Rüggeberg, A., Mienis, F., Andresen, N. and Dullo, C., in prep. Geochemical and physical constraints for the occurrence of living cold-water corals.

Foubert, A., Depreiter, D., Beck, T., Maignien, L., Pannemans, B., Frank, N., Blamart, D. and Henriet, J.-P., 2008. Carbonate mounds in a mud volcano province off north-west Morocco: Key to processes and controls. Marine Geology, 248(1-2), 74-96.

Foubert, A. and Henriet, J.P., 2009. Nature and significance of the recent carbonate mound record: the Mound Challenger Code. Springer-Verlag, Heidelberg, 350 pp.

Foubert, A., Van Rooij, D., Blamart, D. and Henriet, J.-P., 2007. X-ray imagery and physical core logging as a proxy of the content sediment cores in cold-water coral mound provinces: a case study from Porcupine Seabight, SW of Ireland. International Journal of Earth Sciences, 96, 141-158.

Frank, N., Ricard, E., Paque, A., van der Land, C., Colin, C., Blamart, D., Foubert, A., Van Rooij, D., Henriet, J.P., De Haas, H. and Van Weering, T., 2009. The Holocene occurrence of cold-water corals in the NE Atlantic: Implications for coral carbonate mound evolution. Marine Geology, 266, 129-142.

Freiwald, A. and Roberts, J.M., 2005. Cold-water corals and ecosystems - Preface. Cold-Water Corals and Ecosystems, 7-12.

Friedman, I. and O'Neil, J.R., 1977. Compilation of stable isotope fractionation factors of geochemical interest. In: M. Fleischer (Editor), Data of Geochemistry. US Geological Survery Professional Paper pp. 1-12.

Gontharet, S., Pierre, C., Blanc-Valleron, M.M., Rouchy, J.M., Fouquet, Y., Bayon, G., Foucher, J.P., Woodside, J. and Mascle, J., 2007. Nature and origin of diagenetic carbonate crusts and concretions from mud volcanoes and pockmarks of the Nile deep-sea fan (eastern Mediterranean Sea). Deep-Sea Research Part Ii-Topical Studies in Oceanography, 54(11-13), 1292-1311.

Hargreaves, P.M., 1984. The distribution of Decapoda (Crustacea) in the open ocean and near-bottom over an adjacent slope in the northern North-East Atlantic Ocean during Autumn 1979. Journal of the Marine Biological Association of the United Kingdom, 64, 829-857.

Henriet, J.-P., De Mol, B., Pillen, S., Vanneste, M., Van Rooij, D., Versteeg, W., Croker, P.F., Shannon, P.M., Unnithan, V., Bouriak, S., Chachkine, P. and The Porcupine-Belgica 97 Shipboard Party, 1998. Gas hydrate crystals may help build reefs. Nature, 391, 648-649.

Holser, W.T. and Kaplan, I.R., 1966. Isotope geochemistry of sedimentary sulfates. Chemical Geology, 1, 93-135.

Huvenne, V., Beyer, A., de Haas, H., Dekindt, K., Henriet, J.P., Kozachenko, M., Olu-Le Roy, K., Wheeler, A. and the TOBI/Pelagia 197 and CARACOLE cruise participants, 2005. The seabed appearance of different coral bank provinces in the Porcupine Seabight, NE Atlantic: results from sidescan sonar and ROV seabed mapping. In: A. Freiwald and J.M. Roberts (Editors), Cold-water Corals and Ecosystems. Springer-Verlag, Berlin Heidelberg, pp. 535-569.

Huvenne, V.A.I., Bailey, W.R., Shannon, P.M., Naeth, J., di Primio, R., Henriet, J.-P., Horsfield, B., de Haas, H., Wheeler, A.J. and Olu-Le Roy, K., 2007. The Magellan mound province in the Porcupine Basin. International Journal of Earth Sciences, 96, 85-101.

Huvenne, V.A.I., Blondel, P. and Henriet, J.-P., 2002. Textural analyses of sidescan sonar imagery from two mound provinces in the Porcupine Seabight. Marine Geology, 189, 323-341.

James, N.P., Bone, Y. and Kyser, T.K., 2005. Where has all the aragonite gone? - Mineralogy of holocene neritic cool-water carbonates, southern Australia. Journal of Sedimentary Research, 75(3), 454-463.

Kano, A., Ferdelman, T.G., Williams, T., Henriet, J.P., Ishikawa, T., Kawagoe, N., Takashima, C., Kakizaki, Y., Abe, K., Sakai, S., Browning, E., Li, X. and the IODP Expedition 307 Scientists, 2007. Age constraints on the origin and growth history of a deep-water coral mound in northeast Atlantic drilled during Integrated Ocean Drilling Program Expedition 307. Geology, 35(11), 1051-1054.

Kopittke, P.M., Menzies, N.W. and Fulton, I.M., 2004. Gypsum solubility in seawater, and its application to bauxite residue amelioration. Australian Journal of Soil Research, 42(8), 953-960.

Kroopnick, P. and Craig, H., 1972. Atmospheric oxygen - isotopic composition and solubility fractionation. Science, 175(4017), 54-55.

Ku, T.C.W., Walter, L.M., Coleman, M.L., Blake, R.E. and Martini, A.M., 1999. Coupling between sulfur recycling and syndepositional carbonate dissolution: Evidence from oxygen and sulfur isotope composition of pore water sulfate, South Florida Platform, USA. Geochimica Et Cosmochimica Acta, 63(17), 2529-2546.

Lindberg, B., Berndt, C. and Mienert, J., 2007. The Fugloy Reef at 70°N; acoustic signature, geologic, geomorphologic and oceanographic setting. International Journal of Earth Sciences, 96, 201-213.

Longinelli, A., 1989. Oxygen-18 and sulphur-34 in dissolved oceanic sulphate and phosphate. In: P. Fritz and J.C. Fontes (Editors), Handbook of Environmental Isotope Geochemistry. Elsevier, Amsterdam, pp. 219-255.

Malone, M.J., Slowey, N.C. and Henderson, G.M., 2001. Early diagenesis of shallow-water periplatform carbonate sediments, leeward margin, Great Bahama Bank (Ocean Drilling Program Leg 166). Geological Society of America Bulletin, 113(7), 881-894.

Moore, C.H., 2001. Carbonate Reservoirs: Porosity evolution and diagenesis in a sequence stratigraphic framework. Developments in sedimentology, 55. Elsevier, 444 pp.

Moreira, N.F., Walter, L.M., Vasconcelos, C., McKenzie, J.A. and McCall, P.J., 2004. Role of sulfide oxidation in dolomitization: Sediment and pore-water geochemistry of a modern hypersaline lagoon system. Geology, 32(8), 701-704.

Mutti, M. and Bernoulli, D., 2003. Early marine lithification and hardground development on a Miocene ramp (Maiella, Italy): Key surfaces to track changes in trophic resources in nontropical carbonate settings. Journal of Sedimentary Research, 73(2), 296-308.

Noé, S., Titschack, J., Freiwald, A. and Dullo, W.C., 2006. From sediment to rock: diagenetic processes of hardground formation in deep-water carbonate mounds of the NE Atlantic. Facies, 52(2), 183-208.

O'Neil, J.R., Clayton, R.N. and Mayeda, T.K., 1969. Oxygen Isotope Fractionation in Divalent Metal Carbonates. Journal of Chemical Physics, 51(12), 5547-5558.

Rice, A.L., Billet, D.S.M., Thurston, M.H. and Lampitt, R.S., 1991. The institute of oceanographic sciences biology programme in the Porcupine Seabight: background and general introduction. Journal of the Marine Biological Association of the United Kingdom, 71, 281-310.

Richter, D.K., Gotte, T., Gotze, J. and Neuser, R.D., 2003. Progress in application of cathodoluminescence (CL) in sedimentary petrology. Mineralogy and Petrology, 79(3-4), 127-166.

Roberts, J.M., Wheeler, A.J. and Freiwald, A., 2006. Reefs of the deep: The biology and geology of cold-water coral ecosystems. Science, 312(5773), 543-547.

Rüggeberg, A., Dorschel, B., Dullo, W.C. and Hebbeln, D., 2005. Sedimentary patterns in the vicinity of a carbonate mound in the Hovland Mound Province, northern Porcupine Seabight. In: A. Freiwald and J.M. Roberts (Editors), Cold-Water Corals and Ecosystems. Springer-Verlag, Berlin Heidelberg, pp. 87-112.

Rüggeberg, A., Dullo, C., Dorschel, B. and Hebbeln, D., 2007. Environmental changes and growth history of a cold-water carbonate mound (Propeller Mound, Porcupine Seabight). International Journal of Earth Sciences, 96, 57-72.

Shaffer, L.H., 1967. Solubility of gypsum in sea water and sea water concentrates at temperatures from ambient to 65 degrees C. Journal of Chemical and Engineering Data, 12(2), 183-189.

Siesser, W.G. and Rogers, J., 1976. Authigenic pyrite and gypsum in South West African continental slope sediments. Sedimentology, 23(4), 567-577.

Soetaert, K., Hofmann, A.F., Middelburg, J.J., Meysman, F.J.R. and Greenwood, J., 2007. The effect of biogeochemical processes on pH. Marine Chemistry, 105(1-2), 30-51.

Takashima, C. and Kano, A., 2008. Geochemical characterization of a lithified horizon of the Challenger mound, hole U1317B. IODP 307 data report.

Tarutani, T., Clayton, R.N. and Mayeda, T.K., 1969. Effect of Polymorphism and Magnesium Substitution on Oxygen Isotope Fractionation between Calcium Carbonate and Water. Geochimica et Cosmochimica Acta, 33(8), 987-996.

Taylor, B.E., Wheeler, M.C. and Nordstrom, D.K., 1984. Stable isotope geochemistry of acid mine drainage: Experimental oxidation of pyrite. Geochimica et Cosmochimica Acta, 48(12), 2669-2678.

Thode, H.G. and Monster, J., 1965. Sulfur-isotopes geochemistry of petroleum, evaporates and ancient seas. In: A. Young and J.S. Galley (Editors), Fluids in subsurface environments: American Association of Petroleum Geologists Memoir 4, pp. 367-377.

Titschack, J., Thierens, M., Dorschel, B., Schulbert, C., Freiwald, A., Kano, A., Takashima, C., Kawagoe, N., Li, X. and Scientists, I.E., 2009. Carbonate budget of a cold-water coral mound (Challenger Mound, IODP Exp. 307). Marine Geology, 259(1-4), 36-46.

Toran, L. and Harris, R.F., 1989. Interpretation of sulfur and oxygen isotopes in biological and abiological sulfide oxidation. Geochimica et Cosmochimica Acta, 53, 2341-2348.

Van Rooij, D., Blamart, D., Richter, T.O., Wheeler, A.J., Kozachenko, M. and Henriet, J.-P., 2007. Quaternary sediment dynamics in the Belgica mounds province, Porcupine Seabight: Ice rafting events and contour current processes. International Journal of Earth Sciences, 96, 121-140.

Van Rooij, D., Blamart, D. and Unnithan, V., 2001. Cruise report MD123-Géosciences: Leg 2, part GEOMOUND, RCMG, Gent.

Van Rooij, D., De Mol, B., Huvenne, V., Ivanov, M.K. and Henriet, J.-P., 2003. Seismic evidence of current-controlled sedimentation in the Belgica mound province, upper Porcupine slope, southwest of Ireland. Marine Geology, 195(1-4), 31-53.

Wang, J.S., Suess, E. and Rickert, D., 2004. Authigenic gypsum found in gas hydrate-associated sediments from Hydrate Ridge, the eastern North Pacific. Science in China Series D-Earth Sciences, 47(3), 280-288.

Wehrmann, L.M., Knab, N.J., Pirlet, H., Unnithan, V., Wild, C. and Ferdelman, T.G., 2009. Carbon mineralization and carbonate preservation in modern cold-water coral reef sediments on the Norwegian shelf. Biogeosciences, 6(4), 663-680.

Wehrmann, L.M., Templer, S.P., Brunner, B., Bernasconi, S.M., Maignien, L. and Ferdelman, T.G., 2010. The imprint of methane seepage on the geochemical record and early diagenetic processes in cold-water coral mounds on Pen Duick Escarpment, Gulf of Cadiz. Marine Geology, doi:10.1016/j.margeo.2010.08.005.

Wheeler, A.J., Beyer, A., Freiwald, A., de Haas, H., Huvenne, V.A.I., Kozachenko, M., Olu-Le Roy, K. and Opderbecke, J., 2007. Morphology and environment of cold-water coral carbonate mounds on the NW European margin. International Journal of Earth Sciences, 96, 37-56.

White, M., 2001. Hydrography and physical dynamics at the NE Atlantic margin that influence the deep water cold reef ecosystem, Dept. of Oceanography, NUI, Galway, Ireland, Galway.

White, M., 2007. Benthic dynamics at the carbonate mound regions of the Porcupine Sea Bight continental margin. International Journal of Earth Sciences, 96, 1-9.

Xavier, A. and Klemm, D.D., 1979. Authigenic gypsum in deep-sea manganese nodules. Sedimentology, 26(2), 307-310.

Zhong, C., Wen, Y., Mu-hong, C., Jun, L. and Sen-Chang, G., 2007. Formation of authigenic gypsum and pyrite assemblage and its significance to gas ventings in Nansha Trough, South Chine Sea. Marine Geology & Quaternary Geology, 27(2), 90-100.

Chapter 7 - Unique authigenic mineral assemblages reveal different diagenetic histories in neighbouring cold-water coral mounds on Pen Duick Escarpment, Gulf of Cadiz

Abstract

Alpha, Beta and Gamma Mound are three cold-water coral mounds, located on the Pen Duick Escarpment in the Gulf of Cadiz amidst the El Arraiche mud volcano field where focused fluid seepage occurs. Despite the proximity of Alpha, Beta and Gamma Mound, each mound contains a completely different assemblage of authigenic minerals and hence diagenetic history.

The diagenetic alteration of the sedimentary record of both Alpha and Beta mound is strongly influenced by biogeochemical processes occurring at shallow sulfate-methane transition zones (SMTZs). Our combined sedimentological, petrographic and isotopic analyses of early-diagenetic features in gravity cores from both Alpha and Beta Mound indicate that the contrast in mineral assemblages between these mounds is caused by differences in fluid and methane fluxes. Alpha Mound (authigenic dolomite, calcite, framboidal pyrite and gypsum) appears to be affected by strong fluctuations in the fluid flow, causing shifts in redox boundaries whereas Beta Mound (authigenic barite, calcite and euhedral pyrite noddules) seems a less dynamic system.

To a large extent, the diagenetic regimes within Alpha and Beta are controlled by factors such as fluid and methane fluxes deriving from layers underlying the mounds and forcings like pressure gradients caused by bottom currents. However, it also becomes evident that authigenic mineral assemblages are not only very sensitive recorders of the diagenetic history of specific cold-water coral mounds, but also affect diagenetic processes in turn. Dissolution of aragonite, lithification by precipitation of authigenic minerals and subsequent brecciation of these lithified layers may also exert a control on the advective and diffusive fluid flow within these mounds, providing a feedback mechanism on future diagenetic processes.

In contrast to Alpha and Beta Mound, the diagenetic processes in the upper 5 m of Gamma Mound are not influenced by a SMTZ. The large pool of iron-(oxyhydr)oxides, due to the Saharan dust input, resulted in the dominance of dissimilatory iron reduction over bacterial sulfate reduction. Therefore, corals are well preserved in the upper layer. Below 5 m, bacterial sulfate reduction becomes the dominant electron accepting pathway during organic matter degradation and relatively high $\delta^{34}S$ values of the sedimentary pyrite suggest the upward diffusion of hydrogen sulfide from a STMZ below. In this layer, corals are badly preserved and precipitation of calcite and dolomite occurs.

This chapter is mostly based on Pirlet, H., Wehrmann, L., Foubert, A., Brunner, B., Blamart, D., De Mol, L., Van Rooij, D., Dewanckele, J., Cnudde, V., Swennen, R., Henriet, J.-P. (in preparation) Unique authigenic mineral assemblages reveal different diagenetic histories in two neighbouring cold-water coral mounds on Pen Duick Escarpment, Gulf of Cadiz.

7.1 Introduction

Cold-water corals are widespread along the northeast Atlantic continental margin (Roberts *et al.*, 2006). The dominant cold-water corals, *Lophelia pertusa* and *Madrepora oculata,* are known to construct mound-like structures up to 300 m in height in the Rockall Trough and Porcupine Seabight (De Mol *et al.*, 2002; Henriet *et al.*, 1998; Kenyon *et al.*, 2003; van Weering *et al.*, 2003). In 2005, one of these mounds (Challenger Mound, Porcupine Seabight) was drilled to its base during Expedition 307 of the Integrated Ocean Drilling Program (IODP) (Ferdelman *et al.*, 2006; Foubert and Henriet, 2009; Kano *et al.*, 2007). More recently, similar cold-water coral mounds, in a juvenile growth stage, have been discovered in the Gulf of Cadiz on top of escarpments in the close vicinity of mud volcanoes (Fig. 7.1) (Foubert *et al.*, 2008; Van Rooij *et al.*, 2010; Wienberg *et al.*, 2009). These cold-water coral mounds represent excellent laboratories to study the early diagenetic and biogeochemical processes which affect cool-water carbonates given that they are not affected by burial and/or meteoric diagenesis (Foubert and Henriet, 2009). Previous studies indicate that cold-water coral mound sediments represent a specific diagenetic environment with a tight coupling between microbial-mediated organic matter degradation and carbonate mineral diagenesis (Ferdelman *et al.*, 2006; Webster *et al.*, 2008). Wehrmann *et al.* (2009) showed that cold-water coral reef sediments have a low content of organic matter characterized by an elevated degradation state due to a high organic matter turnover by oxic microbial respiration. As a consequence of these low rates of carbon degradation, sediment diagenesis is slow as well. The preservation state of the aragonitic corals is largely controlled by the presence of reactive iron in the siliciclastic fraction of the sediment, which buffers the sulfide produced during bacterial sulfate reduction

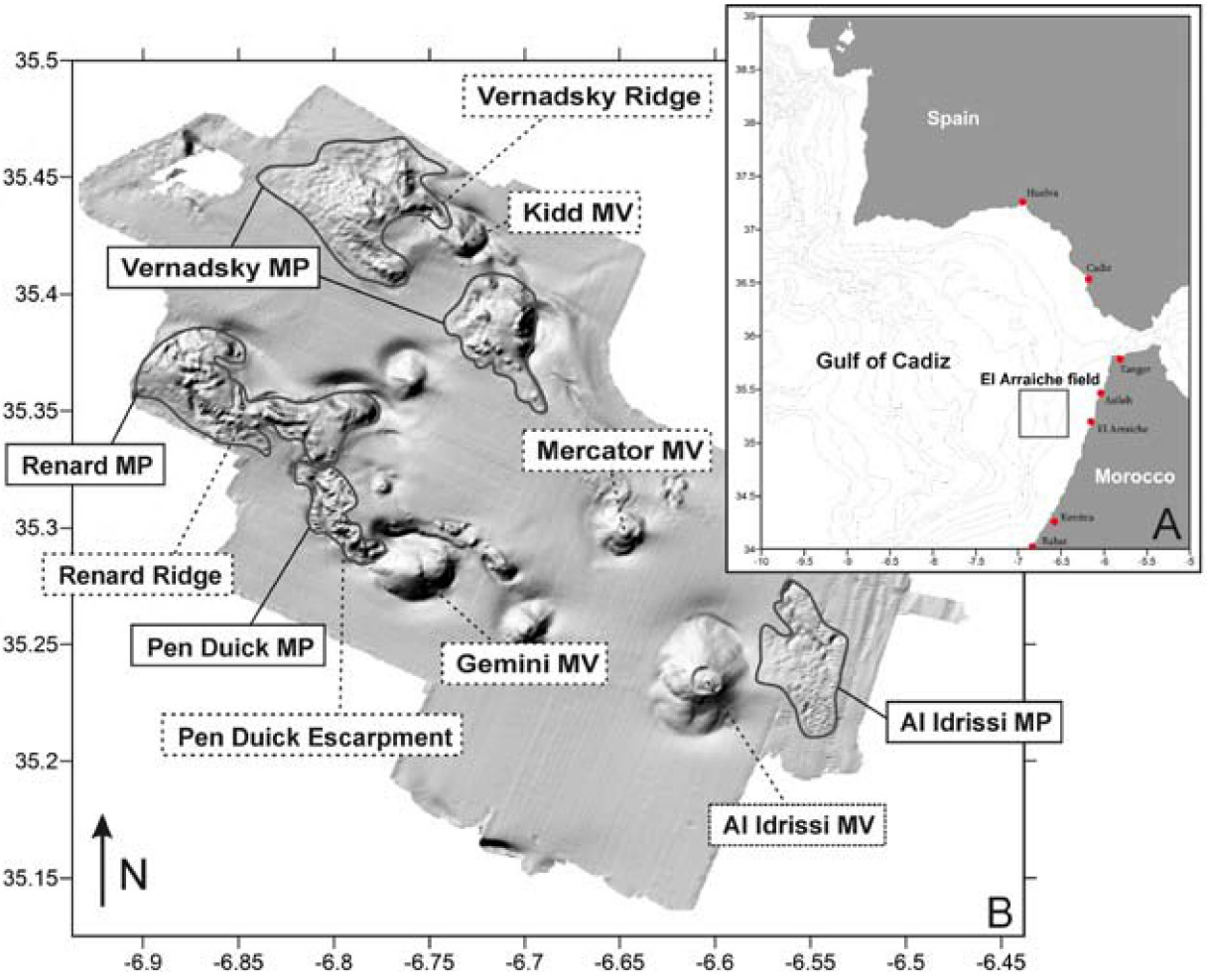

Fig. 7.1 *A. Location of the El Arraiche mud volcano field in the Gulf of Cadiz. B. Multibeam map of the El Arraiche mud volcano field. The various mud volcanoes (MV), mound provinces (MP) and escarpments are indicated. Modified after Foubert et al. (2008).*

(Ferdelman *et al.*, 2006; Wehrmann *et al.*, 2009). In addition, the production of CO_2 during organic matter degradation also affects carbonate diagenesis. This production will essentially lead to a decrease of the carbonate saturation state in the porewater and may thus induce carbonate dissolution. Furthermore, the intermittent growth of coral mounds with episodes of reduced sedimentation or erosion exerts a strong control on early-diagenetic processes as these episodes can relocate redox-fronts in the subsurface (Pirlet *et al.*, 2010).

IODP Expedition 307 revealed that the geochemistry and diagenetic processes within Challenger Mound are not influenced by methane or other hydrocarbons (Ferdelman *et al.*, 2006; Webster *et al.*, 2008). In contrast, anaerobic oxidation of methane (AOM) coupled to sulfate reduction in a shallow sulfate methane transition zone (SMTZ) has been reported in the mounds in the Gulf of Cadiz (Foubert *et al.*, 2008; Maignien *et al.*, 2010; Wehrmann *et al.*, 2010). This microbially-mediated process leads to a drastic alteration of the original sediment resulting in the dissolution and precipitation of carbonates and iron- and sulfur-bearing minerals (Maignien *et al.*, 2010; Wehrmann *et al.*, 2010). Wehrmann *et al.* (2010) and Maignien *et al.* (2010) identified a shallow SMTZ in both Alpha and Beta Mound and discussed the impact on sediment diagenesis. Evidence was found for a variable position of the SMTZ in Alpha Mound which was attributed to fluid dynamics (Wehrmann *et al.*, 2010).

Here, we build upon the findings of Wehrmann *et al.* (2010) and Maignien *et al.* (2010). An in-depth study of the diagenetic features in the sediment of three neighboring cold-water coral mounds (Alpha, Beta and Gamma Mound) in the Gulf of Cadiz is conducted (Fig. 7.1), using sedimentological, mineralogical and petrographic

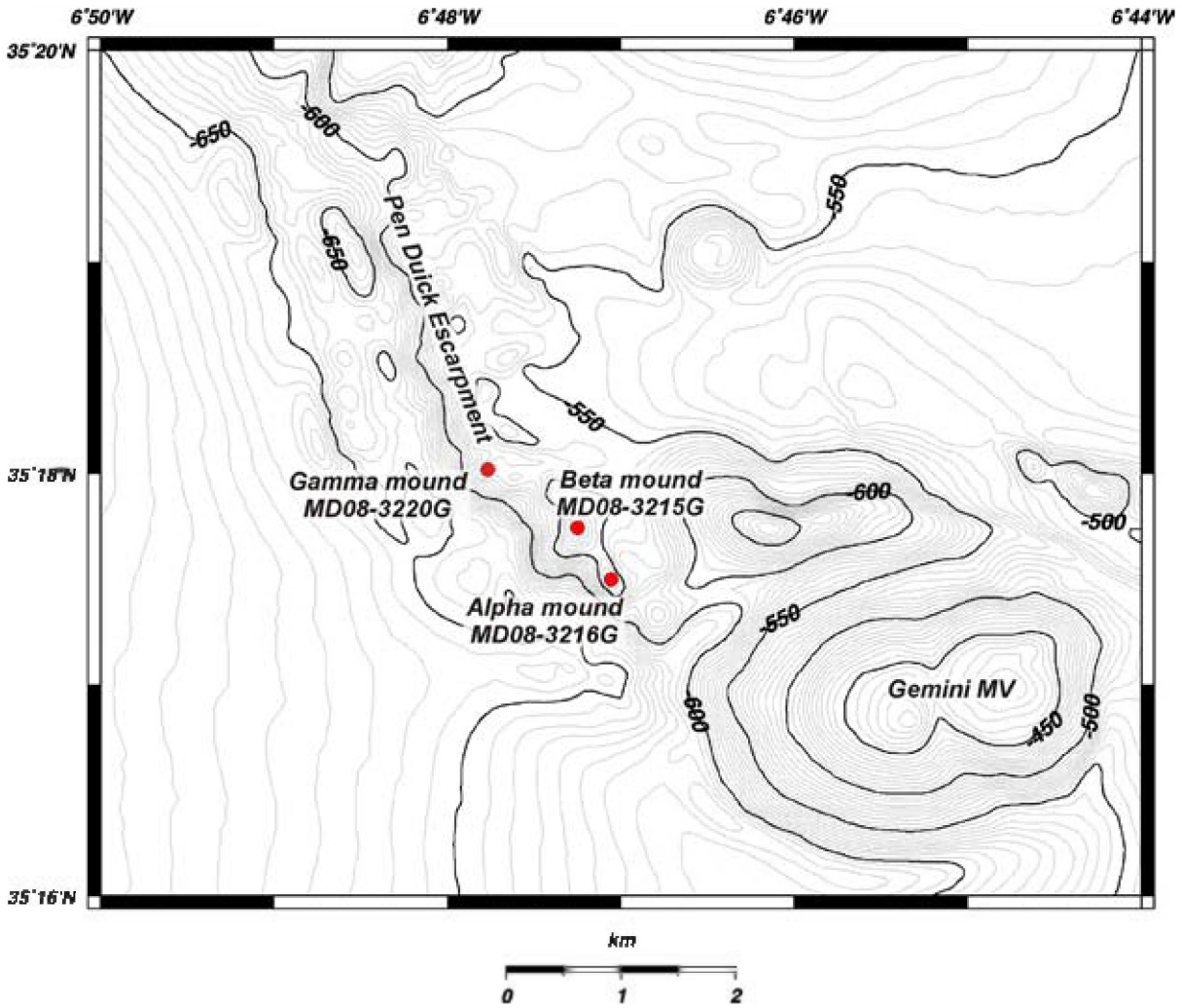

Fig. 7.2 *A multibeam map of the Pen Duick Escarpment, Off Morocco with the location of the gravity cores retrieved from Alpha (MD08-3216G), Beta (MD08-3215G) and Gamma Mound (MD08-3220G) (Van Rooij et al., 2010). Next to the escarpment, Gemini mud volcano (MV) is indicated.*

and isotopic analyses. The detailed identification of the various authigenic minerals and diagenetic features (brecciation, dissolution) allows to reconstruct the diagenetic environment and assess the differences between the three mounds. The role of fluid fluxes from underlying layers and pressure gradients, caused by bottom currents on diagenesis are discussed as well as the effect of lithification and brecciation processes.

7.1.1 Regional setting

The Gulf of Cadiz is situated at the front of the Gibraltar arc, the westernmost tectonic belt of the Alpine-Mediterranean compressional system which has formed by the convergence of the African and Eurasian plates. The geology of this area is extremely complex and still discussed controversially (Gutscher *et al.*, 2002; Maldonado *et al.*, 1999; Sartori *et al.*, 1994; Zitellini *et al.*, 2009). The westward motion of the front of the Gibraltar Arc caused the Gulf of Cadiz to form as a forearc basin and induced the emplacement of an olistostrome in an accretionary wedge-type depositional environment during the Tortonian (Maldonado *et al.*, 1999; Medialdea *et al.*, 2004). The main part of the olistostrome unit covers the central part of the Gulf of Cadiz as a lobe-shaped structure and extends over 300 km into the Atlantic Ocean (Maestro *et al.*, 2003; Maldonado *et al.*, 1999; Medialdea *et al.*, 2004; Somoza *et al.*, 2003). The end of olistostrome emplacement during the Late Miocene coincides with accelerated tectonic subsidence, while thick progradational and aggradational depositional sequences were developed (Maldonado *et al.*, 1999). Plate convergence in the region yields a compressional-transpressional tectonic regime leading to the reactivation of many normal faults and causing mud volcanism and widespread diapirism in the north of the Gulf of Cadiz (Berastegui *et al.*, 1998; Pinheiro *et al.*, 2004; Somoza *et al.*, 2003).

The study area, the El Arraiche mud volcano field (Fig. 7.1), is located on top of the accretionary wedge in water depths between 200-700 m (Van Rensbergen *et al.*, 2005). In this mud volcano field, four cold-water coral mound provinces have been reported which have been named after the steep fault-bounded escarpments and ridges (Foubert *et al.*, 2008) they are located on: (1) the Pen Duick Mound Province, (2) the Renard Mound Province, (3) the Vernadsky Mound Province and (4) the Al Idrisi Mound Province (Fig. 7.1). Alpha, Beta and Gamma Mound are located on the southeastern edge of the Pen Duick Escarpment which hosts a total of 15 mounds (Fig. 7.2). The mounds reach a height up to 60 m, a diameter of about 500 m and occur in water depths ranging between 500-600 m (Foubert *et al.*, 2008). Video imagery and surface samples revealed the presence of reef-forming scleractinians such as *Lophelia pertusa*, *Madrepora oculata* and *Dendrophyllia sp.* however few or no living species were observed (Foubert *et al.*, 2008; Van Rooij *et al.*, 2010). A more elaborate overview of the temporal and spatial distribution of cold-water corals in the study area is given in Wienberg *et al.* (2009).

7.1.2 Hydrodynamic setting

The hydrodynamic setting in the Gulf of Cadiz is controlled by the exchange of Atlantic and Mediterranean water masses through the Strait of Gibraltar. The upper water mass is the North Atlantic Surface Water (NASW, upper 100 m) which, together with the North Atlantic Central Water (NACW, 100-600 m), forms the cool Atlantic Inflow Water (AI) into the Mediterranean (Caralp, 1988; Pelegri *et al.*, 2005). Between 600 and 1500 m two intermediate water masses are observed: Antarctic Intermediate Water (AAIW) from 600 to 900 m and below 900 m, Mediterranean Outflow Water occurs (MOW) (Iorga and Lozier, 1999; Machin *et al.*, 2006; Pelegri *et al.*, 2005). Below 1500 m, North Atlantic Deep Water (NADW) is present. A more elaborate description of the hydrodynamic setting of the study area can be found in Foubert *et al.* (2008) and Van Rooij *et al.* (2010).

7.2 Material and Methods

Cores MD08-3215G, MD08-3216G and MD08-3220G were obtained with a gravity corer during the MD-169 MiCROSYSTEMS cruise with R/V Marion Dufresne in July 2008 (Van Rooij *et al.*, 2010). Core MD08-3215G was taken on the top of Beta Mound (35° 17.74050'N and 6° 47.25040'W) and has a length of 343 cm while MD08-3216G was retrieved from the top of Alpha Mound (35° 17.49590'N and 6° 47.05810'W) and has a total length of 445 cm (Fig. 7.2). Gravity core MD08-3220G was taken on Gamma Mound (35° 18.87270'N and 6° 48.07980'W) and has a total length of 620 cm (Fig. 7.2). After retrieval all cores were cut in sections of 75 cm.

7.2.1 Sedimentological and mineralogical analyses

The mineralogical composition of the bulk sediment of 44 samples in the cores retrieved

Alpha Mound			Beta Mound			Gamma Mound		
Thin-sections	SEM	Micro-CT scans	Thin-sections	SEM	Micro-CT scans	Thin-sections	SEM	Micro-CT scans
91-93	90-91	18-20	3-5	11-12	68-70	143-145	400-401	483-485
162-164	201-202	144-146	116-118	115-116	254-256	209-211	520-521	578-580
191-193	291-292	219-221	220-222	221-222	262-264	335-337	585-586	
289-291	321-322	260-262	254-256	251-252	280-282	443-445		
336-338	371-372	365-367	285-287	291-292	285-287	516-518		
365-367	431-432	381-383	293-295	331-332	309-311	578-580		
429-431	441-442	414-416	309-311	core-catcher		592-594		
		435-437	core-catcher					

Table 7.1 *The depth (cm) of the samples taken from the various cores on Pen Duick Escarpment for thin-sections, micro-CT scans and SEM.*

from Alpha and Beta Mound was identified and quantified using X-ray diffraction (XRD) at the department of Earth and Environmental Sciences, Geology, K.U. Leuven, Belgium. The samples were prepared and measured following the method described in section 2.5.3. Standard thin sections, embedded in a fluorescent resin, from 22 intervals in Alpha, Beta and Gamma Mound were manufactured at the Department of Earth and Environmental Sciences, Geology, K.U. Leuven (Table 7.1). The thin sections were studied using conventional transmitted, reflected and UV light microscopy. A more thorough investigation of the diagenetic features was conducted with cold cathodoluminescence (CL) (see section 2.5.1). Furthermore, 17 bulk sediment samples, taken at various depths in the cores from Alpha, Beta and Gamma Mound (Table 7.1), were dissolved in distilled water and treated in an ultrasonic bath for 20 s. Subsequently, the solution was filtered and dried. The filter was gold-coated and studied with a JEOL 6400 scanning electron microscope (SEM) at Ghent University. The composition of several points was analyzed using Energy Dispersive Spectroscopy (EDS) (see section 2.5.2).

In total, 16 samples were taken from Alpha, Beta and Gamma Mound for micro-CT scans in intervals with obvious signs of diagenetic alteration of the sediment (Table 7.1). The micro-CT scans were conducted at the Centre for X-ray Tomography at Ghent University (UGCT) following the method described in section 2.3. Medical CT scans of the sediment cores from Alpha, Beta and Gamma Mound were performed with a Siemens medical CT at Ghent University Hospital (UZ Gent) (see section 2.3).

7.2.2 Isotope measurements

The stable C and O isotope composition was measured of 19 bulk carbonate samples from Alpha and Beta Mound according to the method described in section 2.8.1. In the present study, a partial extraction procedure was performed to separate the dolomite fraction from the calcite fraction in a sample taken at 181 cm in Alpha Mound following the method described in section 2.8.2. Subsequently, stable isotopic measurements were performed at the University of Erlangen (Germany) on the bulk fraction, as well as on separated calcite and dolomite fractions. All values are reported in per mil relative to Vienna Pee Dee Belemnite (V-PDB).

The sulfur isotopic composition of the pyrite was measured on 15 samples in Alpha Mound, 15 samples in Beta Mound and 24 samples in Gamma Mound at the Max Planck Institute for Marine Microbiology, Bremen (see section 2.9). The isotope measurements of sulfur are reported with respect to Vienna Canyon Diablo Troilite (V-CDT). In order to determine the isotope composition of carbonate associated sulfate (CAS) in the dolomite, a sequential leaching technique was used (section 2.10). The sulfur isotope ratio of the CAS is reported with respect to Vienna Canyon Diablo Troilite (V-CDT), the oxygen isotope composition of CAS is reported with respect to Vienna Standard Mean Ocean

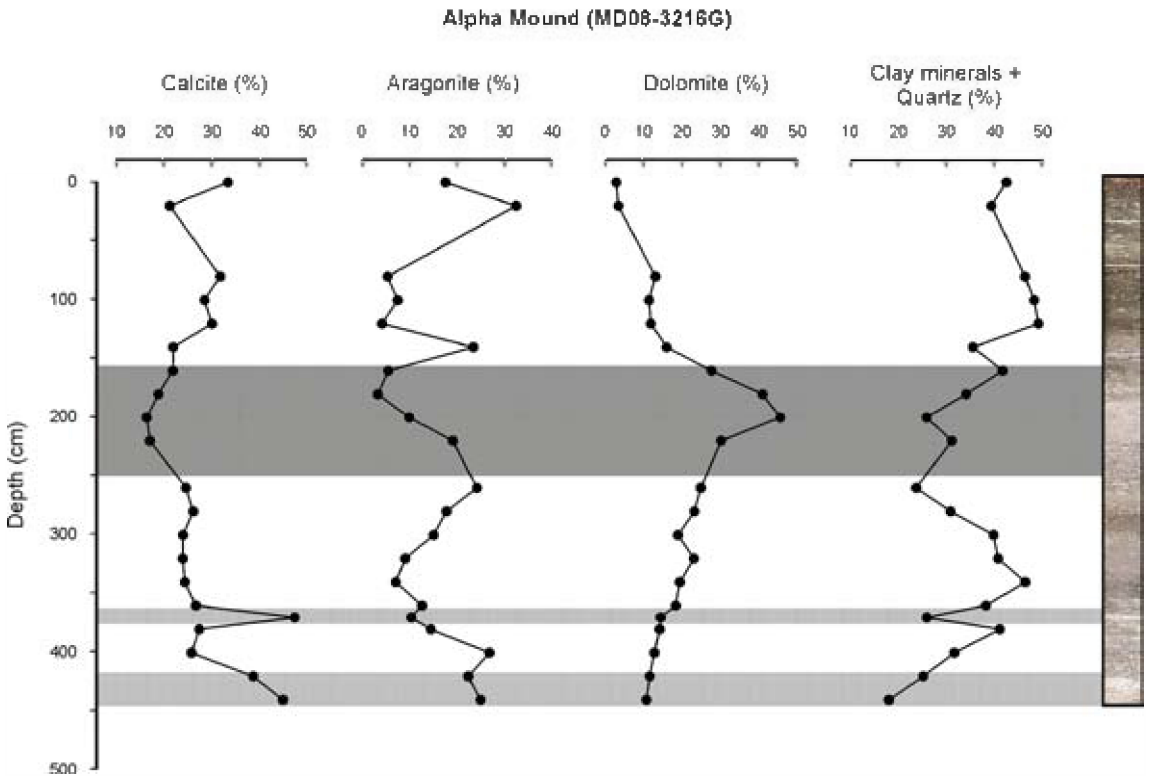

Fig. 7.3 *X-ray diffraction data of the bulk sediment of Alpha Mound (MD08-3216G). The percentages of calcite, aragonite, dolomite and the clay minerals + quartz are indicated and correlated with the core photographs. The lithified layers are indicated in grey.*

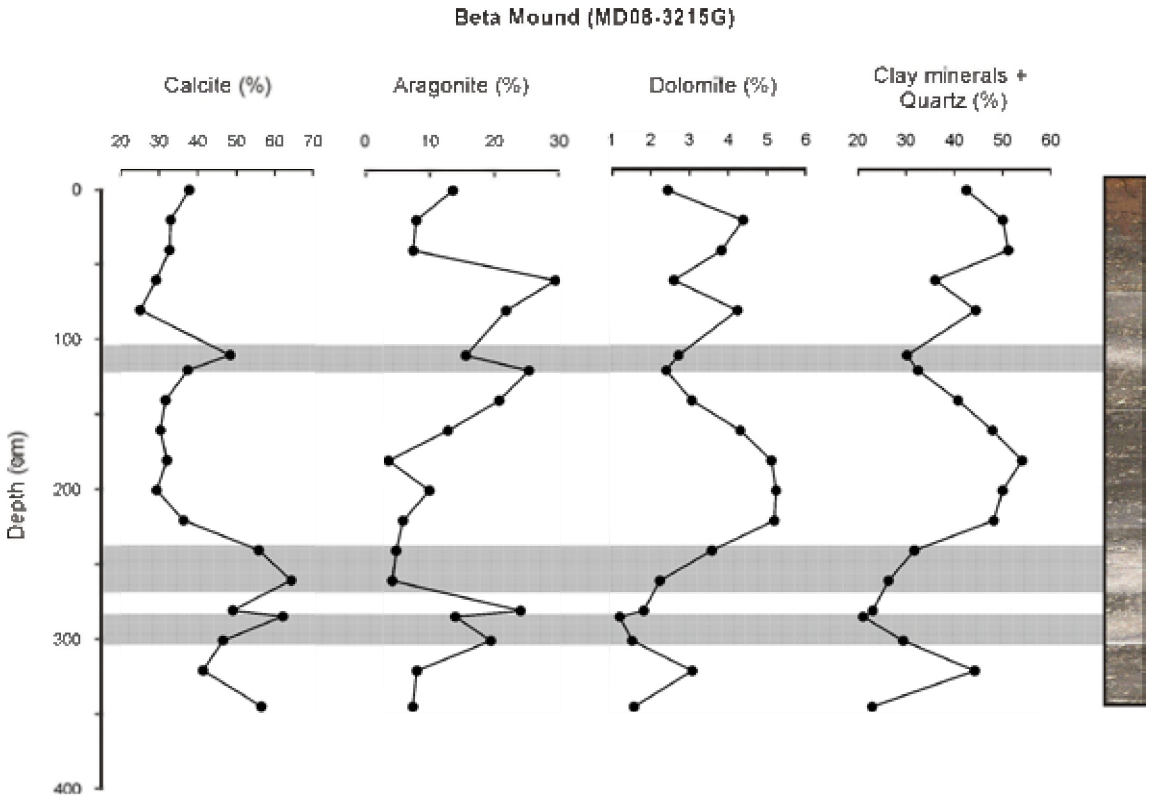

Fig. 7.4 *X-ray diffraction data of the bulk sediment of Beta Mound (MD08-3215G). The percentages of calcite, aragonite, dolomite and the clay minerals + quartz are shown and correlated with the core photographs. The lithified layers are indicated in grey.*

Water (V-SMOW).

7.3 Results

7.3.1 Lithology and mineralogy

The cores taken on Alpha (MD08-3216G), Beta Mound (MD08-3215G) and Gamma Mound (MD08-3220G) contain in varying quantities fragments of *Lophelia pertusa*, *Madrepora oculata*, *Desmophyllum* spp. and *Dendrophyllia* spp. corals, embedded in a matrix of fine to coarse silt. The sediments in the upper part of Alpha and Beta Mound are characterized by a brown to grayish brown colour (Alpha Mound: 0-9 cm, Beta Mound: 0-30 cm) (Fig. 7.3 and 7.4), while in the lower part, the sediments are gray to olive gray. In Alpha Mound, various lighter levels occur with poorly preserved corals and semi-lithified layers (162-255 cm, 367-375 cm, 419-445 cm). Pale layers with dissolved corals and partial lithification are also present in Beta Mound (101-120 cm, 234-268 cm, 281-300 cm, core catcher). In Gamma Mound the upper 470 cm of the core consist of olive brown to grayish brown sediment containing well preserved coral fragments (Fig. 7.11). Below 470 cm, the matrix has a gray colour with lenses of lighter, slightly lithified sediment (544-600 cm) which reveal badly preserved corals.

The dominant mineral in Alpha Mound is calcite with an average content of 27.5% (Fig. 7.3). In the pale, semi-lithified layers in the lower part of the core (367-375 cm, 419-445 cm), the calcite value increases to 47.5%. Dolomite constitutes the second most important carbonate mineral with an average content of 18.9% and peaks of 45.6% in the semi-lithified layer at 162-255 cm (Fig. 7.3). Aragonite varies between 6 and 19% with an average of 13.2%. Beside the carbonate minerals, quartz (average 13.2%) and clay minerals (average 22.7%) are abundantly present (Fig. 7.3). Clay minerals and quartz co-vary with lower values in the pale, lithified layers and are inversely correlated with the distribution of the carbonate minerals (Fig. 7.3). Pyrite and feldspar occur in minor quantities in the samples with an average of respectively 0.2% and 2.3%. In the samples taken at 101, 121 and 361 cm, the presence of gypsum was noticed (0.6-1.9%).
In Beta Mound, calcite constitutes on average 41% of the bulk sediment with peaks up to 62% in the pale semi-lithified layers (Fig. 7.4). Aragonite (average 13.5%) is the second most important carbonate mineral whereas dolomite (average 3.1%) only constitutes a minor fraction of the sediment (Fig. 7.4). The dolomite distribution correlates nicely with the variations of the clay minerals (average 22.3%) and quartz (average 15.9%) with higher values in between the semi-lithified layers (Fig. 7.4). In the core catcher, which corresponds to the deepest sediment retrieved from the core, barite constitutes around 9.1% of the bulk sediment. Pyrite and feldspar occur in minor quantities with an average of respectively 0.4% and 3.1%.

7.3.2 Petrography

7.3.2.1 Alpha Mound

In general, the sediment of Alpha Mound (Fig. 7.5) consists of micritic carbonate mud with a variable amount of biogenic fragments (foraminifera, corals, shells, etc.). Dolomite crystals containing coccoliths and radiolaria were observed in all samples in varying quantities. In the interval between 160 and 220 cm a higher concentration of dolomite rhombs (up to 50 µm) was observed in the matrix and in the pores of biogenic fragments. This was confirmed by the observation of rhombohedric crystals under the SEM which were identified as dolomite using EDS (Fig. 7.5 A, B). Cold CL shows bright orange luminescent dolomite rhombs which sometimes reveal zonation (Fig. 7.5 C, D). At a depth of 371, 431 and 441 cm calcitic overgrowths were observed on the coccoliths and in biogenic fragments (Fig. 7.5 E). The thin sections also reveal the presence of feldspar (bright blue luminescent) and quartz grains. In some intervals circular concentrations of coarse quartz grains are observed which are attributed to the presence of a quartz-agglutinating benthic organism (Fig. 7.5 F). Throughout the entire core, clusters of framboidal pyrite were observed in the sediment matrix and in the pores of biogenic fragments (Fig. 7.5 G, H). Between 190 and 370 cm the framboids have overgrowths of euhedral pyrite crystals. At a depth of 366 cm, a twinned crystal was observed of approximately 800 µm in length (Fig. 7.5 I). This crystal contains small biogenic fragments, dolomite rhombs and encrusts a coral (Fig. 7.5 I, J). The crystal is non-luminescent and was identified as gypsum using Energy Dispersive Spectroscopy (EDS) (Fig. 7.5 K).

7.3.2.2 Beta Mound

The biogenic fragments of Beta Mound are embedded in a matrix of micritic carbonate mud with quartz and feldspar grains (Fig. 7.6). In contrast to Alpha Mound, there are no layers

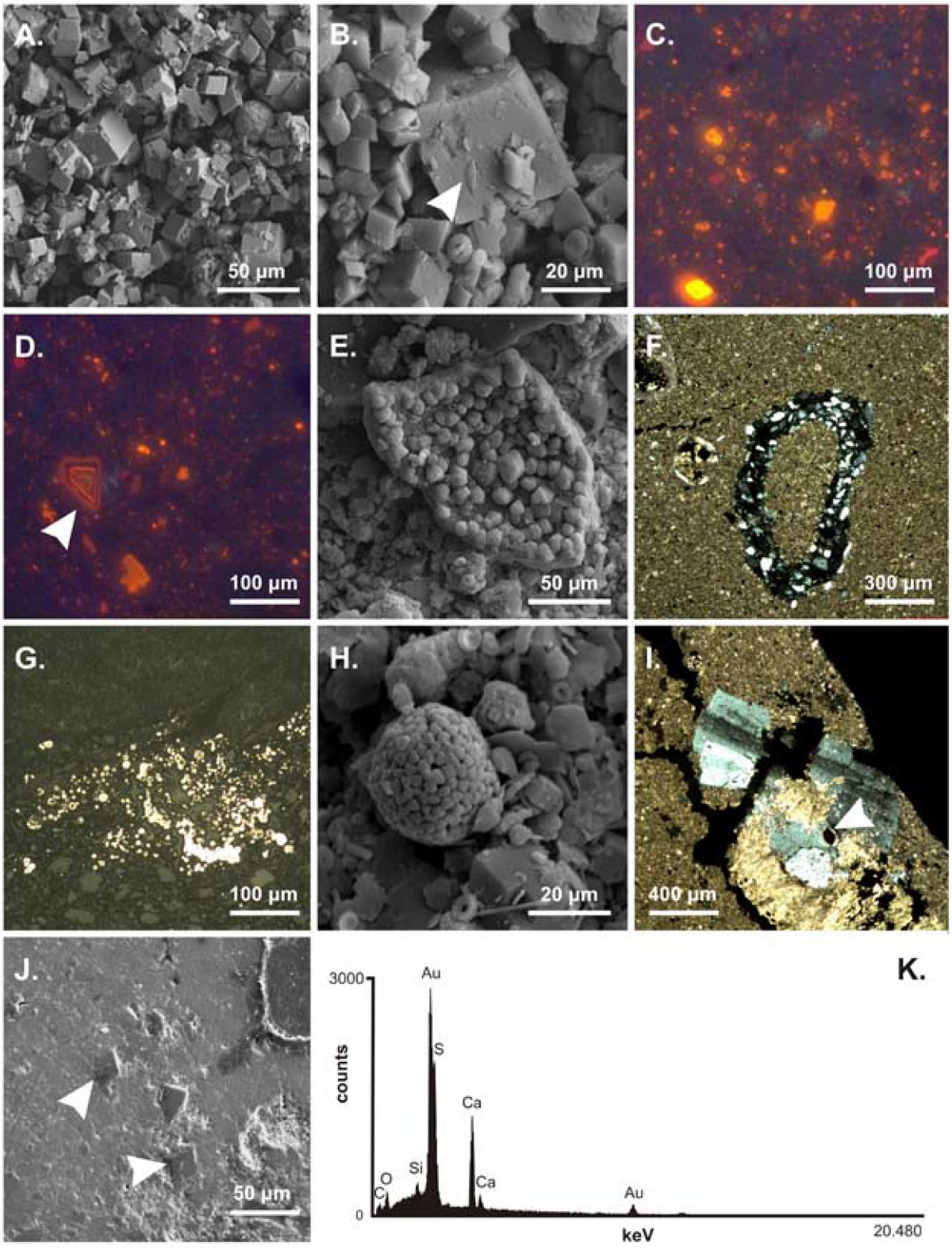

Fig. 7.5 *Petrographic observations of Alpha Mound. A. High concentration of dolomite rhombs at a depth of 201 cm (SEM). B. A detail of a dolomite crystal incorporating coccoliths and other dolomite rhombs (SEM) (201-202 cm). C. Cold Cathode Luminescence (CL) of bright-yellow to orange luminescent dolomite (162-164 cm). D. Cold CL of a zoned dolomite (162-164 cm). E. Intraparticular calcite precipitation in a biogenic fragment (SEM) (431-432 cm). F. Concentration of coarse quartz grains, attributed to a quartz-agglutinating benthic organism (plane-polarized light) (191-192 cm). G. A cluster of framboidal pyrite (reflected light) (91-93 cm). H. A detail of a pyrite framboid (SEM) (291-292 cm). I. A twinned gypsum crystal (white-grey colours), encrusting a coral fragment and incorporating foraminifers (white arrow) (plane-polarized light) (365-367 cm). J. A detail of dolomite rhombs incorporated in a gypsum crystal (SEM) (365-367 cm). K. An EDS-profile of the gypsum crystal (365-357 cm).*

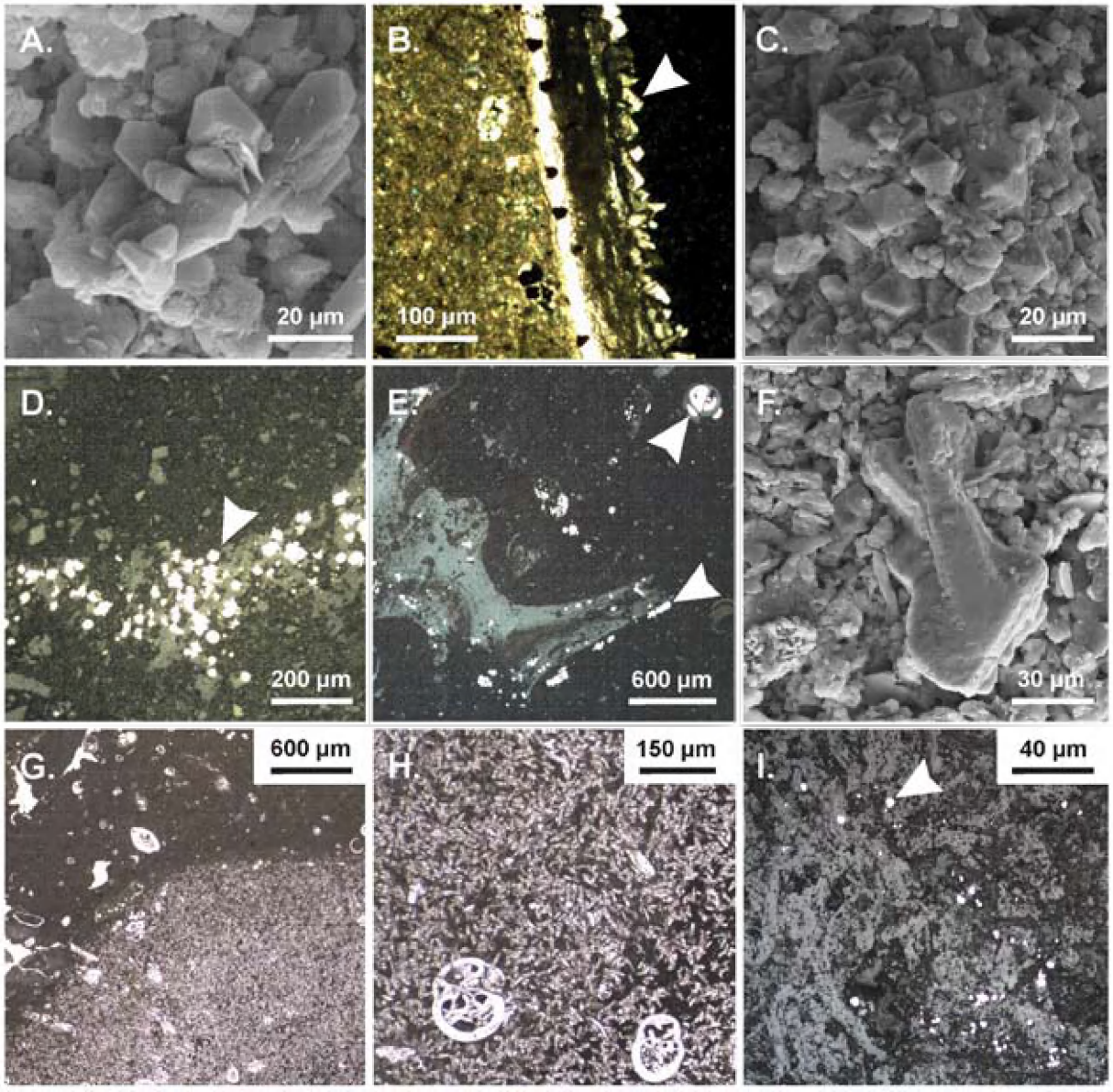

Fig. 7.6 *Petrographic observations of Beta Mound. A. Calcite crystals (core catcher, deepest part of core) (SEM). B. Intraparticular calcite precipitation in the shell of a bivalve (plane-polarized light) (309-311 cm). C. A detail of a cluster of euhedral pyrite (SEM) (core catcher). D. and E. The precipitation of euhedral pyrite inside biogenic fragments such as corals and foraminifera (reflected light) (116-118 and 293-295 cm). F. A twinned barite crystal (SEM) (core catcher). G. The sharp transition between the sediment matrix without barite and a barite nodule (whitish sediment) (core catcher). H. A detail of barite precipitation in the sediment matrix and inside biogenic fragments (core catcher). I. The presence of euhedral pyrite within and around the barite crystals (reflected light) (core catcher).*

with higher occurrence of dolomite rhombs. Cold CL reveals the scattered occurrence of small bright-yellow dolomite crystals. In various intervals (251 cm, 291 cm and the core catcher) calcite overgrowth occurs on coccoliths and in the pores of the biogenic fragments (Fig. 7.6 A, B). Throughout the entire core large quantities of euhedral pyrite were found, scattered in the sediment matrix or as overgrowths on framboidal pyrite (Fig. 7.6 C, D, E). In most samples euhedral pyrite is also present in the pores of biogenic fragments and borings in the corals (Fig. 7.6 D, E). Thin sections of the lithified sediment in the core catcher of MD08-3215G reveal the presence of large quantities of barite which were identified using EDS (Fig. 7.6 F). The barite crystals are mostly uniform and have dimensions between 50 and 100 µm (Fig. 7.6 F, G, H, I). The crystals appear in nodules characterized by a sharp transition with the sediment matrix which contains no barite crystals (Fig. 7.6 G). Around and within the barite crystals, euhedral pyrite

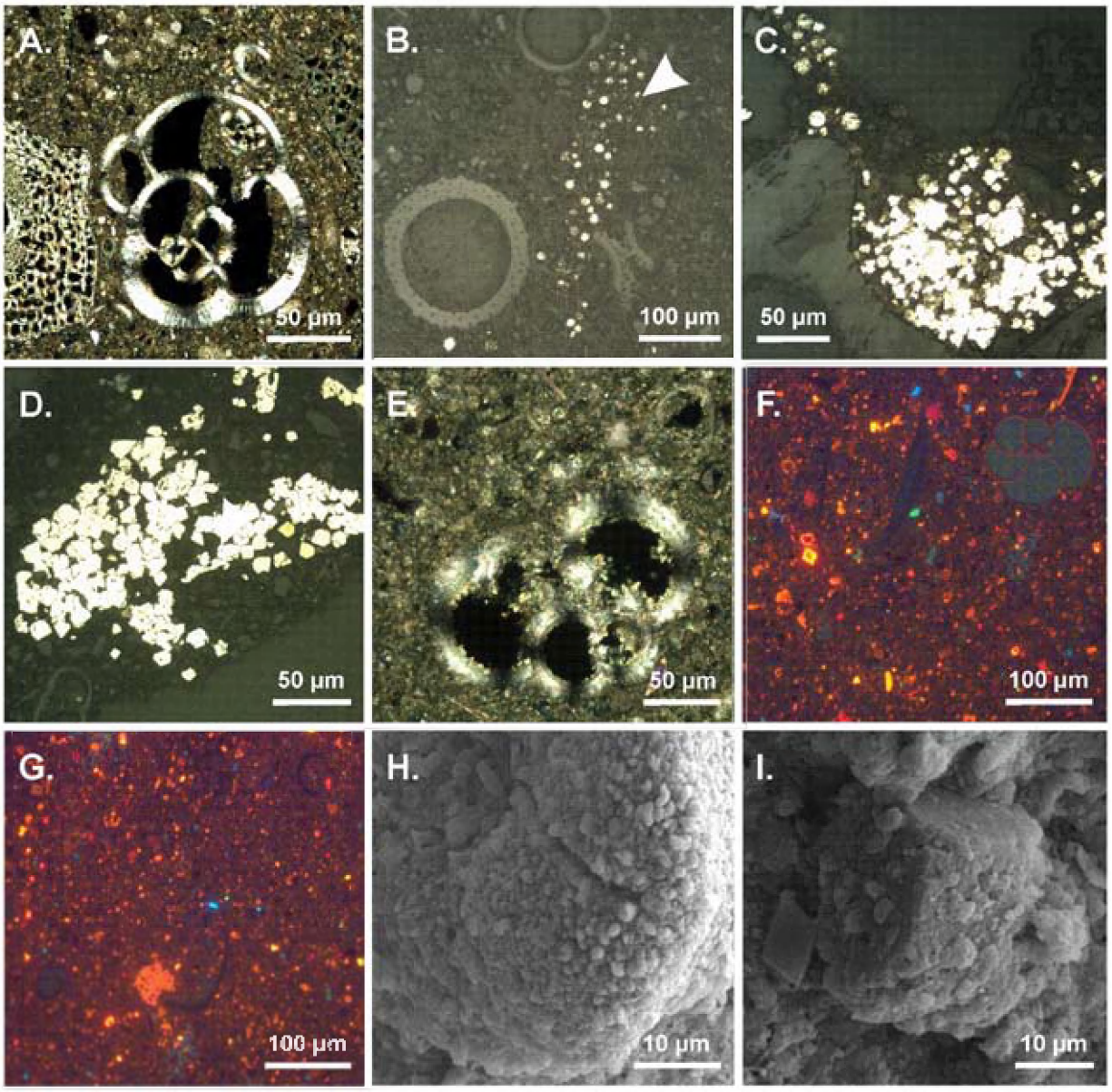

Fig. 7.7 *Petrographic observations of Gamma mound. A. Biogenic fragments embedded in a matrix of micritic carbonate mud (plane-polarized light) (443-445 cm). B. Cluster of pyrite framboids which are mostly mat (reflected light) (335-337 cm). C. and D. Pyrite framboids with euhedral overgrowths (reflected light) (516-518 and 592-594 cm). E. Intraparticular calcite precipitation in the shell of a foraminifera (plane-polarized light) (592-594 cm). F. and G. Cold Cathode Luminescence (CL) revealing bright-yellow to orange luminescent dolomite rhombs (516-518 cm). H. Calcite overgrowths on a biogenic fragment (SEM) (585-586 cm). I. Dolomite rhombs incorporating biogenic fragments (SEM) (520-521 cm).*

was observed (Fig. 7.6 I).

7.3.2.3 Gamma Mound

The sediment matrix of Gamma Mound reveals biogenic fragments such as: foraminifera, corals, shells, etc. embedded in micritic carbonate mud (Fig. 7.7 A). Between 0 and 470 cm, little or no carbonate precipitation or dissolution was observed. In some thin sections small amounts of framboidal pyrite were noticed (Fig. 7.7 B). In most cases the pyrite framboids are mat and do not reflect light (Fig. 7.7 B). Below, 470 cm, large amounts of pyrite were observed in the thin sections. The pyrite occurs as euhedral pyrite or as euhdral overgrowths on framboid clusters (Fig. 7.7 C, D). Calcite precipitation was noticed below 470 cm on biogenic fragments (Fig. 7.7 E, H). Cold CL reveals the presence of bright orange to red luminescent dolomite crystals in the sediment matrix (Fig. 7.7 F, G). On SEM images some dolomite rhombs were observed which

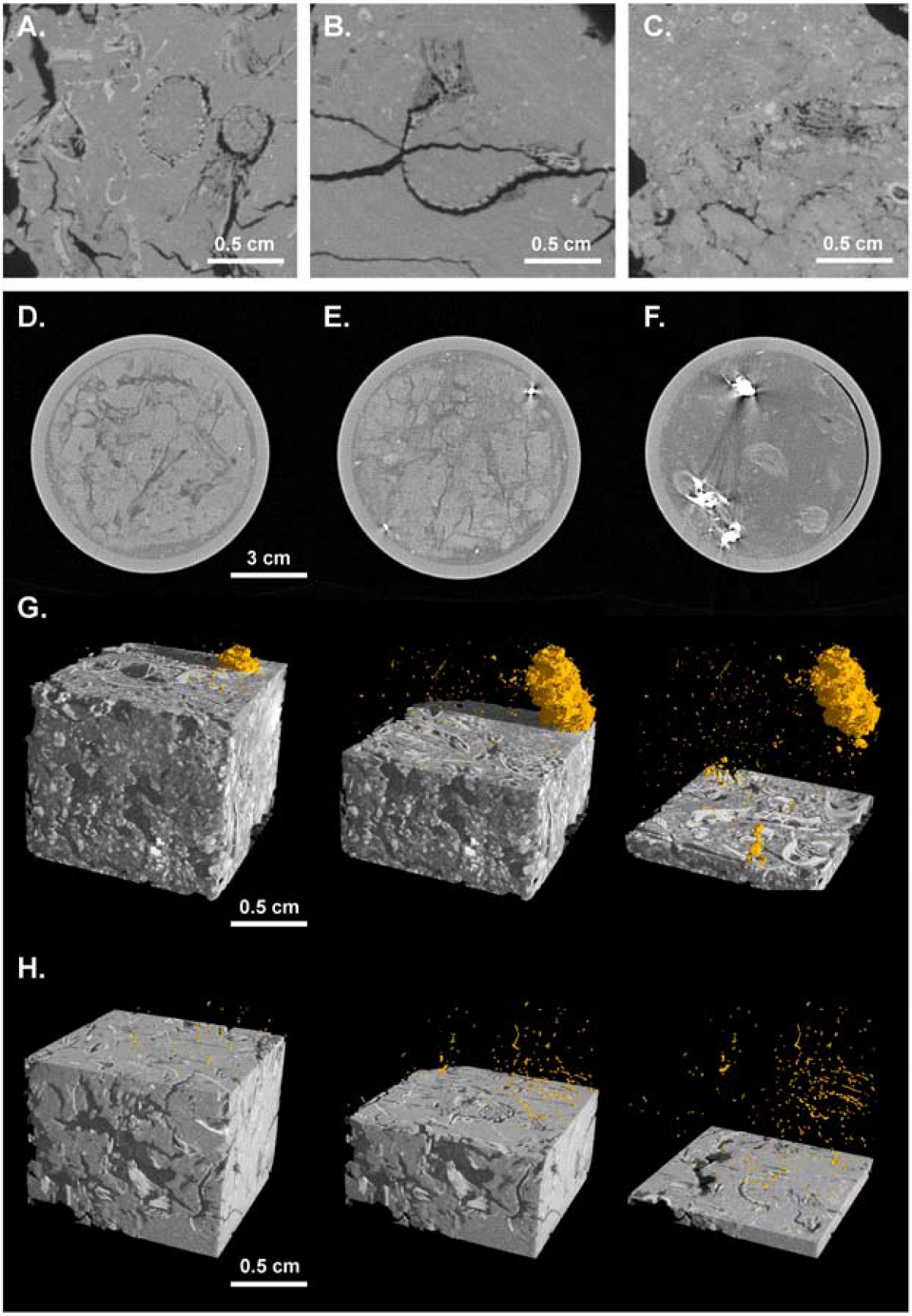
A.
0.5 cm
B.
0.5 cm
C.
0.5 cm
D.
E.
F.
3 cm
G.
0.5 cm
H.
0.5 cm

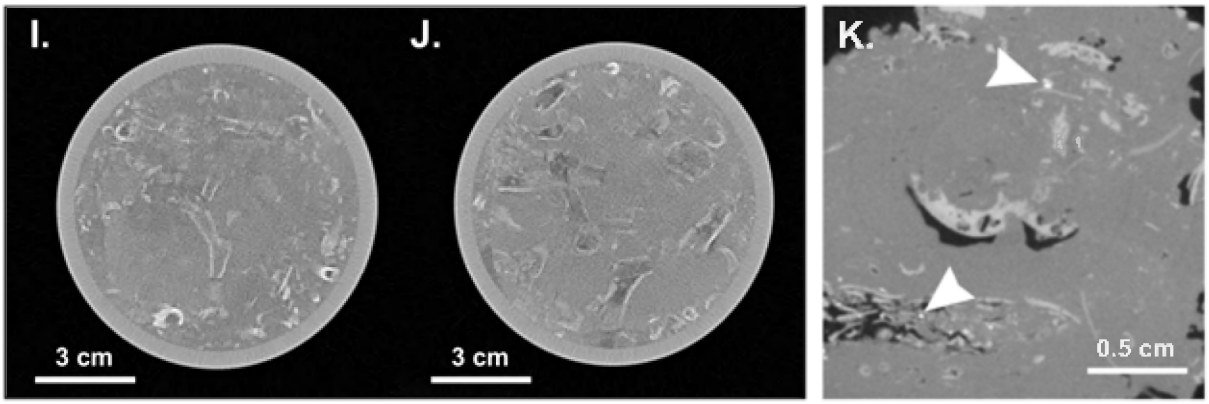

Fig. 7.8 *CT scans. A. and B. Micro-CT scans showing the dissolution of corals and the subsequent creation of moldic porosity in Alpha and Beta Mound (black) (MD08-3216G 219-221 cm and MD08-3215 262-264 cm). C. A micro-CT scan of a brecciated (semi)-lithified layer in Beta Mound containing strongly dissolved corals (MD08-3215G 285-287 cm). D. and E. Medical CT scan of moldic porosity and brecciation inside a (semi)-lithified layer in Beta Mound. F. Medical CT scan of pyrite nodules (white) in Beta Mound which precipitate close to coral fragments. Due to the high density of the pyrite, starburst artifacts are present (Ketcham and Carlson 2001). G. A micro-CT scan of a pyrite nodule (yellow) in the sediment matrix (grey) of Beta Mound. H. A micro-CT scan of pyritized burrows and scattered pyrite (yellow) in the sediment matrix (grey) of Alpha Mound. I. and J. Medical CT scan of dissolved corals in Gamma Mound below 470 cm. K. Micro-CT scan of dissolved corals with small clusters of pyrite (white, indicated with arrows) in Gamma Mound (578-580 cm).*

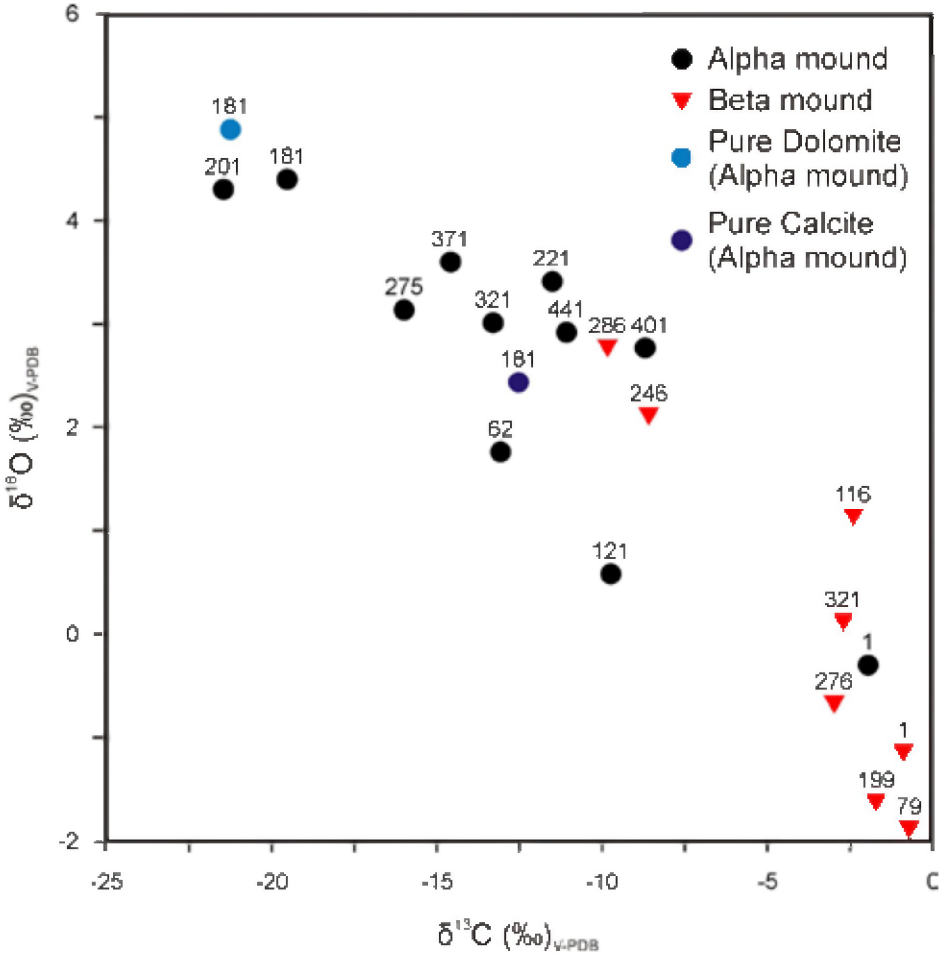

Fig. 7.9 *A plot of the $\delta^{13}C$ versus $\delta^{18}O$ values of the bulk carbonate of Alpha Mound (black dots) and Beta Mound (red triangles). The $\delta^{13}C$ and $\delta^{18}O$ values of the pure dolomite and calcite sampled both at a depth of 181 cm in Alpha Mound are also shown.*

incorporate coccoliths (Fig. 7.7 I).

7.3.3 CT scans

In Alpha (219-220 cm, 435-437 cm) and Beta Mound (254-256 cm, 262-264 cm, 285-287 cm) various samples with strongly dissolved corals were observed (Fig. 7.8 A, B, C). In some cases the corals are completely dissolved and leave moldic pores in the sediment (Fig. 7.8 D, E). The zones with strongly altered corals coincide with (semi)-lithified intervals. These brittle, (semi)-lithified horizons are more sensitive for fracturing and brecciation (Fig. 7.8 C, D, E). In most of the samples these secondary fractures are considered an artifact of the sampling process. However, in the samples taken at 435-437 cm (Alpha Mound) and 285-287 cm (Beta Mound), brecciation is believed to be a genuine feature since these samples reveal a specific fracture network which is completely different from the other samples. The brecciation can also be noticed in the medical CT scans in Alpha Mound (419-445 cm) and Beta Mound (234-268 cm, 281-300 cm) (Fig. 7.8 D, E). The fractures have a width up to several millimeters and are in some cases filled with unconsolidated sediment.
In two samples of Beta Mound (309-311 cm and 280-282 cm) a large pyrite nodule with a diameter up to 0.7 cm was observed (Fig. 7.8 G). These nodules contain biogenic fragments. In the remaining samples of Alpha and Beta Mound only scattered pyrite in the matrix or pyritized burrows were observed (Fig. 7.8 H). In the medical CT scans numerous large pyrite nodules were identified and quantified in Beta Mound (Fig. 7.8 F) while no nodules were noticed in Alpha Mound. These pyrite nodules occur mostly next to coral fragments.
In Gamma Mound, corals are well preserved between 0 and 470 cm although in some cases bio-erosion occurs. Below 470 cm, the corals reveal signs of dissolution (Fig. 7.8 I, J, K). On the micro-CT scans small pyrite clusters (around 1 mm) are recognized in association with dissolved corals (Fig. 7.8 K).

7.3.4 Stable isotope analyses

The $\delta^{13}C$ and $\delta^{18}O$ values of the bulk carbonate of Alpha and Beta Mound are displayed in Fig. 7.9. In both mounds, the decrease in the $\delta^{13}C$ values of the carbonate corresponds to an increase in the $\delta^{18}O$ values. In Alpha Mound, $\delta^{13}C$ values vary between -1.9‰ and -21.5‰ whereas $\delta^{18}O$ values range between -0.3‰ and +4.4‰. Except for the surface sample, all samples in Alpha Mound are depleted in ^{13}C and enriched in ^{18}O with respect to V-PDB. The lowest $\delta^{13}C$ values are recorded in the semi-lithified and dolomite-rich layers (181-201 cm). The $\delta^{13}C$ and $\delta^{18}O$ values of the pure dolomite which was extracted from the

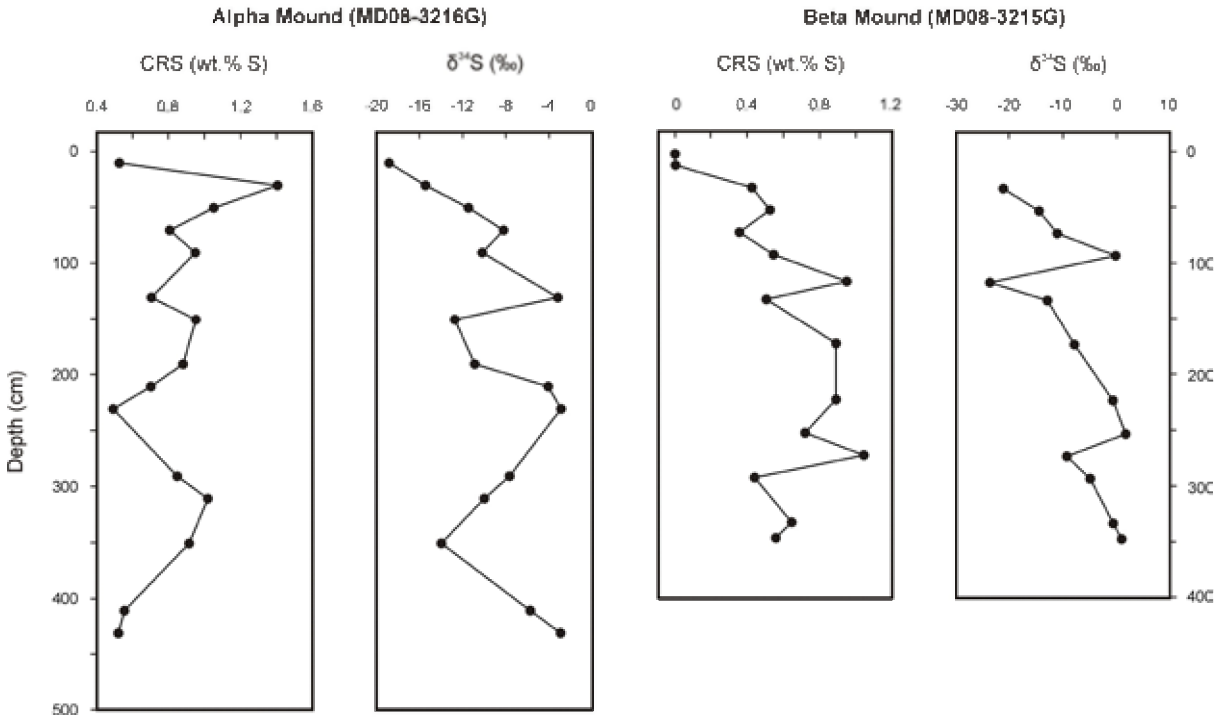

Fig. 7.10 *Weight percentage of the Chromium Reducible Sulfur (CRS) (i.e. mostly pyrite) and the $\delta^{34}S$ values of the pyrite in Alpha and Beta Mound.*

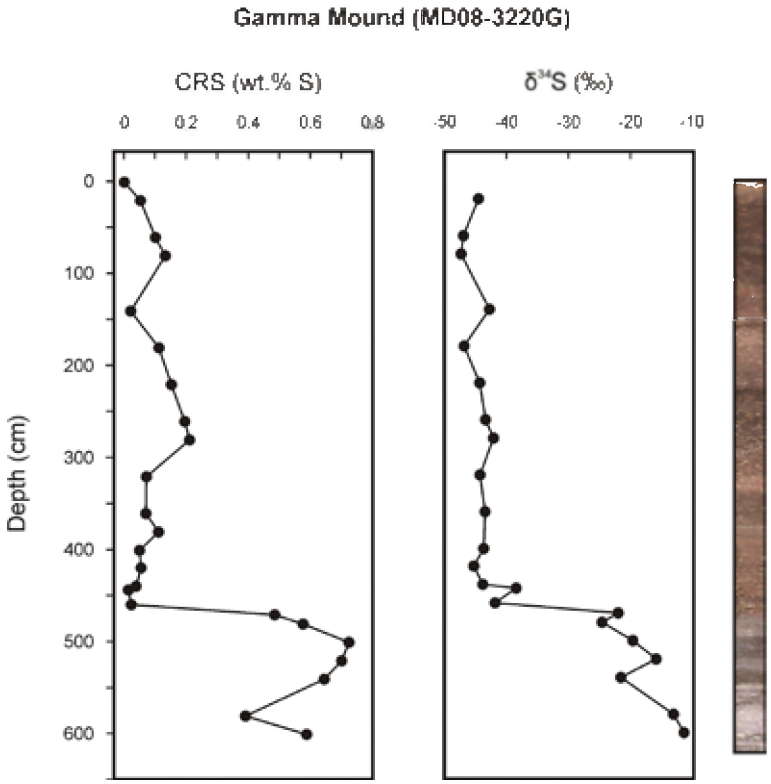

Fig. 7.11 *Weight percentage of the Chromium Reducible Sulfur (CRS) (i.e. mostly pyrite) and the $\delta^{34}S$ values of the pyrite in Gamma Mound. Furthermore, an image stack of the split core surface is shown.*

bulk carbonate in Alpha Mound (181-182 cm) are respectively: -22.3‰ and +4.8‰ (Fig. 7.9). The calcite associated with this dolomite has a $\delta^{13}C$ value of -12.5‰ and a $\delta^{18}O$ value of +2.4‰ (Fig. 7.9). The bulk carbonates of Beta Mound have $\delta^{13}C$ values between -0.7‰ and -9.8‰ and $\delta^{18}O$ values between -1.9‰ and +2.8‰. A significant drop in the $\delta^{13}C$ values and increase in the $\delta^{18}O$ values is observed in the semi-lithified layers of Beta Mound at approximately 246 and 286 cm (Fig. 7.9).

Sulfur isotopes of solid phase pyrite ($\delta^{34}S$-CRS) in Alpha and Beta Mound are shown in (Fig. 7.10). The sulfur isotope composition of the pyrite phase of Alpha Mound varies between -18‰ and -2.9‰ (Fig. 7.10). Three intervals with significantly higher $\delta^{34}S$ values can be identified in the samples taken at a depth of 131 cm, 231 cm and 431 cm. In Beta Mound the $\delta^{34}S$ values for pyrite range between -23.5‰ and +1.7‰ (Fig. 7.10). Three intervals with distinctly heavier isotope composition were indentified (91 cm, 251 cm and 345 cm). Gamma Mound reveals an important shift in the $\delta^{34}S$ values of solid phase pyrite ($\delta^{34}S$-CRS) (Fig. 7.11). Between 0 and 470 cm, very low $\delta^{34}S$ values are recorded between -38‰ and -47‰ whereas below 470 cm, the $\delta^{34}S$ values increase sharply up to a value of -11‰ around 601 cm (Fig. 7.11).

A sample with high dolomite content from Alpha Mound (201 cm) was treated with a two step acid dissolution. Sulfate associated with carbonate that resisted dissolution with acetic acid, presumably mainly dolomite, was liberated by dissolution with concentrated hydrochloric acid. The $\delta^{34}S$ and $\delta^{18}O_{SMOW}$ value of the carbonate associated sulfate (CAS) from the dolomite phase is +21.7‰ and +12.7‰, respectively.

7.4 Discussion

First, the assemblage of authigenic minerals in Alpha and Beta Mound will be discussed and compared. A model is proposed to explain the different diagenetic history in both mounds. In a second step, the preliminary results of Gamma Mound will be discussed.

7.4.1 The authigenic minerals in Alpha and Beta Mound

7.4.1.1 Pyrite

The sedimentary pyrite concentration and the sulfur isotopic composition of the pyrite in Alpha and Beta Mound (Fig. 7.10) are likely the result of a combination of the following processes: (1)

hydrogen sulfide production by organoclastic sulfate reduction during organic matter degradation, (2) hydrogen sulfide production during methanotrophic sulfate reduction (coupled to the anaerobic oxidation of methane (AOM)) in the SMTZ which is diffusing upwards and (3) the subsequent reaction of the produced sulfide with reactive iron phases and dissolved iron in the sediment (Berner, 1970; Wehrmann *et al.*, 2010).

Due to their proximity and similar sedimentary setting, it can be assumed that Alpha and Beta mound received a similar amount of reactive iron and organic material. In both mounds, sulfide production by organoclastic and methanotrophic sulfate reduction, albeit a different depth of SMTZ, has led to the almost complete pyritization of reactive mineral phases (Wehrmann *et al.*, 2010). Nevertheless, a distinct shift in the micro-textures of this sedimentary pyrite is observed between Alpha and Beta Mound. Alpha Mound is predominantly characterized by clusters of framboidal pyrite with some minor euhedral overgrowths (Fig. 7.5 G, H) whereas Beta Mound contains big nodules of euhedral pyrite (Fig. 7.6 C, D, E and 7.8 F, G). Framboidal textures are generally assumed to be the result of rapid pyrite formation from aqueous solutions, highly supersaturated with both iron monosulfides and pyrite, in which kinetics favour the formation of iron monosulfides before pyrite (Passier *et al.*, 1999; Passier *et al.*, 1997; Raiswell, 1982; Sweeney and Kaplan, 1973). Euhedral pyrite grows more slowly at saturation levels that are below those of iron monosulfides after *in situ* sources of iron are exhausted and transportation of reactive iron from adjacent sediments is required (Passier *et al.*, 1999; Passier *et al.*, 1997; Raiswell, 1982; Sweeney and Kaplan, 1973). Thus, the shift in the micro-textures of the pyrite indicates that different saturation levels were present in Alpha and Beta Mound. Given that originally a comparable pool of reactive iron was present in both mounds, this difference in saturation level may be attributed to higher hydrogen sulfide concentrations in Alpha Mound compared to Beta Mound (Merinero *et al.*, 2008; Ohfuji and Rickard, 2005; Passier *et al.*, 1999).

Organoclastic sulfate reduction produces an increase in the $\delta^{34}S$-values with depth as the residual porewater sulfate will become progressively enriched in ^{34}S (Goldhaber and Kaplan, 1980). This trend is also reflected in the sulfur isotope composition of sulfide produced by sulfate reduction, explaining general trends to heavier pyrite values with depth. However, both Alpha and Beta Mound contain 3 zones, characterized by peaks in the $\delta^{34}S$-values (Fig. 7.10). These relatively heavy $\delta^{34}S$-values can be attributed to hydrogen sulfide production during sulfate reduction coupled to AOM which diffuses upwards and overprints the isotopic signature of pyrite formed during organoclastic sulfate reduction (Jørgensen *et al.*, 2004; Neretin *et al.*, 2004). Hence, the zones with higher $\delta^{34}S$-values indicate shifts of the SMTZ to more shallow depths compared to the current situation as was also concluded by Wehrmann *et al.* (2010).

There is an apparent discrepancy between the differences in the pyrite morphologies of Alpha and Beta Mound (attributed to dissimilar sulfide fluxes), and the similarities in the sulfur isotope patterns (attributed to changes in the SMTZ position). It is hypothesized that methane fluxes in Alpha Mound are generally higher, resulting in a shallower SMTZ compared to Beta Mound. However, the position of SMTZ in both Alpha and Beta Mound was subjected to relocations as indicated by the positive shifts in the $\delta^{34}S$ of pyrite. The latter scenario could explain the apparent mismatch between the pyrite morphologies and the sulfur isotope trends of the two mounds.

7.4.1.2 Barite

The barite in Beta Mound has a diagenetic origin as it encrusts biogenic fragments and pyrite crystals (Fig. 7.6 F, H, I). Authigenic barite deposits have been documented along numerous continental margins in association with submarine venting of cold fluids enriched in hydrocarbons and barium (Castellini *et al.*, 2006; Dickens, 2001; Greinert *et al.*, 2002; Riedinger *et al.*, 2006; Snyder *et al.*, 2007; Torres *et al.*, 2003; Torres *et al.*, 1996). The barite crystals precipitate above the SMTZ where upward migrating barium-rich, sulfate-depleted fluids react with sulfate-rich porewater (Torres *et al.*, 1996) and thus couples the carbon, sulfur and barium cycles (Aloisi *et al.*, 2004; Dickens, 2001). A similar process can be evoked for the formation of barite in Beta Mound at ~345 cm. This is in line with a linear decrease of porewater sulfate concentration observed in a core that was taken nearby (Wehrmann *et al.*, 2010) which indicates the current position of the SMTZ between 350 and 450 cm. The source of barium in the barite deposits remains uncertain. Barium could be derived from the dissolution of biogenic barite which is produced in the water column in association with decaying organic matter (Paytan and Griffith, 2007). When porewater gets depleted in sulfate, buried pelagic barite is dissolved, leading to the accumulation of barium in the porewater. However, barium can also be derived from the dissolution of underlying salt deposits and is subsequently transported to the

surface by an upward fluid migration (Castellini *et al.*, 2006). The increase of the natrium and chloride concentration in a 1:1 ratio with depth in the porewater of Beta Mound indicates that upward migrating fluids that were affected by evaporite dissolution (Wehrmann *et al.*, 2010) may be the primary source for barium whereas the dissolution of pelagic barite might act as a secondary contributor. This hypothesis is corroborated by a strong increase with depth of the barium concentration in the porewater at the nearby Gemini mud volcano (Hensen *et al.*, 2007). The precipitation of significant amounts of barite (9.1%) at a single layer in Beta Mound indicates that the SMTZ remained stable at a certain depth for a long period which might be related to a period of reduced or even no sedimentation (Torres *et al.*, 1996).

7.4.1.3 Gypsum

In Alpha Mound authigenic gypsum crystals were found, encrusting corals and dolomite rhombs (Fig. 7.5 I, J, K). The diagenetic formation of gypsum in a cold-water coral mound was already described by Pirlet *et al.* (2010) who concluded that the presence of authigenic gypsum might serve as an indicator for a diagenetic oxidation event. The inflow of seawater is capable of oxidizing iron sulfides, which leads to an acidification of the porewater and causes carbonate dissolution (Ku *et al.*, 1999). Hence, sulfide oxidation induces both sulfate production and an increase in the concentration of calcium in the porewaters due to the dissolution of aragonite. This leads to an oversaturation of the porewater with respect to gypsum (Pirlet *et al.*, 2010). The hypothesis that sporadic seawater inflow occurs in Alpha Mound is supported by the study of Wehrmann *et al.* (2010), who found evidence that such an event recently occurred.

7.4.1.4 Calcite

Authigenic calcite was observed in various (semi)-lithified intervals in Alpha and Beta Mound as intraparticular crystals in biogenic fragments or as overgrowths on coccoliths (Fig. 7.5 E and 7.6 A, B). The semi-lithified layer, observed in Beta Mound between 101 and 120 cm reveals $\delta^{13}C$ and $\delta^{18}O$ values which are close to the values in the 'unaltered' surface samples. Thus, the precipitation of authigenic calcite in this layer may be attributed to early-diagenetic processes which are seawater-related or driven by organic matter degradation close to the sediment-water interface with little or no influence of AOM. Similar early-diagenetic processes steered by bacterial sulfate reduction were also evoked to explain the formation of lithified carbonate layers in the mounds off Ireland (Pirlet *et al.*, 2010; Van der Land *et al.*, 2010; see also chapter 6). On the contrary, the negative $\delta^{13}C$ values (around -10‰) of the bulk carbonate in the other layers with calcite precipitation (Fig. 7.9) indicate that carbonate produced by AOM was incorporated in the calcite cement (Mozley and Burns, 1993). Anaerobic oxidation of methane promotes the precipitation of authigenic carbonate as it increases the alkalinity of the porewater (Aloisi *et al.*, 2002; Aloisi *et al.*, 2000; Ritger *et al.*, 1987). The precipitation of ^{13}C depleted calcite in various layers indicates excursions in the depth of the SMTZ which are also evidenced by the heavy $\delta^{34}S$ values of the sedimentary pyrite (Fig. 7.10) (Wehrmann *et al.*, 2010).

The oxygen isotope composition of authigenic carbonates is controlled by a combination of factors including carbonate mineralogy and chemistry, temperature of precipitation and the oxygen isotopic composition of the interstitial water. In modern conditions, calcite, which precipitates in equilibrium with bottom seawater ($\delta^{18}O$ = 0.94‰ (V-SMOW), T = 11°C (Craig and Gordon, 1965)) will have a $\delta^{18}O$ value of +2.0‰ (V-PDB) if the paleo-thermometer of O'Neil *et al.* (1969) ($10^3 \ln\alpha = 2.78 \times (10^6 T^{-2}) - 2.89$, α = carbonate-water fractionation factor and T = bottom water temperature) is used. A $\delta^{18}O$ value of +2.8‰ (V-PDB) is obtained according to the paleo-thermometer of Friedman and O'Neil (1977) and Tarutani *et al.* (1969) for high-Mg calcite ($10^3 \ln\alpha = 2.78 \times (10^6 T^{-2}) - 2.89 + 0.72$). Calcite precipitation during glacial periods, characterized by cooler bottom waters, could easily produce $\delta^{18}O$ values exceeding +3‰. Given that $\delta^{18}O$ values in the layers with calcite precipitation are between +2‰ and +2.9‰ (Fig. 7.9), it might be concluded that the calcite precipitated in equilibrium with bottom seawater.

7.4.1.5 Dolomite

There is a significant difference in the dolomite content of Alpha and Beta Mound. Beta Mound is characterized by small amounts of dolomite (3-5%) which correlate closely with the quartz and clay mineral content, suggesting a primarily detrital origin of these dolomites (Fig. 7.4). Moreover, little or no dolomite crystals were observed which encrust biogenic fragments. In contrast, Alpha Mound reveals large amounts of dolomite which constitute up to 45% of the sediment (Fig. 7.3). These dolomite crystals have a diagenetic origin as numerous rhombs were observed which incorporate coccoliths and

other biogenic fragments (Fig. 7.5 A, B). Although dolomite occurs abundantly in the geological record, its formation in modern sediments remains uncertain (McKenzie, 1991). Several studies have linked dolomite formation with the microbial activity of sulfate reducers (Van Lith *et al.*, 2003; Vasconcelos and McKenzie, 1997; Vasconcelos *et al.*, 1995; Wright, 1999). Meister *et al.* (2007) and Moore *et al.* (2004) stated that dolomite formation will preferentially form in microbial hotspots such as the SMTZ where AOM results in the strong production of alkalinity. This is in accordance with the strong depletion of dolomite in ^{13}C (-22.3‰) in Alpha Mound (Fig. 7.9). The isotope composition of the calcite ($\delta^{13}C$ = -12.5‰ and $\delta^{18}O$ = +2.4‰) associated with the dolomite shows that this calcite has a (partial) diagenetic origin as well (Fig. 7.9). Overall, the low concentration of calcite in the dolomite layer indicate that, most likely, a significant part of the original carbonate was replaced by dolomite during the dolomitization process (Moore *et al.*, 2004). The parameters which control this dolomitization process remain uncertain. Possibly, authigenic calcite precipitated first and lowered the Ca-concentration in the porewater, thereby increasing the Mg/Ca ratio which favored subsequent dolomitization. This requires a SMTZ which remains stable at a certain depth to sufficiently increase the Mg/Ca ratio.

The oxygen isotope composition of the dolomite in Alpha Mound indicates that dolomite precipitated from interstitial waters with a composition close to seawater with little or no brine influence. The $\delta^{18}O$ value of dolomite which precipitates in isotopic equilibrium with bottom seawater can be calculated with the paleo-thermometer for microbial dolomite at low temperatures (Vasconcelos *et al.*, 2005) ($10^3 \ln\alpha = 2.73 \times (10^6 T^{-2}) + 0.26$). Assuming a $\delta^{18}O_{SMOW}$ value for the bottom seawater of 0.94‰ and a temperature of 11°C (Craig and Gordon, 1965), dolomite with a $\delta^{18}O$ value of +4.6‰ (V-PDB) is formed. This value is coherent with the $\delta^{18}O$ value which is recorded in the dolomite (+4.8‰) in Alpha Mound (Fig. 7.9). Moreover, the $\delta^{18}O$ value would be even higher if the dolomite was precipitated during glacial periods, when bottom waters were cooler. The finding that dolomite in Alpha Mound precipitated from interstitial waters with a composition close to seawater is in contrast with the observations of Wehrmann *et al.* (2010) who postulated the influence of a brine enriched in ^{18}O. The cause of the difference between these findings is rooted in the interpretation of the carbonate mineralogy (high-Mg calcite vs. high-Ca dolomite) as the equilibrium isotope fractionation between dolomite and water is considerably larger than the corresponding isotope fractionation for high-Mg calcite. The study of Wehrmann *et al.* (2010) highlights the presence of high-Mg calcite in the coral mounds on Pen Duick Escarpment, whereas dolomite was reported to occur only in low quantities. This is in contrast to the present study, where only little high-Mg calcite and considerable quantities of high-Ca dolomite were detected by XRD. It is assumed that the carbonate identified as "high-Mg calcite" in Wehrmann *et al.* (2010) corresponds to the carbonate that is identified in the present study as "high-Ca dolomite". Strictly speaking, neither of the fractionation factors used in Wehrmann *et al.* (2010) and this study truly correspond to the isotope equilibrium between water and the observed carbonate mineral. Hence, the results of both studies have to be interpreted as end-member calculations.

Cold CL of the dolomite crystals reveals alternating dark and bright luminescent zones. This zonation indicates a change in the porewater chemistry which might be linked with alternating (sub)-oxic and reducing conditions controlling the concentration and oxidation state of Fe and Mn in the porewater (Richter *et al.*, 2003). Hence, the dolomite probably formed in different phases recording different redox conditions related to shifts in the location of the SMTZ. The alternation of (sub)-oxic and reducing conditions is probably also recorded in the isotopic values of the CAS extracted from a dolomite-rich sample, which may reflect the isotopic composition of porewater sulfate during dolomite formation. The $\delta^{18}O_{CAS}$ (+12.7‰) and $\delta^{34}S_{CAS}$ values (+21.7‰) of the dolomite reveal no significant enrichment compared to the isotopic value of sea-water sulfate ($\delta^{18}O_{seawater}$ = +8.6‰ and $\delta^{34}S_{seawater}$ = +20.3‰, (Longinelli, 1989)) as would be expected if dolomite formed close to the SMTZ. However, it must be considered that dolomite forming close to the SMTZ cannot incorporate large amounts of sulfate because sulfate concentrations are low. Probably, sulfate with an isotopic value close to seawater was incorporated during dolomite formation in a (sub)-oxic phase.

7.4.2 The role of the lithified layers

The occurrence of various lithified layers in the upper layers of both Beta and Alpha Mound as a result of the precipitation of authigenic minerals indicates that early diagenesis is an important and very active process in the stabilization of these mound structures. The lithified layers will stabilize the steep flanks of the mounds and form a protection against erosional processes. Indeed,

exhumed rockslabs and firmgrounds have been observed on the coral mounds in Cadiz (Foubert *et al.*, 2008) but also on the mounds off Ireland (de Haas *et al.*, 2009; Noé *et al.*, 2006; Van der Land *et al.*, 2010; Wienberg *et al.*, 2008).
The semi-lithified layers are characterized by poorly preserved aragonitic corals and other biogenic fragments (Fig. 7.8 C, D, E). The moldic shape of the pores indicates that aragonite dissolution occurred after or during carbonate precipitation, otherwise the molds of the biogenic fragments would not have been preserved. Probably, aragonite dissolution is the result of diffusing hydrogen sulfide, derived from sulfate reduction, which acts as a weak acid (Soetaert *et al.*, 2007). Dissolution and precipitation of carbonates also impacts the permeability of the coral mound and may strongly affect fluid pathways. The precipitation of calcite and dolomite results in a decrease of the permeability (Davis *et al.*, 2006) and therefore, the (semi)-lithified layers might act as a barrier for upward migrating fluids (Hovland, 2002; Naudts *et al.*, 2008). However, given that lithified layers are more prone to brittle deformation, processes such as sediment loading and hydrostatic pressure build-up (Conti *et al.*, 2004; Conti *et al.*, 2008) may result in the brecciation which was observed in some of the layers of Alpha and Beta Mound (Fig. 7.8 C, E). Due to this brecciation, the lithified layers will no longer act as a barrier and may even serve as pathways for fluid flow. Hence, diagenetic processes such as dissolution of aragonite, lithification by precipitation of authigenic minerals and subsequent brecciation of these lithified layers may affect advective and diffusive fluid flow within the mounds.

7.4.3 Early diagenesis in Alpha versus Beta Mound

Alpha and Beta Mound are located on the same escarpment, in a similar water depth with a distance of 540 m between both mounds (Fig. 7.2). Therefore, it can be assumed that they received a similar sediment input and are influenced by the same water masses. Moreover,

Diagenetic feature	Alpha mound	Beta mound
Framboidal pyrite	Large clusters throughout entire core	Minor quantities
Euhedral pyrite	Present in minor quantities as overgrowths on framboids	Large nodules up to +/- 1 cm throughout entire core
Barite	Not present	Barite nodules in core catcher
Gypsum	Present in minor quantities at 101, 121 361 and 366 cm	Not present
Calcite	Present as overgrowths on coccoliths and intraparticular crystals in intervals: 367-375 cm and 419-445 cm	Present as overgrowths on coccoliths and intraparticular crystals in intervals: 101-120 cm, 234-268 cm, 281-300 cm and the core catcher
Dolomite	Present in large quantities in interval 162-255 cm and moderate to minor quantities in other parts of the core	Present in minor quantities
Moldic porosity	162-255 cm, 367-375 cm and 419-445 cm	234-268 cm and 281-300 cm
Brecciation	419-445 cm	234-268 cm and 281-300 cm

Table 7.2 *An overview of the diagenetic features present in Alpha and Beta Mound.*

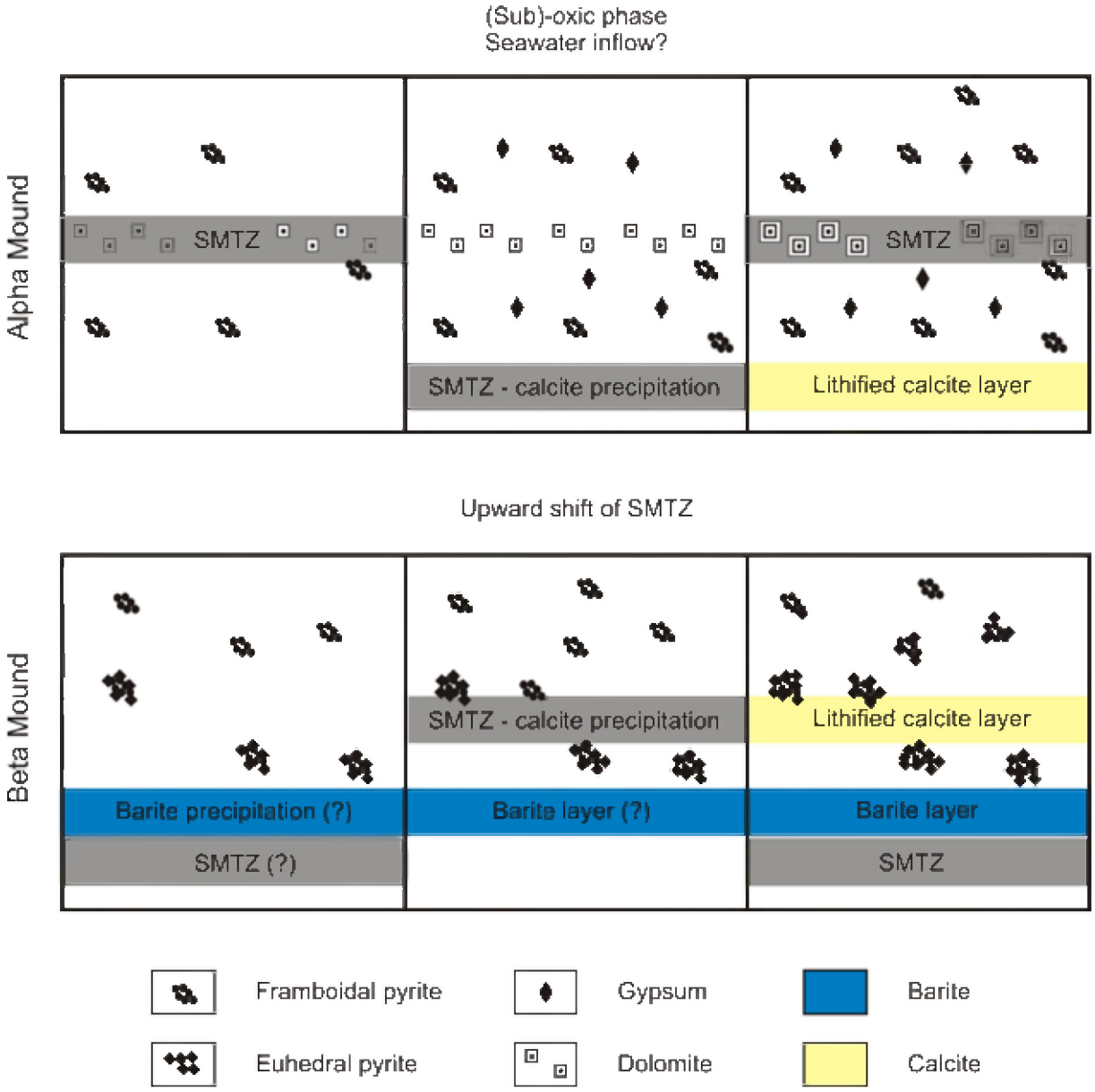

Fig. 7.12 *Proposed models for the precipitation of the various authigenic minerals in Alpha and Beta Mound tied to a shift in the position of the SMTZ.*

the major driver for diagenetic processes: sulfate reduction coupled to AOM in the SMTZ is the same for both mounds. Nevertheless, Alpha and Beta Mound are characterized by a different assemblage of authigenic minerals (Table 7.2) and hence, diagenetic history. Most likely this heterogeneity between both mounds can be attributed to differences in the intensity of sulfate reduction coupled to AOM, in the dynamics of the fluctuations of the position the SMTZ and in the diffusive and advective fluid flow patterns in the mound.

Alpha Mound appears to have experienced higher methane fluxes than Beta Mound. This is corroborated by the extensive precipitation of dolomite depleted in ^{13}C, which requires a stable SMTZ with a strong production of alkalinity by AOM (Fig. 7.12). The high methane fluxes in Alpha Mound are also supported by the dominance of framboidal pyrite over euhedral pyrite, which is likely associated with extensive production of sulfide coupled to AOM. Alpha Mound was probably also more affected by shifts in the position of redox boundaries than Beta Mound. The zonation of the dolomite under CL indicates that dolomite precipitated in various episodes, which were likely characterized by varying redox conditions related to shifts in the position of the SMTZ (Fig. 7.12). Such a dynamical behavior of the location of the SMTZ could be caused by

episodic lateral inflow of seawater. This scenario was already postulated by Wehrmann *et al.* (2010) to explain the almost-linear pore-water sulfate profile in a close-by core at present.
Seawater inflow could trigger the oxidation of sulfide minerals causing carbonate dissolution and the formation of authigenic gypsum crystals (Pirlet *et al.*, 2010) which were observed in Alpha Mound (Fig. 7.12). Other cores, obtained from Alpha Mound reported no such influx in the porewater (Foubert *et al.*, 2008; Maignien *et al.*, 2010), which may point to spatial and/or temporal differences in the seawater inflow. In this regard, the presence and spatial distribution of brecciated layers may be an important sedimentary feature as they may serve as a conduit for this sideward inflow. Depreiter (2009) proposed a pumping-model where currents cause pressure gradients around obstacles on the seabed which lead to the sideward inflow of seawater and a lowering of the SMTZ. In this context, Alpha Mound may be more prone to erosion events and seawater inflow due to its position, at the southeastern edge of Pen Duick Escarpment.
In contrast to Alpha Mound, Beta Mound appears to be exposed to lower methane fluxes and a more static position of the SMTZ. The latter scenario with a fixed position of the SMTZ for a longer period of time, is supported by the precipitation of significant amounts of barite (Fig. 7.12) (Torres *et al.*, 1996). In addition, the porewater data of Beta Mound also indicates that the current position of the SMTZ is below this layer, rich in barite (Wehrmann *et al.*, 2010). Apparently, the flux of dissolved sulfide from this SMTZ is not as intense as for Alpha Mound. Under these conditions, formation of euhedral pyrite dominates. Nevertheless, there is also evidence for relocations of the SMTZ in Beta Mound to shallower depths, which led to the formation of calcite depleted in ^{13}C between 250 and 300 cm (Fig. 7.12). Most likely, the SMTZ did not remain long enough at this position to sufficiently increase the Mg/Ca ratio of the porewater to induce dolomite precipitation. However, the depletion of magnesium in the porewater with depth (Wehrmann *et al.*, 2010) indicates that dolomite is being formed at the present position of the SMTZ, below the barite layer.

7.4.4 Early diagenesis in Gamma Mound

In constrast to Alpha and Beta Mound, Gamma Mound does not reveal the occurrence of large amounts of iron sulfides in the upper 470 cm of the core (Fig 7.11). In some thin sections small clusters of framboidal pyrite were observed which show signs of re-oxidation as in most cases, the framboids do not reflect the light. The brownish colour of the sediment hints that iron-(oxyhydr)oxides are present in the upper 470 cm of the core (Fig. 7.7 B). Hence, it might be concluded that bacterial sulfate reduction is proceeding at very low rates and is largely outcompeted by dissimilatory iron reduction (DIR). In this case bacteria will use ferric iron as electron acceptor for organic matter oxidation (Haese, 2000; Lovley, 1991; Lovley, 1997). Generally, the zone of DIR is restricted to the first tens of cm of the sediment. The fact that this zone extends in Gamma Mound until a depth of 470 cm is attributed to the large pool of reactive iron. Enhanced concentrations of iron-(oxyhydr)oxides are present in the sediment due to the input of Saharan dust which constitutes the dominant source of iron in the Atlantic (Baker *et al.*, 2006). Alpha and Beta Mound also recieve this iron-(oxyhydr)oxides-rich dust input, however, in these mounds the zone of DIR is restricted to the upper 40 cm due to the presence of a shallow SMTZ which actively removes iron-(oxyhydr)oxides as a consequence of the production of hydrogen sulfide. This leads to the precipitation of significant amounts of iron-sulfides in the latter mounds.
The $\delta^{34}S$ values of the pyrite in the upper 470 cm of Gamma Mound reveal a depletion in ^{34}S of around 70‰ compared to the isotopic value of seawater sulfate (Fig. 7.11). This depletion cannot be completely attributed to microbial sulfate reduction since cultural experiments yielded only depletions between 10‰ and 30‰ with maximum values up to 50‰ (Bickert, 2000; Kaplan and Rittenberg, 1964). Larger fractionation values may be due to re-oxidation of sulfide followed by disproportionation of thiosulfate and/or elemental sulfur (e.g. Böttcher, 2001; Canfield and Thamdrup, 1994; Jørgensen, 1990). This is in accordance with the petrographic observation which observed signs of re-oxidation in the framboids clusters (Fig. 7.7 B).
The sharp increase in iron sulfides below 470 cm indicates that bacterial sulfate reduction becomes the dominant the dominant terminal electron pathway during organic matter oxidation. Petrographic observations reveal large clusters of euhedral pyrite and euhedral overgrowths on framboids which indicate that porewater became gradually undersaturated with respect to iron monosulfides. Also, a sharp increase in the $\delta^{34}S$ values of the pyrite is observed below 470 cm. The relatively high $\delta^{34}S$ values recorded around 600 cm may point towards the upwards diffusion of hydrogen sulfide deriving from sulfate reduction associated with anaerobic oxidation of

methane (AOM) in a SMTZ below (Jørgensen *et al.*, 2004; Neretin *et al.*, 2004).
The reactions associated with sulfate reduction also affected the carbonate saturation state (Soetaert *et al.*, 2007). This resulted in the dissolution of aragonitic biogenic fragments as observed in the CT-scans (Fig. 7.8 I, J, K). Furthermore, precipitation of calcite on biogenic fragments and some dolomite rhombs were noticed in thin sections and SEM images (Fig. 7.7 E, F, G, H, I). Further mineralogical and isotopic analyses are necessary to better constrain the origin of these authigenic carbonate minerals in Gamma Mound.

7.5 Conclusions

The diagenetic processes in both Alpha and Beta Mound are steered by sulfate reduction coupled to AOM in a shallow SMTZ. Nevertheless, both mounds reveal a specific assemblage of authigenic minerals: calcite, framboidal pyrite, gypsum and dolomite in Alpha Mound and calcite, euhedral pyrite and barite in Beta Mound. These assemblages point to a different diagenetic history which may be attributed to variations in the intensity of sulfate reduction coupled to AOM, in the dynamics of the fluctuations in the depth of the SMTZ and in the diffusive and advective fluid flow patterns in the mound.
In this regard, the sedimentary diagentic features of the mounds also affect the advection and diffusion of dissolved compounds, thereby influencing the ongoing diagenetic processes. Generation of secondary porosity by the dissolution of aragonite, for example, may contribute to an enhanced flux of methane, promoting subsequent lithification by precipitation of authigenic minerals, which in turn, may reduce the overall permeability of the sediment. The formation of lithified layers contributes to the stabilization of the mounds, but also forms layers that are susceptible to brittle deformation, opening pathways for subsequent fluid migration and thus amplifying the dynamics of the entire diagenetic system. Hence, the cold-water coral mounds from the Pen Duick Escarpment are not just the result of coral growth, subsequent sediment infill and the shaping by currents, but also an expression of their internal diagenetic dynamics.
In contrast to Alpha and Beta Mound, Gamma Mound does not reveal indications for the occurrence of a SMTZ in the upper 5 m of the sediment. The brown colour of the sediment, the low amount of iron sulfides and the extremely low $\delta^{34}S$ values of the sedimentary pyrite indicate that bacterial sulfate reduction is largely outcompeted by dissimilatory iron reduction (DIR). This is attributed to the large pool of iron-(oxyhydr)oxides in the sediment as a result of the Saharan dust input. The dominance of DIR resulted in the good preservation of the corals. The sharp increase in iron sulfides below 470 cm indicates that bacterial sulfate reduction becomes the dominant terminal electron pathway during organic matter oxidation. The relatively high $\delta^{34}S$ values of the sedimentary pyrite reveal the upward diffusion of hydrogen sulfide from an SMTZ below. Below, 470 cm corals are badly preserved and calcite and dolomite precipitation occurs.

References

Aloisi, G., Bouloubassi, I., Heijs, S.K., Pancost, R.D., Pierre, C., Damste, J.S.S., Gottschal, J.C., Forney, L.J. and Rouchy, J.M., 2002. CH4-consuming microorganisms and the formation of carbonate crusts at cold seeps. Earth and Planetary Science Letters, 203(1), 195-203.

Aloisi, G., Pierre, C., Rouchy, J.M., Foucher, J.P., Woodside, J. and party, M.s., 2000. Methane-related authigenic carbonates of eastern Mediterranean Sea mud volcanoes and their possible relation to gas hydrate destabilisation. Earth and Planetary Science Letters, 184, 321-338.

Aloisi, G., Wallmann, K., Bollwerk, S.M., Derkachev, A., Bohrmann, G. and Suess, E., 2004. The effect of dissolved barium on biogeochemical processes at cold seeps. Geochimica et Cosmochimica Acta, 68(8), 1735-1748.

Baker, A.R., Jickells, T.D., Witt, M. and Linge, K.L., 2006. Trends in the solubility of iron, aluminium, manganese and phosphorus in aerosol collected over the Atlantic Ocean. Marine Chemistry, 98(1), 43-58.

Berastegui, X., Banks, C.J., Puig, C., Taberner, C., Waltham, D. and Fernandez, M., 1998. Lateral diapiric emplacement of Triassic evaporites at the southern margin of Guadalquivir Basin, Spain. In: A. Mascle (Editor), Cenozoic Foreland Basins of Western Europe. Geological Society Special Publication, pp. 49-68.

Berner, R.A., 1970. Sedimentary pyrite formation. American Journal of Science, 268(1), 1-23.

Bickert, T., 2000. Influence of Geochemical Processes on Stable Isotope Distribution in Marine Sediments. In: H.D. Schulz and M. Zabel (Editors), Marine Geochemistry. Springer-Verlag, Berlin Heidelberg, pp. 309-333.

Böttcher, M.E., 2001. Sulfur isotope fractionation in the biogeochemical sulfur cycle of marine sediments. Isotopes in Environmental and Health Studies, 37(2), 97-99.

Canfield, D.E. and Thamdrup, B., 1994. The production of 34S-depleted sulfide during bacterial disproportionation of elemental sulfur. Science, 266, 1973-1975.

Caralp, M.H., 1988. Late Glacial to Recent Deep-sea Benthic Foraminifera from the Northeastern Atlantic (Cadiz Gulf) and Western Mediterranean (Alboran Sea): Paleoceanographic Results. Marine Micropaleontology, 13, 265-289.

Castellini, D.G., Dickens, G.R., Snyder, G.T. and Ruppel, C.D., 2006. Barium cycling in shallow sediment above active mud volcanoes in the Gulf of Mexico. Chemical Geology, 226(1-2), 1-30.

Conti, S., Fontana, D., Gubertini, A., Sighinolfi, G., Tateo, F., Fioroni, C. and Fregni, P., 2004. A multidisciplinary study of middle Miocene seep-carbonates from the northern Apennine foredeep (Italy). Sedimentary Geology, 169(1-2), 1-19.

Conti, S., Fontana, D. and Lucente, C.C., 2008. Authigenic seep-carbonates cementing coarse-grained deposits in a fan-delta depositional system (middle Miocene, Marnoso-arenacea Formation, central Italy). Sedimentology, 55(2), 471-486.

Craig, H. and Gordon, L.I., 1965. Deuterium and oxygen-18 variations in the ocean and marine atmosphere. In: E. Tongiori (Editor), Stable isotopes in oceanic studies and paleotemperatures. Consiglio Nazionale Delle Ricerche, Laboratorio di Geologia Nucleare, Pisa, pp. 9-130.

Davis, J.M., Roy, N.D., Mozley, P.S. and Hall, J.S., 2006. The effect of carbonate cementation on permeability heterogeneity in fluvial aquifers: An outcrop analog study. Sedimentary Geology, 184(3-4), 267-280.

de Haas, H., Mienis, F., Frank, N., Richter, T.O., Steinacher, R., De Stigter, H., van der Land, C. and Van Weering, T.C.E., 2009. Morphology and sedimentology of (clustered) cold-water coral mounds at the south Rockall Trough margins, NE Atlantic Ocean. Facies, 55, 1-26.

De Mol, B., Van Rensbergen, P., Pillen, S., Van Herreweghe, K., Van Rooij, D., McDonnell, A., Huvenne, V., Ivanov, M., Swennen, R. and Henriet, J.-P., 2002. Large deep-water coral banks in the Porcupine Basin, southwest of Ireland. Marine Geology, 188, 193-231.

Depreiter, D., 2009. Sources, modes and effects of seabed fluid flow. PhD Thesis, Ghent University, Ghent, 207 pp.

Dickens, G.R., 2001. Sulfate profiles and barium fronts in sediment on the Blake Ridge: Present and past methane fluxes through a large gas hydrate reservoir. Geochimica et Cosmochimica Acta, 65(4), 529-543.

Ferdelman, T.G., Kano, A., Williams, T., Henriet, J.P. and Scientists, I.E., 2006. IODP Expedition 307 drills cold-water coral mound along the Irish continental margin. Scientific Drilling, 2, 11-16.

Foubert, A., Depreiter, D., Beck, T., Maignien, L., Pannemans, B., Frank, N., Blamart, D. and Henriet, J.-P.,

2008. Carbonate mounds in a mud volcano province off north-west Morocco: Key to processes and controls. Marine Geology, 248(1-2), 74-96.
Foubert, A. and Henriet, J.P., 2009. Nature and significance of the recent carbonate mound record: the Mound Challenger Code. Springer-Verlag, Heidelberg, 350 pp.
Friedman, I. and O'Neil, J.R., 1977. Compilation of stable isotope fractionation factors of geochemical interest. In: M. Fleischer (Editor), Data of Geochemistry. US Geological Survery Professional Paper pp. 1-12.
Goldhaber, M.B. and Kaplan, I.R., 1980. Mechanisms of Sulfur Incorporation and Isotope Fractionation during Early Diagenesis in Sediments of the Gulf of California. Marine Chemistry, 9(2), 95-143.
Greinert, J., Bollwerk, S.M., Derkachev, A., Bohrmann, G. and Suess, E., 2002. Massive barite deposits and carbonate mineralization in the Derugin Basin, Sea of Okhotsk: precipitation processes at cold seep sites. Earth and Planetary Science Letters, 203(1), 165-180.
Gutscher, M.A., Malod, J., Rehault, J.P., Contrucci, I., Klingelhoefer, F., Mendes-Victor, L. and Spakman, W., 2002. Evidence for active subduction beneath Gibraltar. Geology, 30(12), 1071-1074.
Haese, R.R., 2000. The Reactivity of Iron. In: H.D. Schulz and M. Zabel (Editors), Marine Geochemistry. Springer-Verlag, Berlin Heidelberg, pp. 233-261.
Henriet, J.-P., De Mol, B., Pillen, S., Vanneste, M., Van Rooij, D., Versteeg, W., Croker, P.F., Shannon, P.M., Unnithan, V., Bouriak, S., Chachkine, P. and The Porcupine-Belgica 97 Shipboard Party, 1998. Gas hydrate crystals may help build reefs. Nature, 391, 648-649.
Hensen, C., Nuzzo, M., Hornibrook, E., Pinheiro, L.M., Bock, B., Magalhaes, V.H. and Bruckmann, W., 2007. Sources of mud volcano fluids in the Gulf of Cadiz - indications for hydrothermal imprint. Geochimica et Cosmochimica Acta, 71(5), 1232-1248.
Hovland, M., 2002. On the self-sealing nature of marine seeps. Continental Shelf Research, 22(16), 2387-2394.
Iorga, M.C. and Lozier, M.S., 1999. Signatures of the Mediterranean outflow from a North Atlantic climatology 1. Salinity and density fields. Journal of Geophysical Research-Oceans, 104(C11), 25985-26009.
Jaccard, S.L., Galbraith, E.D., Sigman, D.M., Haug, G.H., Francois, R., Pedersen, T.F., Dulski, P. and Thierstein, H.R., 2009. Subarctic Pacific evidence for a glacial deepening of the oceanic respired carbon pool. Earth and Planetary Science Letters, 277(1-2), 156-165.
Jørgensen, B.B., 1990. A Thiosulfate Shunt in the Sulfur Cycle of Marine-Sediments. Science, 249(4965), 152-154.
Jørgensen, B.B., Böttcher, M.E., Luschen, H., Neretin, L.N. and Volkov, I.I., 2004. Anaerobic methane oxidation and a deep H2S sink generate isotopically heavy sulfides in Black Sea sediments. Geochimica et Cosmochimica Acta, 68(9), 2095-2118.
Kano, A., Ferdelman, T.G., Williams, T., Henriet, J.P., Ishikawa, T., Kawagoe, N., Takashima, C., Kakizaki, Y., Abe, K., Sakai, S., Browning, E., Li, X. and the IODP Expedition 307 Scientists, 2007. Age constraints on the origin and growth history of a deep-water coral mound in northeast Atlantic drilled during Integrated Ocean Drilling Program Expedition 307. Geology, 35(11), 1051-1054.
Kaplan, I.R. and Rittenberg, S.C., 1964. Microbiological fractionation of sulphur isotopes. Journal of General Microbiology, 34, 195-212.
Kenyon, N.H., Akhmetzhanov, A.M., Wheeler, A.J., van Weering, T.C.E., de Haas, H. and Ivanov, M.K., 2003. Giant carbonate mud mounds in the southern Rockall Trough. Marine Geology, 195, 5-30.
Ketcham, R.A. and Carlson, W.D., 2001. Acquisition, optimization and interpretation of X-ray computed tomography imagery: applications to the geosciences. Computers & Geosciences, 27, 381-400.
Ku, T.C.W., Walter, L.M., Coleman, M.L., Blake, R.E. and Martini, A.M., 1999. Coupling between sulfur recycling and syndepositional carbonate dissolution: Evidence from oxygen and sulfur isotope composition of pore water sulfate, South Florida Platform, USA. Geochimica et Cosmochimica Acta, 63(17), 2529-2546.
Longinelli, A., 1989. Oxygen-18 and sulphur-34 in dissolved oceanic sulphate and phosphate. In: P. Fritz and J.C. Fontes (Editors), Handbook of Environmental Isotope Geochemistry. Elsevier, Amsterdam, pp. 219-255.
Lovley, D.R., 1991. Dissimilatory Fe(Iii) and Mn(Iv) Reduction. Microbiological Reviews, 55(2), 259-287.
Lovley, D.R., 1997. Microbial Fe(III) reduction in subsurface environments. Fems Microbiology Reviews, 20(3-4), 305-313.
Machin, F., Pelegri, J.L., Marrero-Diaz, A., Laiz, I. and Ratsimandresy, A., 2006. Near-surface circulation in the southern gulf of cadiz. Deep Sea Research Part II: Topical Studies in Oceanography, 63,

1161-1181.
Maestro, A., Somoza, L., Medialdea, T., Talbot, C.J., Lowrie, A., Vazquez, J.T. and Diaz-del-Rio, V., 2003. Large-scale slope failure involving Triassic and Middle Miocene salt and shale in the Gulf of Cadiz (Atlantic Iberian Margin). Terra Nova, 15(6), 380-391.
Maignien, L., Depreiter, D., Foubert, A., Reveillaud, J., De Mol, L., Boeckx, P., Blamart, D., Henriet, J.P. and Boon, N., 2010. Anaerobic oxidation of methane in a cold-water coral carbonate mound from the Gulf of Cadiz. International Journal of Earth Sciences, doi: 10.1007/s00531-010-0528-z.
Maldonado, A., Somoza, L. and Pallares, L., 1999. The Betic orogen and the Iberian-African boundary in the Gulf of Cadiz: geological evolution (central North Atlantic). Marine Geology, 155(1-2), 9-43.
McKenzie, J.A., 1991. The dolomite problem: An outstanding controversy. In: D.W. Müller, J.A. McKenzie and H. Weissert (Editors), Controversies in Modern Geology. Academic Press, London, pp. 35-54.
Medialdea, T., Vegas, R., Somoza, L., Vazquez, J.T., Maldonado, A., Diaz-Del-Rio, V., Maestro, A., Cordoba, D. and Fernandez-Puga, M.C., 2004. Structure and evolution of the "Olistostrome" complex of the Gibraltar Arc in the Gulf of Cadiz (eastern Central Atlantic): evidence from two long seismic cross-sections. Marine Geology, 209(1-4), 173-198.
Meister, P., Mckenzie, J.A., Vasconcelos, C., Bernasconi, S., Frank, M., Gutjahr, M. and Schrag, D.P., 2007. Dolomite formation in the dynamic deep biosphere: results from the Peru Margin. Sedimentology, 54(5), 1007-1031.
Merinero, R., Lunar, R., Martinez-Fiias, J., Somoza, L. and Diaz-del-Rio, V., 2008. Iron oxyhydroxide and sulphide mineralization in hydrocarbon seep-related carbonate submarine chimneys, Gulf of Cadiz (SW Iberian Peninsula). Marine and Petroleum Geology, 25(8), 706-713.
Moore, T.S., Murray, R.W., Kurtz, A.C. and Schrag, D.P., 2004. Anaerobic methane oxidation and the formation of dolomite. Earth and Planetary Science Letters, 229(1-2), 141-154.
Mozley, P.S. and Burns, S.J., 1993. Oxygen and Carbon Isotopic Composition of Marine Carbonate Concretions - an Overview. Journal of Sedimentary Petrology, 63(1), 73-83.
Naudts, L., Greinert, J., Artemov, Y., Beaubien, S.E., Borowski, C. and De Batist, M., 2008. Anomalous sea-floor backscatter patterns in methane venting areas, Dnepr paleo-delta, NW Black Sea. Marine Geology, 251(3-4), 253-267.
Neretin, L.N., Böttcher, M.E., Jørgensen, B.B., Volkov, I.I., Luschen, H. and Hilgenfeldt, K., 2004. Pyritization processes and greigite formation in the advancing sulfidization front in the Upper Pleistocene sediments of the Black Sea. Geochimica et Cosmochimica Acta, 68(9), 2081-2093.
Noé, S., Titschack, J., Freiwald, A. and Dullo, W.C., 2006. From sediment to rock: diagenetic processes of hardground formation in deep-water carbonate mounds of the NE Atlantic. Facies, 52(2), 183-208.
O'Neil, J.R., Clayton, R.N. and Mayeda, T.K., 1969. Oxygen Isotope Fractionation in Divalent Metal Carbonates. Journal of Chemical Physics, 51(12), 5547-5558.
Ohfuji, H. and Rickard, D., 2005. Experimental syntheses of framboids - a review. Earth-Science Reviews, 71(3-4), 147-170.
Passier, H.F., Middelburg, J.J., de Lange, G.J. and Bottcher, M.E., 1999. Modes of sapropel formation in the eastern Mediterranean: some constraints based on pyrite properties. Marine Geology, 153(1-4), 199-219.
Passier, H.F., Middelburg, J.J., deLange, G.J. and Bottcher, M.E., 1997. Pyrite contents, microtextures, and sulfur isotopes in relation to formation of the youngest eastern Mediterranean sapropel. Geology, 25(6), 519-522.
Paytan, A. and Griffith, E.M., 2007. Marine barite: Recorder of variations in ocean export productivity. Deep-Sea Research Part Ii-Topical Studies in Oceanography, 54(5-7), 687-705.
Pelegri, J.L., Aristegui, J., Cana, L., Gonzalez-Davila, M., Hernandez-Guerra, A., Hernandez-Leon, S., Marrero-Diaz, A., Montero, M.F., Sangra, P. and Santana-Casiano, M., 2005. Coupling between the open ocean and the coastal upwellng region off northwest Africa: water recirculation and offshore pumping of organic matter. Journal of Marine Systems, 54(1-4), 3-37.
Pinheiro, L., Ivanov, M.K., Sautkin, A., Akhmanov, G., Magalhaes, V., Volkonskaya, A., Monteiro, J.H., Somoza, L., Gardner, J., Hamouni, N. and Cunha, M.R., 2004. Mud volcanism in the Gulf of Cadiz: results from the TTR-10 cruise. Marine Geology, 195, 131-151.
Pirlet, H., Wehrmann, L.M., Brunner, B., Frank, N., Dewanckele, J., Van Rooij, D., Foubert, A., Swennen, R., Naudts, L., Boone, M., Cnudde, V. and Henriet, J.P., 2010. Diagenetic formation of gypsum and dolomite in a cold-water coral mound in the Porcupine Seabight, off Ireland. Sedimentology,

57, 786-805.
Raiswell, R., 1982. Pyrite Texture, Isotopic Composition and the Availability of Iron. American Journal of Science, 282(8), 1244-1263.
Richter, D.K., Gotte, T., Gotze, J. and Neuser, R.D., 2003. Progress in application of cathodoluminescence (CL) in sedimentary petrology. Mineralogy and Petrology, 79(3-4), 127-166.
Riedinger, N., Kasten, S., Groger, J., Franke, C. and Pfeifer, K., 2006. Active and buried authigenic barite fronts in sediments from the Eastern Cape Basin. Earth and Planetary Science Letters, 241(3-4), 876-887.
Ritger, S., Carson, B. and Suess, E., 1987. Methane-Derived Authigenic Carbonates Formed by Subduction Induced Pore-Water Expulsion Along the Oregon Washington Margin. Geological Society of America Bulletin, 98(2), 147-156.
Roberts, J.M., Wheeler, A.J. and Freiwald, A., 2006. Reefs of the deep: The biology and geology of cold-water coral ecosystems. Science, 312(5773), 543-547.
Sartori, R., Torelli, L., Zitellini, N., Peis, D. and Lodolo, E., 1994. Eastern Segment of the Azores-Gibraltar Line (Central-Eastern Atlantic) - an Oceanic Plate Boundary with Diffuse Compressional Deformation. Geology, 22(6), 555-558.
Snyder, G.T., Dickens, G.R. and Castellini, D.G., 2007. Labile barite contents and dissolved barium concentrations on Blake Ridge: New perspectives on barium cycling above gas hydrate systems. Journal of Geochemical Exploration, 95(1-3), 48-65.
Soetaert, K., Hofmann, A.F., Middelburg, J.J., Meysman, F.J.R. and Greenwood, J., 2007. The effect of biogeochemical processes on pH. Marine Chemistry, 105(1-2), 30-51.
Somoza, L., Diaz-del Rio, V., Leon, R., Ivanov, M.K., Fernandez-Puga, M.C., Gardner, J., Hernandez-Molina, F.J., Pinheiro, L., Rodero, J., Lobato, A., Maestro, A., Vazquez, J.T., Medialdea, T. and Fernandez-Salas, L.M., 2003. Seabed morphology and hydrocarbon seepage in the Gulf of Cadiz mud volcano area: Acoustic imagery, multibeam and ultra-high resolution seismic data. Marine Geology, 195, 153-176.
Sweeney, R.E. and Kaplan, I.R., 1973. Pyrite Framboid Formation - Laboratory Synthesis and Marine Sediments. Economic Geology, 68(5), 618-634.
Tarutani, T., Clayton, R.N. and Mayeda, T.K., 1969. Effect of Polymorphism and Magnesium Substitution on Oxygen Isotope Fractionation between Calcium Carbonate and Water. Geochimica et Cosmochimica Acta, 33(8), 987-996.
Torres, M.E., Bohrmann, G., Dube, T.E. and Poole, F.G., 2003. Formation of modern and Paleozoic stratiform barite at cold methane seeps on continental margins. Geology, 31(10), 897-900.
Torres, M.E., Brumsack, H.J., Bohrmann, G. and Emeis, K.C., 1996. Barite fronts in continental margin sediments: A new look at barium remobilization in the zone of sulfate reduction and formation of heavy barites in diagenetic fronts. Chemical Geology, 127(1-3), 125-139.
Van der Land, C., Mienis, F., De Haas, H., Frank, N., Swennen, R. and Van Weering, T.C.E., 2010. Diagenetic processes in carbonate mound sediments at the southwest Rockall Trough margin. Sedimentology, 57, 912-931.
Van Lith, Y., Warthmann, R., Vasconcelos, C. and Mckenzie, J.A., 2003. Sulphate-reducing bacteria induce low-temperature Ca-dolomite and high Mg-calcite formation. Geobiology, 1(1), 71-79.
Van Rensbergen, P., Depreiter, D., Pannemans, B., Moerkerke, G., Van Rooij, D., Marsset, B., Akhmanov, G., Blinova, V., Ivanov, M.K., Rachidi, M., Magalhaes, V., Pinheiro, L. and Henriet, J.-P., 2005. The El Arraiche mud volcano field at the Moroccan Atlantic slope, Gulf of Cadiz. Marine Geology, 219, 1-17.
Van Rooij, D., Blamart, D., De Mol, L., Mienis, F., Pirlet, H., Wehrmann, L.M., Maignien, L., Templer, S.P., De Haas, H., Barbieri, R., Hebbeln, D., Frank, N., Larmagnat, S., Stadnitskaia, A., Stivaletta, N., Van Weering, T.C.E., Zhang, Y., Hamoumi, N., Duyck, P., Henriet, J.P. and party, T.M.M.s., 2010. Cold-water coral mounds on the Pen Duick Escarpment, Gulf of Cadiz: the MiCROSYSTEMS approach. Marine Geology, doi: 10.1016/j.margeo.2010.08.012.
van Weering, T.C.E., de Haas, H., Akhmetzhanov, A.M. and Kenyon, N.H., 2003. Giant Carbonate Mounds along the Porcupine and SW Rockall Trough Margins. In: J. Mienert and P.P.E. Weaver (Editors), European margin sediment dynamics: side-scan sonar and seismic images. Springer-Verlag, Heidelberg, pp. 211-216.
Vasconcelos, C. and McKenzie, J.A., 1997. Microbial mediation of modern dolomite precipitation and diagenesis under anoxic conditions (Lagoa Vermelha, Rio de Janeiro, Brazil). Journal of Sedimentary Research, 67(3), 378-390.
Vasconcelos, C., McKenzie, J.A., Bernasconi, S., Grujic, D. and Tien, A.J., 1995. Microbial Mediation as a

Possible Mechanism for Natural Dolomite Formation at Low-Temperatures. Nature, 377(6546), 220-222.

Vasconcelos, C., McKenzie, J.A., Warthmann, R. and Bernasconi, S.M., 2005. Calibration of the delta O-18 paleothermometer for dolomite precipitated in microbial cultures and natural environments. Geology, 33(4), 317-320.

Webster, G., Blazejak, A., Cragg, B.A., Schippers, A., Sass, H., Rinna, J., Tang, X., Mathes, F., Ferdelman, T.G., Fry, J.C., Weightman, A.J. and Parkes, R.J., 2008. Subsurface microbiology and biogeochemistry of a deep, cold-water carbonate mound from the Porcupine Seabight (IODP Expedtion 307). Environmental Microbiology, doi: 10.1111/j.1462-2920.2008.01759.x.

Wehrmann, L.M., Knab, N.J., Pirlet, H., Unnithan, V., Wild, C. and Ferdelman, T.G., 2009. Carbon mineralization and carbonate preservation in modern cold-water coral reef sediments on the Norwegian shelf. Biogeosciences, 6(4), 663-680.

Wehrmann, L.M., Templer, S.P., Brunner, B., Bernasconi, S.M., Maignien, L. and Ferdelman, T.G., 2010. The imprint of methane seepage on the geochemical record and early diagenetic processes in cold-water coral mounds on Pen Duick Escarpment, Gulf of Cadiz. Marine Geology, doi:10.1016/j.margeo.2010.08.005.

Wienberg, C., Beuck, L., Heidkamp, S., Hebbeln, D., Freiwald, A., Pfannkuche, O. and Monteys, X., 2008. Franken Mound: facies and biocoenoses on a newly-discovered “carbonate mound” on the western Rockall Bank, NE Atlantic. Facies, 54(1), 1-24.

Wienberg, C., Hebbeln, D., Fink, H.G., Mienis, F., Dorschel, B., Vertino, A., Correa, M.L. and Freiwald, A., 2009. Scleractinian cold-water corals in the Gulf of Cadiz-First clues about their spatial and temporal distribution. Deep-Sea Research Part I-Oceanographic Research Papers, 56(10), 1873-1893.

Wilkin, R.T. and Barnes, H.L., 1996. Pyrite formation by reactions of iron monosulfides with dissolved inorganic and organic sulfur species. Geochimica et Cosmochimica Acta, 60(21), 4167-4179.

Wright, D.T., 1999. The role of sulphate-reducing bacteria and cyanobacteria in dolomite formation in distal ephemeral lakes of the Coorong region, South Australia. Sedimentary Geology, 126(1-4), 147-157.

Zitellini, N., Gracia, E., Matias, L., Terrinha, P., Abreu, M.A., DeAlteriis, G., Henriet, J.P., Danobeitia, J.J., Masson, D.G., Mulder, T., Ramella, R., Somoza, L. and Diez, S., 2009. The quest for the Africa-Eurasia plate boundary west of the Strait of Gibraltar. Earth and Planetary Science Letters, 280(1-4), 13-50.

Chapter 8 - Conclusions and outlook

8.1 Conclusions

The present research focused on the sediment matrix in cold-water coral mounds in the Porcupine Seabight (Off Ireland) and the Gulf of Cadiz (Off Morocco). In part 2, the potential of the terrigenous sediment fraction as paleo-environmental was explored. First, a pilot study was conducted on the Late Quaternary sediment intervals in a gravity core retrieved from Challenger Mound. This pilot study was used to develop a methodological strategy to disentangle the various signals recorded in the terrigenous sediment fraction and assess the potential difficulties inherent to these methods. In a next step, this methodological strategy was applied on the entire sequence in Challenger Mound which was drilled during IODP expedition 307. Based on the results of chapter 3 and 4, the following conclusions are highlighted:

- Based on the neodymium and strontium isotope ratios of the sediment throughout the entire Challenger mound sequence, the British-Irish Isles are identified as the primary contributor of terrigenous sediment in Challenger Mound with a variable amount of volcanic material. Iceland and the Tertiary volcanic provinces of the NW British Isles may be considered as the source area for this volcanic material.
- A minority of the samples reveal a minor input of sediment from old cratons which can be found on Greenland, Scandinavia or Canada.
- In the Late Quaternary sequence of Challenger Mound, glacial intervals are characterized by siliciclastic sediment with a bimodal grain-size distribution, typical for ice-rafting. The fact that little or no sorting occurred indicates that bottom currents were reduced during cold stages.
- The Late Quaternary interglacial intervals in Challenger Mound reveal evidence for strong sorting processes due to enhanced bottom currents. Hence, reworking of biogenic and ice-rafted material, deposited during glacial times, was observed.
- The absence of coral fragments in the Late Quaternary intervals deposited during deglaciations, shows that coral growth was suppressed. It is put forward that the deglaciations of the BIIS seriously altered the hydrography and terrigenous input in the Porcupine Seabight and therefore affected coral growth. Thus, the role of the BIIS is ambiguous as the influx of glacial sediments is an important factor for the infill of the coral framework and thus mound build-up, while deglaciations seem to suppress coral growth.
- The Early-Pleistocene ice-rafted horizons which occur in the lower mound phase of Challenger Mound are linked with the British-Irish Isles. Hence, for the first time, evidence is put forward for the presence of a recurring, marine-based ice sheet on the British-Irish Isles since the earliest Pleistocene, implying significant mid-latitudinal glaciations, even in the earliest stages of Northern Hemisphere glacial expansion. Therefore, early and significant ice accumulation in mid-latitudinal regions, such as the British-Irish Isles, should be accounted for in reconstructions and modelling studies addressing the mechanisms that steer Northern Hemisphere ice sheet development and their impact on Quaternary climate variability.
- The clay mineralogy in the lower mound phase (M1) of Challenger Mound is primarily steered

by weathering processes on the British-Irish Isles. Thus, Challenger Mound provides a unique record of the Early-Pleistocene continental climate on the nearby British-Irish Isles. Interglacial periods are characterized by an enhanced smectite content indicating the presence of a temperate climate with sufficient precipitation to allow hydrolysis. Glacial periods record an increase in illite due to the decrease of hydrolytic processes and the increase of direct rock erosion. Abrupt smectite peaks are superimposed on this cyclic glacial-interglacial pattern and are linked to the initial stage of chemical weathering during deglaciations. Below the mound base, the increased smectite content attests of the increased temperature and hence, increased chemical weathering during the Miocene.

- The clay mineralogy of the upper mound phase (M2) of Challenger reveals a more chaotic pattern due to the absence of a dense coral framework which results in the increased influence of differentiation processes and the presence of numerous unconformities. Nevertheless an increase is observed in the chlorite content compared to M1, while kaolinite reveals a decrease. This is attributed to the prolonged and more extensive glaciations after the MPT, which result in an increase of the physical weathering processes.

In part 3 of the presented work, the early-diagenetic processes in cold-water coral mounds were investigated. First, the diagenetic formation of gypsum and dolomite was studied in Perseverance Mound in the Porcupine Seabight. Furthermore, the relation with calcite precipitation and aragonite dissolution close to the seabed was discussed. In a next step, the diagenetic processes were studied in Alpha, Beta and Gamma Mound, three cold-water coral mounds located in the Pen Duick Mound Province in the Gulf of Cadiz. In contrast to Perseverance Mound, the mounds on Pen Duick Escarpment are influenced by a shallow sulfate methane transition zone. Based on the results of chapter 6 and 7, the following conclusions are highlighted:

- The diagenetic formation of gypsum and dolomite in Perseverance Mound is attributed to a phase of seawater inflow. This led to penetration of oxygenated fluids into formerly anoxic sediments. Oxidation of sulfide minerals (e.g. pyrite) caused dissolution of aragonite and increased sulfate and calcium concentration, triggering the precipitation of gypsum and dolomite. In the future, the occurrence gypsum in marine sediments could be a powerful tool to indentify oxidation processes in carbonate sediments.
- The inflow of oxidizing seawater may be caused by increased bottom currents which resulted in partial erosion and enhanced inflow of sea water in the mound.
- In Perseverance Mound, upward diffusing bicarbonate deriving from coral dissolution due to sulfide oxidation, was reprecipitated near the surface as calcite due to the increase in pH. This precipitation led to a lithification of the sediment.
- The widely distributed moldic porosity in the lithified layer indicates that a new phase of dissolution occurred during or after lithification, when the lithified layer was buried by Holocene sediments. The dissolution of aragonitic biogenic fragments may be attributed to the production of hydrogen sulfide during microbial sulfate reduction. Due to the low content of reactive iron in the lithified layer, hydrogen sulfide was not extracted from the porewater as iron sulfide. Subsequently, hydrogen sulfide will act as a weak acid and result in aragonite dissolution.
- Alpha and Beta Mound are both affected by a shallow SMTZ which induced the precipitation of 1) carbonates with a depleted $\delta^{13}C$ signature and 2) sedimentary pyrite characterized by heavy $\delta^{34}S$ values.
- Various lithified layers occur in the cold-water coral mounds in Cadiz as a result of authigenic mineral precipitation. This lithification not only stabilizes the mounds, but also forms layers that are susceptible to brittle deformation, opening pathways for subsequent fluid migration and thus influencing the diagenetic environment.
- In Alpha Mound, the presence of a SMTZ around a depth of 200 cm can be inferred based on the presence of significant amounts of dolomite, characterized by a depleted $\delta^{13}C$ value. Dolomite will preferentially form in microbial hotspots such as the SMTZ, given that AOM results in the strong production of alkalinity. Most likely, calcite precipitated first, lowering the Ca-concentration in the porewater and thus increasing the Mg/Ca ratio which subsequently favoured dolomitization. The high methane fluxes in Alpha Mound are also corroborated by the dominance of framboidal pyrite over euhedral pyrite, which is likely associated with extensive production of sulfide coupled to AOM. The zonation of the dolomite under CL indicates that dolomite precipitated in various episodes, which were probably characterized by varying redox

conditions related to shifts in the position of the SMTZ. Such a dynamical behavior of the location of the SMTZ could be caused by episodic lateral inflow of seawater. This diagenetic oxidation event may also be responsible for gypsum precipitation in Alpha Mound.

- Beta Mound appears to be exposed to lower methane fluxes and a more static position of the SMTZ compared to Alpha Mound. The more fixed position of the SMTZ for a longer period of time, is supported by the precipitation of significant amounts of barite around 345 cm. Apparently, the flux of dissolved sulfide from this SMTZ is not as intense as for Alpha Mound. Under these conditions, formation of euhedral pyrite dominates. Nevertheless, the precipitation of calcite between 250 and 300 cm with depleted ^{13}C values can be attributed to an upward shift in the SMTZ.
- In constrast to Alpha and Beta Mound, Gamma Mound does not reveal indications for the occurrence of a SMTZ in the upper 5 m of the sediment. The brown colour of the sediment, the low amount of iron sulfides and the extremely low $\delta^{34}S$ values of the sedimentary pyrite indicate that bacterial sulfate reduction is largely outcompeted by dissimilatory iron reduction (DIR). This is attributed to the large pool of iron-(oxyhydr)oxides in the sediment as a result of the Saharan dust input. The dominance of DIR resulted in the good preservation of the corals. The sharp increase in iron sulfides below 470 cm indicates that bacterial sulfate reduction becomes the dominant terminal electron pathway during organic matter oxidation. The relatively high $\delta^{34}S$ values of the sedimentary pyrite reveal the upward diffusion of hydrogen sulfide from an SMTZ below. Below, 470 cm corals are badly preserved and calcite and dolomite precipitation occurs.

8.2 Outlook

The present thesis provides new data on the terrigenous fraction and early diagenetic processes in cold-water coral mounds. However, this research also raises new questions which may be addressed in future research. Some of the unanswered, burning issues are listed below.

- Lab experiments are necessary to better understand the relation between the presence of a coral framework and sediment infill.
- More work is needed on the provenance of the Early-Pleistocene ice-rafted layers in order to better constrain the spatial dimensions of the ice sheet on the British-Irish Isles.
- The relation between the terrigenous fraction in the sediment and diagenetic processes affecting the sediment should be further explored. The presence of terrigenous material provides a pool of reactive iron which buffers the diagenetic alteration of the carbonates. In this regard, the drilling of a cold-water coral mound in the Rockall Trough would be highly interesting. These mounds received less terrigenous input compared to the mounds in the Porcupine Seabight and hence, the diagenetic alterations may be in a more evolved state. In addition, such drilling would help to evaluate the role of terrigenous material in mound build-up.
- Not much is known about the change in the diagenetic processes when a mound gets buried and moves from an open to a closed diagenetic system. The drilling of one of the buried mounds in the Magellan Mound Province or the Melilla Mound Field might provide crucial data on how recent mounds evolve, through a series of diagenetic processes, towards fossil carbonate mounds in terrestrial outcrops.
- The simulation of diagenetic processes in lab environments by means of a bioreactor system will help to put better constraints on the precipitation of enigmatic minerals such as dolomite.
- Monitoring of seawater inflow in cold-water coral mound sediments, as observed in Alpha Mound and Perseverance Mound, is necessary to better understand and assess the impact of diagenetic oxidation processes.
- A core transect on a cold-water coral mound will contribute in acquiring a better insight in the spatial distribution of the fluid flow processes in coral mounds and their impact on early diagenesis. In addition, such transect will yield important information on mound build-up.

Acknowledgements

First, I would like to thank my promotor, Jean-Pierre Henriet for offering me this opportunity and providing the perfect framework to conduct my research.

A huge thanks goes to my two partners in crime/science: Mieke Thierens and Laura Wehrmann, who I could always rely on. Without the two of you, my thesis would have been half as thick and twice as boring... Laura is additionally acknowledged for making me appreciate the colour pink and John Denver just a little bit more.

Christophe Colin, merci pour toute l'aide apportée à ma thèse. Tes explications et nos discussions étaient de grande importance pour ma recherche. Je veux aussi remercier Dominique Blamart, Norbert Frank et les autres gens de Gif qui m'ont aidé.

A special thanks goes to the cold-water coral team from Gent. David, Lies and Andres, thanks for all the help, nice coral discussions and entertainment (David actually works on contourites but is thanked anyway). Also, a big thanks to the other people of the RCMG for appreciating my insanely funny jokes: Lieven, Rindert, Mieke, Jasper, Maarten, Katrien, Davy, Tine, Anita, Javiera, Marcske, Sonja, Els, Isabelle, Vera, Jens, Peter, Koen, Arne, Jeroen, Wim, Dries, Matthi, Athanas, Jefster and Tist.

I want to thank Benjamin Brunner for the isotopic measurement and the assistance writing my manuscripts.

Furthermore, I would like to thank Frank Vanhaecke, Kris Latruwe and Ellen Dewaele of the Atomic and Mass Spectrometry unit (aka the 'S12') for their help with the isotope measurements and sample preparation.

Jan Dewanckele, Matthieu Boone and Veerle Cnudde are thanked for all their assistance with the CT scans.

The people of Leuven: Anneleen Foubert, Herman Nijs and Rudy Swennen are acknowledged for their help with the XRD-analyses, the thin sections and the interesting scientific discussions.

I would also like to thank the people of the cold-water coral mound community for all the nice moments on conferences, cruises and fieldtrips (Silvia Spezafferri, Stephan Margreth, Giordana Gennari, Hiske Fink, Markus Eisele, Boris Dorschel, Nina Joseph, Jürgen Titschack, Veerle Huvenne, Furu Mienis, Henk de Haas, Cees van der Land, Sacha Flögel, Stefanie Templer, Lois Maignien, Rory O'Donnell, Ben De Mol, Anne-Christine da Silva, Morten Bjerager and all the others I forgot...).

Thanks to all the people of the S8 who helped me during my thesis or provided entertainment (Stephen Louwye, Stijn Glorie, Johan De Grave, Kenneth Mertens, Sabine Van Cauwenberghe, Jan Mortier, Thomas Verleye, Annos Zwertvaegher, Koen Verhoeven, Bert Van Bocxlaer, Tim Debacker, Tim De Kock, Marijn Boone, Nicole Selen, Nicole Vindevogel, Veerle Vandenhende, Karen Fontijn, Ingrid Smet...). A special thanks goes to Kurt Blom for the last-minute repair of my computer. Bite the (eolian?) dust, Murphy!

I would like to acknowledge the jury for reading and correcting my thesis.

Finally, I want to thank my family and friends. You are the best.